AD NUMBER:	AD0460484

LIMITATION CHANGES

TO:

Approved for public release; distribution is unlimited.

FROM:

Distribution authorized to U.S. Gov't. agencies and their contractors; Administrative/Operational Use; 16 Feb 1965. Other requests shall be referred to Department of the Air Force, Washington DC 20330

AUTHORITY

20190516 - CFSTI PER SEG LTR, 1 JUN 1965

NA-64-177

ADVANCED X-15A ABLATION SYSTEM DESIGN, TESTS, AND ANALYSIS

NORTH AMERICAN AVIATION, INC. / LOS ANGELES DIVISION

Serial No. 30

File No. ____________ Report No. NA-64-177

NORTH AMERICAN AVIATION, INC.

LOS ANGELES DIVISION
INTERNATIONAL AIRPORT
LOS ANGELES 9, CALIFORNIA

"ADVANCED X-15A-2 ABLATION

SYSTEM DESIGN, TESTS, AND ANALYSIS"

DDC
APR 9 1965
TISIA B

PREPARED BY

Robert H. Johnson

APPROVED BY

H. A. Evans, Manager
X-15 Program

E. W. Johnston, Asst. Manager
X-15 Program

No. of Pages 168

Date 2-14-64

REVISIONS

DATE	REV. BY	PAGES AFFECTED	REMARKS

1006-C-2 REV. 8-62

ABSTRACT:

An investigation of ablation materials was conducted for application to an advanced, Mach 8 modification of the X-15 Research Airplane. Performance of the selected material, Thermo-Lag T-500, was evaluated in plasma tunnel tests and in flight tests. Estimates were made of required ablator weight and thicknesses at stagnation and non-stagnation areas of the Advanced X-15A-2. Performance data, resulting from actual flight tests, plasma tunnel tests and analytical predictions, were compared.

TITLE:

"Advanced X-15A-2 Ablation System Design, Tests, and Analysis".

AUTHOR:

Robert H. Johnson, Supervisor, Advanced X-15.

FOREWORD:

The studies described in this report were made from 13 May 1963 to 7 February 1964 as a part of the rebuild of X-15A-2 under Contract No. AF33(657)11614. The report represents the efforts of R. H. Johnson, P. O. Paxson, J. B. Bodne and H. Shatzkin, who were assigned to the project. K. MacDowell of the Materials Laboratory is acknowledged for his support on the flight test portion of the study. Acknowledgement is also made to J. Bartley of the Emerson Electric Company, who assisted in the plasma tunnel tests.

TABLE OF CONTENTS

	Page
FOREWORD	i
ABSTRACT	i
TABLE OF CONTENTS	ii
LIST OF ILLUSTRATIONS	iv
LIST OF TABLES	viii
INTRODUCTION	1
ABLATION SYSTEM DEVELOPMENT PROGRAM	
Screening of Ablation Materials	3
Plasma Tunnel Tests	4
Test Facility Selection	4
Test Specimens and Testing Techniques	4
Analysis of Test Results	6
Leading Edge Tests	7
Flat Plate Tests	10
Flight Tests	14
Flight Test No. 1	14
Flight Test No. 2	17
Flight Test No. 3	17
Flight Test No. 4	18
Flight Test No. 5	19
Flight Test No. 6	20
Heat Shield Design	21
Aerodynamic Heating	21
Thickness Requirements	22
Ablation System Weight	22

TABLE OF CONTENTS

	Page
REFERENCES	25
APPENDIX A - FUSELAGE BOW SHOCK-WING LEADING EDGE SHOCK INTERACTION ANALYSIS	
APPENDIX B - PROTUBERANCE HEAT TRANSFER	
APPENDIX C - PLASMA TUNNEL MODEL PHOTOGRAPHS	

LIST OF ILLUSTRATIONS

Figure No.	Title	Page
1	Advanced X-15 Research Airplane	26
2	Removable Wing Tip Panel	27
3	Performance Characteristics, X-15A-2	28
4	Advanced X-15A-2 Design Mission	29
5	Summary of Maximum Temperatures, Unprotected Inconel-X	30
6	Plasma Tunnel Selection, Stagnation Point Duplication	31
7	Cutaway View of Plasma Tunnel Test Model	32
8	Heat Flux - Enthalpy Simulation, Stagnation Regions	33
9	Shear Stress - Enthalpy Simulation, Stagnation Regions	34
10	Flat Panel Plasma Tunnel Model	35
11	Flight Simulation, Flat Surfaces	36
12	Design Mission Simulation	37
13	Design Mission Simulation, Heat Flux	38
14	Effect of Thickness, Test Condition 1, T-500-6A	39
15	Effect of Thickness, Test Condition 2, T-500-6A	40
16	Effect of Thickness, Test Condition 3, T-500-6A	41
17	Effect of Test Conditions, T-500-6A	42
18	Effect of Material, Test Condition 1	43
19	Effect of Material, Test Condition 2	44
20	Effect of Material, Test Condition 3	45
21	Linear Recession Rate, T-500-6A	46
22	Surface Recession During Test	47
23	Plasma Tunnel - Leading Edge Effective Heat of Ablation, T-500-6A	48

LIST OF ILLUSTRATIONS

Figure No.	Title	Page
24	Variable Heat Flux Results, T-500-6A, Substrate Temperatures	49
25	Sketch of .805 in. Thick Model After Variable Heat Flux Test	50
26	Sketch of .550 in. Thick Model After Variable Heat Flux Test	51
27	Sketch of .354 in. Thick Model After Variable Heat Flux Test	52
28	Variable Heat Flux Tests, T-500-6A, Comparison of Theory With Tests, Material Loss	53
29	Effect of Thickness, Test Condition 2A, T-500-4, T.C. No. 1	54
30	Effect of Thickness, Test Condition 3A, T-500-4, T.C. No. 1	55
31	Effect of Thickness, Test Condition 4A, T-500-4, T.C. No. 1	56
32	Effect of Slots and Holes, Test Condition 3A, T-500-4A, T.C. No. 1	57
33	Effect of Heat Flux - Slotted Model, T-500-4A, T.C. No. 1	58
34	Effect of Thickness, Test Condition 2A, T-500-4, T.C. No. 2	59
35	Effect of Thickness, Test Condition 3A, T-500-4, T.C. No. 2	60
36	Effect of Thickness, Test Condition 4A, T-500-4, T.C. No. 2	61
37	Effect of Slots and Holes, Test Condition 3A, T-500-4A, T.C. No. 2	62
38	Effect of Heat Flux - Slotted Model, T-500-4A, T.C. No. 2	63
39	Plasma Tunnel - Flat Plate Effective Heat of Ablation, Effect of Thickness, T-500-4A	64

LIST OF ILLUSTRATIONS

Figure No.	Title	Page
40	Plasma Tunnel - Flat Plate Effective Heat of Ablation, Clean Models, T-500-4A.	65
41	Plasma Tunnel - Flat Plate Effective Heat of Ablation, Models With Voids, Slots, Holes, T-500-4A.	66
42	Flat Plate Substrate Temperature Correlations, Test Condition 2A.	67
43	Flat Plate Substrate Temperature Correlations, Test Condition 3A.	68
44	Flat Plate Substrate Temperature Correlations, Test Condition 4A.	69
45	Ablation Material Test Regions on X-15.	70
46	Flight Test No. 1, Speed Brake, Cork	71
47	Flight Test No. 2, Speed Brake, Bare Skin	72
48	Flight Test No. 2, Ventral Stagnation Line, Cork	73
49	Flight Test No. 3, Ventral Stagnation Line, T-500-6A	74
50	Flight Test No. 3, Speed Brake, T-500-4	75
51	Flight Test No. 4, Speed Brake, T-500-4A	76
52	Flight Test No. 5, Heating Pattern Near A Protuberance	77
53	Flight Test No. 5, Panel F-4, T-500-4A	78
54	Flight Test No. 6, Ventral Stagnation Line Ablation Material Measurements	79
55	Flight Test No. 6, Ventral Stagnation Line, T-500-6A	80
56	Flight Test No. 6, Panel F-4 Ablation Material Measurements	81
57	Flight Test No. 6, Panel F-4, T-500-4A	82
58	Points on X-15 For Representative Heat Flux Calculations	83

FORM 18-G-1 REV. 9-61

LIST OF ILLUSTRATIONS

Figure No.	Title	Page
59	Typical Stagnation Line Section	84
60	Stagnation Line Points	85
61	Flat Plate Geometry Point Description	86
62	Flat Plate Points	87
63 - 78	Design Mission Heat Flux, Shear Stress and Static Pressure For 16 Points On The X-15	88
79	Fuselage Centerline Variation of Heat Flux at t=150 sec.	104

FORM 18-G-1 REV. 9-61

LIST OF TABLES

Table No.	Title	Page
I	Summary of Plasma Tunnel Test Conditions	5
II	Leading Edge Test Conditions	8
III	Summary of Leading Edge Tests, Effective Heats of Ablation	9
IV	Flat Plate Test Conditions	11
V	Summary of Flat Plate Tests, Effective Heats of Ablation, T-500-4A	12
VI	Summary of Flat Plate Tests, Effective Heats of Ablation, Cork 2755	15
VII	Summary of Ablation Material Flight Tests	16
VIII	Typical Heat Shield Thicknesses	23
IX	Head Shield Weight	24

INTRODUCTION

North American Aviation, Inc., Los Angeles Division (NAA-LAD) has designed an ablation thermal protective system for the No. 2 X-15 Research Airplane, as a part of the repair and improvement of this airplane. Repair of the right-hand wing of the vehicle was necessary as the result of an accident experienced in 1962. Some features of the improvements being made are presented in Figure 1. The main gear is being lengthened to accommodate the mounting of external ramjets. The change in the main gear configuration necessitates an improved nose gear configuration. Increased internal volume is being achieved by adding a 29-inch fuselage extension in the middle of the aircraft. Liquid hydrogen tanks and their related plumbing are being provided for installation in this area. A new windshield configuration, incorporating fused silica, is being installed in the present canopy. A capability of 8000 ft/sec velocity is being achieved by addition of external propellants. The added heat, caused by the increased velocity, is being accommodated by the use of an ablative material.

A removable wing panel, shown in Figure 2, is being incorporated into the tip of the right wing. This panel will be used to investigate the performance of heat resistant materials and experimental rib and spar designs, the effects of surface discontinuities, etc.

The estimated performance characteristics of the Advanced X-15, now designated as the X-15A-2, are shown in Figure 3. For reference purposes, the performance capabilities of the current X-15 are shown with the envelope of some of the maximum flights which have been performed. While capable of attaining the extreme altitudes as shown, the X-15A-2 flights will be directed principally toward 250,000 feet altitudes for stellar photography experiments and 100,000 feet altitudes at about 8,000 ft/sec velocity for hypersonic airbreathing propulsion experiments.

The X-15A-2 design mission, shown in Figure 4, is that for which the ablation protection system has been designed. This mission was chosen for the following reasons:

1. Maximum velocity (Mach 8) is achieved.
2. Thermal conditions are severe in comparison to other planned missions.

Basically, the problem of heat protection of the X-15A-2 is one of converting a design on the heat sink concept to one capable of accommodating a higher heat load with virtually no redesign of the basic structure. Figure 5 shows the peak temperatures which would be generated in the design mission without heat protection. The severe thermal environment of the design mission would subject the unprotected structure to conditions exceeding the limits of structural integrity. This imposes the requirement of an external heat protection system with sufficient heat blockage to preclude redesign of the basic structure of the vehicle.

The following criteria were established as a basis for developing the required heat protection system:

1. The peak temperatures of the existing structure must be held within design limits.

2. Heat protection would be required for the entire vehicle during the total flight. Although it is possible to provide partial vehicle protection, or partial mission protection and maintain acceptable temperatures, the comprehensive thermal and structural analyses required could not be accomplished within the established contract schedules and cost.

3. The heat protection system should add the minimum practical weight.

4. The thermal protection system must be compatible with basic vehicle functions on the ground and in flight.

5. Application and removal of the heat protection system must be effected under field conditions and must not interfere with the intended functions of the vehicle.

6. Initial costs of technical development, costs of raw materials, and costs of application and removal, must be within practical limits.

The present report discusses principally studies to determine the amounts of ablation material required for adequate heat protection.

ABLATION SYSTEM DEVELOPMENT PROGRAM

SCREENING OF ABLATION MATERIALS

Contract schedules and funds did not permit an extensive screening for an optimum ablation system. A cursory review of the literature and an industry survey indicated that there existed a scarcity of knowledge on the behavior of ablation materials in the low heat flux - low enthalpy region. In addition, no data could be found in the literature on ablation performance under relatively high aerodynamic shear stress, a parameter of considerable importance for the X-15.

The following materials were considered for preliminary screening:

1. Emerson Electric Thermo-Lag T-500.
2. Dow-Corning DC 325.
3. Armstrong Cork #2755.
4. NASA Purple Blend.
5. Molded Refrasil Phenolics.
6. General Electric Century Series Materials.

In reply to early contacts, the Emerson Electric Company submitted a proposal to supply a material, Thermo-Lag T-500, which would provide the requisite heat protection with an estimated ablator weight of 400 pounds per mission. This was considered an acceptable weight for the vehicle. Information was available on the performance of Thermo-Lag T-500 in environments approaching that of interest and on the production and application of Thermo-Lag type ablators, both in the molded as well as in the sprayable forms. The Thermo-Lag T-500 formulation incorporates sublimating salts with sublimation temperatures of about 530°F. The presence of these salts limits substrate (backwall) temperatures to sublimation temperatures until the salts are completely consumed. Limiting the substrate temperatures obviates a comprehensive thermal analysis of the X-15A-2 structure.

Previous test results indicated that Purple Blend did not have the requisite resistance to shear stresses. This material was, therefore, eliminated without further testing. The other materials were screened in preliminary plasma arc tunnel tests, and none showed ablation efficiencies as high as that of Thermo-Lag T-500 when compared on the basis of time to attain a substrate temperature of 500°F. Refrasil phenolic molded parts with oriented laminae at the leading edge, were a close second to Thermo-Lag T-500 on the above basis. Refrasil phenolic, however, is available only as molded parts and therefore not considered suitable for use on broad surfaces of non-stagnation areas. On the basis of the above screening, Emerson Electric Thermo-Lag

T-500 was selected as the basic material for the ablation system of the X-15A-2. Stagnation regions are coated with pre-molded T-500-6a. Non-stagnation regions are coated with spray application of T-500-4a.

PLASMA TUNNEL TESTS

TEST FACILITY SELECTION

Selection of a suitable plasma arc facility was based on a comparison of operating envelopes to determine which available facility afforded the broadest range of test conditions covering the flight mission. Figure 6 shows a plot of flight velocity versus altitude for the 8,000 ft/sec design mission and the operating envelopes of several available test facilities, including the NAA/LAD one megawatt, 2-1/2-inch nozzle plasma tunnel. The NAA/LAD plasma facility covers the broadest range of the flight mission and was selected, accordingly, as the test facility. Four test conditions were initially selected within the operation envelope, as indicated in Figure 6, to simulate four velocity-altitude points on the mission profile curve. The plasma facility was then calibrated in order to determine equipment settings for these four points. It was possible to get almost exact duplication of the flight parameters, enthalpy, pressure and heat flus, at the leading edge stagnation line. Plasma tunnel test conditions are listed in Table I. Included are an "off-design" point (Test Condition 5) and the variable tunnel condition, which is described below (see also reference 1.).

TEST SPECIMENS AND TESTING TECHNIQUES

The criterion for designs of the plasma tunnel test specimens was that actual aircraft structure should be duplicated as nearly as practical. Fortunately, the aircraft leading edge diameters (3/4-inch for the wing and 1-inch for the horizontal and vertical tails) fall within the capability of the NAA/LAD plasma tunnel. A diameter of 3/4-inch was selected for the leading edge test specimen. The model, illustrated in Figure 7, was made of steel to simulate thermally the metal heat sink effect of the actual structure. Ablation material was molded and bonded directly to the leading edge model. The full-scale model was mounted in the tunnel with the leading edge inclined 37 degrees to the air flow to duplicate the aircraft wing sweep. Temperature of the steel was measured with a chromel-alumel thermocouple and recorded with time. With this model it was possible to obtain the high degree of flight simulation shown in Figures 8 and 9. Shear stress was slightly low because for a given tunnel condition, the tunnel velocity is slightly lower than the corresponding flight velocity. One of the initially selected test conditions, corresponding to the lowest velocity of Figure 6, was abandoned after preliminary testing showed that adequate coverage could be obtained with the heat flux enthalpy range of the other test conditions.

TABLE I

SUMMARY OF PLASMA TUNNEL TEST CONDITIONS

Test Condition	Stagnation Enthalpy (btu/lb)	Pitot Pressure (Atm)	Percent Oxygen	Tunnel Mach	Tunnel Velocity ft/sec	Simulated Flight Vel. ft/sec [1]	Simulated Flight Alt. 1000 ft. [2]
1	1279	.716	21	3.72	6590	7700	102.8
2	979	.528	21	3.76	5948	6650	103.3
2A	979	.528	10	3.76	5948	6650	103.3
3	768	.386	21	3.80	5313	5800	104.1
3A	768	.386	10	3.80	5313	5800	104.1
4	541	.301	21	3.71	4448	4730	100.6
4A	541	.301	10	3.71	4448	4730	100.6
6	1576	.201	21	3.55	6990	8600	136.8
Variable	413-1088	.322-698	21	3.72-3.80	3903-6194	4000-7030	91-100.5

1 Based on Stagnation enthalpy

2 Based on Pitot pressure

Flat panel specimens (see Figure 10), simulating one dimensional heat flow, were 0.048-inch steel plates coated with various thicknesses of ablation material. Two 28-gage chromel-alumel thermocouples were affixed to the rear of the plate. Thermocouple number one was welded to the rear of a 1/2-inch diameter isolated from the rest of the plate by a groove 1/16-inch wide and .038-inches deep. The centerline of the circle was 5/8-inches away from the centerline of the plate. When tested at an inclination of 45-degress to the flow, this thermocouple location corresponded to the maximum heat flux on the surface of the plate. Thermocouple number two was installed at the centerline of the plate and served principally as back-up instrumentation. Other type models, i.e., cones and cylinders, were initially selected, but failed to produce meaningful results. Cold wall heat flux simulation, obtained with the flat panel models, is shown in Figure 11. While the flat panel values are somewhat higher than those generally anticipated on the fuselage, they are indicative of flight conditions at special fuselage areas having protuberances. It is felt that reasonably accurate values of performance at lower heat fluxes can be predicted by extrapolating values obtained at higher heat fluxes. The designation 2A, 3A, 4A, indicated that the tunnel was run with a reduced partial pressure of oxygen to compensate for the higher static pressure on the models than on the surfaces of the airplane.

In addition to the steady-state conditions above, the plasma tunnel was slightly modified to obtain conditions that varied with time (see reference 1). It was possible, by using mechanical cams to regulate air flow and manual control of power input in accordance with a pre-recorded plot, to simulate the design mission speed and altitude histories from 80 to 400 seconds after launch. Figure 12 shows the simulation attained. Figure 13 shows a comparison of cold wall heat flux between the wing leading edge during the design mission and a leading edge model in the plasma tunnel tested for the conditions shown in Figure 12. While the peak heat flux value was not attained, this type of test simulated the transient effects of heat flux, enthalpy, pressure and other significant parameters on ablation performance. No unexpected or deliterious effects were noted.

Steady state tests for both leading edge and flat plate models were terminated when the substrate temperature reached 700°F. The temperature history of all thermocouples was recorded along with surface temperature measurements obtained with an optical pyrometer.

ANALYSIS OF TEST RESULTS

Ablation performance was expressed in terms of "effective heat of ablation" by dividing cold wall (80°F) heat flux by average mass loss rate. For both leading edge and flat panel tests, the average mass loss rate was obtained by dividing the total mass loss by the time required for the total mass loss. The time period for total mass loss was a value established by a correlation between substrate temperature-time histories and observations of colored movies of the tests. The time at which the bare metal substrate showed in the movies usually corresponded with an abrupt change in the slope of the temperature plot.

Leading Edge Tests

Steady State Tests

Pertinent conditions at the stagnation line of the 37 degree swept leading edge models are listed in Table II. The shear stress is based on Reynold's analogy and the tunnel velocity (u_∞). The Prandtl No. was taken as .705; the wall enthalpy (h_w) was 129 btu/lb. Figures 14, 15, and 16 show the effect of the initial thickness of the molded glass cloth reinforced T-500-6a, on the substrate temperature-time history. Figure 17 shows the effect of test condition on the substrate temperature-time history for a constant initial thickness of about .5-inches. Figure 18, 19, and 20, show the relative performance of different ablator materials at the different test conditions. The "shingled" T-500-6a is seen to be slightly superior to the regular T-500-6a. The ablation material is identical, but the glass cloth laminated within the material was oriented 15 degrees away from a line along the model leading edge, producing an effect similar to shingles on a roof. The phenolic refrasil leading edges exhibited very little change in contour during the tests. The substrate temperature history has a characteristic "non-receding ablator" shape. A substrate temperature of 500°F was considered to be an upper limit for a bondline adhesive and the effective heat of ablation of the phenolic refrasil is based on the time required to reach 500°F. It is seen that although the phenolic refrasil does not recede a significant amount, it is slightly inferior to the T-500-6a when compared on the basis described above.

Table III summarizes the cold wall effective heats of ablation of the leading edge models. Run number 9 data are based on movies since the thermocouple failed on this model. Since such close approximations to flight conditions were achieved in the leading edge plasma tests, it is justifiable to analyze the data with the effective heat of ablation approach. Attempts were made to isolate the effect of shear stress by treating the tunnel data with a multiple regression analysis. Due to the relatively small sampling of data available, the effects of shear could not be delineated. Accordingly, the test results are shown as a function of cold wall heat flux.

Figure 21 illustrates the validity of the assumption of a linear recession rate when applied to the Thermo-Lag molded T-500-6a test results.

From careful studies of the movies taken during the tests, it was possible to sketch the surface of the ablator, as viewed from the side, at various times during the test. From these lines, called isochrones, the surface recession can be shown as a function of time. Figure 22 shows this surface recession for a selected test. The region shown is the portion of the model which had the most rapid ablation. During the initial portion of the test, the char layer is building up, hence the surface recession is small. Near the end of the test, the char itself is being eroded away, causing a more rapid surface recession.

TABLE II

LEADING EDGE TEST CONDITIONS

Test Condition	Heat Flux [1] $\frac{btu}{ft^2\ sec}$	Shear Stress [2] lbs/ft^2	Stag. Line Static Press. lbs/ft^2	Stag. Line Oxygen Press. lbs/ft^2
1	109	9.24	968	230
2	67	6.91	714	148
3	42	5.17	522	110
4	23	3.66	407	85.5
6	71.4	5.1	272	57.1

1 Calculated using tunnel conditions of Table I and a radius of 1/2 inch, 37° sweep, wall temperature 80° F.

2 Based on $\lambda = \frac{P_r^{2/3}}{g} u_\infty \sin\Omega \frac{\dot{q}_{cw}}{h_s - h_w}$

TABLE III

SUMMARY OF LEADING EDGE TESTS

EFFECTIVE HEATS OF ABLATION

Run. No.	Test Cond.	Init. Thick. In.	Material	Mat'l Density lbs/ft3	Heat Flux btu/ft2sec	Run Time Sec.	h_{eff} btu/lb	
47	1	.26	T-500-6a	90	109	81	4540	4560 (Avg.)
8	1	.35	"	"	"	126	5240	
24	1	.35	"	"	"	125	5190	
13	1	.50	"	"	"	140	4075	
9	1	.50	"	"	"	140[4]	4075	
46	1	.785	"	"	"	124	2300 [1]	
48	2	.263	"	"	67	235	8000	5620 (Avg.)
16	2	.35	"	"	"	201	5140	
17	2	.50	"	"	"	260	4650	
49	3	.263	"	"	42	301	6410	6160 (Avg.)
31	3	.35	"	"	"	358	5730	
50	3	.506	"	"	"	577	6380	
70	6	.516	"	"	71.4	570	10500	
92	1	.50	T-500-6a[2]	"	109	200	5810	
102	1	.50	Phen. Ref.	110	109	142[3]	3380	
93	2	.50	T-500-6a[2]	90	67	320	5720	
103	2	.50	Phen. Ref.	110	67	220[3]	3210	
104	3	.50	"	110	42	240[3]	2200	

1 Not used in analysis
2 Lamina oriented 15° away from leading edge
3 Time to substrate temp. of 500°F.
4 Based on Movies

Figure 23 shows effective heat of ablation versus cold wall heat flux as determined from the plasma tests. Results obtained from T-500-6a for tunnel points along the design mission are shown. A linear variation of heat of ablation with heat flux, $h_{eff} = 7200-23.6\dot{q}_{cw}$, is chosen to represent the data for further calculations.

It is interesting to note that the slopes of effective heat of ablation versus cold wall heat flux are negative. This seems to contradict the generally accepted trend that ablation efficiency increases with increasing enthalpy and associated heat flux. The inverse proportionality is probably attributable to the high shear stresses occurring with increase in heat flux.

Variable Heat Flux Tests

In the previous section, a linear variation of effective heat of ablation with heat flux was chosen to represent the steady state data. To demonstrate the validity of the assumptions involved, three leading edge models were tested with the variable tunnel conditions shown in Figure 13. This type of test will illustrate any unusual transient ablation effects, if any, and generally check out the linear recession rate assumption. Models having three different initial thicknesses were tested. The time histories of the substrate temperatures are shown in Figure 24. In no case did the temperature go above 500°F. The thickest model was inadvertently removed from the plasma stream after about 30 seconds of testing. It was re-inserted in the stream and run for another 316.8 seconds. This accounts for the somewhat different temperature behavior. Figure 25, 26, and 27 show sketches of the three models made after the tests. Approximately .09 inches of char layer formed on the models. Measurements of virgin material loss were also made. Figure 28 shows a comparison between measured and calculated virgin material loss. The calculation was based on the linear effective heat of ablation shown in Figure 23. Reasonable agreement is noted, with the theory being slightly conservative. Further checks of the theory were made with flight tests, which will be discussed in a following section.

Flat Plate Tests

With the flat plate models shown in Figure 10, the tunnel conditions listed in Table I resulted in the local heating parameters listed in Table IV. The heat flux distribution over the plate and the location of the region of maximum heat flux was determined by tests with 1/4 inch of cork glued to the model. The maximum values of heating rate for the various test conditions were determined with a flat plate model designed as a copper calorimeter. Shear stress values were calculated in a manner similar to those for the leading edges. For the flat plate models, a recovery enthalpy equal to .85 times the total enthalpy was used.

Figures 29 through 33 show temperature-time histories of the metal substrate at thermocouple No. 1 (see Figure 10). Figures 34 through 38 show similar results for thermocouple No. 2.

Table V summarizes the flat plate data with Thermo-Lag T-400-4a ablation material sprayed on the models.

TABLE IV

FLAT PLATE TEST CONDITIONS

Test Cond.	Heat Flux T.C. #1 btu/ft^{2}sec	Shear Stress lbs/ft^2	Local Static Pressure lb/ft^2	Local Oxygen Pressure lb/ft^2	Heat Flux T.C. #2 btu/ft^{2}sec
2A	90.3	13.3	558	55.8	65
3A	63.7	11.3	408	40.8	45
4A	41.2	9.63	318	31.8	33.5

TABLE V

SUMMARY OF FLAT PLATE TESTS

EFFECTIVE HEATS OF ABLATION; T-500-4a

Thermocouple #1 Density=63 $\#/ft^3$

Run No.	Test Cond.	Init. Thick. In.	Heat Flux $btu/ft^2 sec$	Run Time Sec.	h_{eff} btu/lb.	Remarks
71	2A	.10	90.3	47	8080	
72	"	.10	"	45	7740	
85	"	.10	"	52	8950	
61	"	.07	"	26	6380	Model had voids
105	"	.07	"	37	9100	
62	"	.04	"	17	7310	
73	3A	.10	63.7	95	11530	
63	"	.07	"	65	11260	Model had voids
106	"	.07	"	69	11960	
74	"	.07	"	80	13870	
84	"	.07	"	84*	14560	
64	"	.04	"	39	11830	
75	4A	.10	41.2	230	18050	
65	"	.07	"	134	15020	Model had voids
107	"	.07	"	235	26350	
76	"	.04	"	87	17060	
66	"	.04	"	78	15300	
86	"	.04	"	58	11380	
87	3A	.10	63.7	63	7650	1/32 in. slot ⊥ flow
88	"	.10	"	53	6430	1/32 in. slot ∥ flow
89	"	.10	"	50	6075	1/4 in. dia. hole
90	"	.10	"	72	8750	1/4 in. dia. hole-putty filled
91	4A	.10	41.2	135	10590	1/32 in. slot ⊥ flow

* Based on Thermocouple #2 and movies.

Some of the models had known voids (air pockets) which resulted from an improper drying time between successive spray coats when the models were being made. Other tests were made to determine if there were any differences in the thermal behavior of the material due to a different solvent system. It was necessary to develop a low volatile solvent system to be compatible with desert conditions. No discernable effects are noted on thermal performance due to the solvent system. Other tests were made with slots 1/32 inch wide sawed into the ablation coating. The slots were aligned both parallel to and perpendicular to the flow. Two tests to simulate screw holes left through the ablation material were performed. In one test, the 1/4 inch diameter hole was left open; in the other, the hold was filled with a putty formed of the basic T-500 material. The test results showed that slots and holes reduced the efficiency of the ablator. These data are very conservative, however, since the ratio of boundary layer thickness to slot and hole depth was small. For the thick, turbulent boundary layers on the airplane, the effect of slots and holes is expected to be negligibly small.

Figure 39 shows effective heat of ablation versus cold wall heat flux for models without voids, slots or holes. The data are plotted to indicate the effect of initial ablation thickness, if any. There are too few data points to establish any firm trends. From the data shown, an initial thickness of .07 inches appears most efficient. Figure 40 presents averaged data for all runs without holes, slots, or voids. A linear variation of $h_{eff} = 23000 - 168\ q_{cw}$ is seen to fit the data reasonable well. Since these data are obtained under laminar flow conditions, some accounting must be made for the turbulent boundary layers which are anticipated on the airplane. However, due to the low enthalpies of the design mission, and the relatively low mass loss rates of ablation material during flight, the heat blockage due to "outgassing" of the subliming gasses is small, whether the flow is laminar or turbulent. At this stage of development, it is judicious to take a somewhat conservative approach, particularly in the absence of low heat flux, turbulent data. Figure 41 shows all data points obtained with slots, holes, and voids. The linear variation shown, $h_{eff} = 13,800 - 101\ q_{cw}$ is sixty percent of the heat of ablation shown in Figure 40. By using this lower heat of ablation, the calculated thickness requirements should be conservative, even with turbulent flow, and with slots, holes, and voids in the ablation coating. Some low heat flux data ($q \cong 13$ btu/ft^{2}sec) obtained by Emerson Electric on models with slots running parallel to and perpendicular to the flow, (see Reference 2) had cold wall effective heats of ablation ranging from 14,100 to 42,600 btu/lb. Hence, the variation shown in Figure 41 should be conservative at the lower heating conditions. Maximum use will be made of flight test data on the X-15 to align the low heating rate ablation performance.

A comparison between calculated and measured substrate temperatures was made for certain of the flat plate plasma tunnel tests. For these comparisons, an effective heat of ablation of $23,000-168\ q_{cw}$ was used along with an assumed ablation temperature of 630°F. The 630°F temperature was selected since the measured substrate temperatures appeared to "plateau" at about that value. Figures 42 through 44 show substrate temperature correlations for clean (without voids, slots, etc) models.

FORM 15-C-1 REV. 9-61

Twelve runs were also made with varying thicknesses of Armstrong Cork 2755 ablation material. The cork showed an average effective heat of ablation of about 2630 btu/lb. The results of the test are listed in Table VI. Temperature-time histories are not shown since, in general, the substrate temperature remained at approximately the initial temperature until the cork burned through, then rose very rapidly to 700°F, the temperature at which the test was terminated.

FLIGHT TESTS

At this writing, ablation material experiments have been performed on six (6) X-15-1 or X-15-3 flights. Table VII lists pertinent flight parameters and the types of experiments performed. Although the speed, heating rates and flight duration of the current X-15 are less than those anticipated for the X-15A-2 design mission, the tests served to evaluate the ablators under service conditions, and to correlate flight test performance with plasma tunnel and analytically predicted performances. Some conditions, not readily simulated in the laboratory, are the engine and flight induced vibration of the X-15 vehicle, the cyrogenic environment and the field conditions under which ablation protection systems are applied and refurbished. The following discussions will deal principally with thermal performance correlations.

Various regions of the airplane were used for testing as shown in Figure 45. Reasonably high heating rates can be obtained on Panel F-4, which is located near the nose of the airplane. This region is also free of shock waves from other portions of the airplane, and the heating rates may be calculated with confidence. The lower speed brakes, when opened, also attain relatively high heating rates, and provide a convenient test region. The ventral leading edge was used to test pre-molded Thermo-Lag T-500-6A specimens and a cork leading edge configuration. The under surface of the fuselage near the liquid oxygen tank provides a test region with cryogenic temperatures and severe temperature gradients.

TEST NUMBER 1

An 0.08-inch thick sheet of Armstrong Cork 2755 was bonded with epoxy to the lower right hand speed brake. Figure 46 shows a comparison between measured and calculated substrate temperatures. The thermocouple was located 28.5-inches aft of the speed brake hinge line. An effective heat of ablation of 2500 was used in the calculation.

Post-flight inspection revealed that the epoxy adhesive with a very small amount of cork imbedded in it, remained on some regions of the speed brake. This, and the fact that subsequent plasma tunnel tests indicated a slightly higher effective heat of ablation, tends to account for the over-prediction of the calculated temperature.

TABLE VI

SUMMARY OF FLAT PLATE TESTS

EFFECTIVE HEATS OF ABLATION; CORK 2755

Density - 30.5 lbs/ft^3

Run No.	Test Cond.	Init. Thick In.	Heat Flux btu/ft^{2}sec	Run Time Sec.	h_{eff} btu/lb.
52	2A	.25	90.3	14	1980
53	"	.125	"	7.4	2100
54	"	.08	"	-	- *
55	3A	.25	63.7	28.2	2800
56	"	.125	"	12.2	2450
57	"	.08	"	9.6	3000
58	4A	.25	41.2	49.2	3170
59	"	.125	"	18.4	2380
60	"	.08	"	9.6	1950

* Bad Run

TABLE VII

SUMMARY OF ABLATION MATERIAL FLIGHT TESTS

Test No.	Flight No.	Flight Date	Maximum Velocity ft/sec	Altitude At Max Vel 1000 ft	Material Tested	Principle Test Region
1	1-37-59	7-9-63	5360	142	Cork 2755	R.H. Lower Speed Brake
2	1-38-61	7-18-63	5630	98.1	Cork 2755 DC/325	Ventral Leading Edge Upper & Lower Speed Brakes
3	1-39-63	10-7-63	4070	78.4	Thermo-Lag T-500-6A & T-500-4	Entire Lower Ventral, including Leading Edge. Panel F-4
4	1-40-64	10-29-63	3950	72.4	T-500-4A	R.H. Lower Speed Brake
5	1-42-66	12-5-63	5888	100.3	T-500-4A	Cryogenic Area Panel F-4
6	3-25-42	1-16-64	4750	69	T-500-4A	Ventral Leading Edge Panel F-4

FORM 15-C-1 REV. 9-61

TEST NUMBER 2

Two layers of 1/8-inch thick sheets of cork were wrapped around the ventral leading edge to form a 1/4-inch thick glove, which extended aft of the leading edge about 6-inches. Sheets of cork, 1/8-inch thick, were also bonded to the forward portions of the left and right hand lower speed brakes. A sheet of Dow-Corning DC/325 ablator, .07-inches thick, was prepared in the laboratory and bonded to the upper right-hand speed brake. The thermocouples which were located beneath the cork and DC/325 on the speed brakes, were inoperative for the flight thus preventing a valid comparison between the two. The DC/325 was ablated completely away and a small amount of cork remained near the forward portion of the speed brake.

When the speed brakes are opened, flow separation occurs over approximately the front half of the speed brake, and some portion of the ventral ahead of the speed brake hinge line. The flow reattachment region on the speed brake was evident from post-flight inspection of the cork sheet on the right hand speed brake. An attempt to calculate the heating in the separated region was not made. A thermocouple, aft of the separated region, and the cork sheet was operative. A comparison of calculated and measured bare skin temperatures, shown in Figure 47, indicates reasonable agreement for this area of the speed brake.

The cork covering the leading edge was completely burned away at the stagnation line and approximately around to the shoulder (90° from the stagnation line). The extent of erosion was progressively greater further away from the fuselage, i.e., lower on the stagnation line. This is probably attributable to the enthalpy gradient which exists ahead of the ventral caused by shock waves from other portions of the airplane. Aft of the shoulder, the cork was charred, but not significantly eroded away. It is possible that this portion of the cork was in a laminar flow region. Figure 48 shows a comparison between measured and calculated leading edge temperatures. The time at which the cork was completely eroded away at the leading edge appears to be accurately predicted, although the calculated peak temperature is too high. A reduced heat of ablation is used to account for the aerodynamic shear stress.

TEST NUMBER 3

Representatives from Emerson Electric Company, makers of Thermo-Lag, applied their ablation material to the lower ventral for this test. The leading edge coating was made up of two segments of pre-molded T500-6A. Thickness at the stagnation line was .5-inch. The two segments were butted together, with the joint running perpendicular to the leading edge. Adhesive used was HT-424. The remainder of the lower ventral was sprayed with T-500-4 to a thickness of about 0.09-inches. The need for a less volatile solvent system became apparent during the spray application. The desirability of a protective coat of lacquer to keep moisture off the ablation material was also indicated on this test.

Six flight tests have been accomplished at this writing, and needless to say, the techniques of material application, pre-flight and post-flight measurements have improved with each flight. A material thickness measuring technique, developed for test No. 6, has revealed that flat plate (i.e., speed brake and panel F-4) thickness measurements for tests No. 3, 4, and 5 are questionable. Based on measurements made for Test No. 6, all previous char thickness measurements, which were thought to represent virgin material loss, are larger than the actual virgin material loss by as much as .01 inches. A factor which also contributes to measurement uncertainty is the fact that due to the high efficiency of the Thermo-Lag and low total heat loads of flight, the amount ablated is small to begin with; also, measurements are difficult to make in the field. Consequently, for Tests Nos. 3, 4, and 5, two "measured" thicknesses will be shown; the actual char thickness measurement and a lower "corrected" value. Ordinarily, such questionable measurements would not be reported, but are included in the event that subsequent tests will indicate a more appropriate "correction factor". The improved measuring techniques are discussed in detail in the section, Test No. 6.

Figure 49 shows the calculated cold wall (80°F) heat flux to the ventral leading edge for Test No. 3. Also shown is the calculated virgin material loss (ΔS) for the flight. The measured virgin material loss shown (not a char thickness measurement) is reasonably accurate. The bars indicate the range of measurements obtained along the leading edge. Good agreement is noted between the measured and the calculated material loss. Figure 50 shows material loss, heat flux, and substrate temperature for the speed brake area. The measured material loss (ΔS) is actually a measurement of the char layer thickness and may be too high by as much as .01 inches. A lower value of (ΔS) is shown for reference. The method used to calculate thicknesses for the design mission is seen to agree with the char layer thickness measurement and over-predict the "corrected" measurement. Excellent substrate temperature agreement is noted. An ablation temperature of 630°F is used for temperature calculations.

TEST NUMBER 4

For this flight, the right hand lower speed brake was coated with approximately 0.09-inches of T-500-4A. The 4A means that a new solvent system, compatible with desert environment, was used. Thermal performance of the material was determined to be unaffected by the solvent system in the plasma tunnel tests. The ventral leading edge coating, which was flown on the previous flight, was left on. Since its shape had changed slightly, no material loss measurements were made on the leading edge. It performed satisfactorily, however, which indicates that the ablation material could possibly be used for more than one flight.

Material loss, heat flux and substrate temperatures for the speed brake area are shown in Figure 51. The calculation methods are the same as for Test No. 3. As for the previous test, both the measured char thickness and a "corrected" value for virgin material loss are shown. The design calculation method over-predicts the "corrected value". Again, good temperature correlation is noted.

TEST NUMBER 5

The principle purpose of this flight test was to check the structural compatibility of Thermo-Lag with cryogenic temperatures under actual field conditions. The lower fuselage was coated with approximately .035-inches of T-500-4A from Fuselage Station 196 to Fuselage Station 244. The coating also extended 3-inches onto the lower portion of both the right and left hand side fairings (see Figure 45). A total of 22 ft.^{2} were coated. Approximately 14-inches of the aft portion of the coating extended over the LOX tank, where -300°F temperatures occur. On the forward portion of the coating, two hydraulic vent line pipes, 1-inch in diameter, protruded about 3-inches into the air stream.

Prior to flight, a portion of the coating ahead of the LOX tank, near the left hand side fairing, developed cracks after the airplane was fueled. After a captive flight, some ablation material was noted to be lost and a total area of about 1/2-sq. ft. had poor adhesion to the skin. To prevent any possibility of temperature gradients causing skin buckling in this region, a large portion of the coated area was removed, leaving the LOX tank area and a small area around each protuberance (hydraulic vent pipe) intact. The exact cause of the lack of adhesion has not been determined, since it has not been possible to reproduce the exact type of failure in the laboratory. The difference in contraction between the Thermo-Lag and Inconel-X and the presence of water and ice on the coating, are felt to be contributing factors. However, a similar region on the right hand side of the airplane was unaffected.

The heating around the protuberances proved to be a very interesting phenomena. As mentioned before, a small patch of ablation material was left around the hydraulic vent line pipes. Due to the unfavorable conditions under which the ablation material had to be removed (i.e. in the field, at night, with the LOX tanks full and cold outside temperatures) the patch around the pipes was somewhat poorly shaped. Also, careful thickness measurements could not be made. Hence, the test results are qualitative. Figure 52 clearly illustrates, however, the heating pattern around the protuberance. The region immediately upstream of the pipe had high heating; immediately downstream was a wake, with low heating. The extent of the separated region upstream of the pipe appears to be about 1-1/2 diameters. This and the char thickness measurements made after the flight in the vicinity of the protuberance, are in general agreement with the protuberance heat transfer theory discussed in Appendix B. The photograph from which Figure 52 was made, was obtained through the courtesy of NASA at Edwards Air Force Base.

The old char layer, which had formed from Tests No. 3 and 4, was carefully sanded away on Panel F-4, leaving about .075 inches of virgin material to be tested. Figure 53, shows heat flux and virgin material loss for the panel F-4. No temperatures were measured. The design method calculation is seen to be somewhat conservative compared with both the measured char thickness and the "corrected" virgin material loss measurements.

TEST NUMBER 6

The purposes of this test were to obtain flat surface and leading edge ablation material loss data, and to obtain quantative data on heat transfer near the hydraulic vent line protuberances. The 8 x 8 -inch pre-fabricated panels of T-500-4A, which were cemented to the skin around the hydraulic vent lines to obtain protuberance data, blew off during the flight. Panel F-4 was coated with about .086-inches of T-500-4A and the ventral leading edge was fitted with a pre-molded coating of T-500-6A, which was .256 thick at the stagnation line. It was possible to remove the ventral coating after the flight without damaging it, thus very good post-flight measurements were obtained. Figure 54 shows the post-flight measurements. It is interesting to note that the virgin material loss decreases rather uniformly (except at the joint) as the bottom of the fuselage is approached. This was also observed on Test No. 2 with the cork leading edge. The change in heating rate at the stagnation line, which causes this, is probably attributal to the entropy gradient ahead of the ventral. The shock system of the airplane is known to alter the local flow characteristics. The calculated material loss is seen to agree with the measured values near the lower portion of the ventral. The lower portion of the ventral would be least affected by the shock system. The very bottom of the ventral leading edge has a slightly larger material loss due to the three dimensional flow effect at the end of the ventral. An additional ablation loss of about .01 inches occurs in the vicinity of the butt joint between the two leading edge segments of ablation material (T-500-6A). Figure 55 shows the calculated time histories of the ventral leading edge material loss and heat flux..

The instrument used to measure flat surface ablation material thickness is a conical-tipped penetrometer with a dial gage that reads in thousandths of an inch. On previous flights, a small area of the char layer was scraped away with a sharp instrument. The point of the penetrometer was then pushed onto the exposed virgin material, thus obtaining a measurement of the char thickness. The char thickness was assumed to represent the amount of virgin material ablated away. Measurements made after flight Test No. 6 indicated that the char thickness is a reasonable representation of the virgin material loss, however, the point of the penetrometer apparently penetrates the exposed virgin material, when measured as described above, giving a depth reading which is too large by as much as .01 inches. A preferred technique of measuring is to provide small diameter measuring holes which penetrate the ablation material to the vehicle skin. The initial virgin material thickness is then measured with the penetrometer. After the flight, the

the total coating thickness, including char, is similarily measured. The char layer is now carefully scraped away upstream and downstream of the measuring holes for a distance sufficient to allow the base of the penetrometer to rest flat against the exposed virgin material (approximately 3-inches). The thickness of the remaining virgin material may then be measured. Measurements on panel F-4, made with the preferred way described above, are shown in Figure 56. Char thicknesses for the two upstream points shown on this figure when measured with the old technique, were .031 and .023 inches. These values are seen to be significantly larger than the char thickness determined using the preferred technique. Figure 57 shows the calculated heat flux and material loss time histories for the flight. An average of the char thicknesses on the panel, as measured with the old technique, is shown for reference purposes.

HEAT SHIELD DESIGN

The heat shield selected for the X-15A-2 is comprised of Emerson Electric's Thermo-Lag ablation material. Leading edges are made of pre-molded segments of T-500-6A (density of 90 lbs/ft) which are attached with an adhesive to the airplane leading edges. The rest of the airplane is sprayed with T-500-4A (density of 63 lbs/ft) and heat cured. The entire coating is then sprayed with a protective coating of lacquer. A complete description of application procedures, detailed thicknesses, and removal procedures, are contained in reference 3. The following sections will discuss typical aerodynamic heating conditions over the airplane, typical thickness requirements as determined by both Emerson Electric and NAA, and a breakdown of the ablation system weight by areas of the vehicle.

AERODYNAMIC HEATING

Figure 58 shows a sketch of the airplane indicating the approximate locations of 16 points on the vehicle. Heating rates at these locations are representative of the spread in heating and other local flow properties such as pressure and shear stress. Figures 59 through 62 describe the local vehicle geometry. Figures 63 through 78 represent design mission time histories of heat flux, shear stress, and local static pressure. Figure 79 shows the fuselage heating distribution at the time of peak heating. All stagnation line heat fluxes are based on the substrate geometry, i.e., the leading edge radii have not been increased to account for the ablation coating. With the ablation coating installed, all leading edge radii are increased by 1/8-inch.

Complete definition of the heating on the vehicle required calculations at 159 vehicle locations plus local hot spots.

THICKNESS REQUIREMENTS

Emerson Electric engineers were requested to calculate Thermo-Lag thickness requirements for the sixteen points shown above. Their results are presented in references 2 and 4. A comparison between the Emerson Electric and NAA calculations is shown in Table VIII. Reasonably close agreement is noted between the two calculations. Emerson thicknesses in the low heat flux region are greater than NAA calculations. The NAA calculations in the low heat flux regions are more closely correlated with flight test data. More than 159 points were computed by NAA to determine the complete airplane thickness distribution, and to calculate the weight of the ablation system. Included in these calculations were analyses to account for the bow shock effect on the wing leading edge (see Appendix A) and local protection required near protuberances (see Appendix B).

ABLATION SYSTEM WEIGHT

Based on drawings and actual measures of the X-15A-2 vehicle, an analysis was formulated to calculate installed ablation system weight, given the thickness distribution, and the material density. The airplane was divided in several regions, such as wing, side fairings, fuselage, etc., to allow separate calculations for these areas. Table IX lists areas of the airplane and the corresponding weight. Thicknesses used for these values include design margins. The total heat shield weight of 303.4 lbs. is below the initial target value of 400 lbs.

TABLE VIII

TYPICAL HEAT SHIELD THICKNESSES

Point No.	Location On Airplane	Max. Heat Flux btu/ft^{2}sec	Virgin Mat'l Loss, Ref 2 Inches	Virgin Mat'l Loss, NAA Inches	Design Thickness Inches
1	Fus. Sta. 9.28, lower	53	.156	.188	.190
3	Fus. Sta. 75, lower	27	.089	.092	.100
5	Fus. Sta. 200, lower	6.5	.048	.031	.037
7	Wing Leading Edge	157*	.446	.560	.700**

* Based on 3/8 inch radius

** Includes .09 in. for bow shock effects

TABLE IX

HEAT SHIELD WEIGHT

REGION	TOTAL SURFACE AREA - FT^2	WEIGHT LBS.
Fuselage	433.24	84.30
Side Fairings	313.71	45.10
Wings	206.30	47.06
Horizontal Stabilizers	101.33	42.69
Upper Vertical	85.12	23.33
Lower Vertical (including movable)	75.40	31.03
Canopy	24.60	6.03
Helium Bottle and Shield	11.16	1.52
Nortronics Nose Section	2.99	2.03
Wing Leading Edges	-	9.00
Horizontal Leading Edges	-	5.70
Lower Vertical Leading Edge	-	2.70
Upper Vertical Leading Edge	-	2.50
Canopy Leading Edge	-	.40
TOTAL	1,253.85	303.4

REFERENCES

1. NA63-1159, "A Technique for Simulating a Trajectory by Continuously Varying Flow Conditions in the NAA Hyperthermal Electric Arc Facility" dated 5 November 1963.

2. Emerson Electric Report No. 1637, "Advanced X-15 Program - Preliminary Establishment of Heat Shield Requirements for Aft Body Locations" dated 30 November 1963.

3. NA64-78, "Application of Thermo-Lag T-500 Ablation Materials to the Advanced X-15A-2", dated 7 February 1964.

4. Emerson Electric Report No. 1622, "Advanced X-15 Program - Preliminary Establishment of Heat Shield Requirements For the Wing, Canopy and Empennage Stagnation Regions", dated 17 October 1963.

Figure 1.

ADVANCED X-15 RESEARCH AIRPLANE

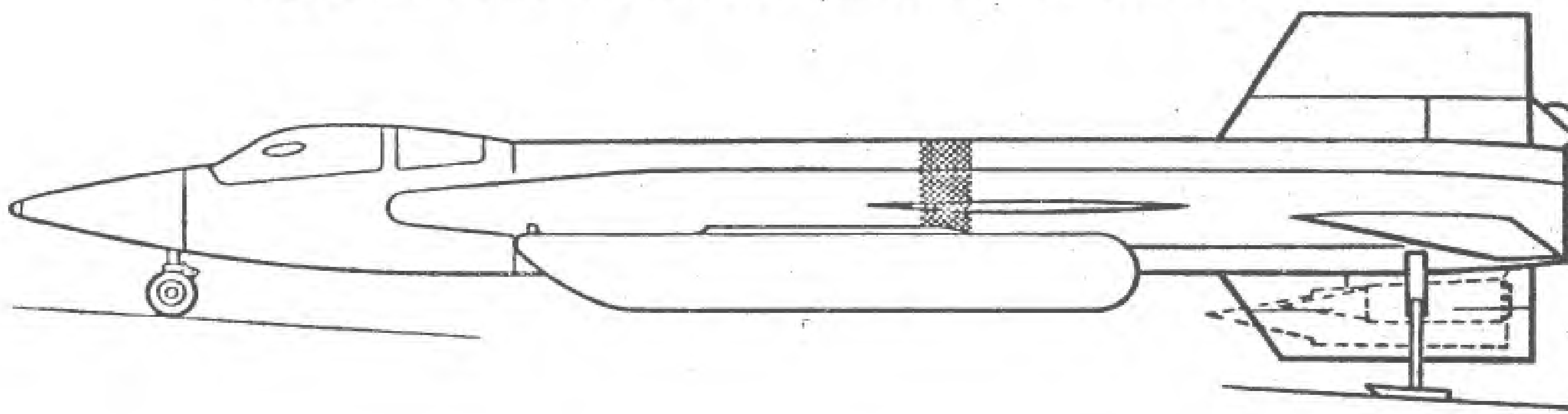

- MAIN LDG GEAR LENGTHENED TO ACCOMMODATE MOUNTING OF EXTERNAL RAMJETS
- IMPROVED NOSE GEAR CONFIGURATION
- FUSELAGE EXTENDED 29 IN. FOR INTERNAL VOLUME
- LH_2 TANKS AND PLUMBING PROVIDED
- INCORPORATES TWO EXTERNAL TANKS (LOX & NH_3) 13,500 LB PROPELLANT-3000 FPS AT 100,000 FT
- IMPROVED WINDSHIELD DESIGN
- USES ABLATION MATERIAL TO SUPPRESS HEAT TO BASIC STRUCTURE

Figure 2.

REMOVABLE WING TIP PANEL

- MATERIALS INVESTIGATION
  - RENE 41
  - COLUMBIUM
  - MOLYBDENUM
- EXPERIMENTAL DESIGN CONFIGURATION
  - RIBS
  - SPARS
- SURFACE DISCONTINUITY STUDIES
- INSTRUMENTATION DEVELOPMENT
- GAS EJECTION & TRANSPIRATION COOLING RESEARCH

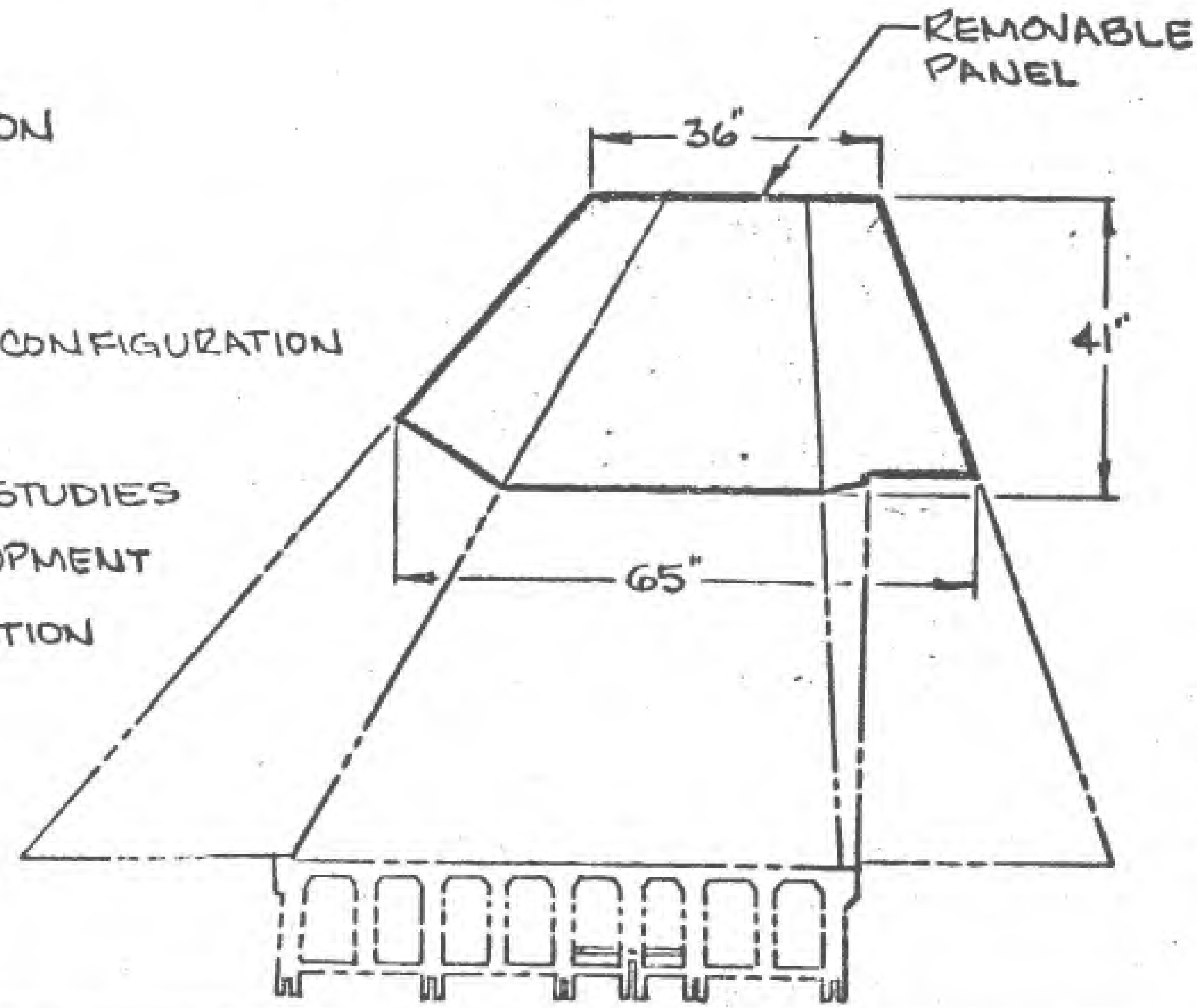

FORM 10811

PREPARED BY: A.F.T.	NORTH AMERICAN AVIATION, INC.	PAGE NO. 29 OF
CHECKED BY:		REPORT NO. NA64-177
DATE: 1-22-64		MODEL NO. X-15A-2

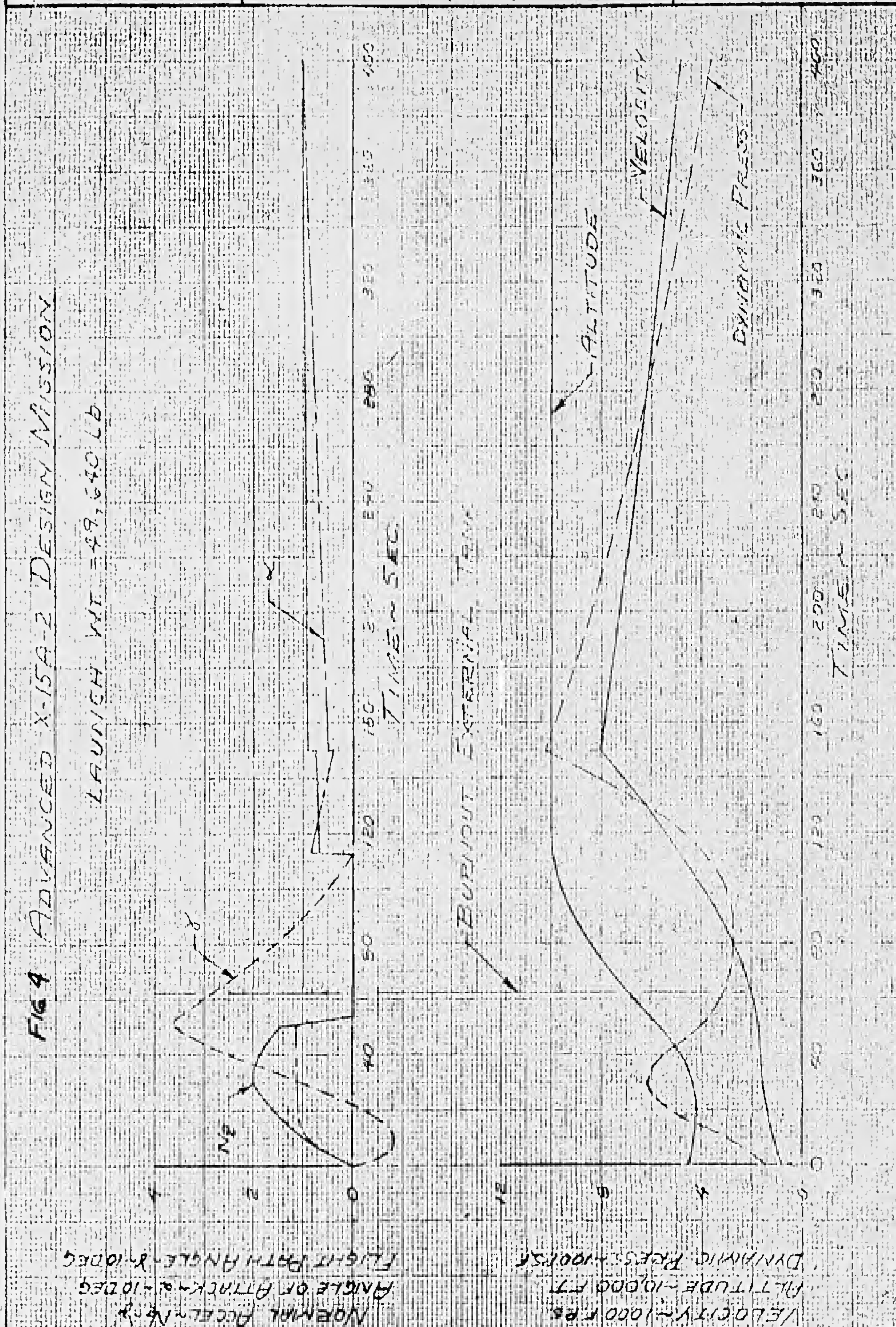

Figure 3.

PERFORMANCE CHARACTERISTICS
X-15A-2

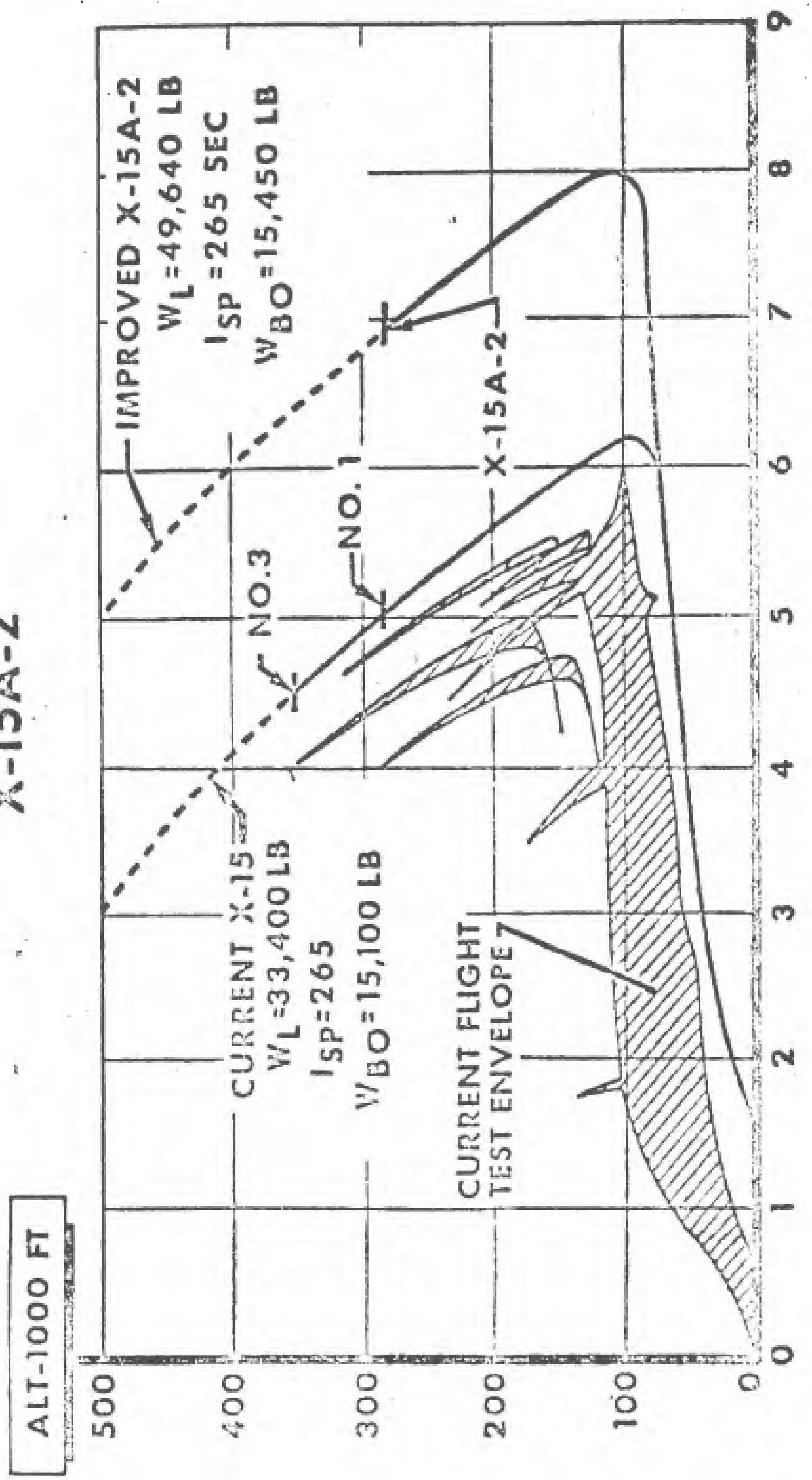

North American Aviation, Inc.
International Airport
Los Angeles 9, California

NA-64-177

Figure 5.

SUMMARY OF MAXIMUM TEMPERATURES UNPROTECTED INCONEL - X

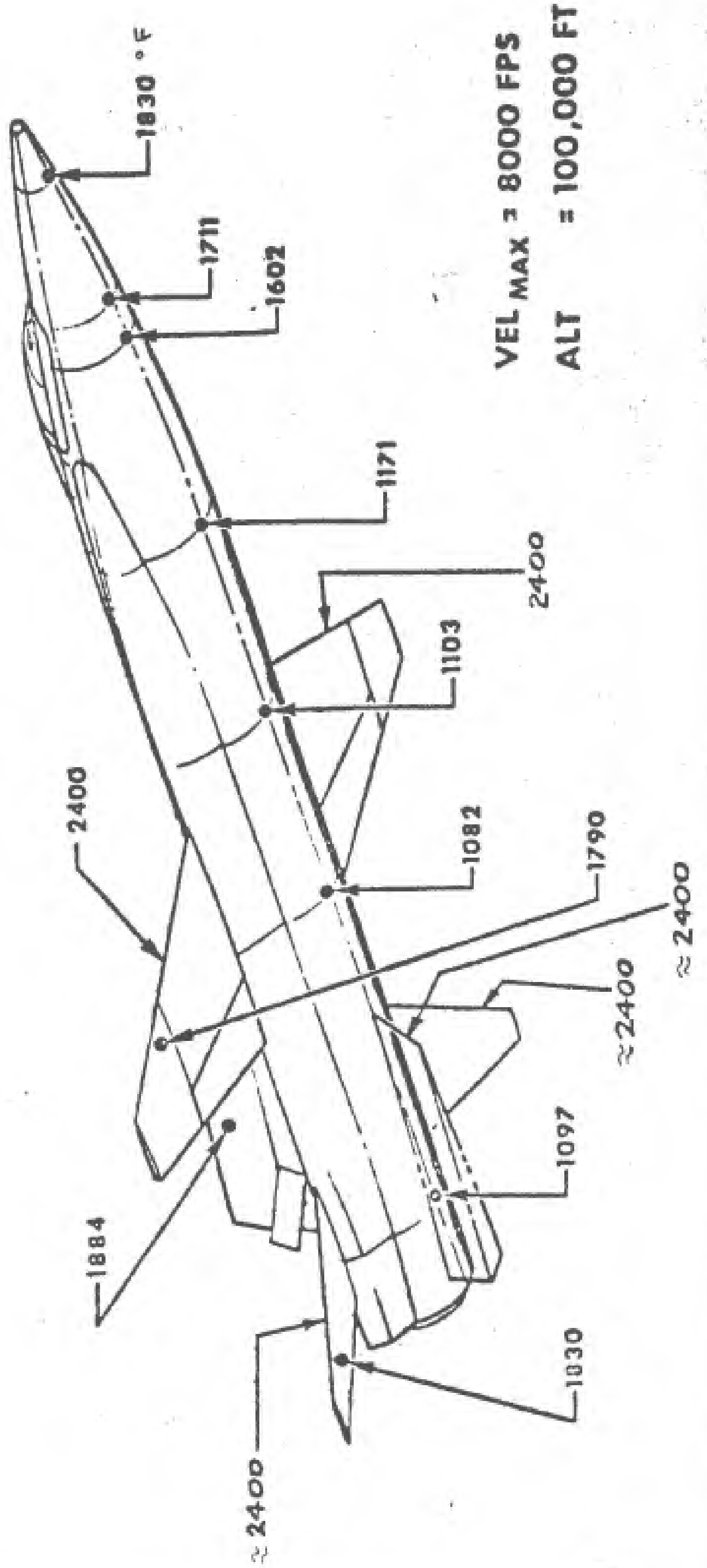

Figure 6.

PLASMA TUNNEL SELECTION
STAGNATION POINT DUPLICATION

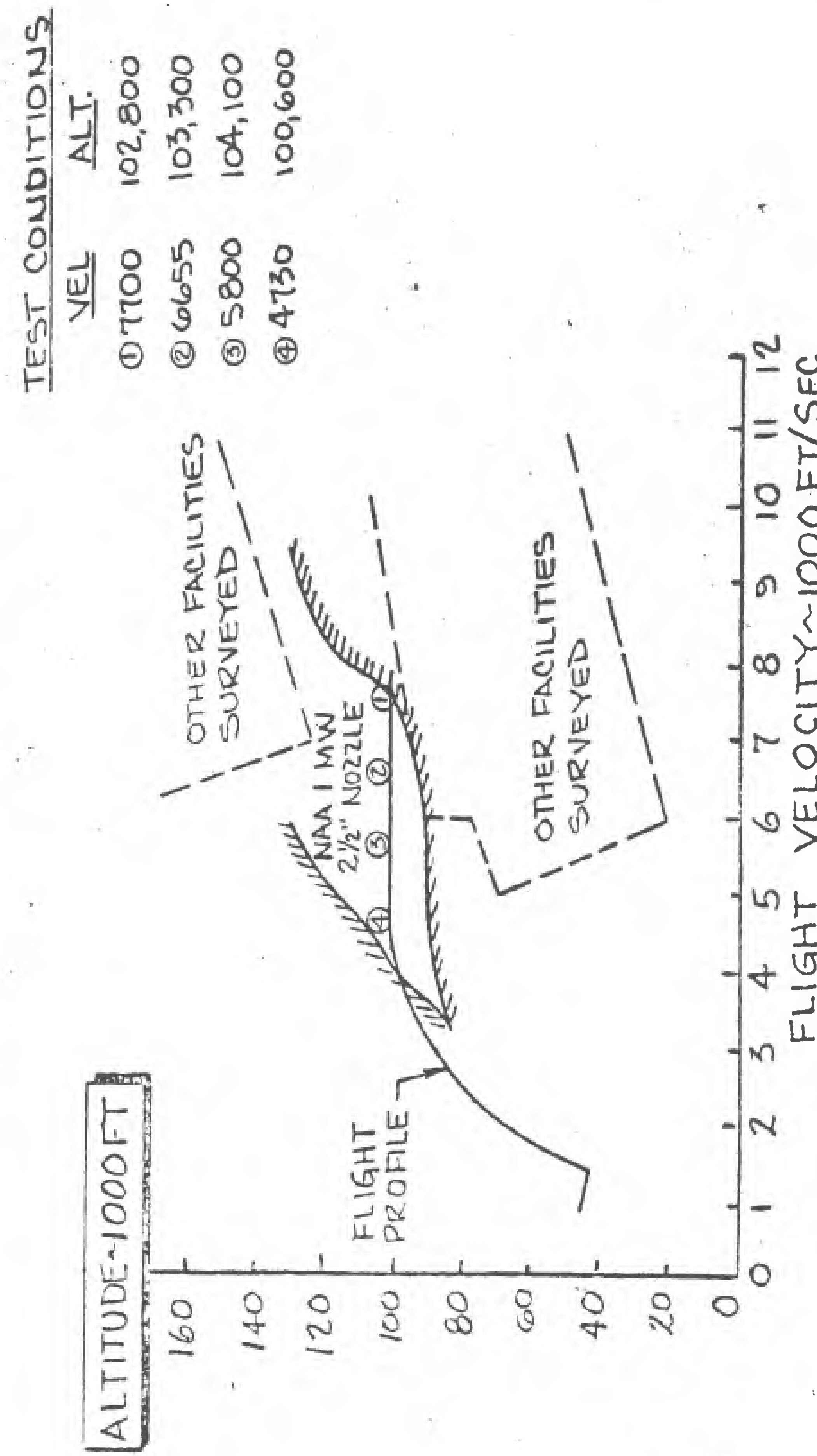

Figure 7.

CUTAWAY VIEW OF PLASMA TUNNEL TEST MODEL

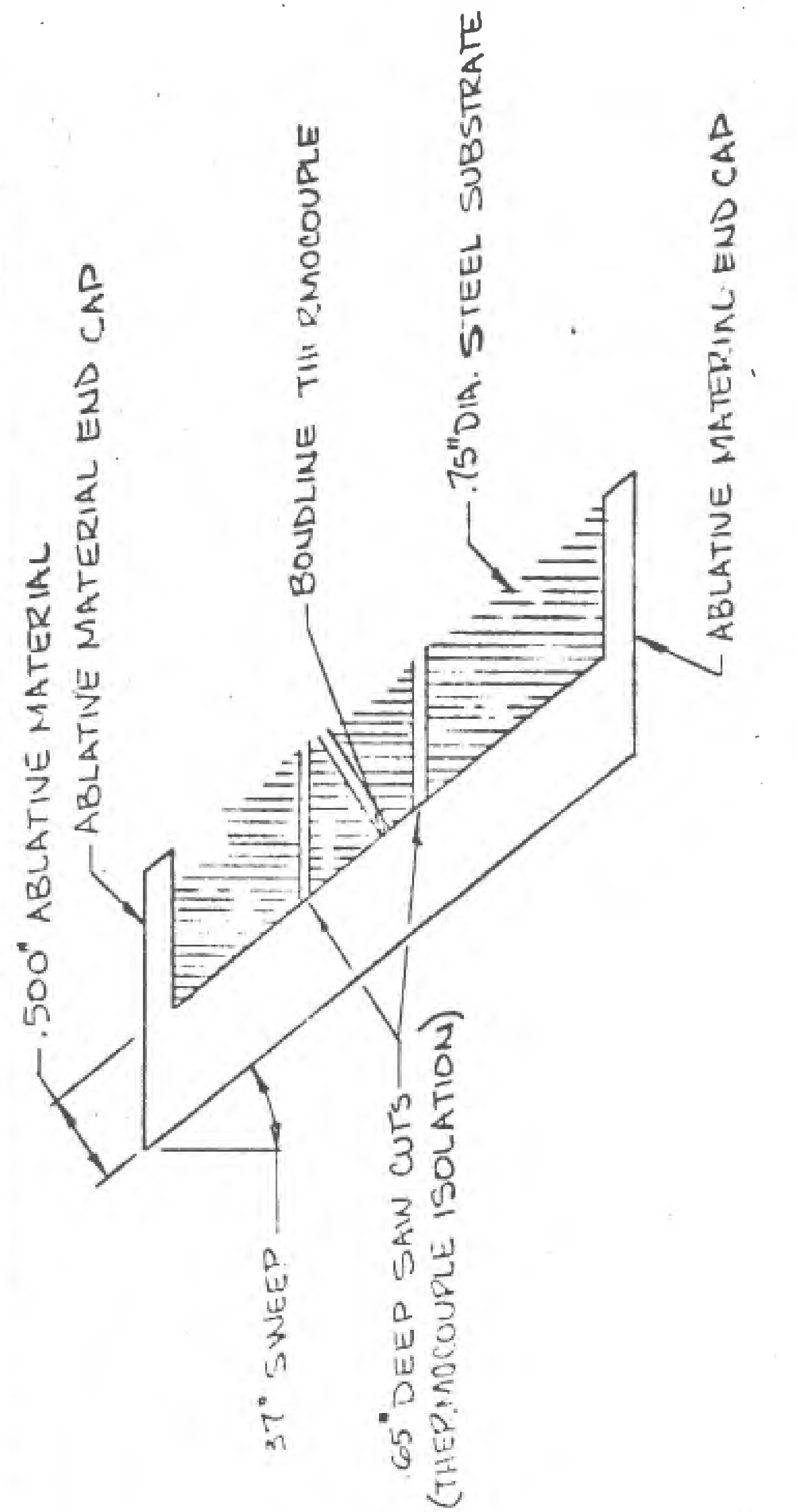

STAGNATION LINE PLASMA TUNNEL MODEL

FORM 1021-5

PREPARED BY:	NORTH AMERICAN AVIATION, INC.	PAGE NO. 33 OF
CHECKED BY:		REPORT NO. NA-64-177
DATE:		MODEL NO.

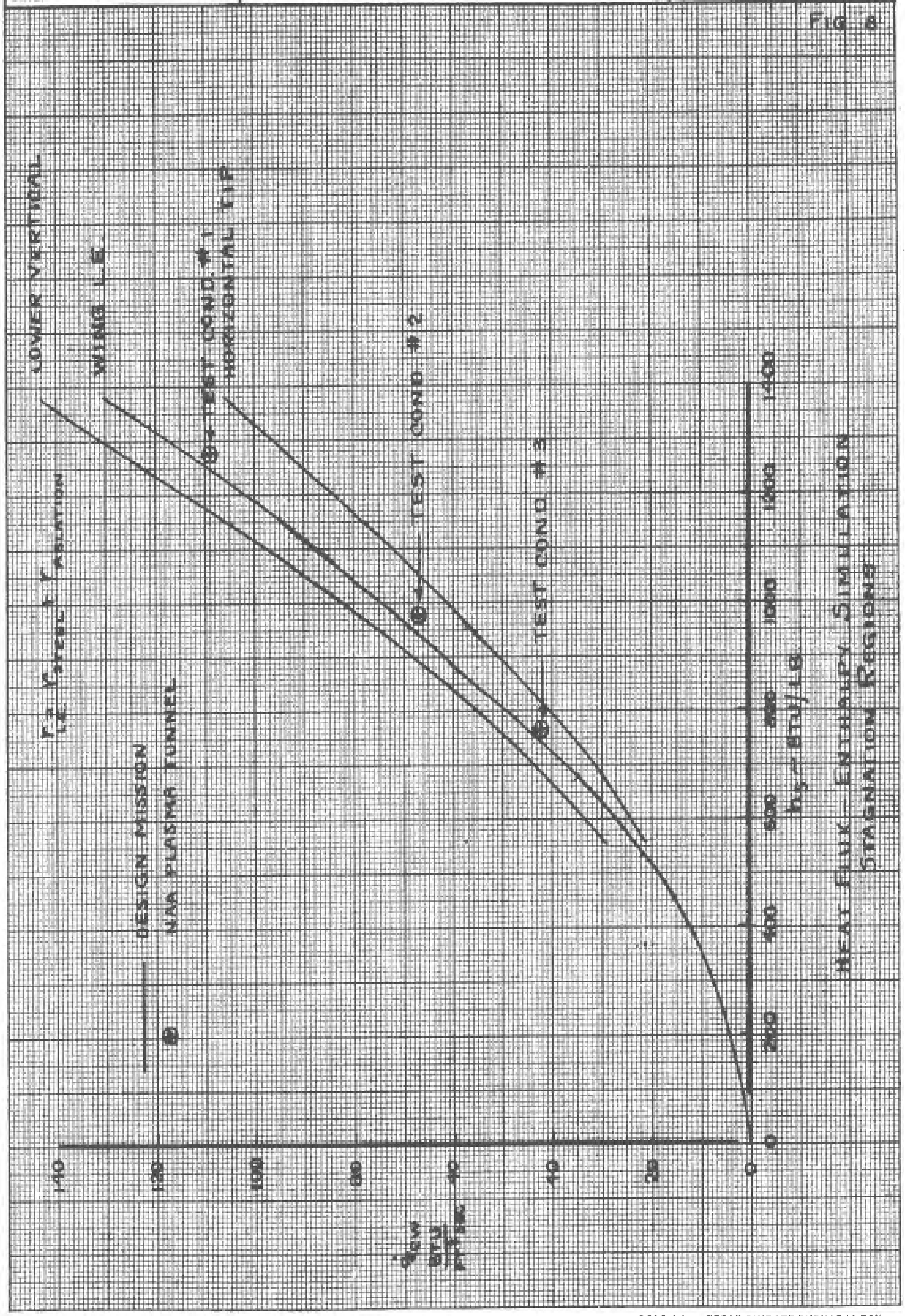

FORM 1021-5

NORTH AMERICAN AVIATION, INC.	
PREPARED BY:	PAGE NO. 34 OF
CHECKED BY:	REPORT NO. NA-64-177
DATE:	MODEL NO.

FIG. 9

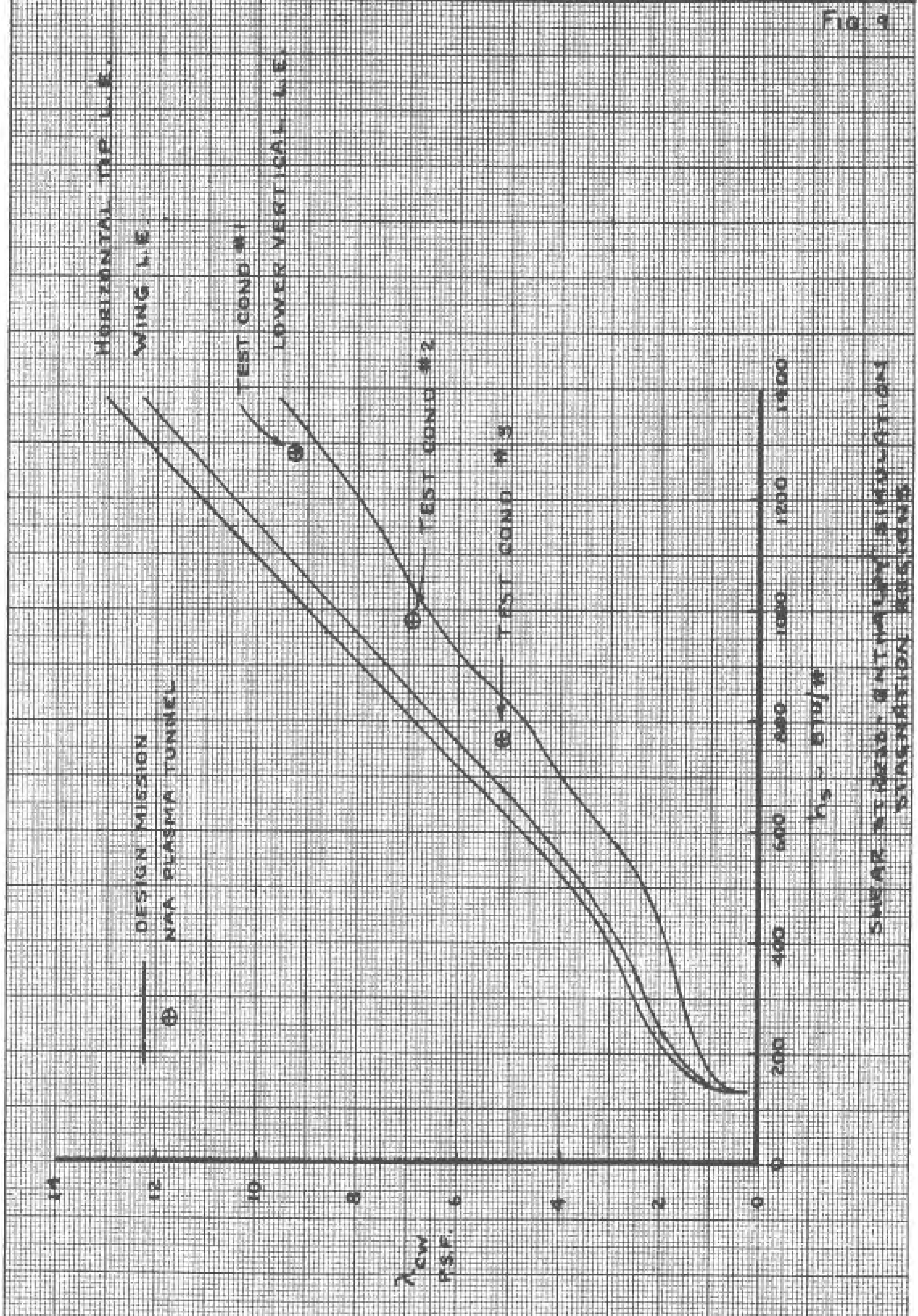

K&E ALBANENE TRACING PAPER LA 0498

Figure 10

FLAT PANEL PLASMA TUNNEL MODEL

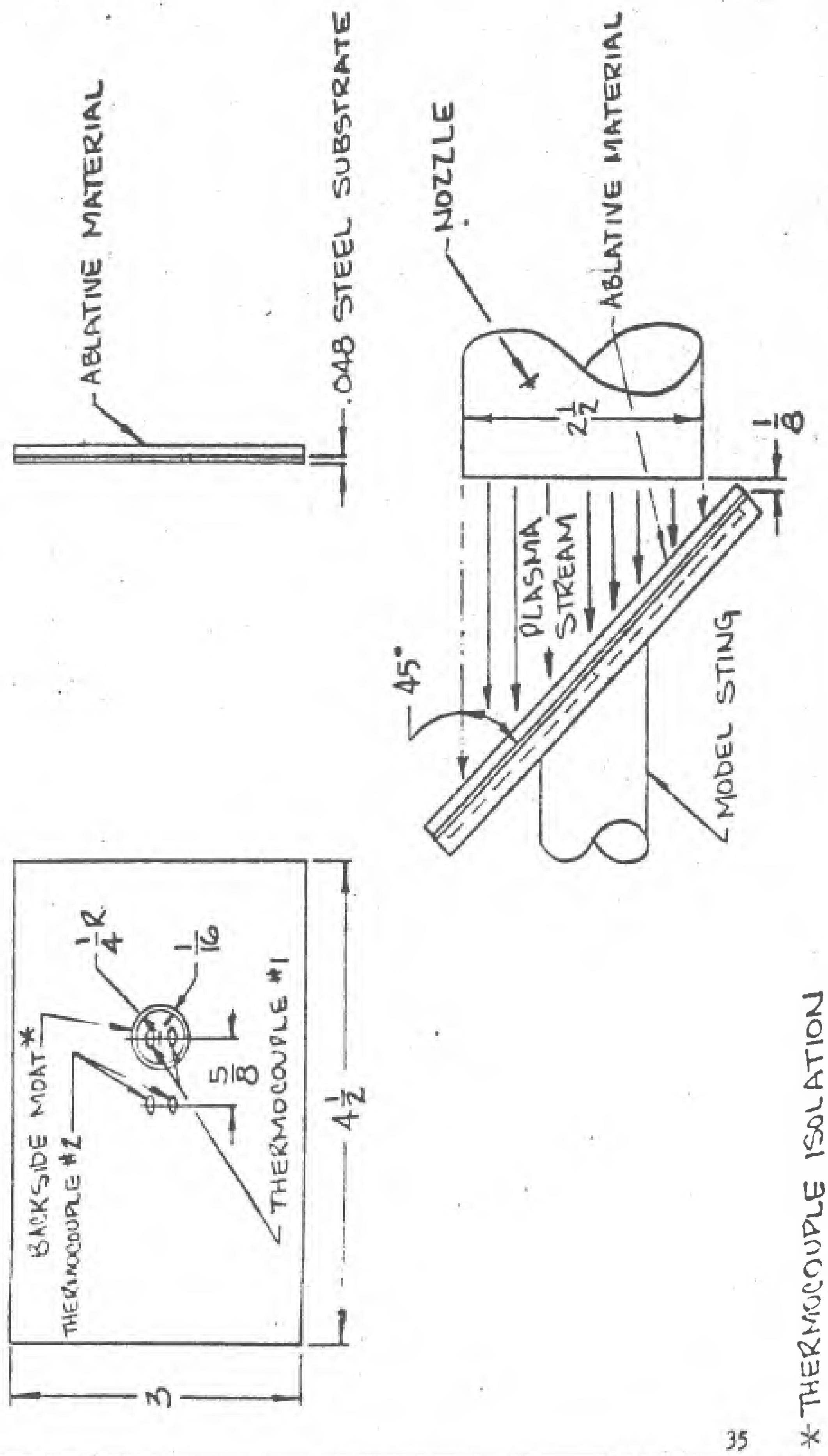

FIG. 11

FLIGHT SIMULATION
FLAT SURFACES

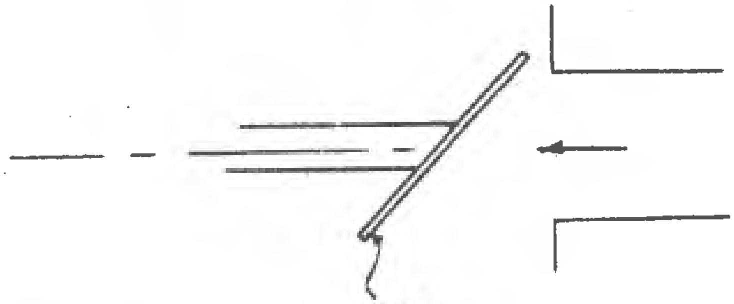

—— FUSELAGE LOWER ℄ @ PEAK HEATING

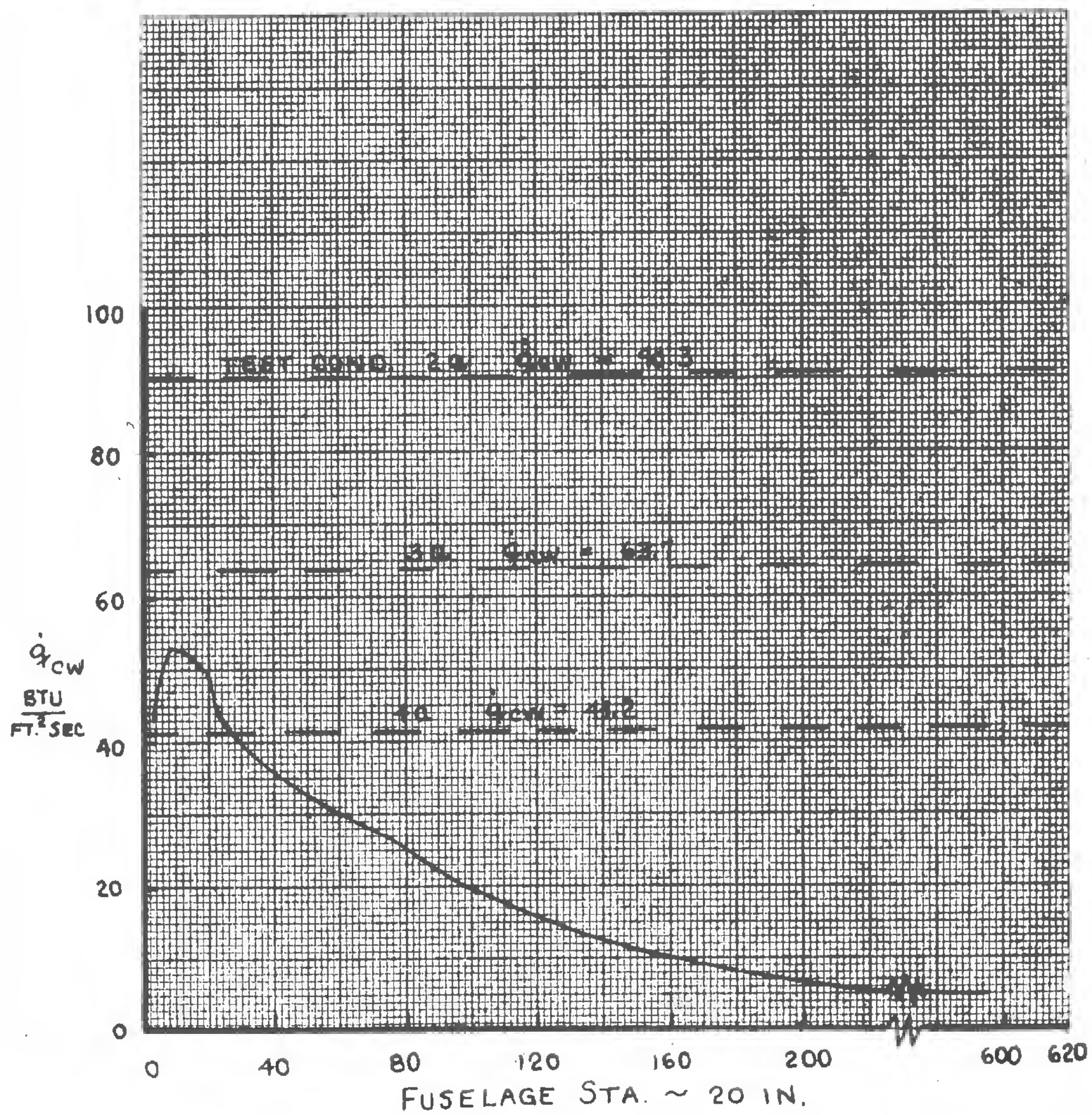

Figure 12

DESIGN MISSION SIMULATION

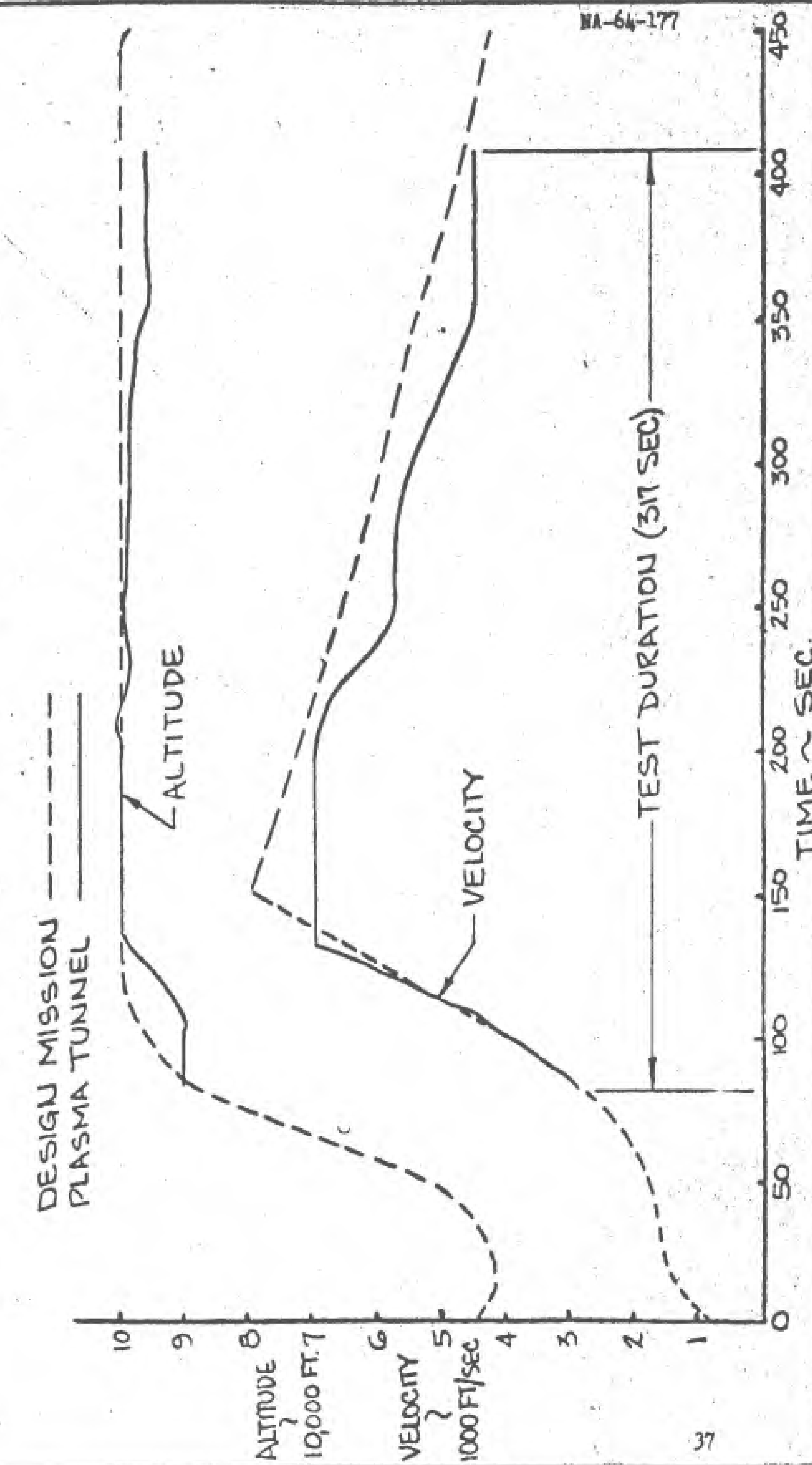

Figure 13

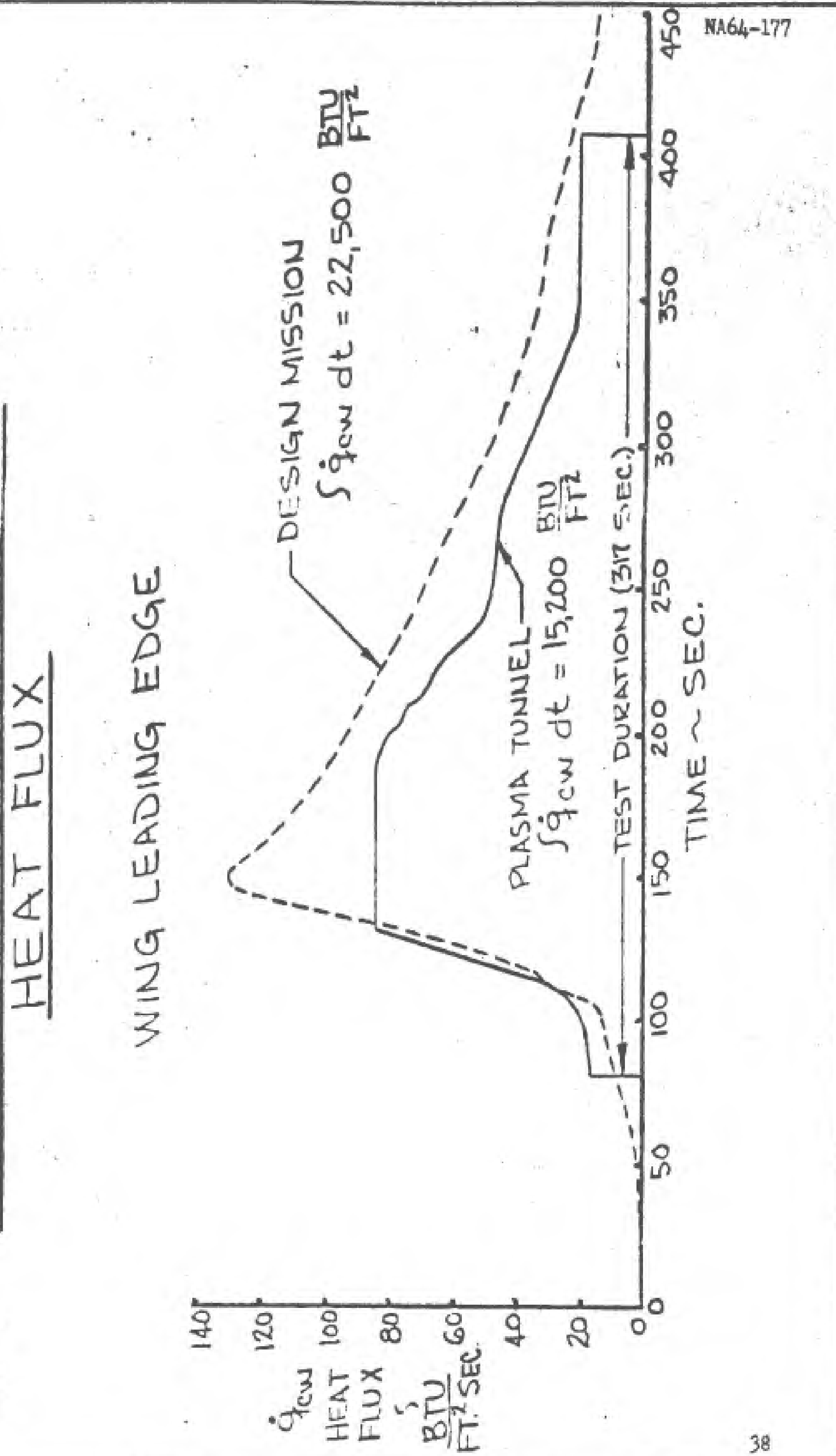
DESIGN MISSION SIMULATION
HEAT FLUX
WING LEADING EDGE
DESIGN MISSION
$\int \dot{q}_{cw}\, dt = 22{,}500 \frac{BTU}{FT^2}$
PLASMA TUNNEL
$\int \dot{q}_{cw}\, dt = 15{,}200 \frac{BTU}{FT^2}$
TEST DURATION (317 SEC.)
$\dot{q}_{cw}$ HEAT FLUX ~ $\frac{BTU}{FT^2 SEC.}$
140
120
100
80
60
40
20
0
0
50
100
150
200
250
300
350
400
450
TIME ~ SEC.

FORM 1021-S

PREPARED BY:	NORTH AMERICAN AVIATION, INC.	PAGE NO. 39 OF
CHECKED BY:		REPORT NO. NA-64-177
DATE:		MODEL NO.

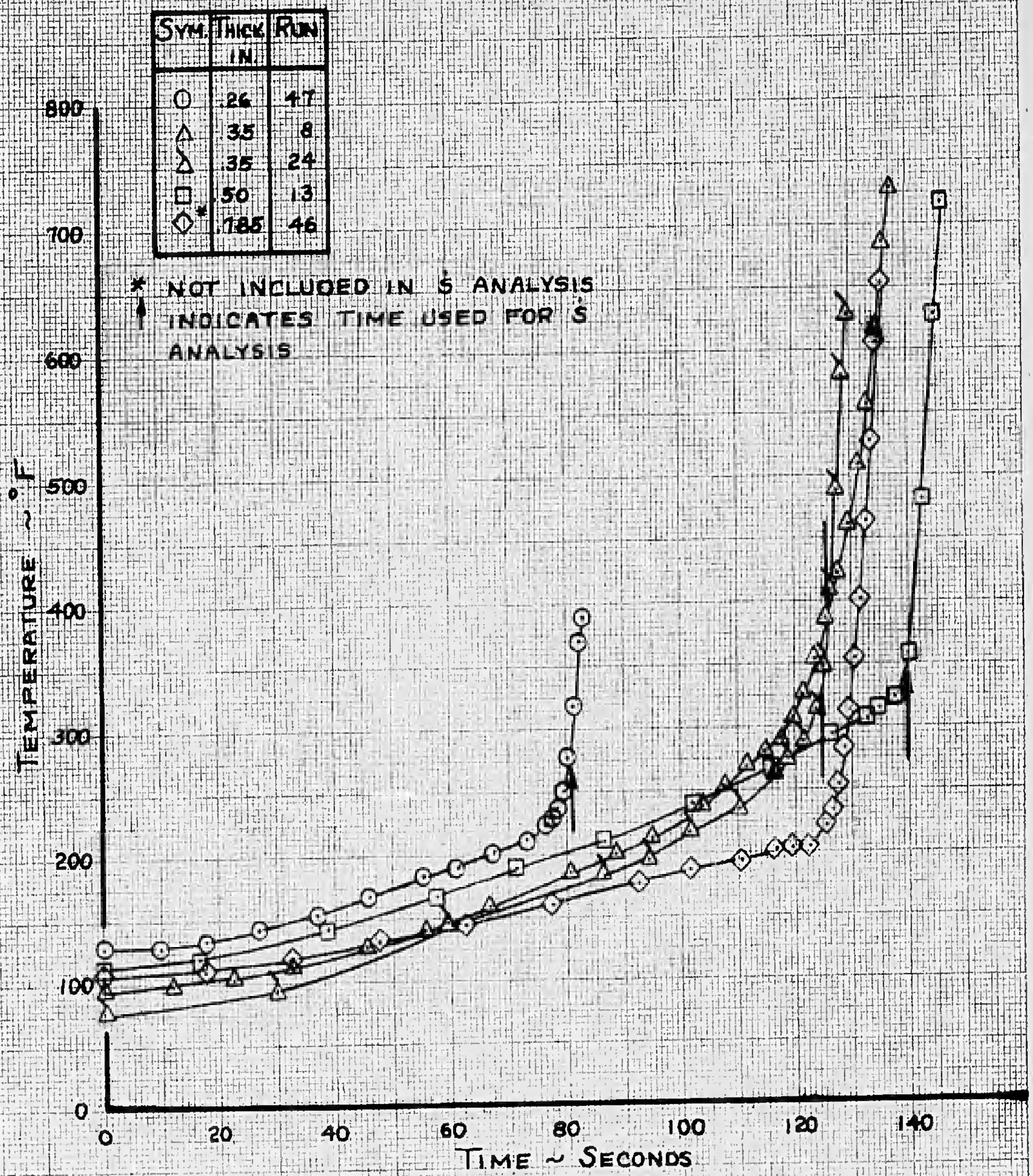

FIG 14 EFFECT OF THICKNESS

TEST CONDITION I
T-500-6A

FORM 1021-B

PREPARED BY:	NORTH AMERICAN AVIATION, INC.	PAGE NO. 40 OF
CHECKED BY:		REPORT NO. NA-64-177
DATE:		MODEL NO.

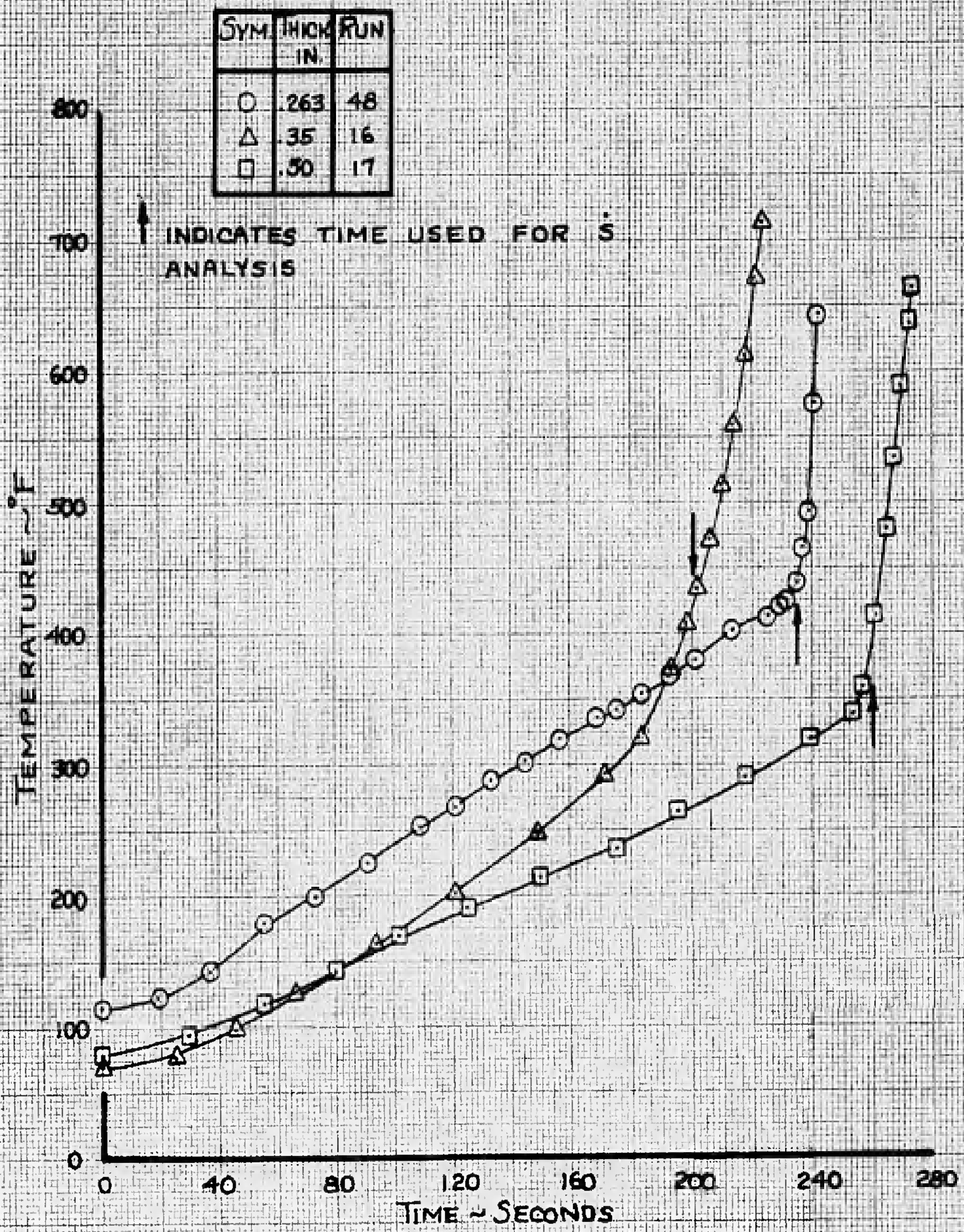

FIG. 15 EFFECT OF THICKNESS

TEST CONDITION 2

T-500-6A

FORM 1021-3

PREPARED BY:	NORTH AMERICAN AVIATION, INC.	PAGE NO. 41 OF
CHECKED BY:		REPORT NO. NA-64-177
DATE:		MODEL NO.

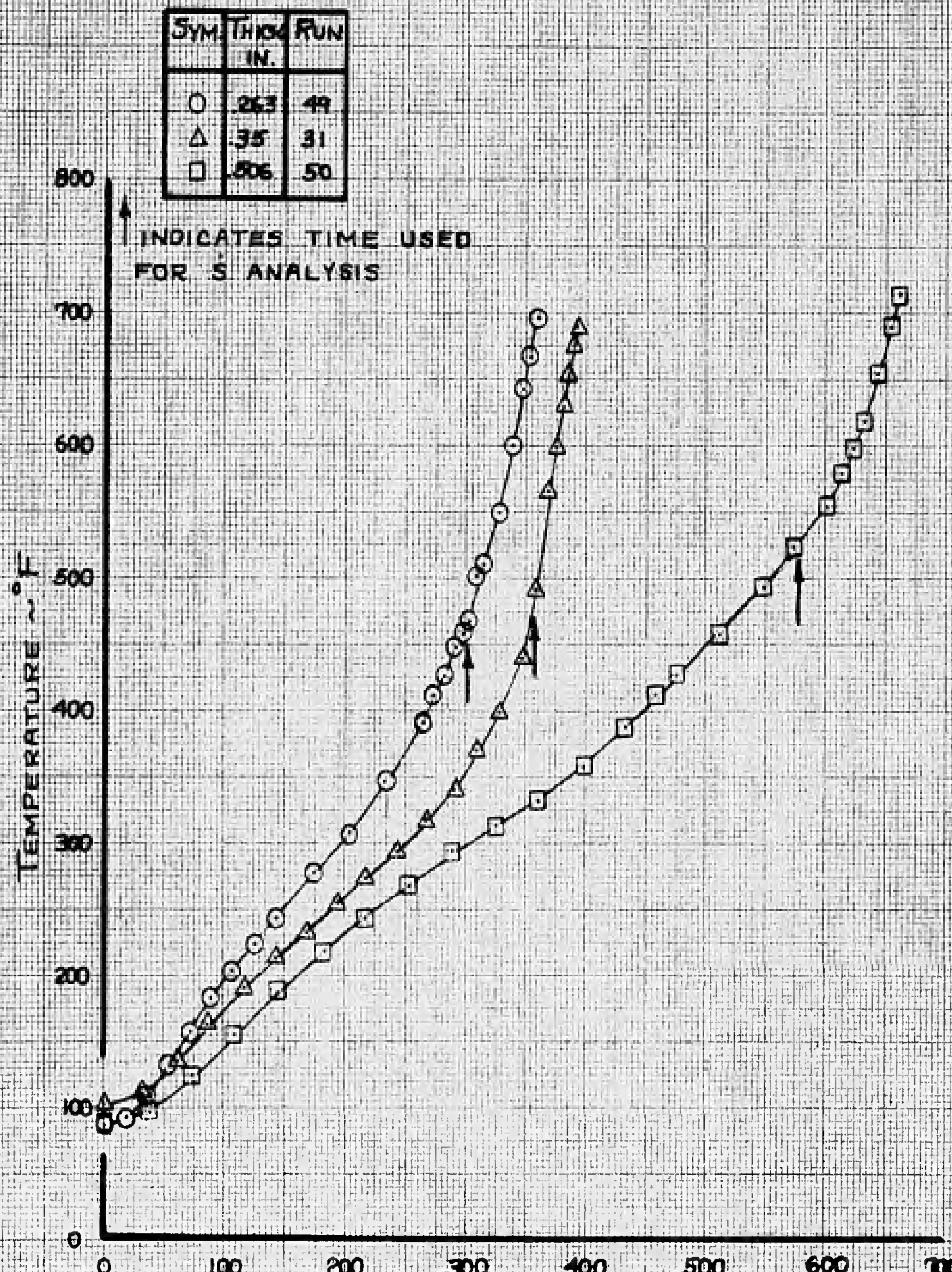

FIG. 16 EFFECT OF THICKNESS

TEST CONDITION 3

T-500-6A

FORM 1021-S

PREPARED BY:	NORTH AMERICAN AVIATION, INC.	PAGE NO. 42 OF
CHECKED BY:		REPORT NO. NA-64-177
DATE:		MODEL NO.

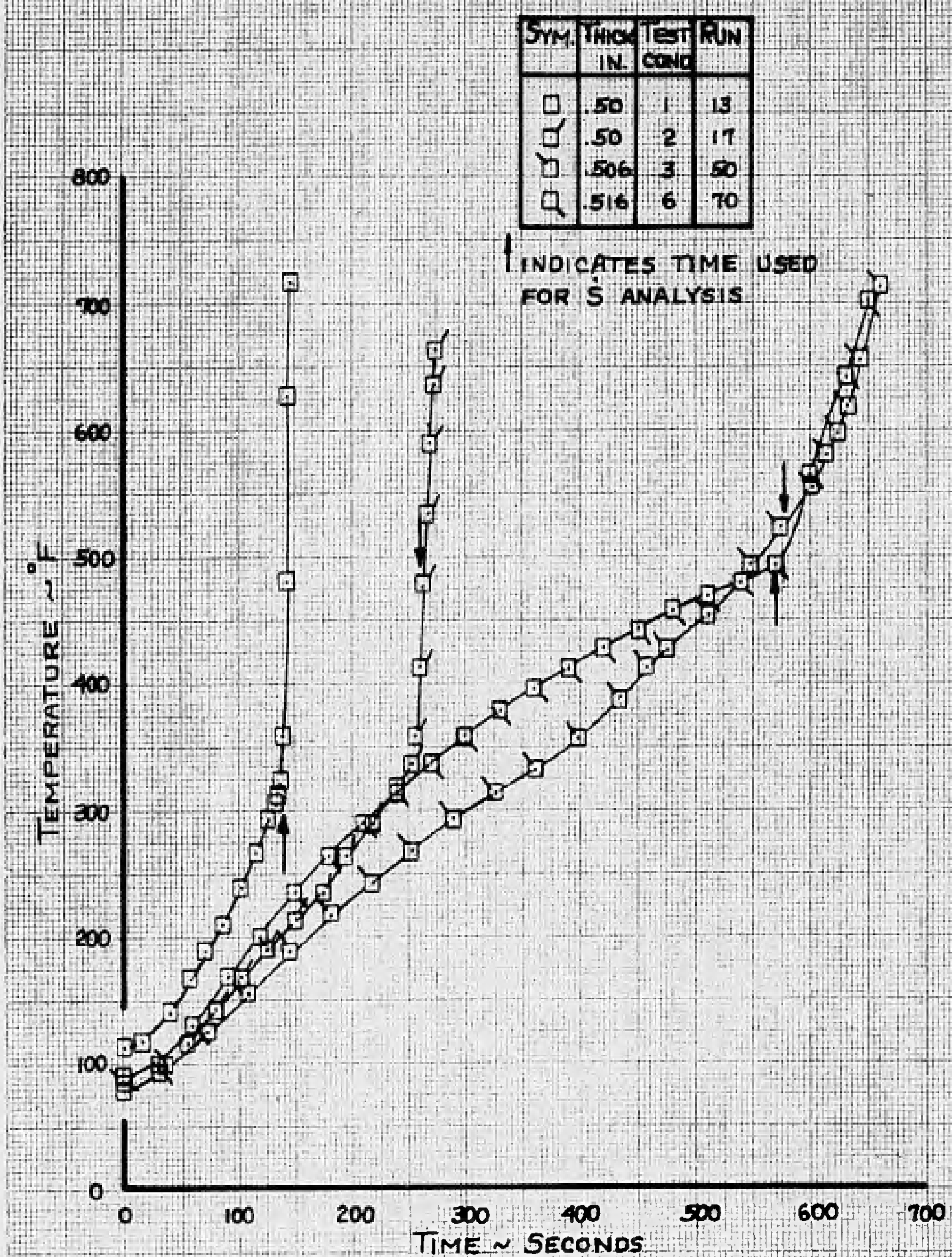

FIG. 17 EFFECT OF TEST CONDITION

T-500-6A

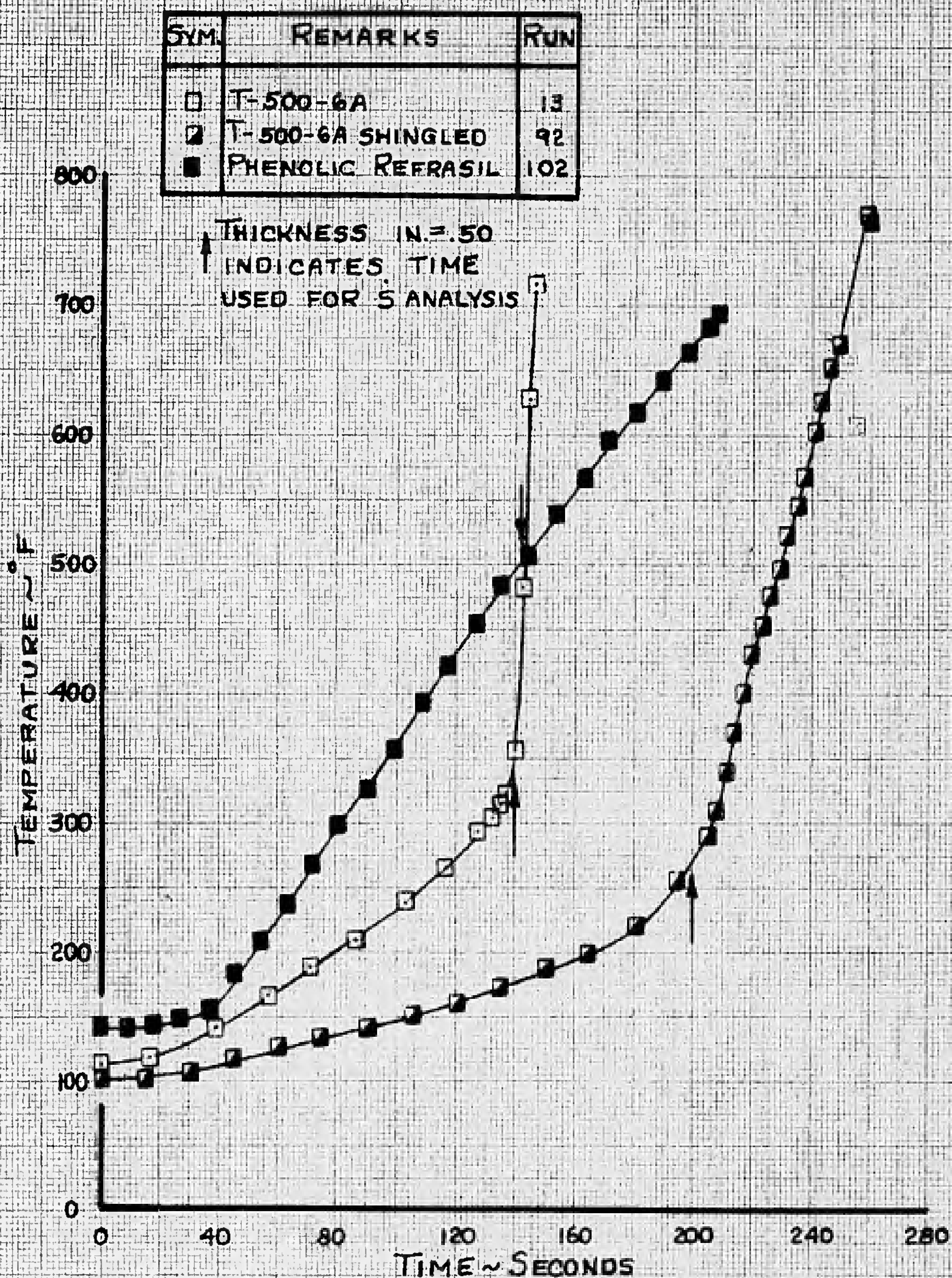

FIG. 18 EFFECT OF MATERIAL

TEST CONDITION I

FORM 1021-B

PREPARED BY:	NORTH AMERICAN AVIATION, INC.	PAGE NO. 44 OF
CHECKED BY:		REPORT NO. NA-64-177
DATE:		MODEL NO.

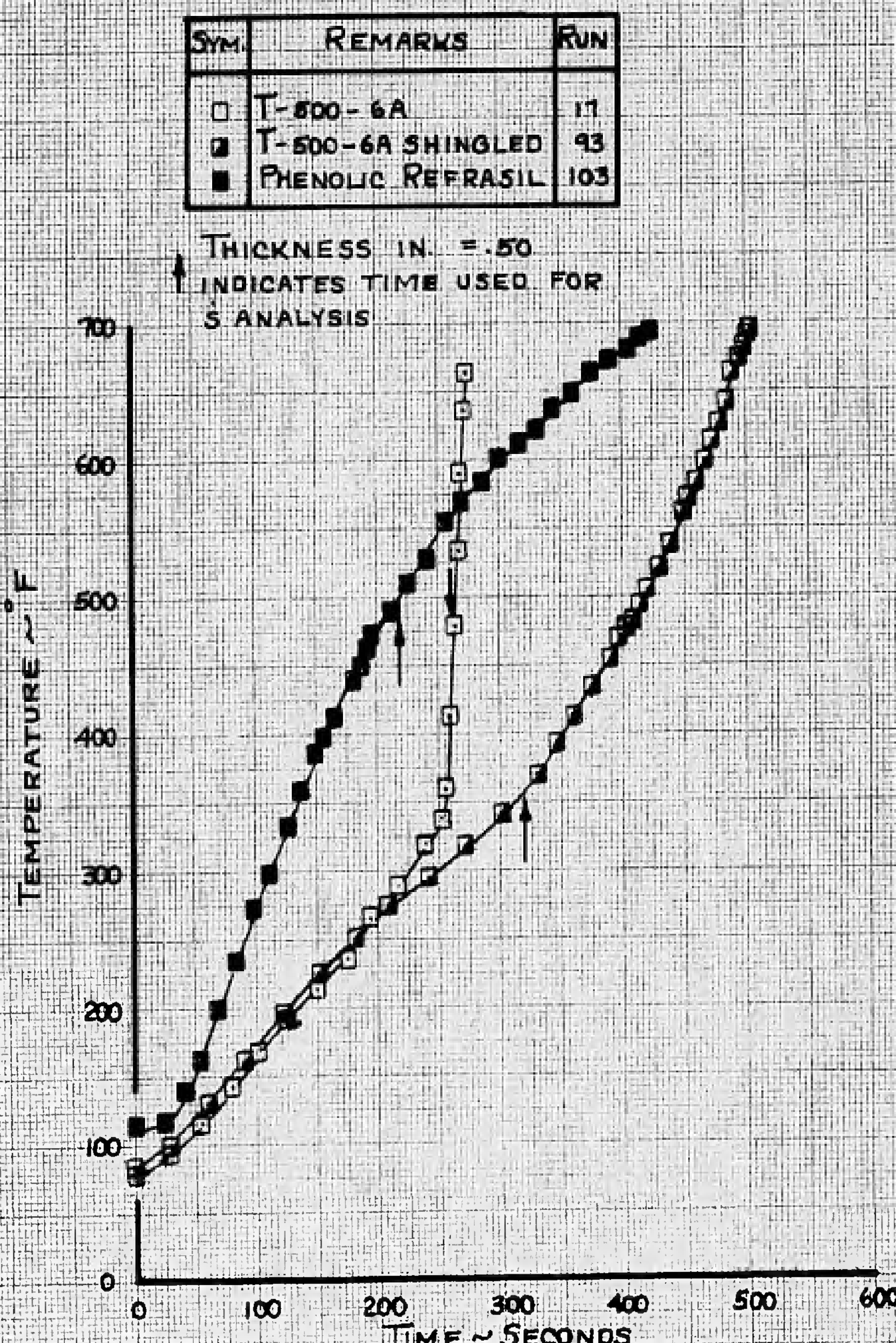

FIG. 19 EFFECT OF MATERIAL

TEST CONDITION 2

FORM 1021-B

PREPARED BY:	NORTH AMERICAN AVIATION, INC.	PAGE NO. 45 OF
CHECKED BY:		REPORT NO. NA-64-177
DATE:		MODEL NO.

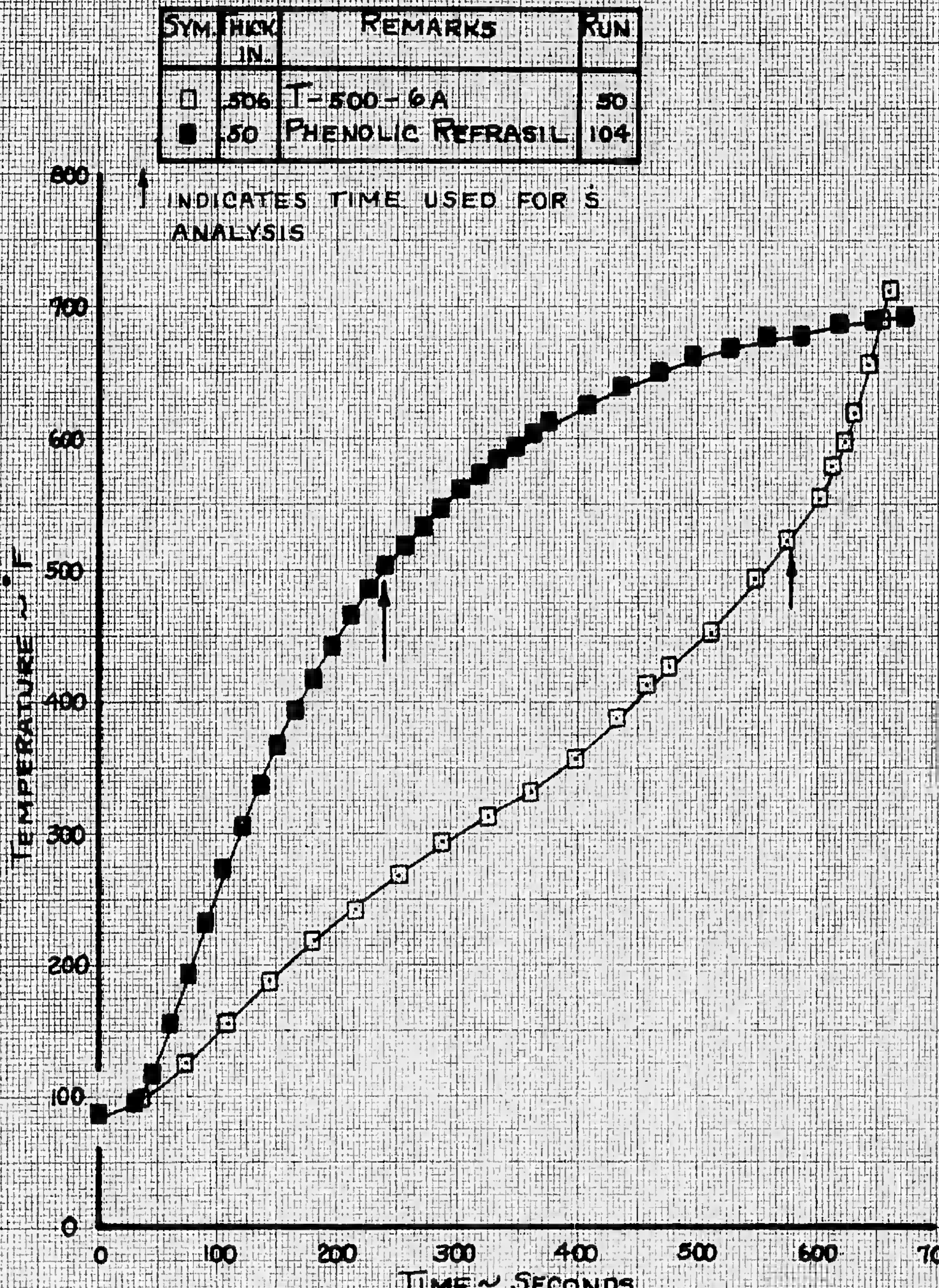

FIG 20 EFFECT OF MATERIAL

TEST CONDITION 3

FIG. 21

LINEAR RECESSION RATE - T-500-6A

○ TEST COND. # 1
△ " " 2
□ " " 3

NOS. IN ( ) INDICATE RUN NOS.

——— BASED ON AVERAGE RECESSION RATE

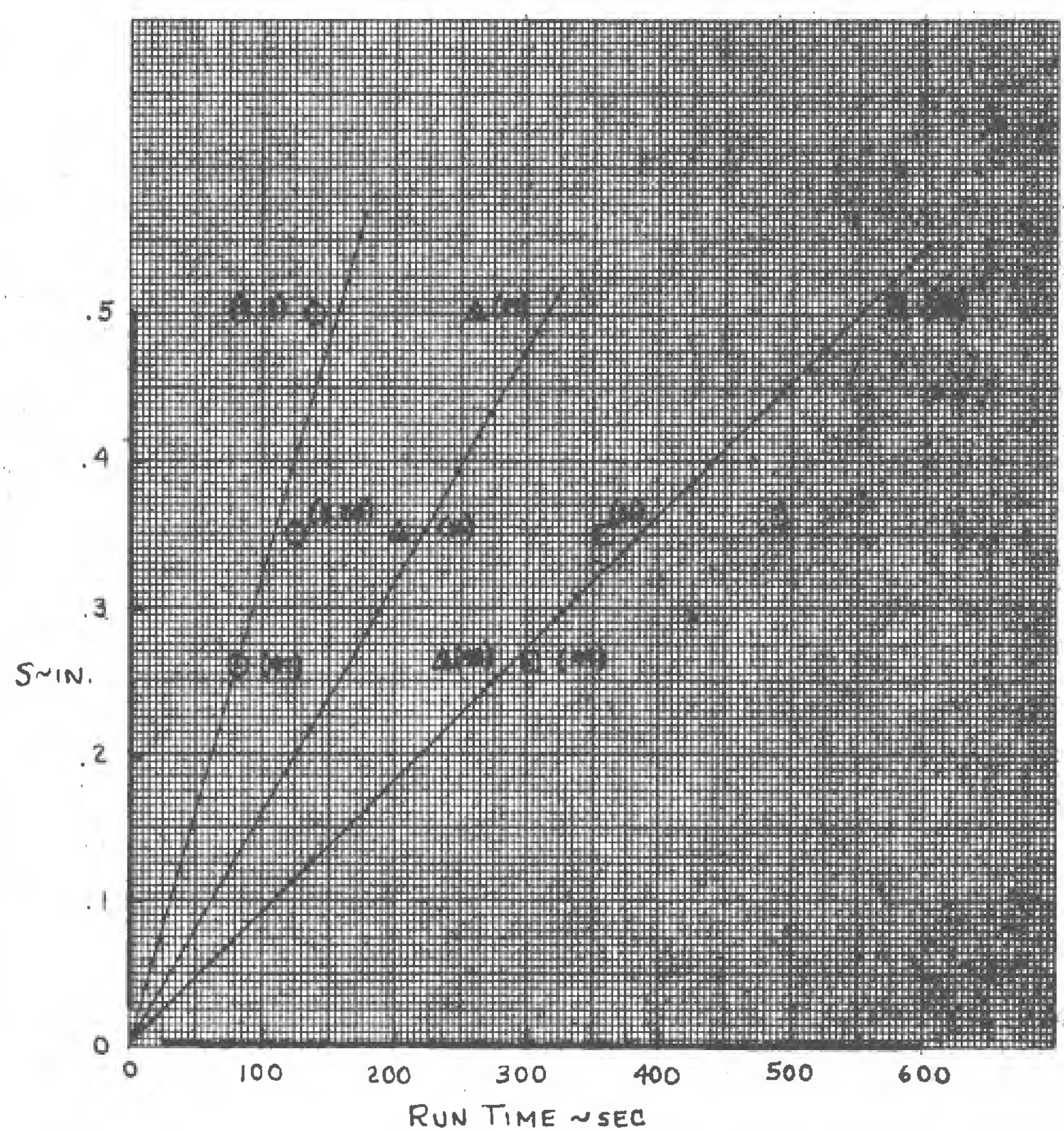

PREPARED BY: JB	NORTH AMERICAN AVIATION, INC.	PAGE NO. 47 OF
CHECKED BY:	SURFACE RECESSION	REPORT NO. NA-64-177
DATE: 1/21/64	DURING TEST	MODEL NO.

FIG. 22

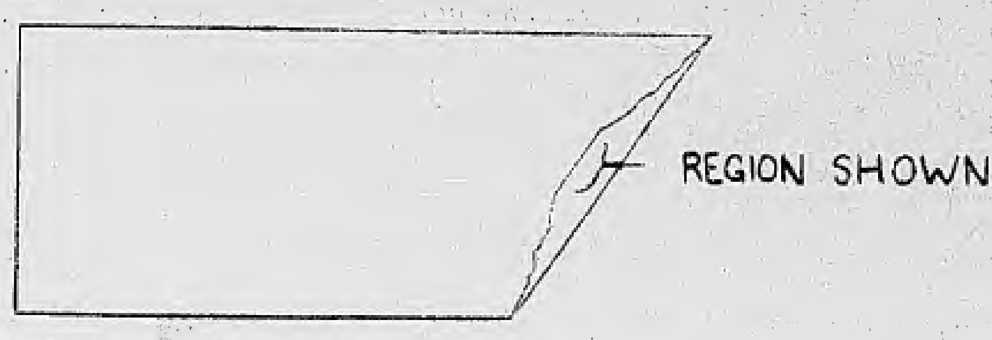

SKETCH OF MODEL DURING TEST (TYPICAL)

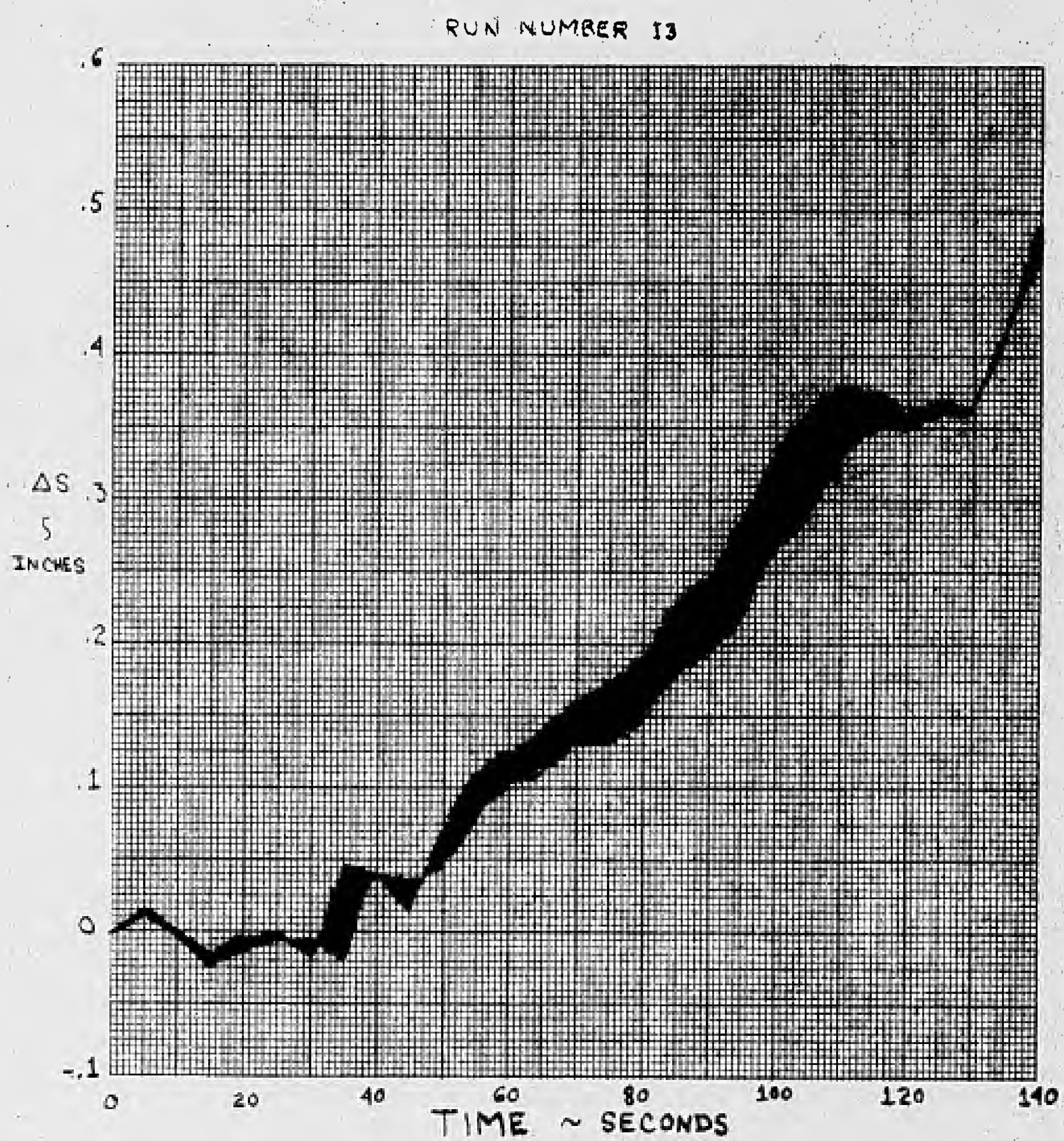

FORM 1021-B

PREPARED BY:	NORTH AMERICAN AVIATION, INC.	PAGE NO. 48 OF
CHECKED BY:		REPORT NO NA-64-177
DATE:		MODEL NO.

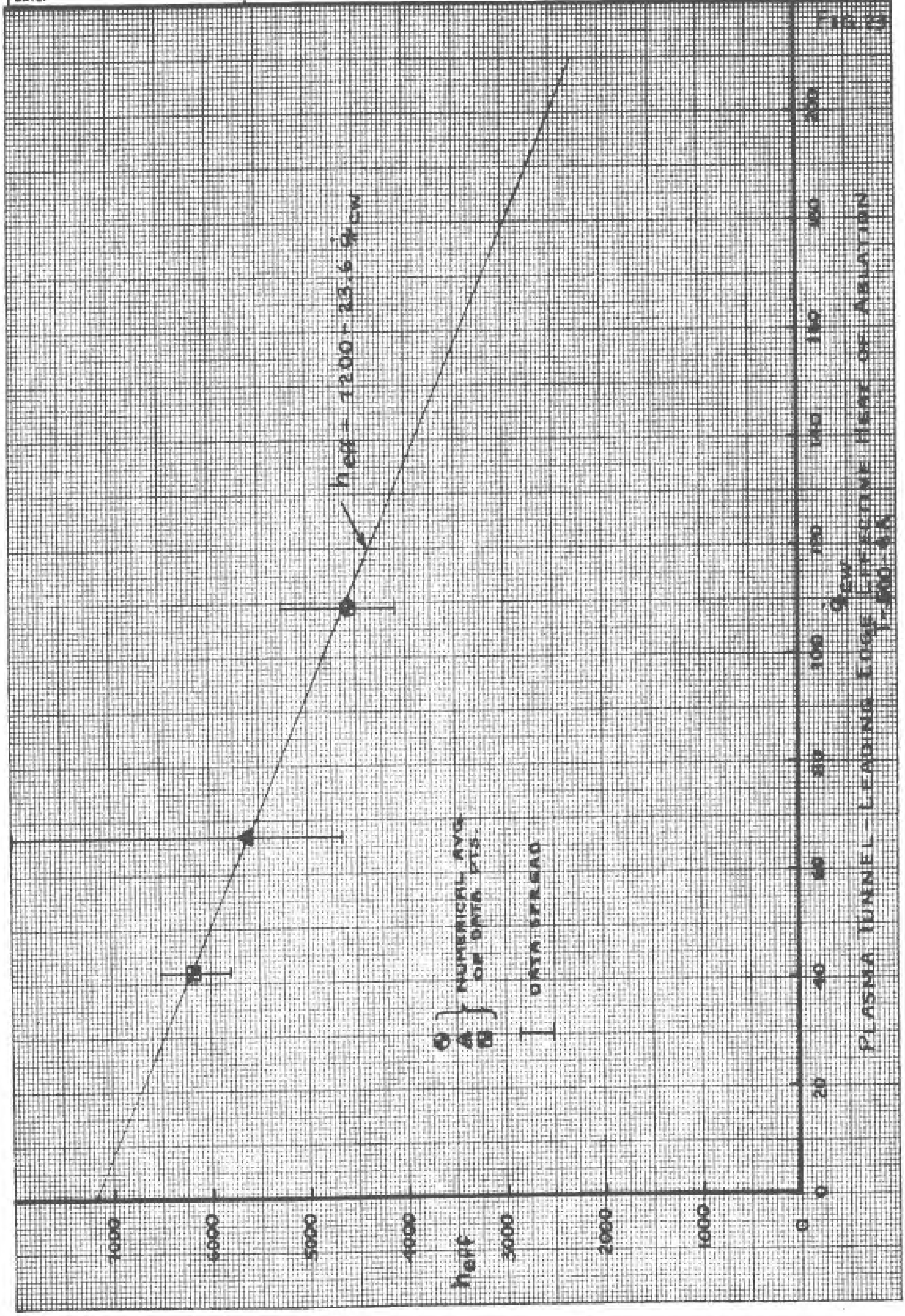

FORM 1021-9

NORTH AMERICAN AVIATION, INC.		
PREPARED BY: R.J.		PAGE NO. 49 OF
CHECKED BY:		REPORT NO. NA-64-177
DATE: 10/1/63		MODEL NO.

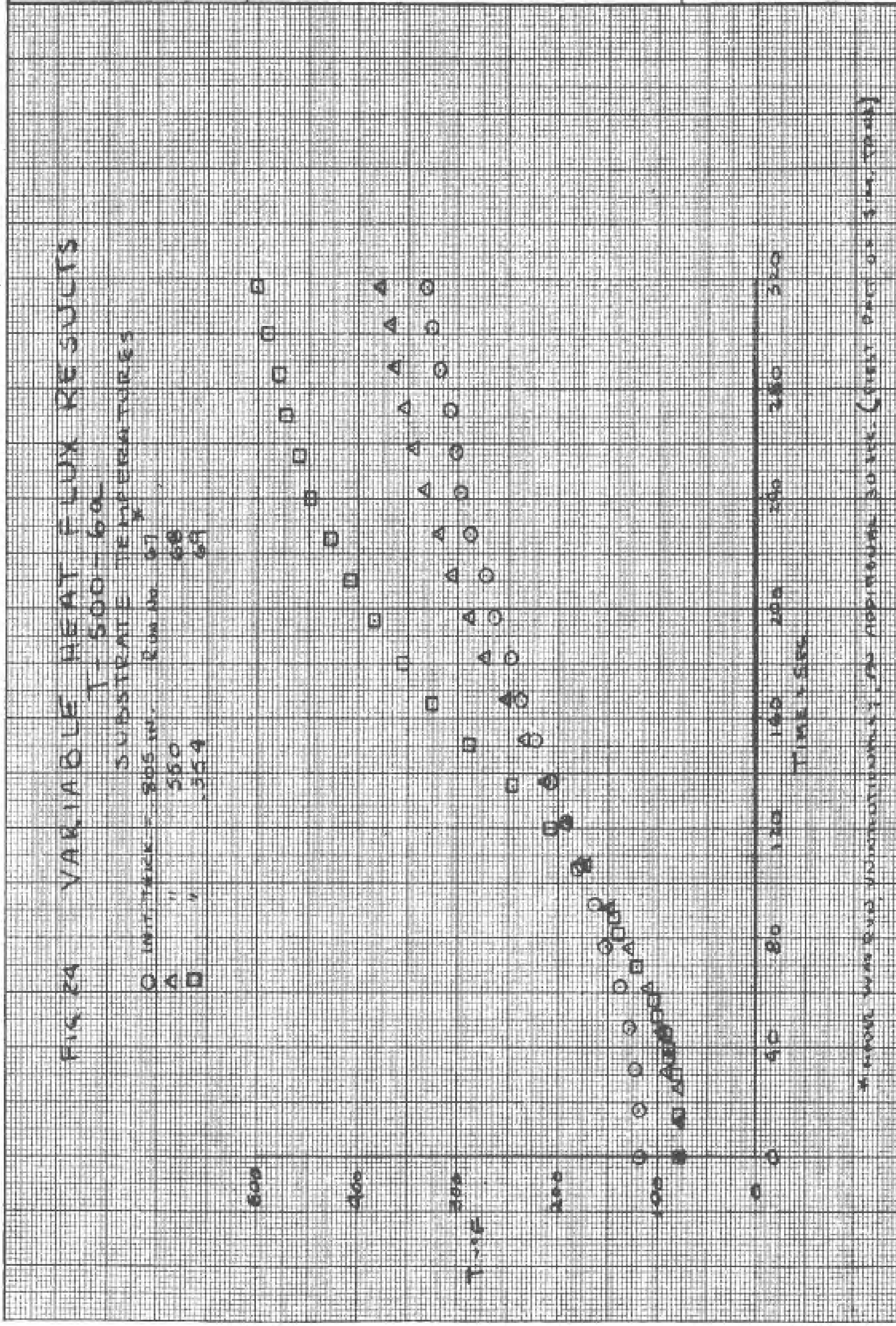

PREPARED BY: DLD	NORTH AMERICAN AVIATION, INC.	PAGE NO. 50 OF
CHECKED BY:		REPORT NO. NA-64-177
DATE: 10/2/63		MODEL NO.

1) ADDED MEAS. TO VIRGIN MAT'L ON 10/31/63. R.H.J.

2) ADDED NOTE ON 10/31/63

PT-8 RUN 67 [TRAJECTORY]

L.E. EMERSON MODEL #102

.805 IN. THICK THERMOLAG

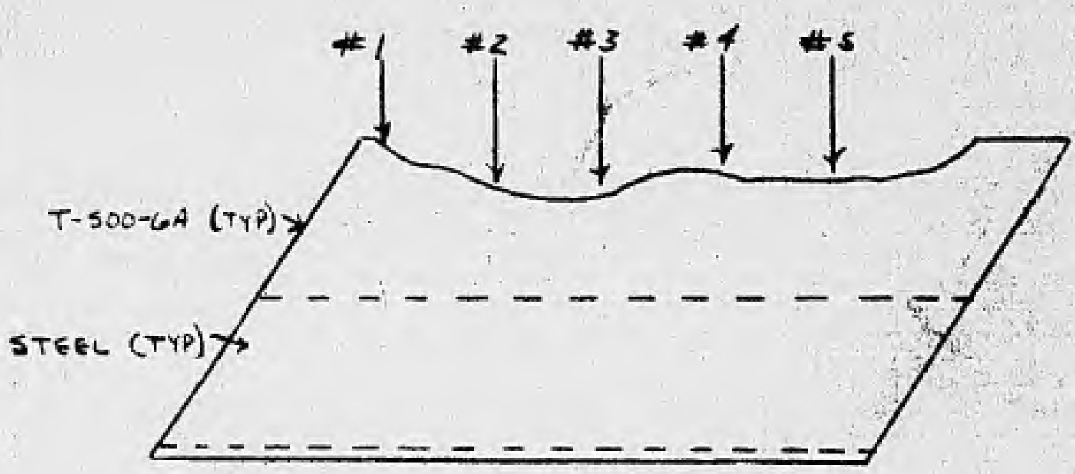

THICKNESS REMAINING	(TO SURFACE)	(TO VIRGIN MAT'L)
STATION #1:	.600 IN.	
STATION #2:	.531 IN.	
STATION #3:	.522 IN.	.465
STATION #4:	.565 IN.	
STATION #5:	.637 IN.	

NOTE: THIS MODEL WAS EXPOSED TO AN ADDITIONAL 30 SEC. OF TEST. THE FIRST 30 SEC. OF THE VAR. HEAT FLUX WAS RUN, THEN STOPPED. THE MODEL THEN WAS RUN THE FULL TEST OF 316.8 SEC. MORE.

Figure 25 - Sketch of .805 in. thick Model After Variable Heat Flux Test

PREPARED BY: DED	NORTH AMERICAN AVIATION, INC.	PAGE NO. 51 OF 5
CHECKED BY:		REPORT NO. NA-64-177
DATE: 10/2/63		MODEL NO.

ADDED MEAS. TO VIRGIN MAT'L ON 10/31/63. R.H.J.

PT-8 RUN 68 [TRAJECTORY]
L.E. EMERSON MODEL #11
.550 IN. THICK THERMOLAG

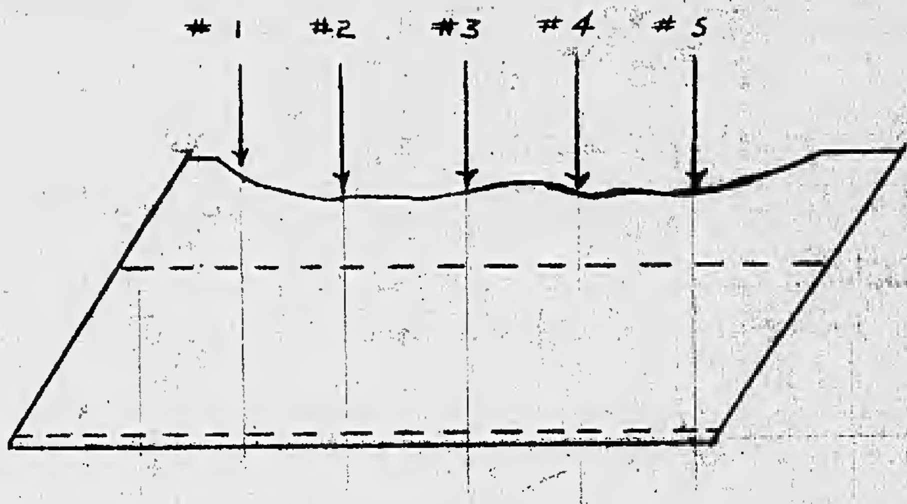

THICKNESS REMAINING	(TO SURF.)	(TO VIRGIN MAT'L)
STATION #1:	.414 IN.	
STATION #2:	.382 IN.	
STATION #3:	.420 IN.	.260
STATION #4:	.402 IN.	.250
STATION #5:	.437 IN.	

Figure 26 - Sketch of .550 in. Thick Model After Variable Heat Flux Test

PREPARED BY: DED	NORTH AMERICAN AVIATION, INC.	PAGE NO. 52 OF
CHECKED BY:		REPORT NO. NA-64-177
DATE: 10/2/63		MODEL NO.

ADDED MEAS. TO VIRGIN
MAT'L ON 10/31/63. RHJ.

PT-8 RUN 69 [TRAJECTORY]
L.E. EMERSON MODEL # 70
.354 IN. THICK THERMOLAG

THICKNESS REMAINING	(TO SURFACE)	(TO VIRGIN MAT'L)
STATION #1:	.255 IN.	
STATION #2:	.182 IN.	
STATION #3:	.125 IN.	.044
STATION #4:	.116 IN.	.024
STATION #5:	.235 IN.	

Figure 27 - Sketch of .354 in. Thick Model After Variable Heat Flux Test

FORM 1021-S

PREPARED BY:	**NORTH AMERICAN AVIATION, INC.**	PAGE NO. 53 OF
CHECKED BY:		REPORT NO. NA-64-177
DATE:		MODEL NO.

FIG. 28

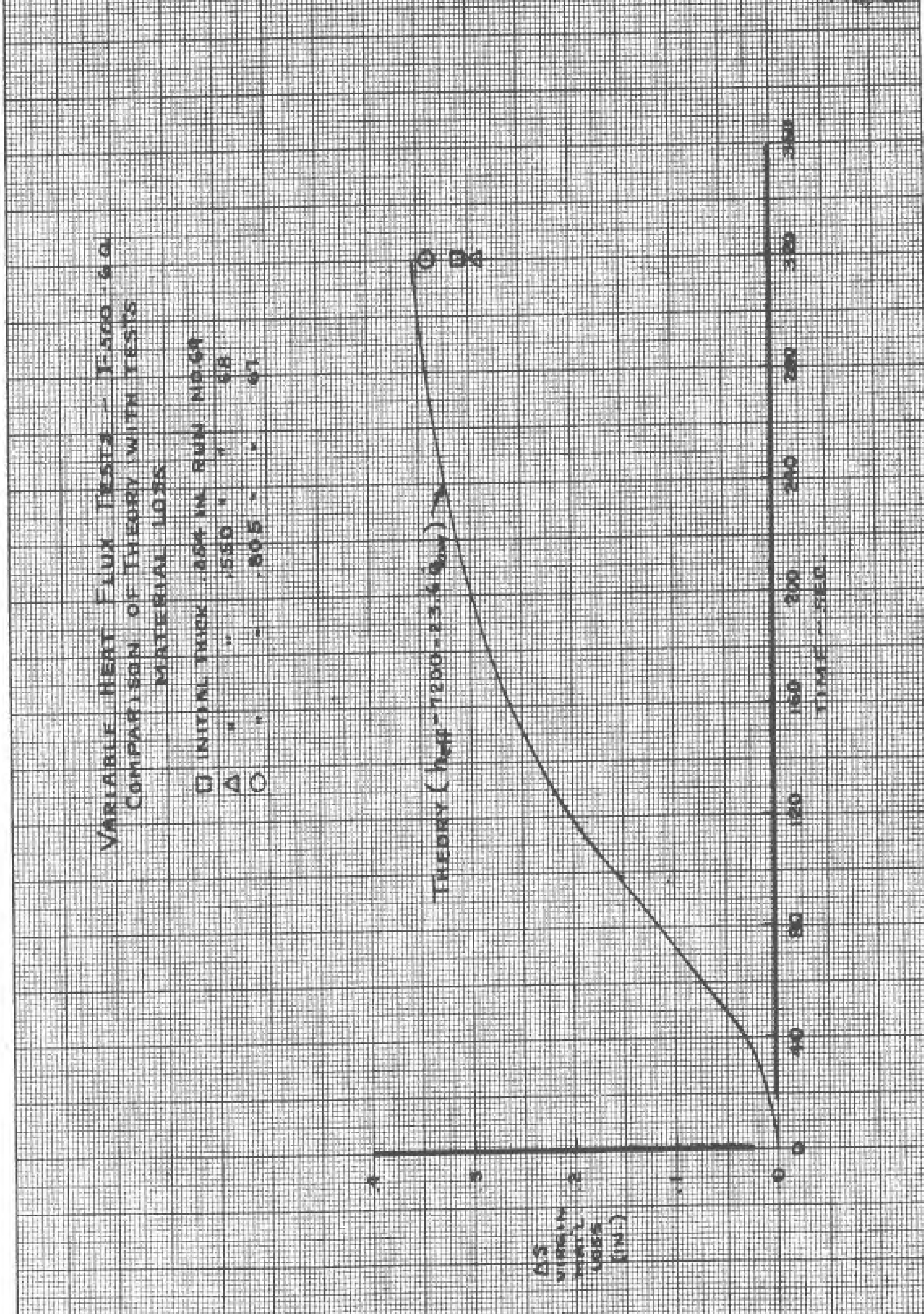

K&E ALBANENE TRACING PAPER LA 0498

FORM 1021-S

PREPARED BY:	NORTH AMERICAN AVIATION, INC.	PAGE NO. 54 OF
CHECKED BY:		REPORT NO. NA-64-177
DATE:		MODEL NO.

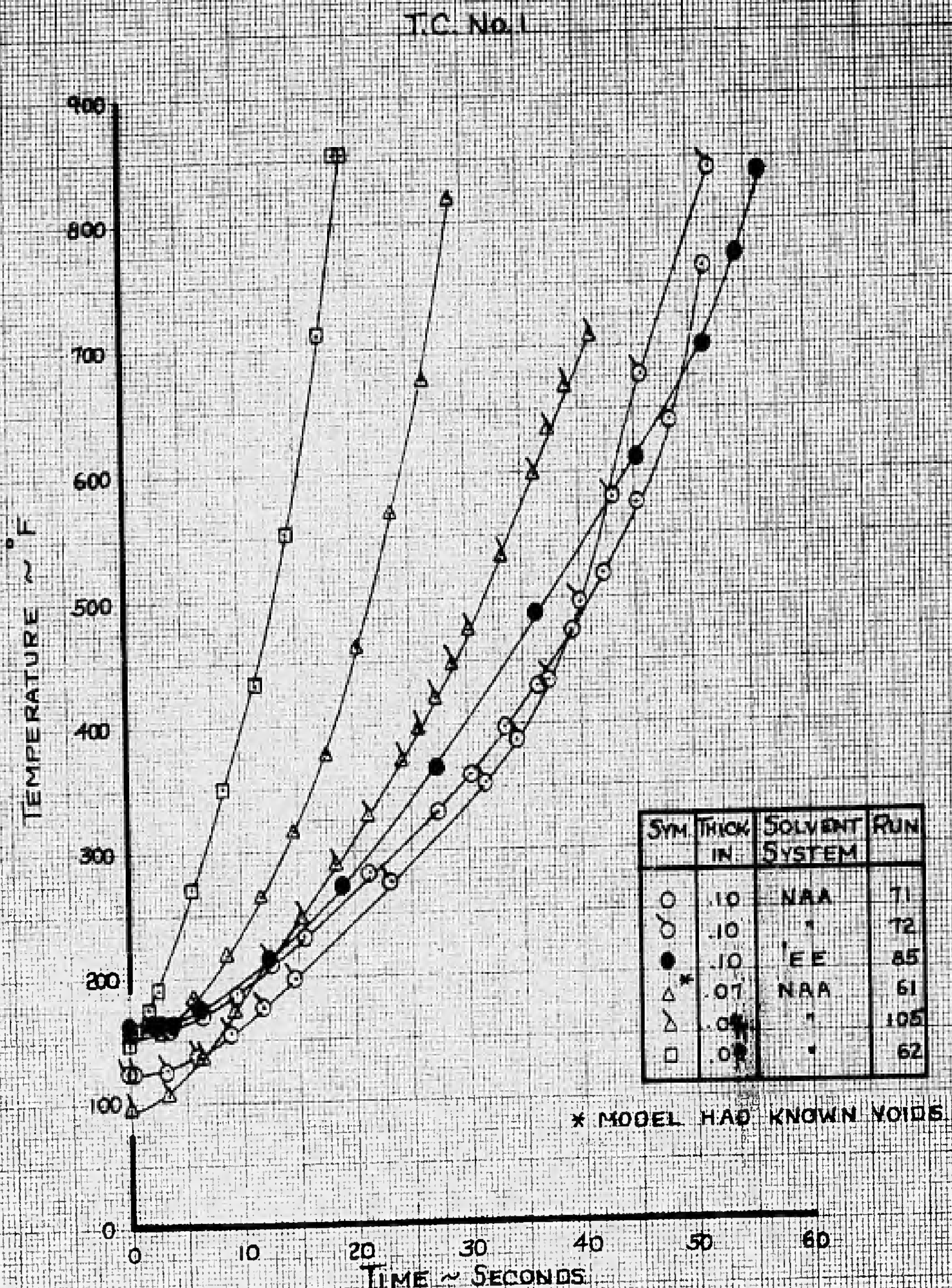

Fig. 29 EFFECT OF THICKNESS

TEST CONDITION 2a
T-500-4

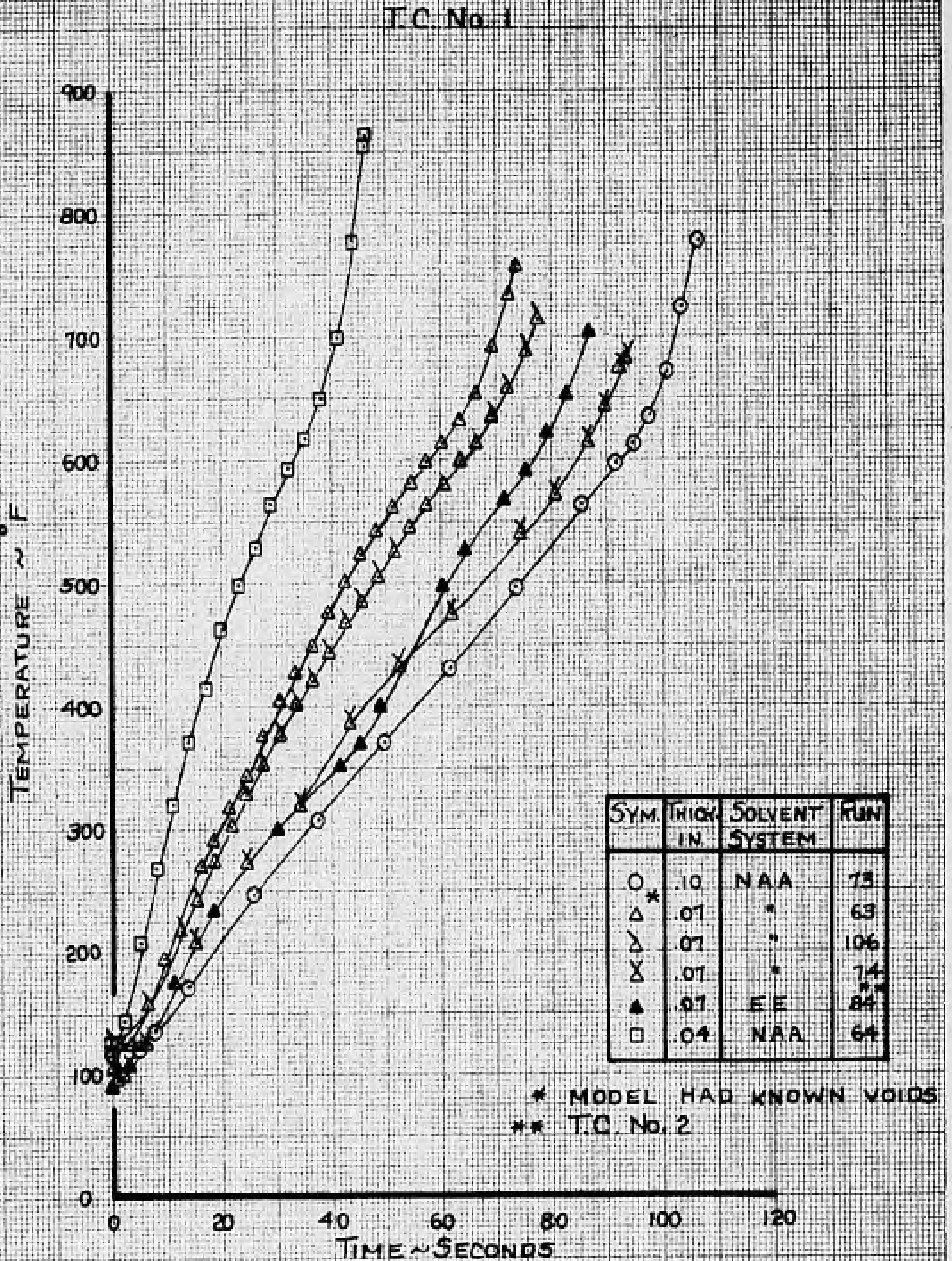

FIG. 30 EFFECT OF THICKNESS

TEST CONDITION 3a
T-500-4

FORM 1021-8

PREPARED BY:	NORTH AMERICAN AVIATION, INC.	PAGE NO. 56 OF
CHECKED BY:		REPORT NO. NA-64-177
DATE:		MODEL NO.

T.C. No. 1

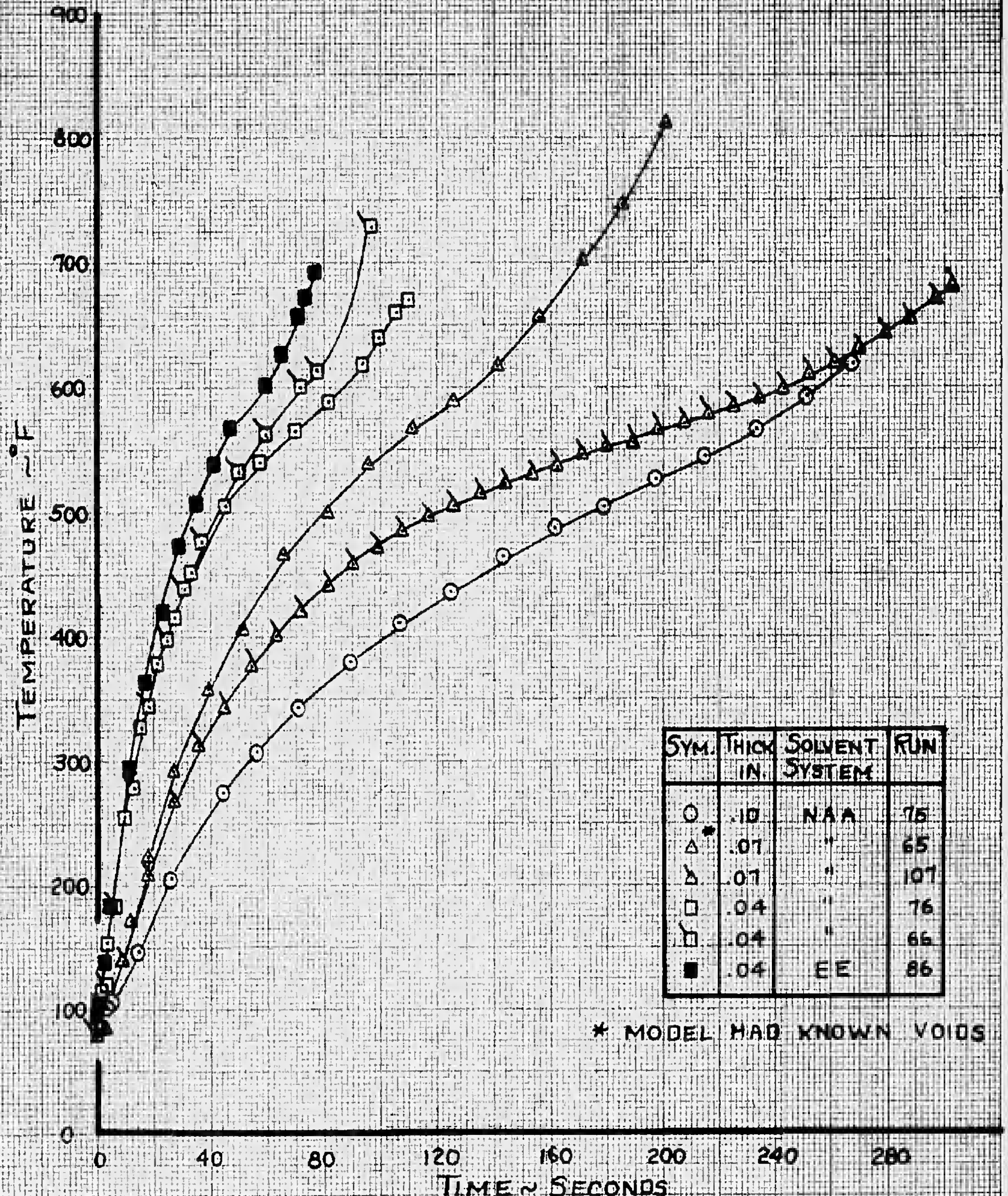

SYM.	THICK IN.	SOLVENT SYSTEM	RUN
○	.10	NAA	75
△*	.07	"	65
△ (flagged)	.07	"	107
□	.04	"	76
□ (flagged)	.04	"	66
■	.04	EE	86

* MODEL HAD KNOWN VOIDS

FIG. 31 EFFECT OF THICKNESS

TEST CONDITION 4a

T-500-4

FORM 1021-S

PREPARED BY:	NORTH AMERICAN AVIATION, INC.	PAGE NO. 57 OF
CHECKED BY:		REPORT NO. NA-64-177
DATE:		MODEL NO.

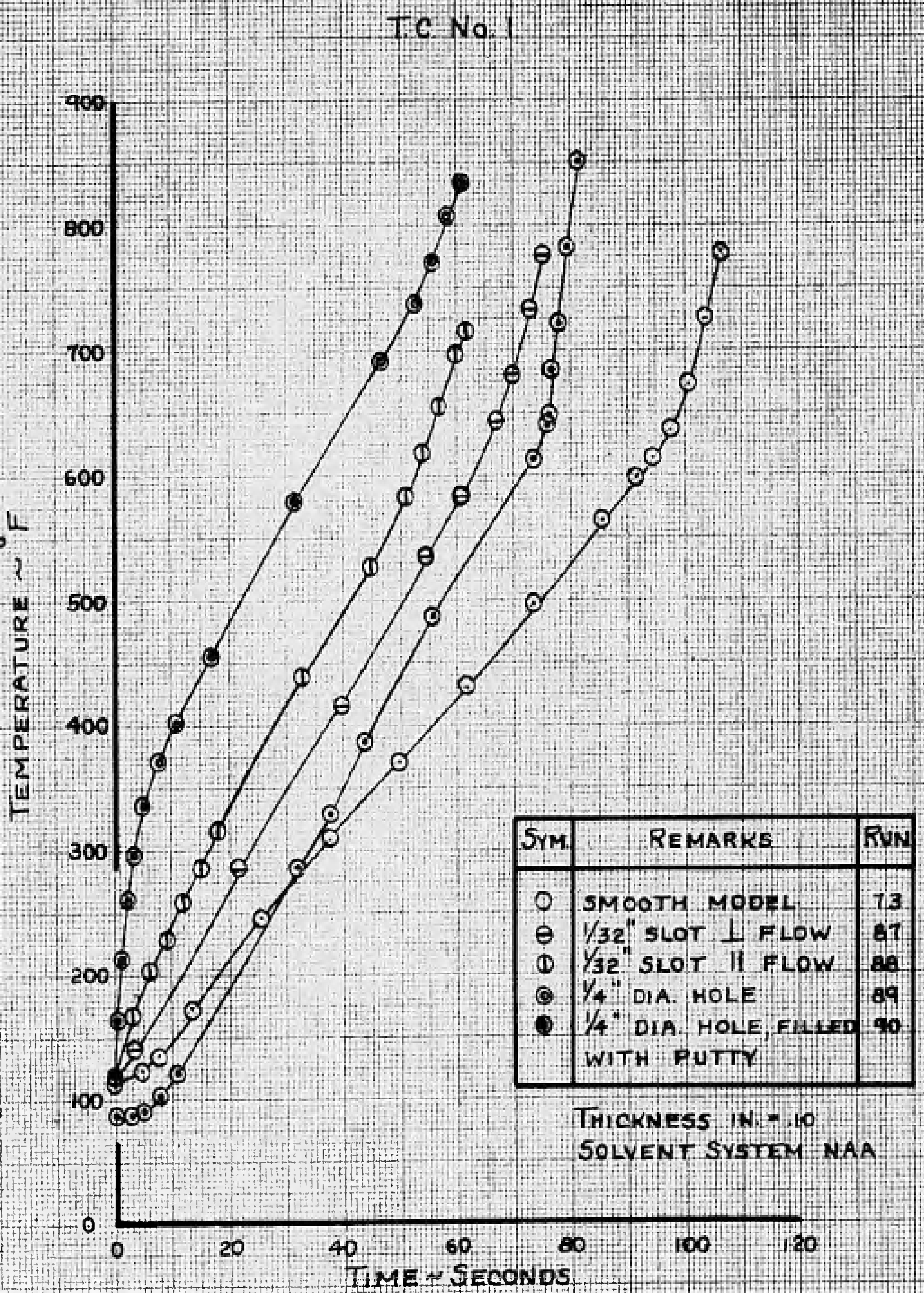

FIG. 32 EFFECTS OF SLOTS AND HOLES

TEST CONDITION 3a
T-500-4

FORM 1021-S

PREPARED BY:	NORTH AMERICAN AVIATION, INC.	PAGE NO. 58 OF
CHECKED BY:		REPORT NO. NA-64-177
DATE:		MODEL NO.

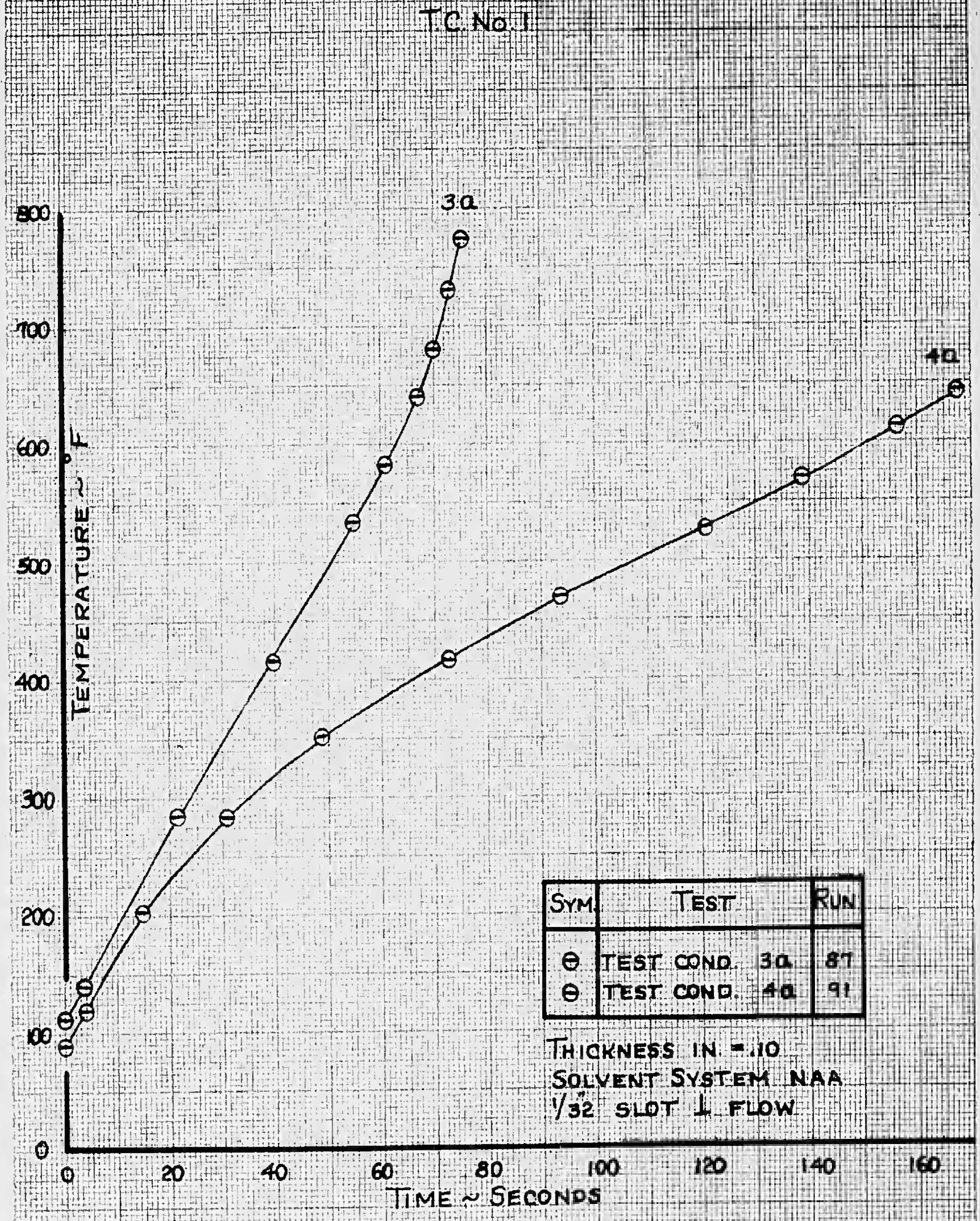

FIG. 33 EFFECT OF HEAT FLUX-SLOTTED MODEL

T-500-4A

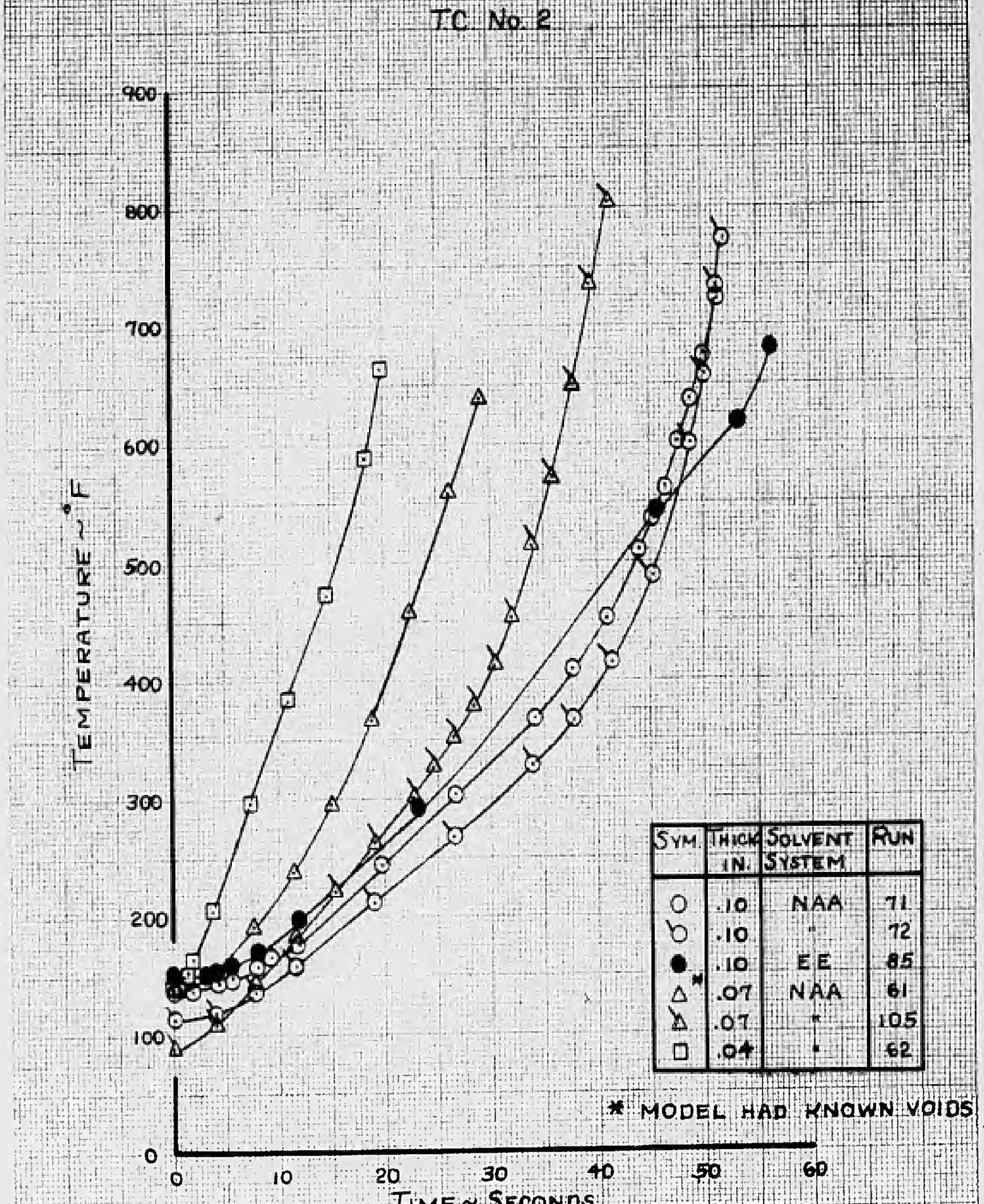

FIG. 34 EFFECT OF THICKNESS

TEST CONDITION 2a
T-500-4

FORM 1021-B

PREPARED BY:	NORTH AMERICAN AVIATION, INC.	PAGE NO. 60 OF
CHECKED BY:		REPORT NO NA-64-177
DATE:		MODEL NO.

T.C. No. 2

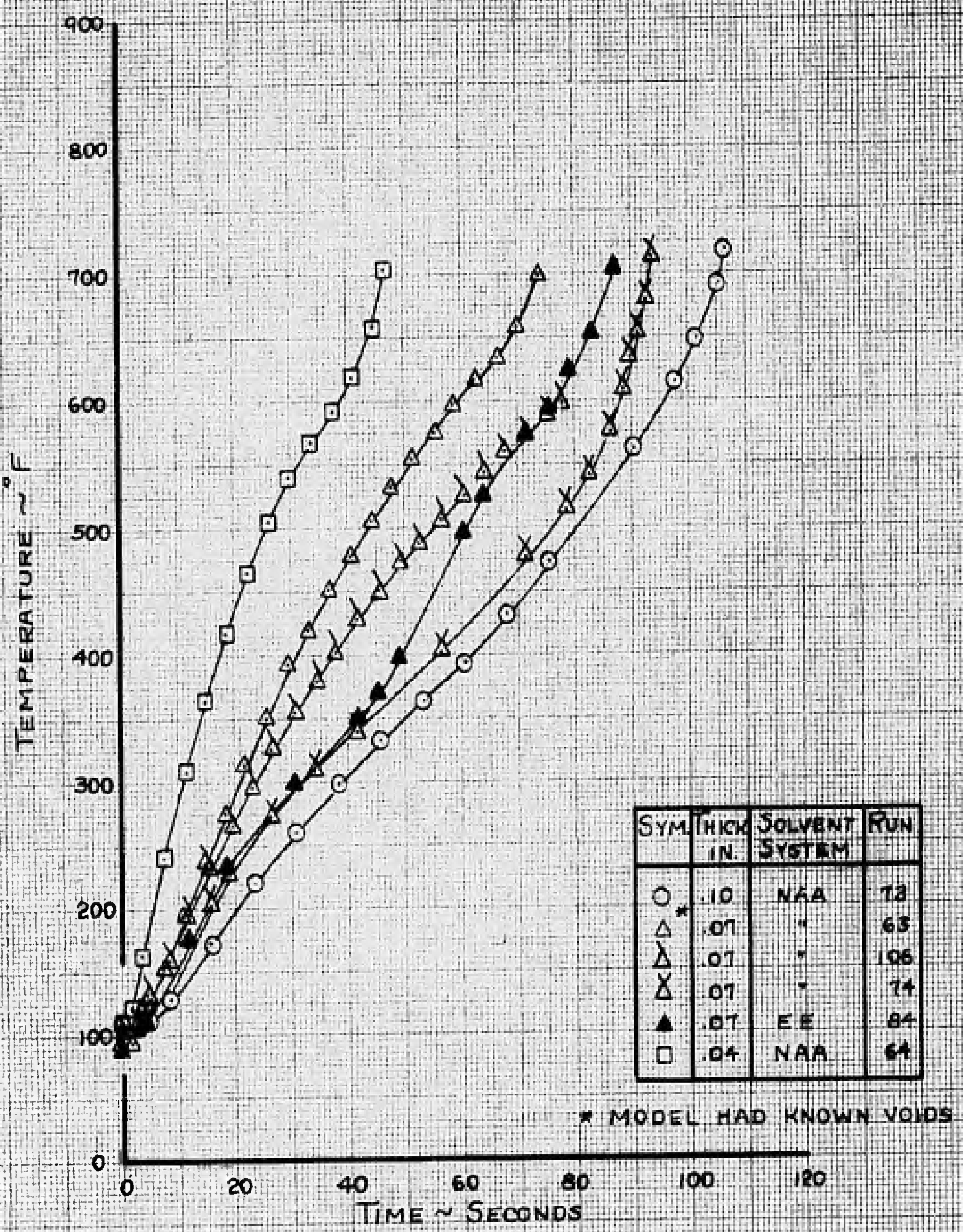

FIG. 35 EFFECT OF THICKNESS

TEST CONDITION 3a

T-500-4

FORM 1021-8

PREPARED BY:	NORTH AMERICAN AVIATION, INC.	PAGE NO. 61 OF
CHECKED BY:		REPORT NO. NA-64-177
DATE:		MODEL NO.

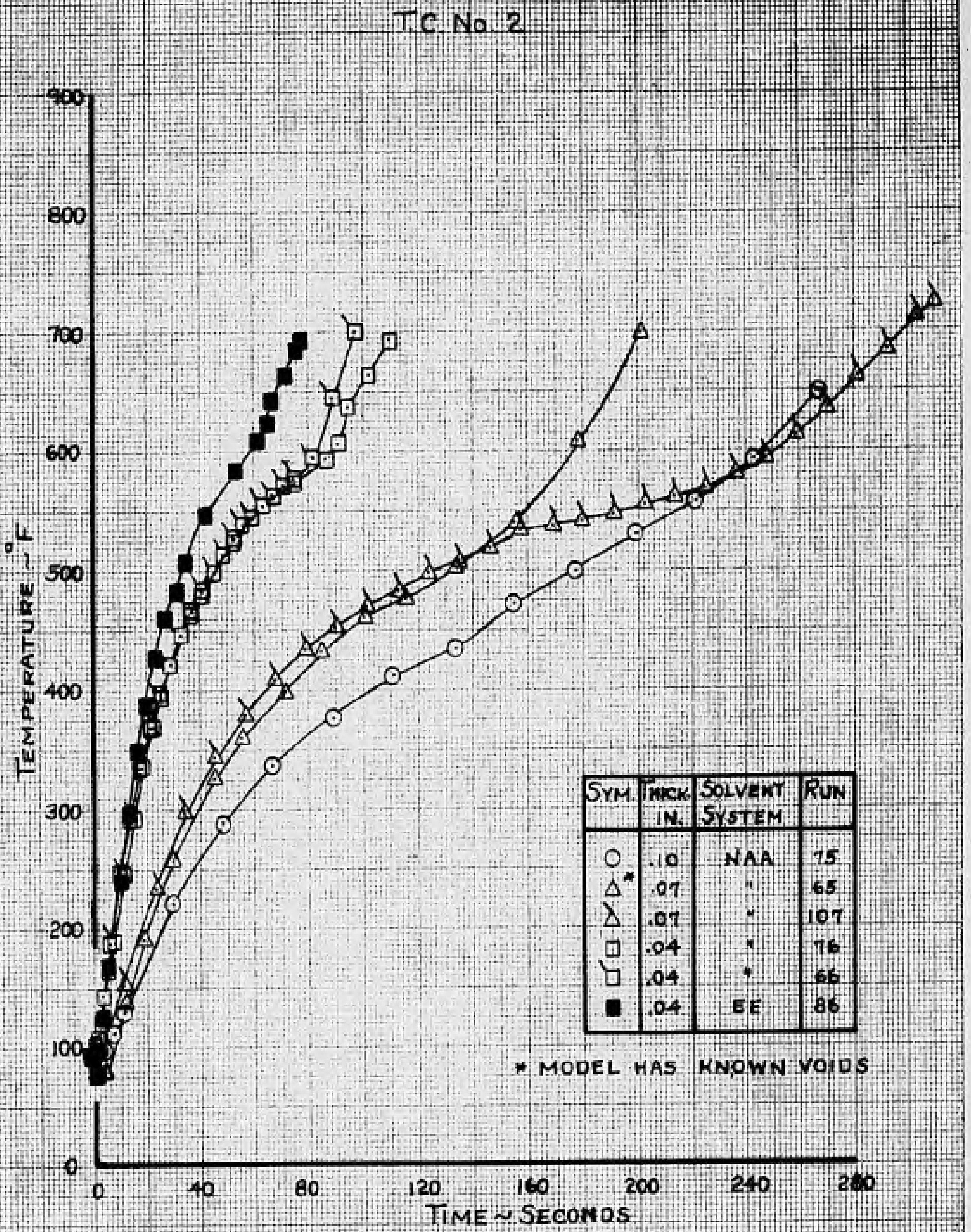

FIG. 36 EFFECT OF THICKNESS

TEST CONDITION 4a

T-500-4

FORM 1021-B

PREPARED BY:	NORTH AMERICAN AVIATION, INC.	PAGE NO. 62 OF
CHECKED BY:		REPORT NO. NA-64-177
DATE:		MODEL NO.

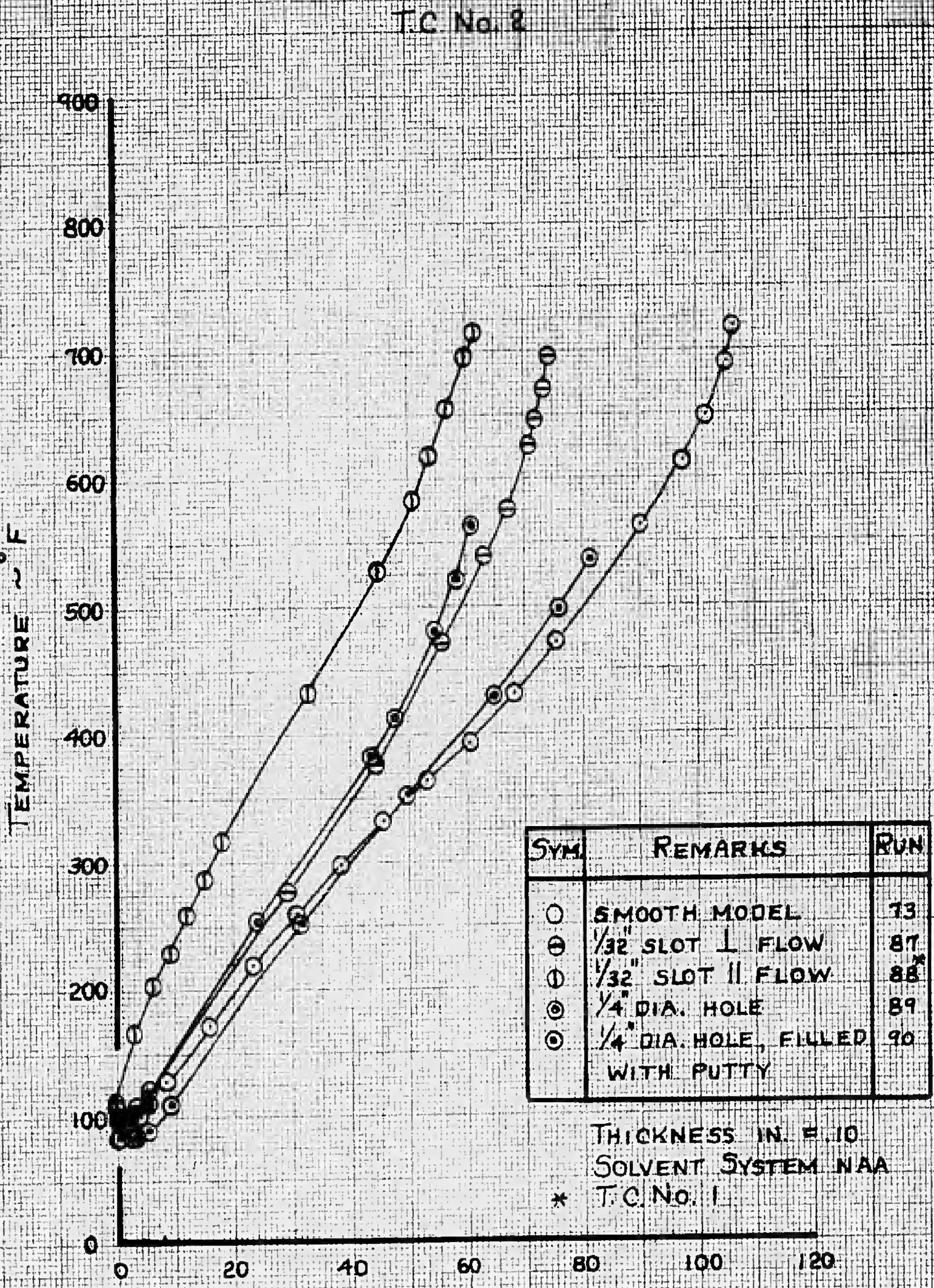

FIG. 37 EFFECTS OF SLOTS AND HOLES

TEST CONDITION 3a

T-500-4A

FORM 1021-9

PREPARED BY:	NORTH AMERICAN AVIATION, INC.	PAGE NO. 63 OF
CHECKED BY:		REPORT NO. NA-64-177
DATE:		MODEL NO.

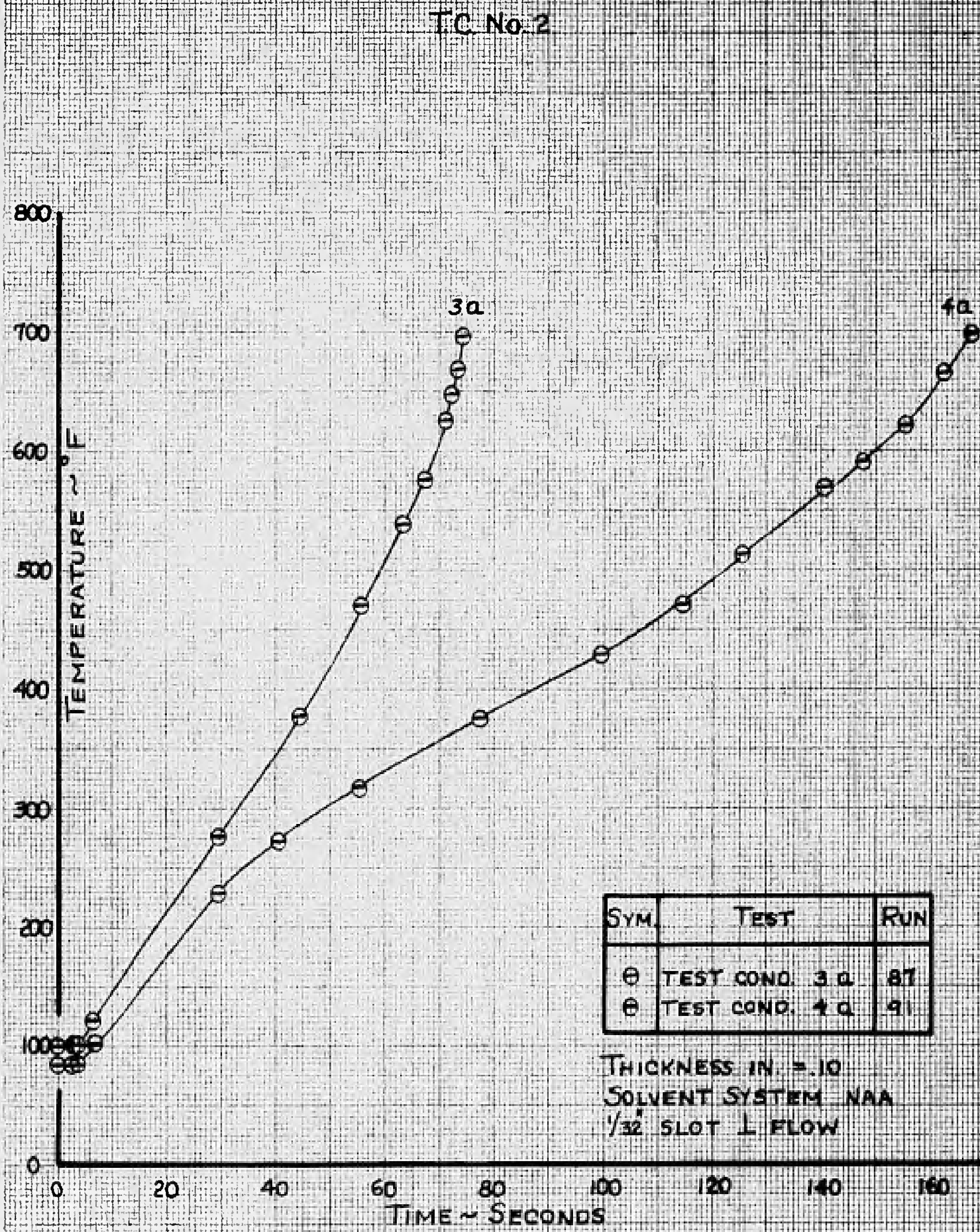

FIG. 38 EFFECT OF HEAT-FLUX SLOTTED MODEL

T-500-4A

PLASMA TUNNEL - FLAT PLATE EFFECTIVE HEAT OF ABLATION FIG. 39
CLEAN MODELS T-500-4a

○ $S_{INIT.}$ = 10 IN.
△ = .07 IN.
□ = .04 IN.
AVG. OF DATA POINTS OMITTING RUNS WITH VOIDS, SLOTS AND HOLES

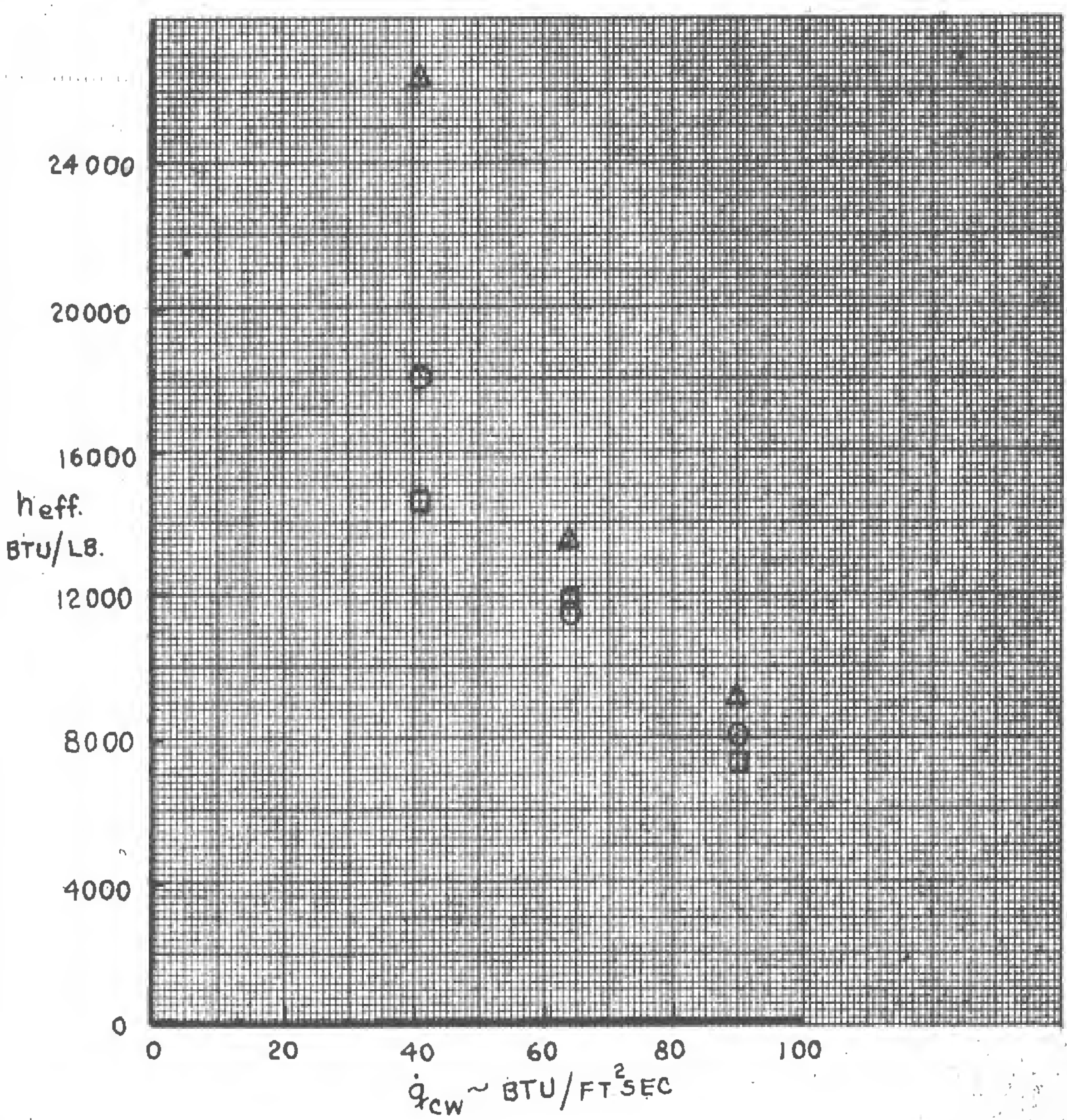

FIG. 40

PLASMA TUNNEL-FLAT PLATE EFFECTIVE HEAT OF ABLATION

CLEAN MODELS T-500-4a

x AVERAGE OF DATA POINTS

I SPREAD OF DATA

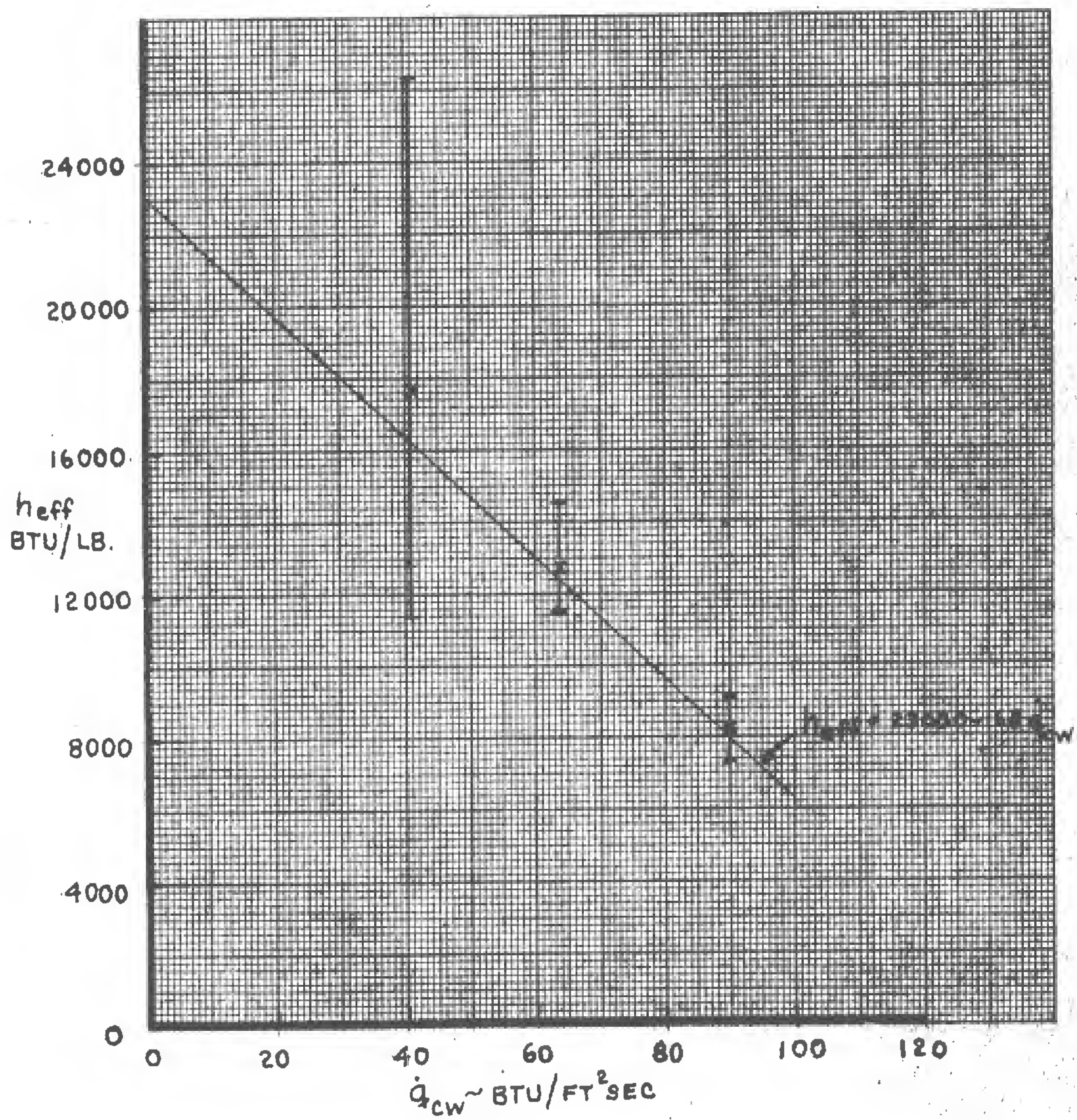

FIG. 41

PLASMA TUNNEL - FLAT PLATE EFFECTIVE HEAT OF ABLATION

MODELS WITH VOIDS, SLOTS, HOLES, T-500-4a

○ MODELS WITH SLOTS AND HOLES

▲ " " VOIDS

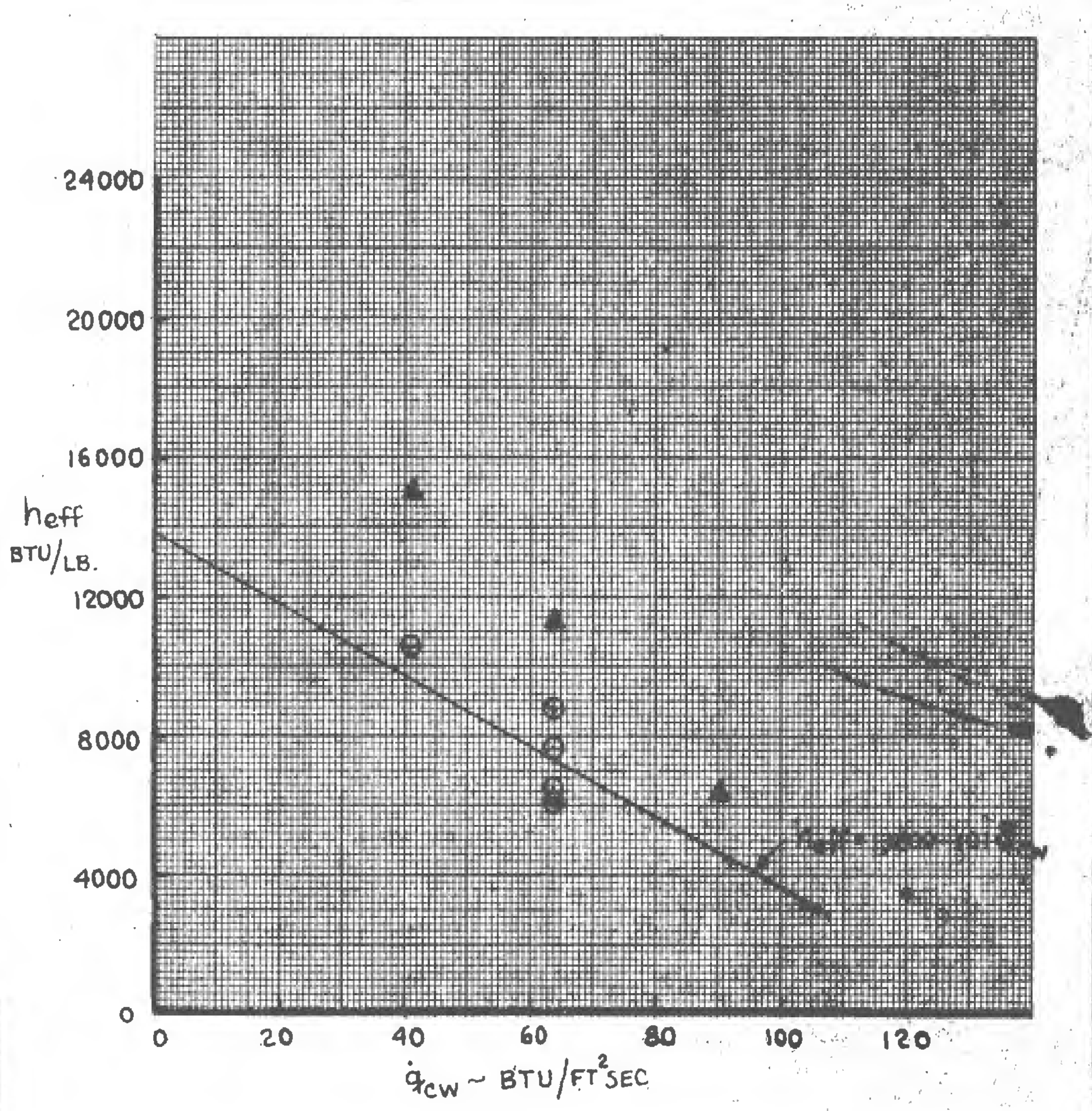

FORM 1021-S

PREPARED BY:	NORTH AMERICAN AVIATION, INC.	PAGE NO. 67 OF
CHECKED BY:		REPORT NO. NA-64-177
DATE:	T-500 4 A	MODEL NO.

FIG. 42

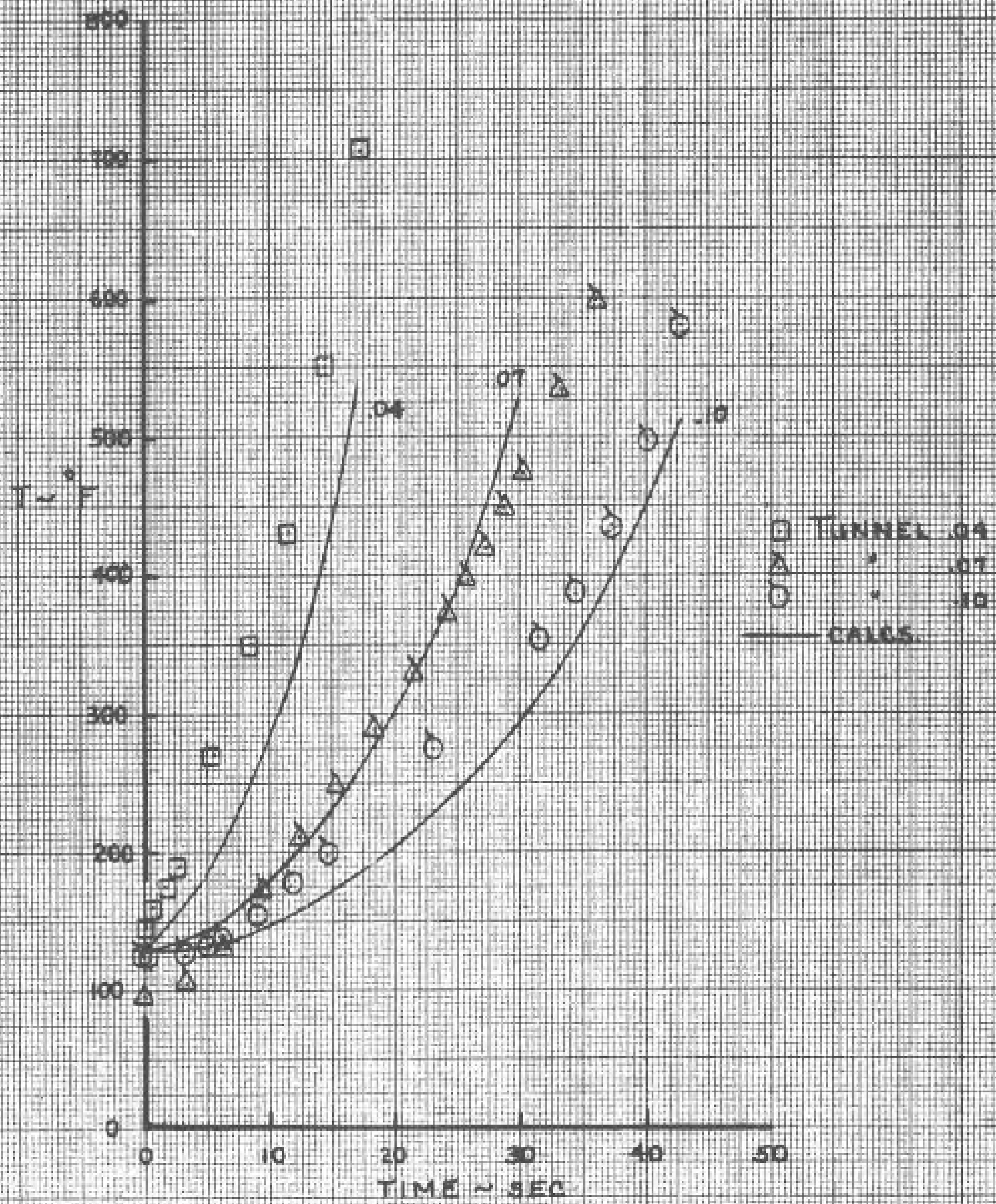

TEST COND. 2 A

FLAT PLATE SUBSTRATE TEMPERATURE CORRELATIONS

FIG. [illegible]

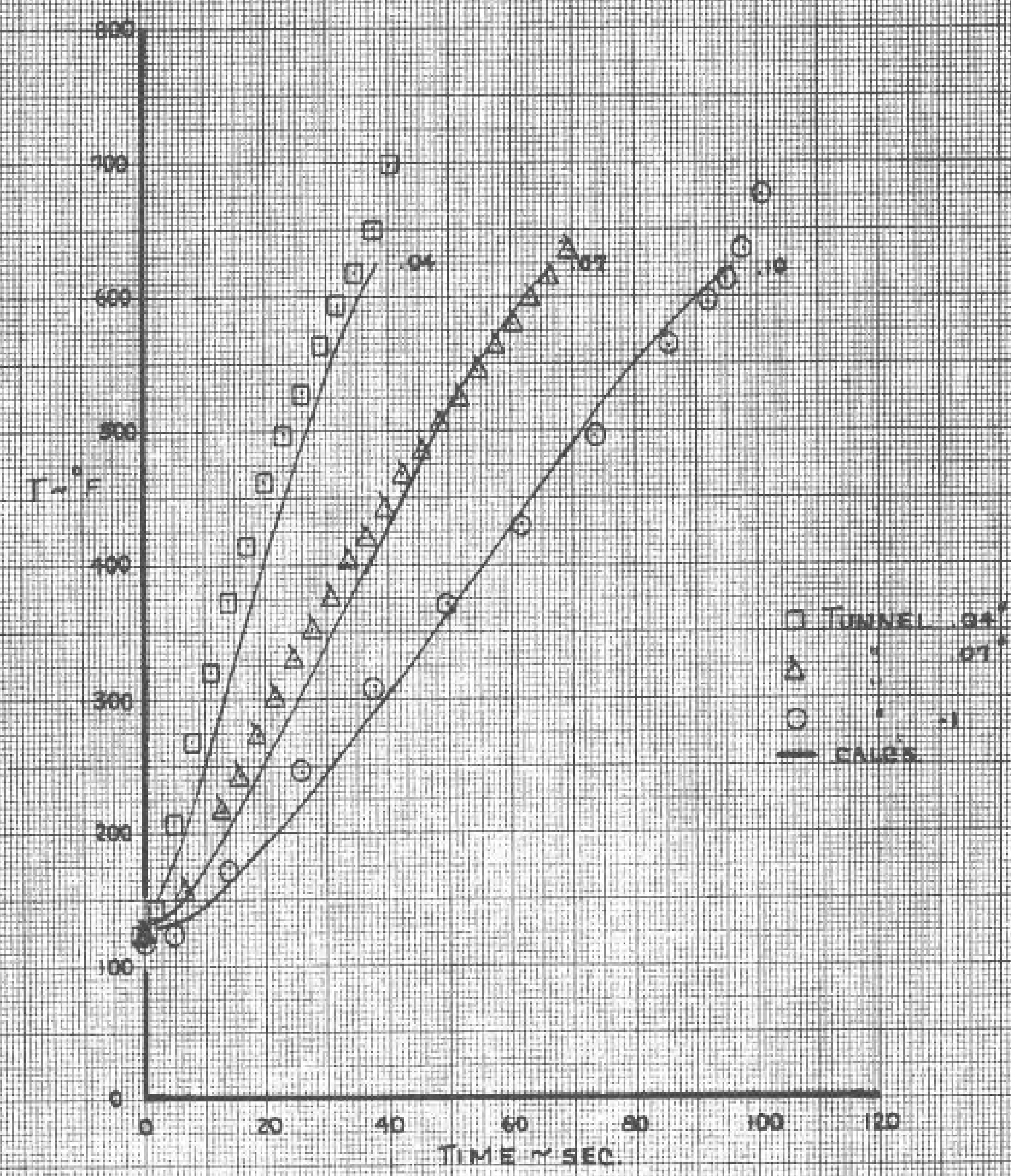

TEST COND. 3A

FLAT PLATE SUBSTRATE TEMPERATURE CORRELATIONS

FORM 1021-B

PREPARED BY:	NORTH AMERICAN AVIATION, INC.	PAGE NO. 69 OF
CHECKED BY:		REPORT NO. NA-64-177
DATE:	T- 500 - 4A	MODEL NO.

FIG. 44

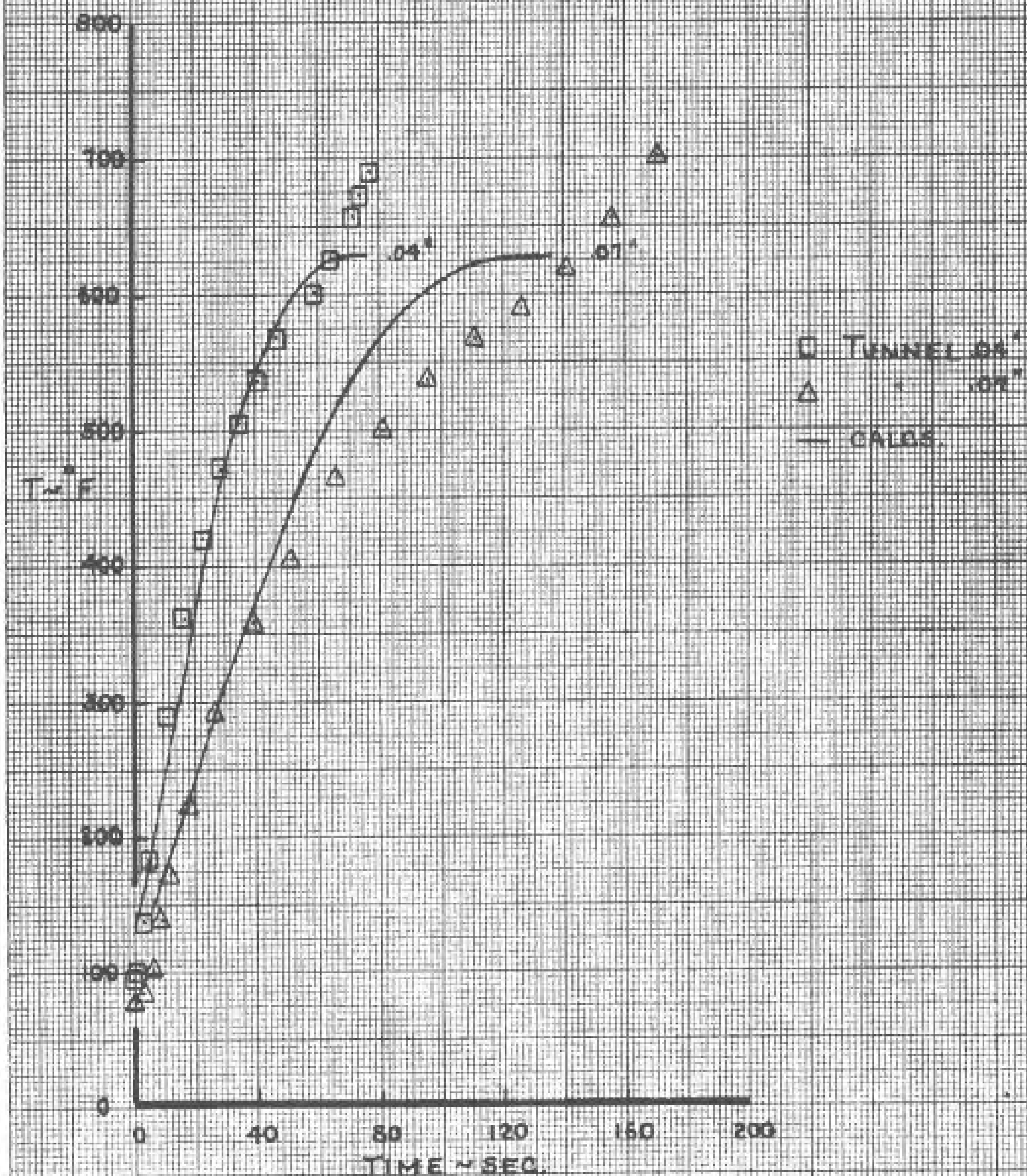

TEST COND. 4 A

FLAT PLATE SUBSTRATE TEMPERATURE CORRELATIONS

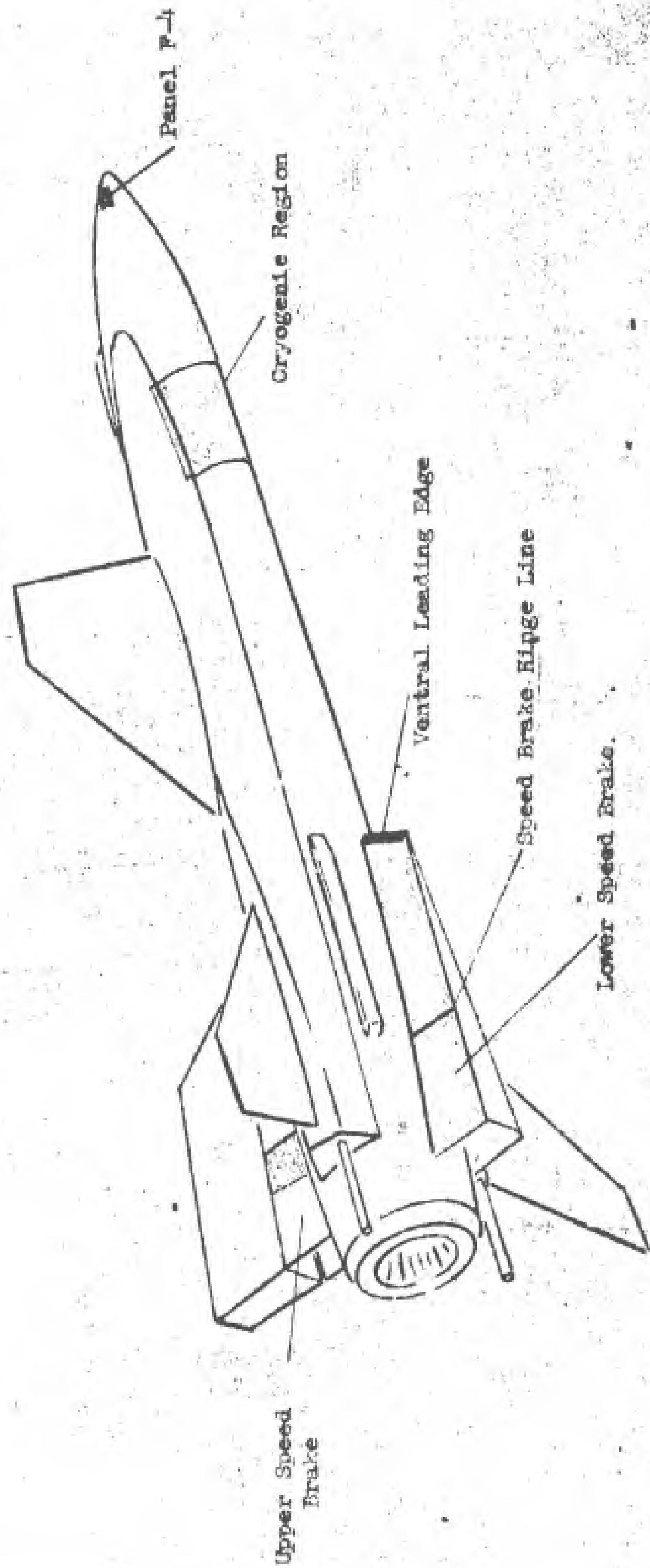

Figure 45.- Ablation Material Test Regions on X-15

FORM 1021-S

PREPARED BY:	**NORTH AMERICAN AVIATION, INC.**	PAGE NO. 71 OF
CHECKED BY:	FLT. TEST #1 (FLT. 1-37-59)	REPORT NO NA-64-177
DATE:	SPEED BRAKE, CORK	MODEL NO.

FIG. 4[illegible]

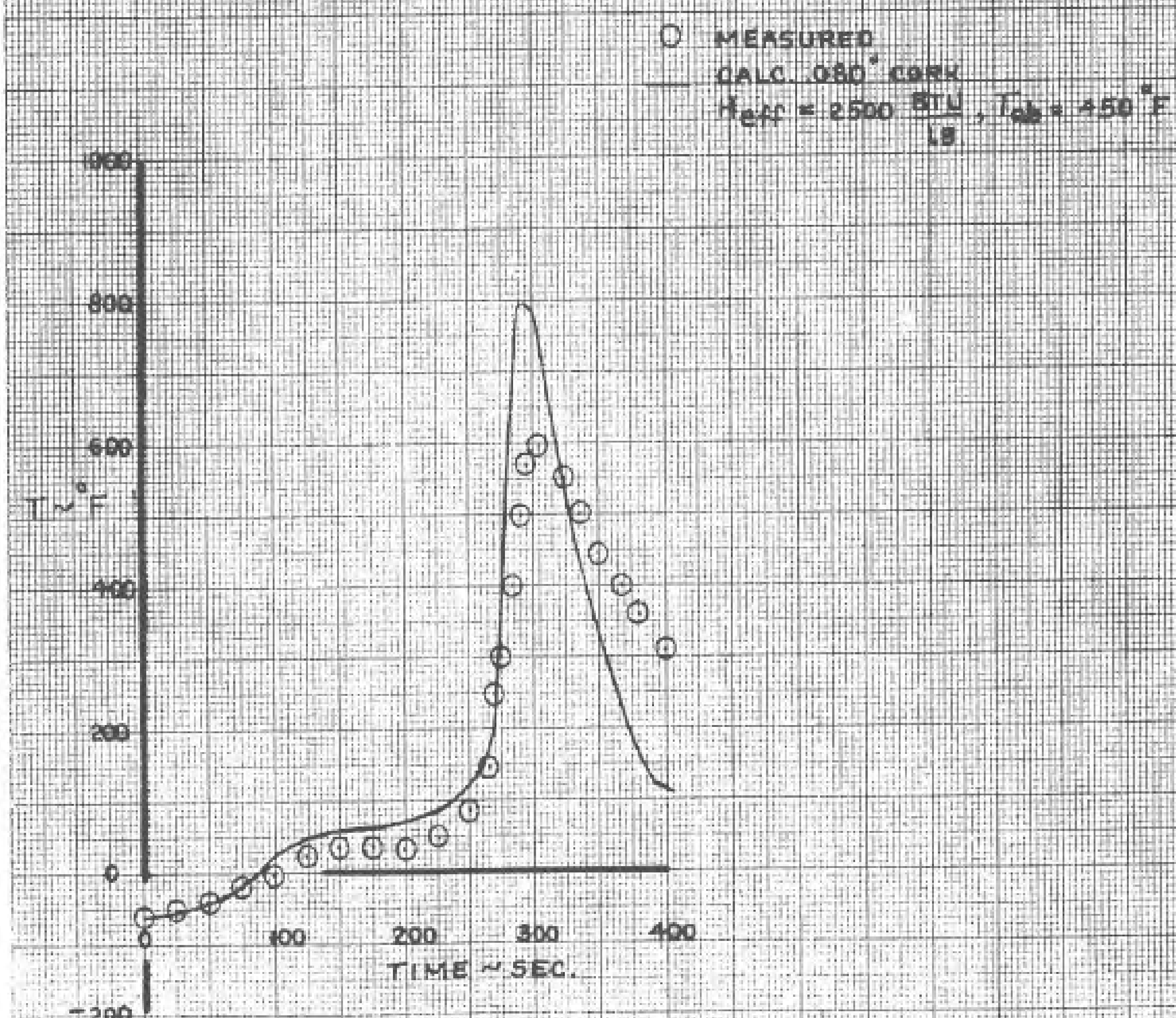

FORM 1021-B

PREPARED BY:	NORTH AMERICAN AVIATION, INC.	PAGE NO. 72 OF
CHECKED BY:	FLT. TEST # 2 (FLT. 1-38-61)	REPORT NO NA-64-177
DATE:	SPEED BRAKE BARE SKIN	MODEL NO.

FIG. 47

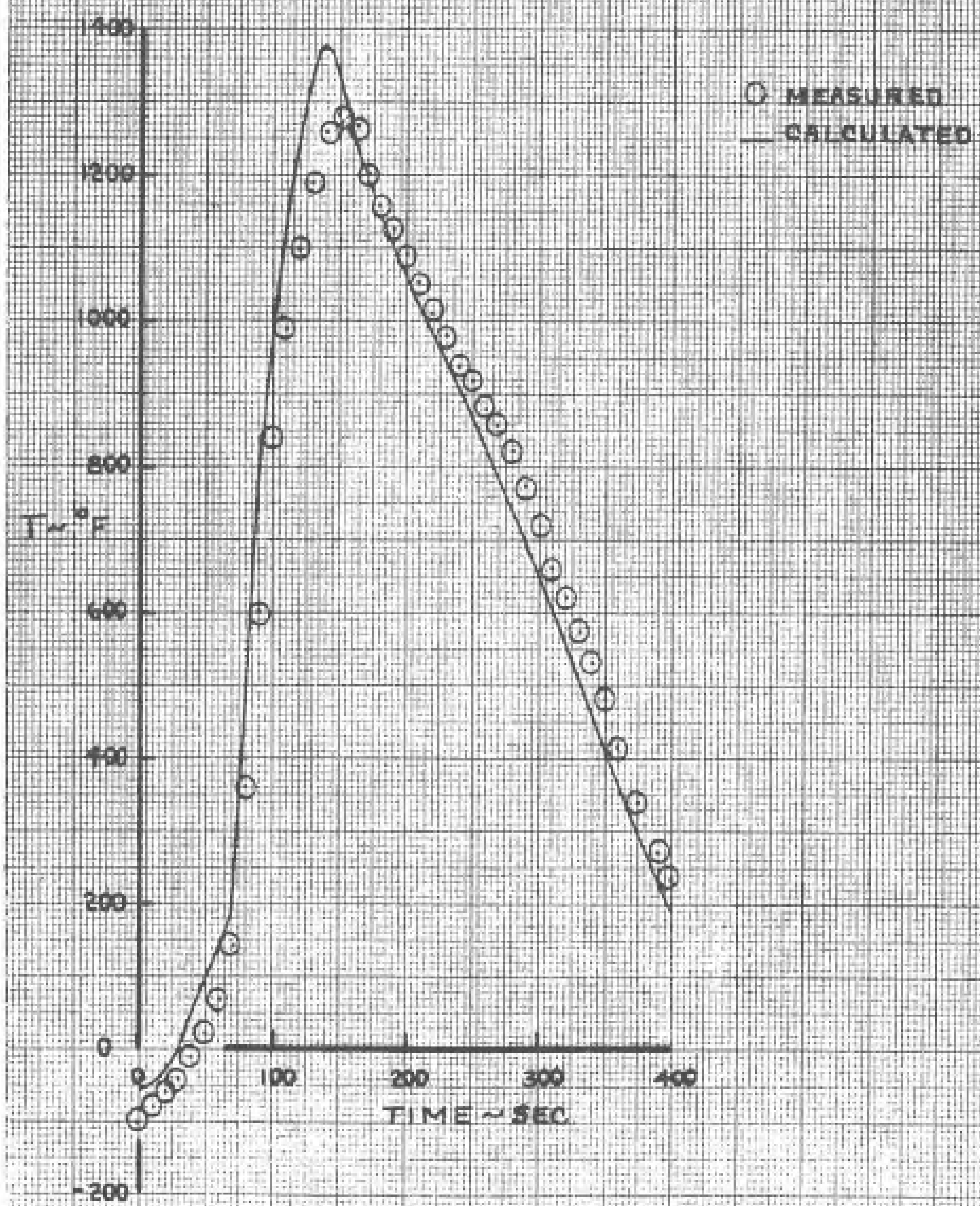

FORM 1021-B

PREPARED BY:	NORTH AMERICAN AVIATION, INC.	PAGE NO. 73 OF
CHECKED BY:	FLT. TEST #2 (FLT. 1-38-61)	REPORT NO. NA-64-177
DATE:	VENTRAL STAGNATION LINE, CORK	MODEL NO

FIG.

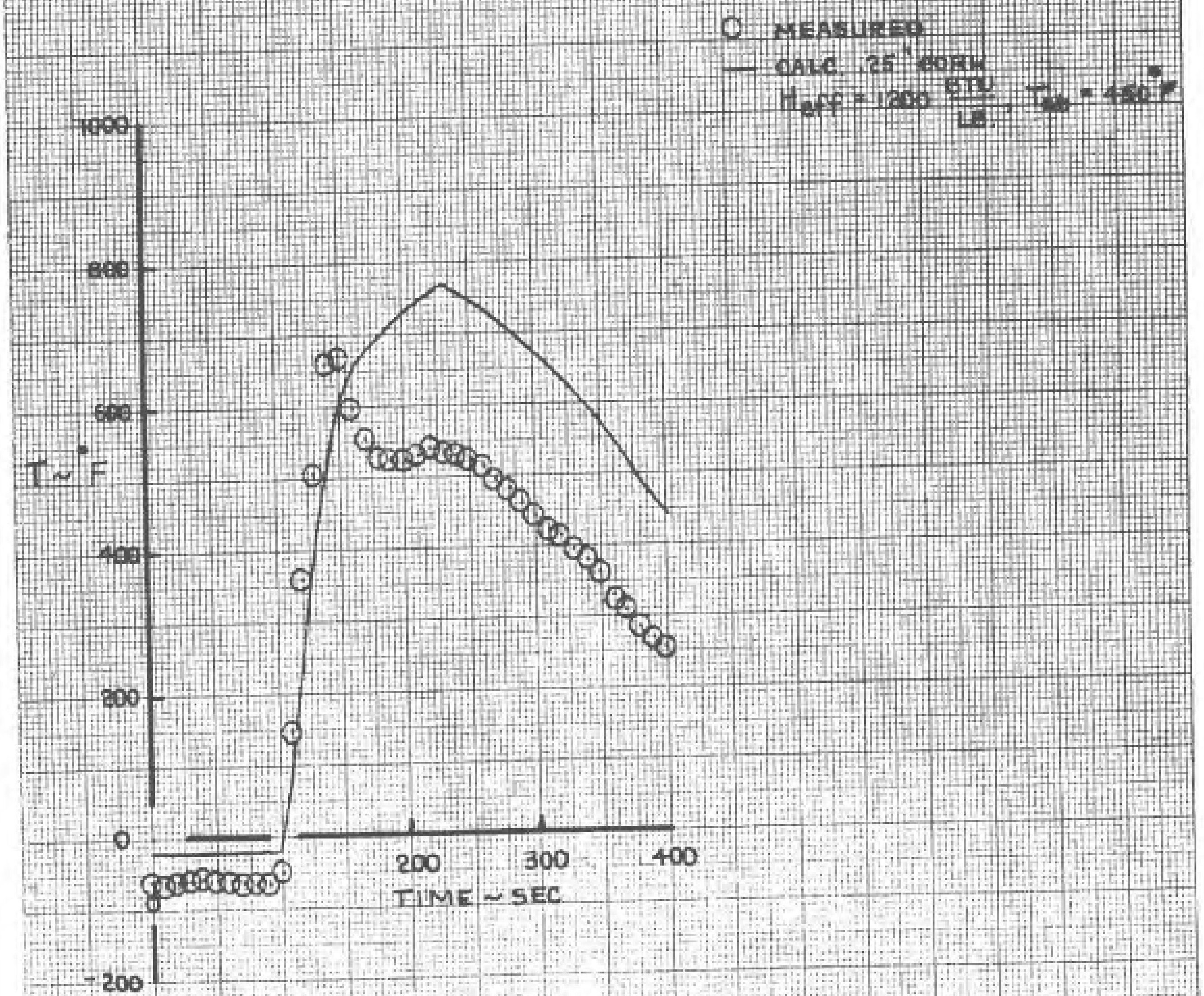

FORM 1021-B

PREPARED BY:	NORTH AMERICAN AVIATION, INC.	PAGE NO. 74 OF
CHECKED BY:	FLT. TEST #3 (FLT. 1-39-63)	REPORT NO. NA-64-177
DATE:	VENTRAL STAGNATION LINE	MODEL NO.

T-500-6A

FIG. 49

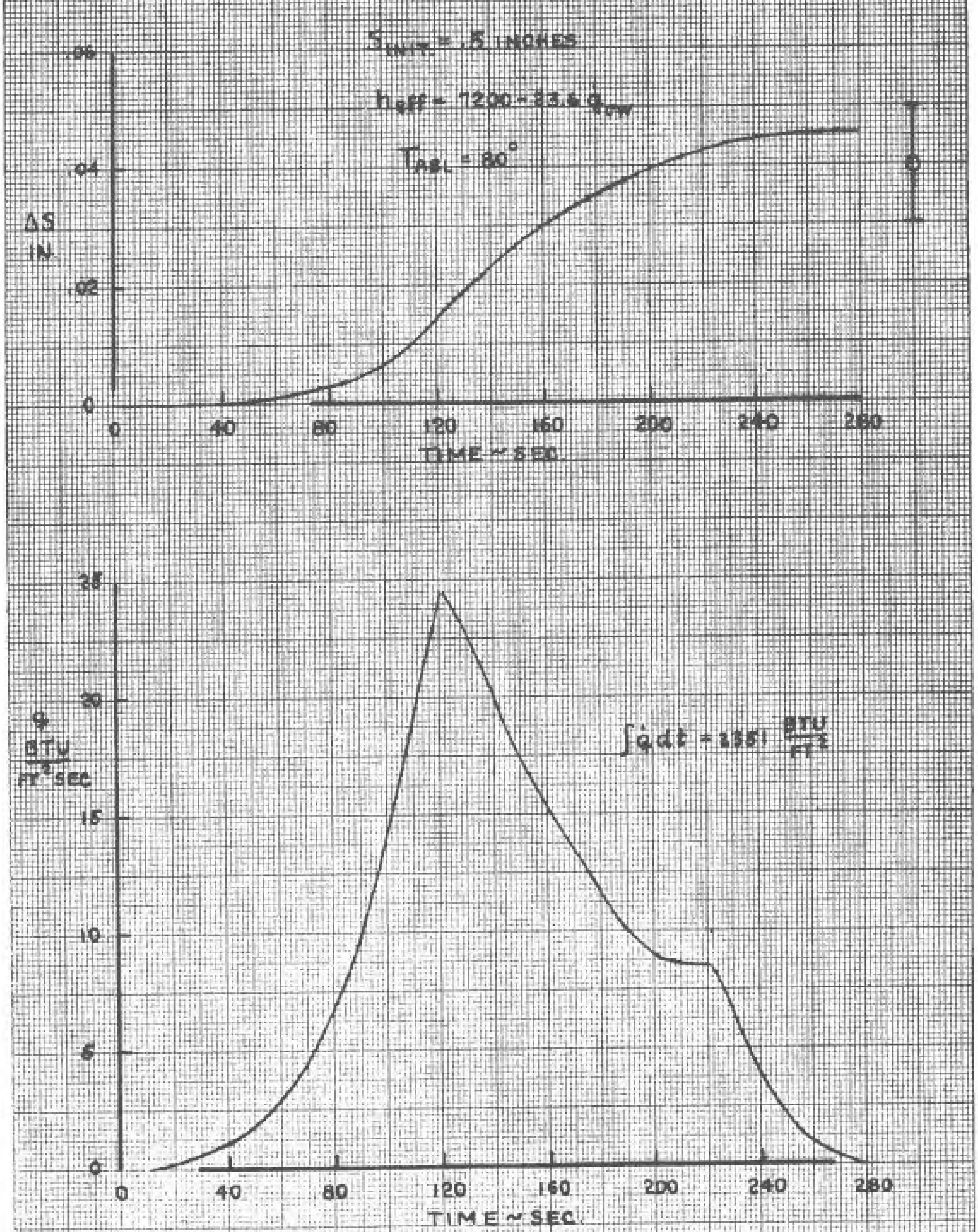

FORM 1021-S

PREPARED BY:	**NORTH AMERICAN AVIATION, INC.**	PAGE NO. 75 OF
CHECKED BY:	FLT. TEST #3 (FLT. 1-39-63)	REPORT NO NA-64-177
DATE:	SPEED BRAKE - T-500-4	MODEL NO.

FIG. 50

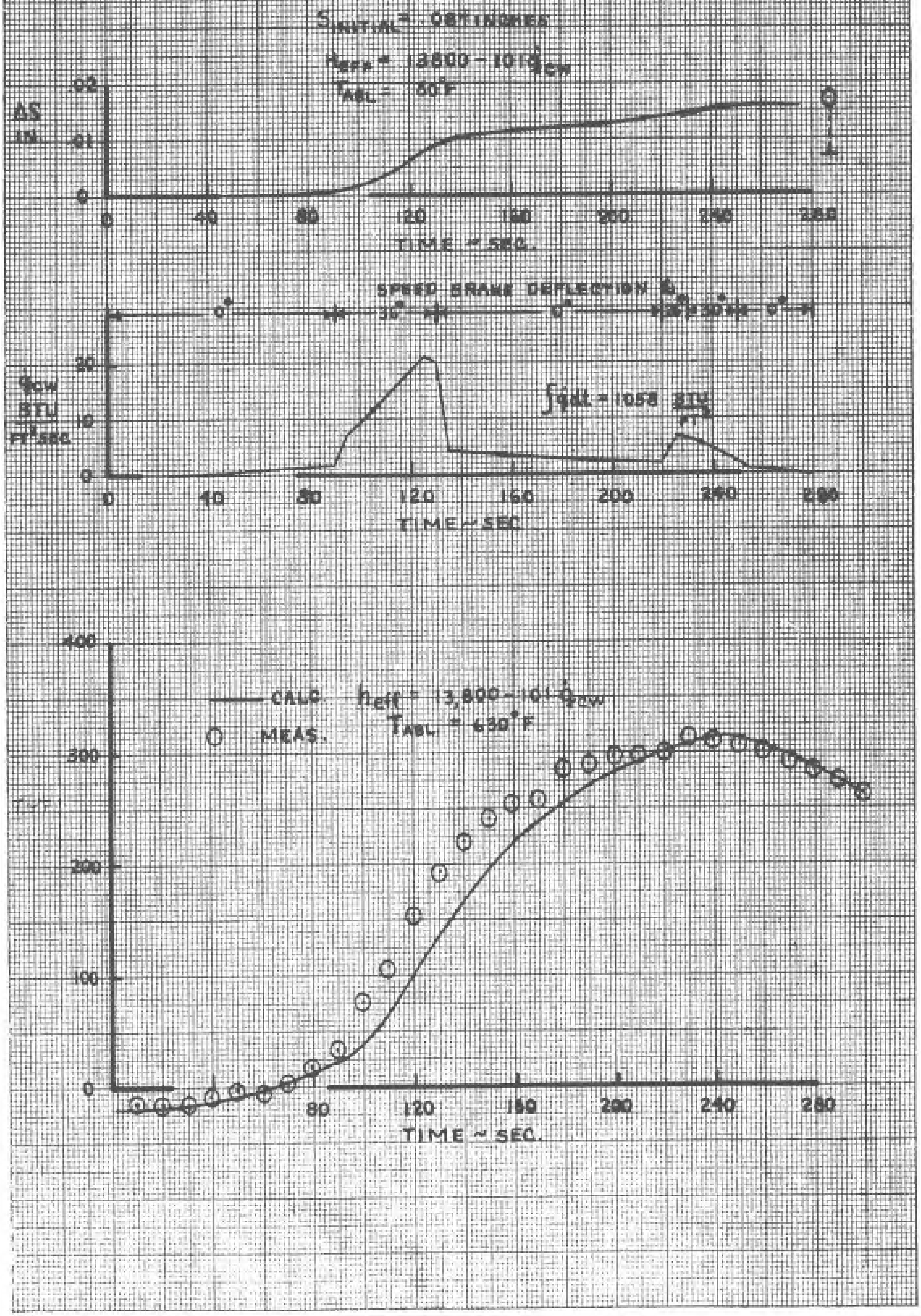

FORM 1021-8

PREPARED BY:	NORTH AMERICAN AVIATION, INC.	PAGE NO. 76 OF
CHECKED BY:	FLT. TEST #4 FLT. 1-40-64)	REPORT NO. NA-64-177
DATE:	SPEED BRAKE T-500-4A	MODEL NO.

FIG. 8

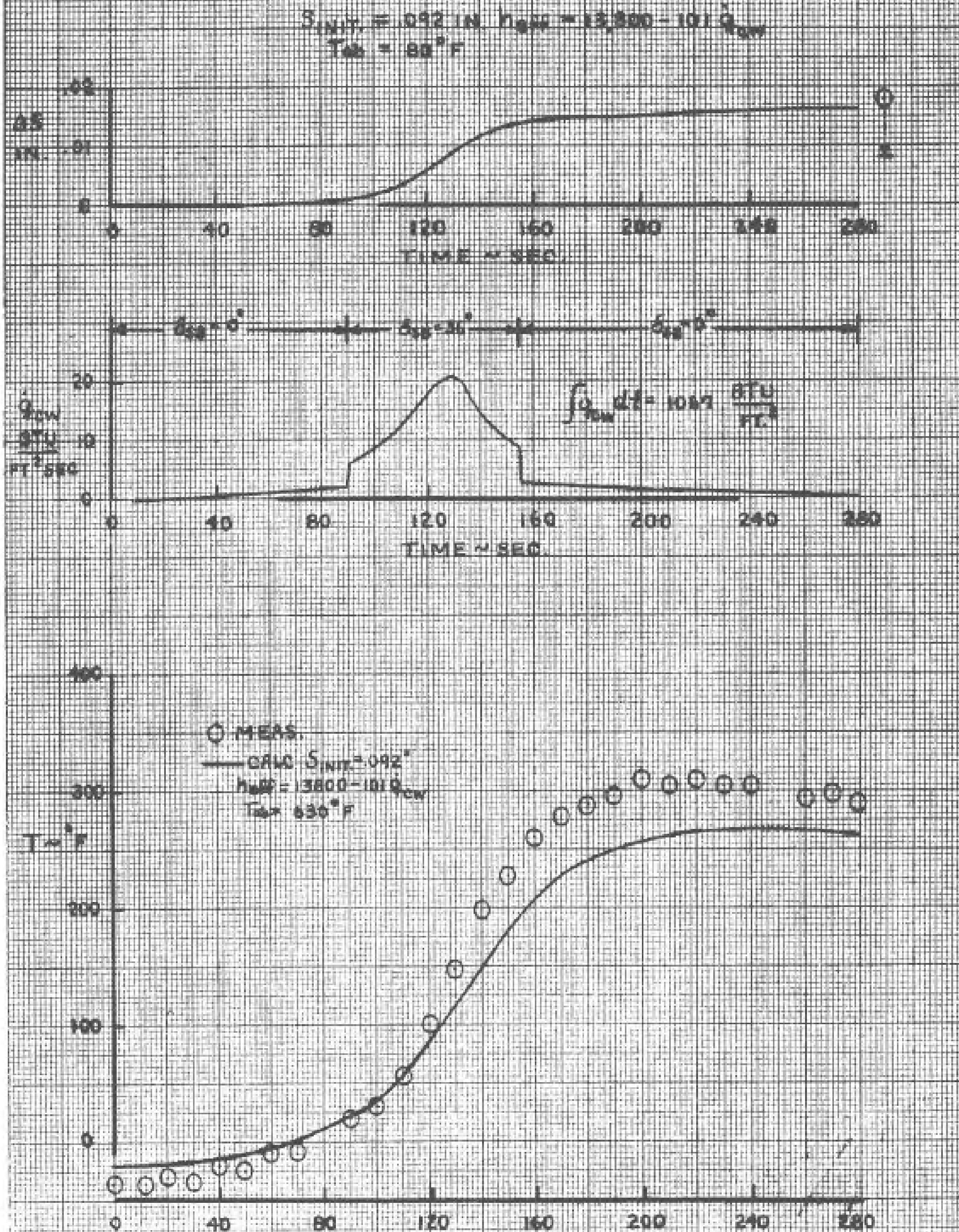

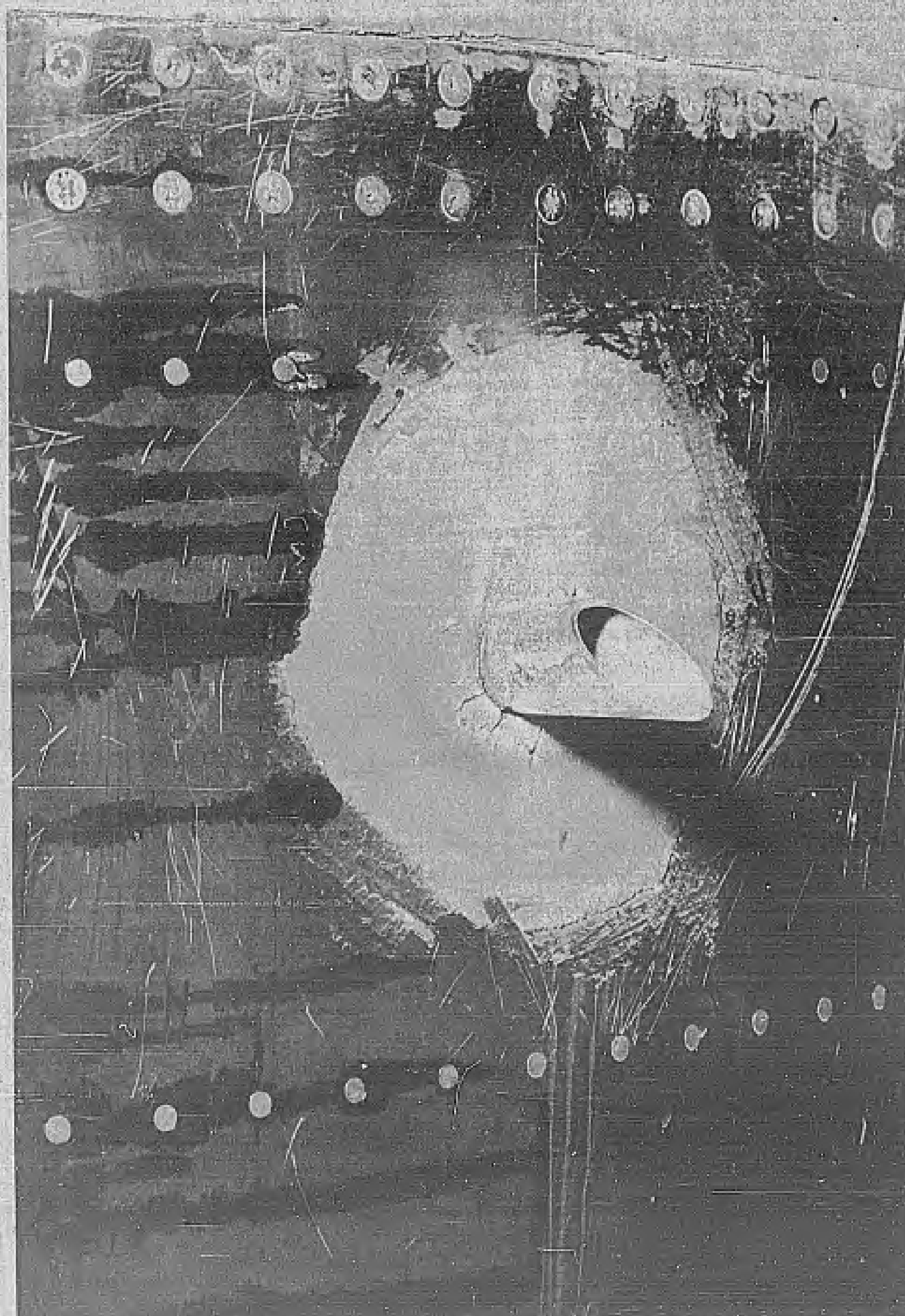

Figure 57 - Flight Test No. 5 Heating Pattern Near Protuberance

FORM 1021-S

PREPARED BY:	**NORTH AMERICAN AVIATION, INC.**	PAGE NO. 78 OF
CHECKED BY:	FLIGHT TEST #5 (FLT. 1-42-66)	REPORT NO. NA-64-177
DATE:	PANEL F-4 TEST	MODEL NO.

FIG. 53

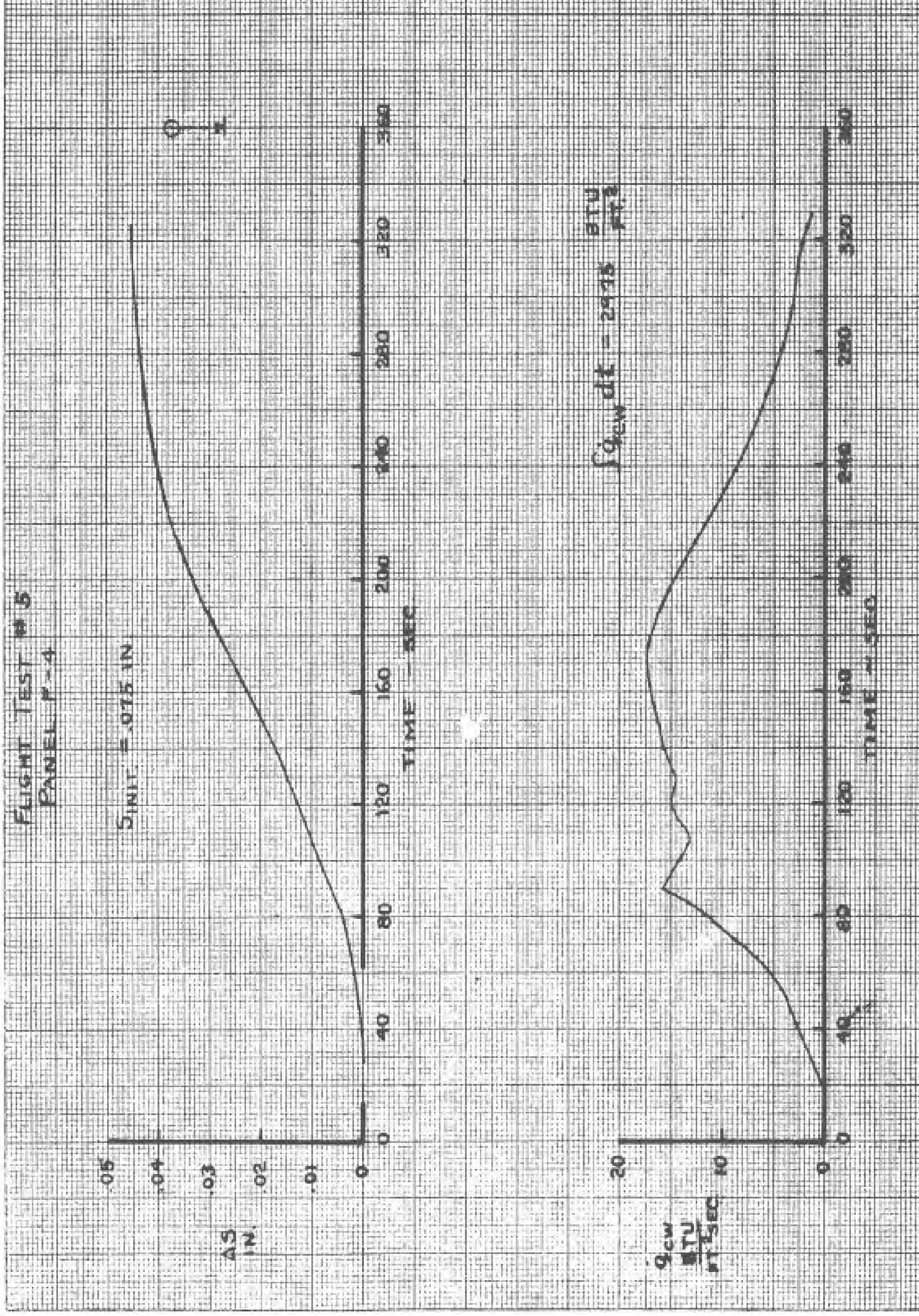

FIG. 54

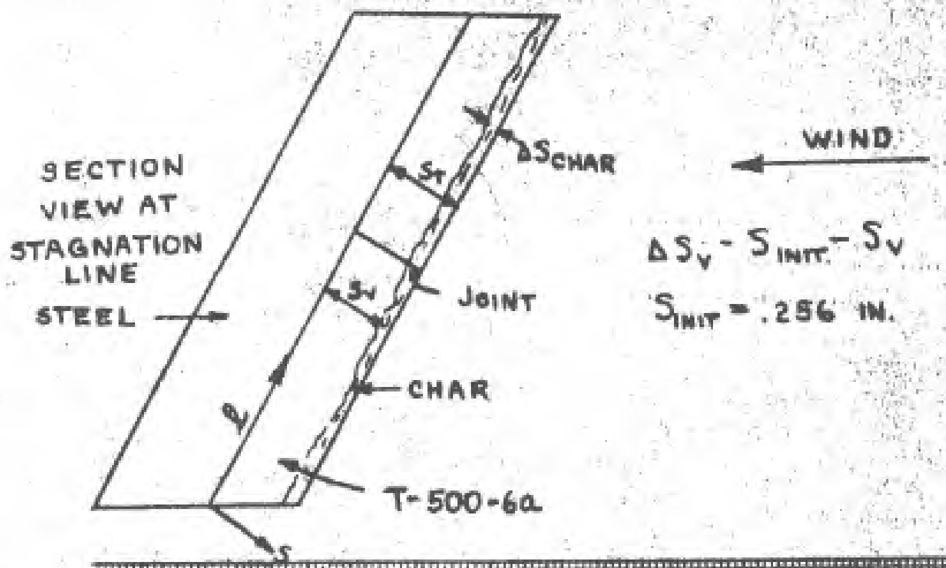
SECTION VIEW AT STAGNATION LINE
STEEL
WIND
ΔS_{CHAR}
S_T
S_V
JOINT
CHAR
T-500-6a
ℓ
S
$\Delta S_V = S_{INIT} - S_V$
$S_{INIT} = .256$ IN.

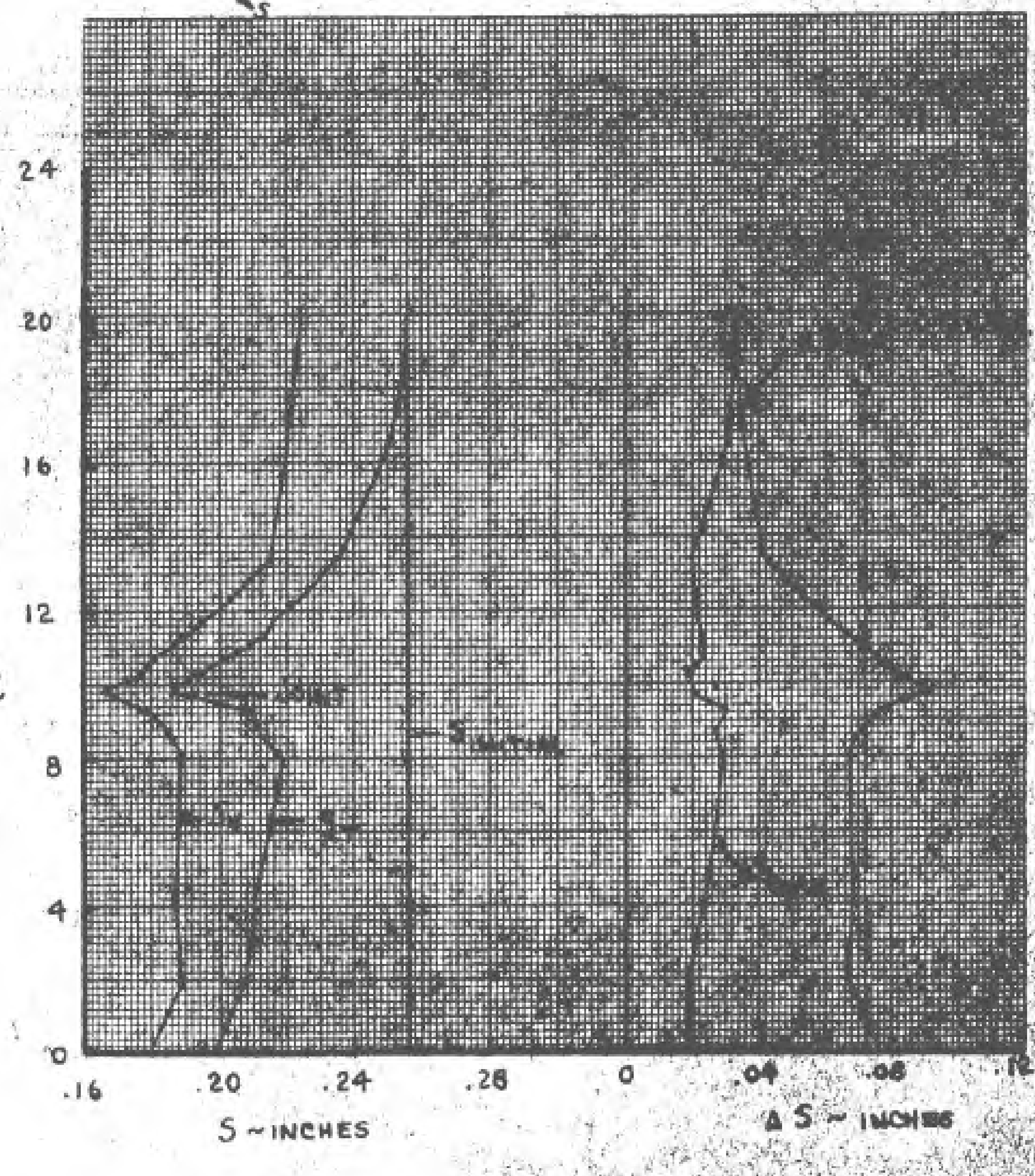
24
20
16
12
8
4
0
ℓ
JOINT
$S_{INITIAL}$
S_V
S_T
.16
.20
.24
.28
0
.04
.08
.12
S ~ INCHES
ΔS ~ INCHES

FORM 1021-B

PREPARED BY:	NORTH AMERICAN AVIATION, INC.	PAGE NO. 80 OF
CHECKED BY:	FLIGHT TEST #6 (FLT. 3-25-42)	REPORT NO NA-64-177
DATE:	VENTRAL STAGNATION LINE T-500-6A	MODEL NO.

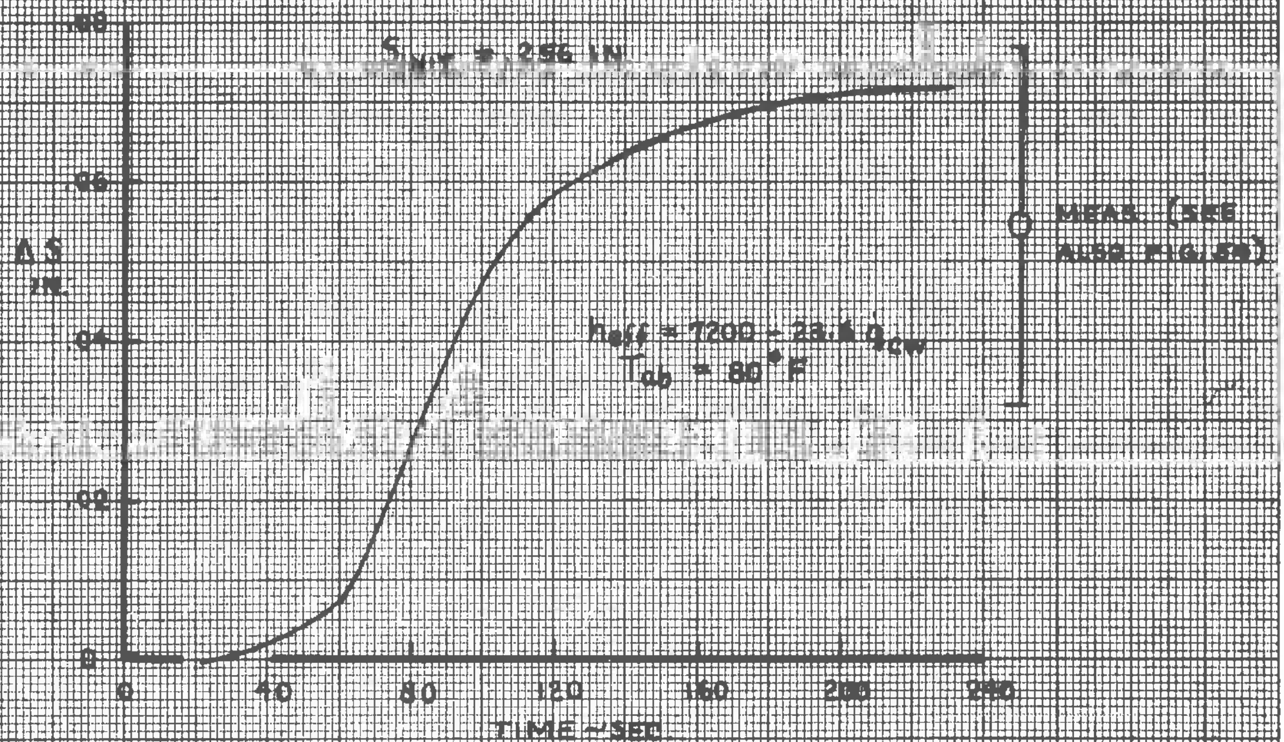

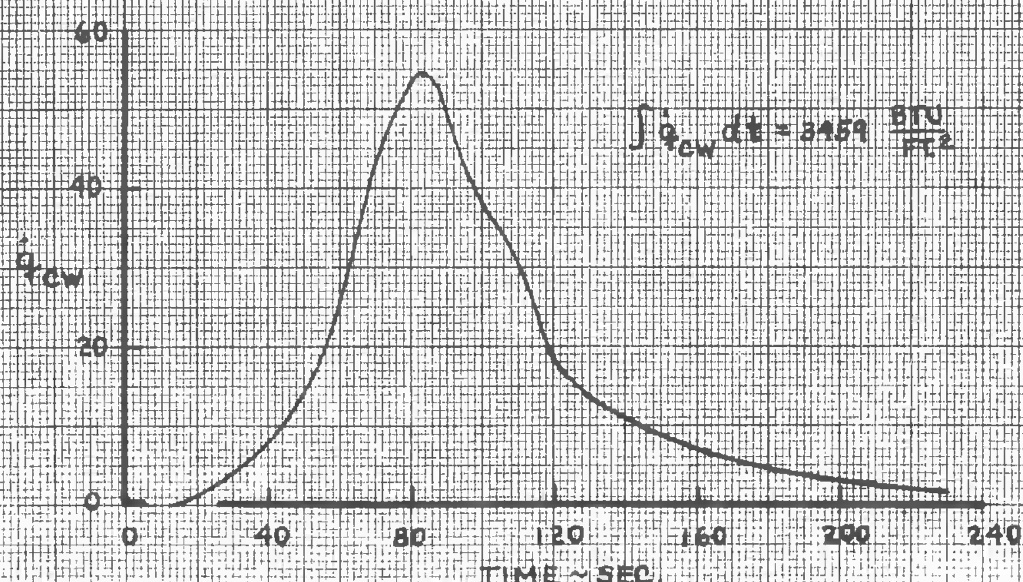

PREPARED BY: B	NORTH AMERICAN AVIATION, INC.	PAGE NO. 81 OF
CHECKED BY:	FIG. 56 FLIGHT TEST NO. 6 PANEL F-4	REPORT NO. NA-64-177
DATE: 2/5/64	ABLATION MATERIAL MEASUREMENTS	MODEL NO.

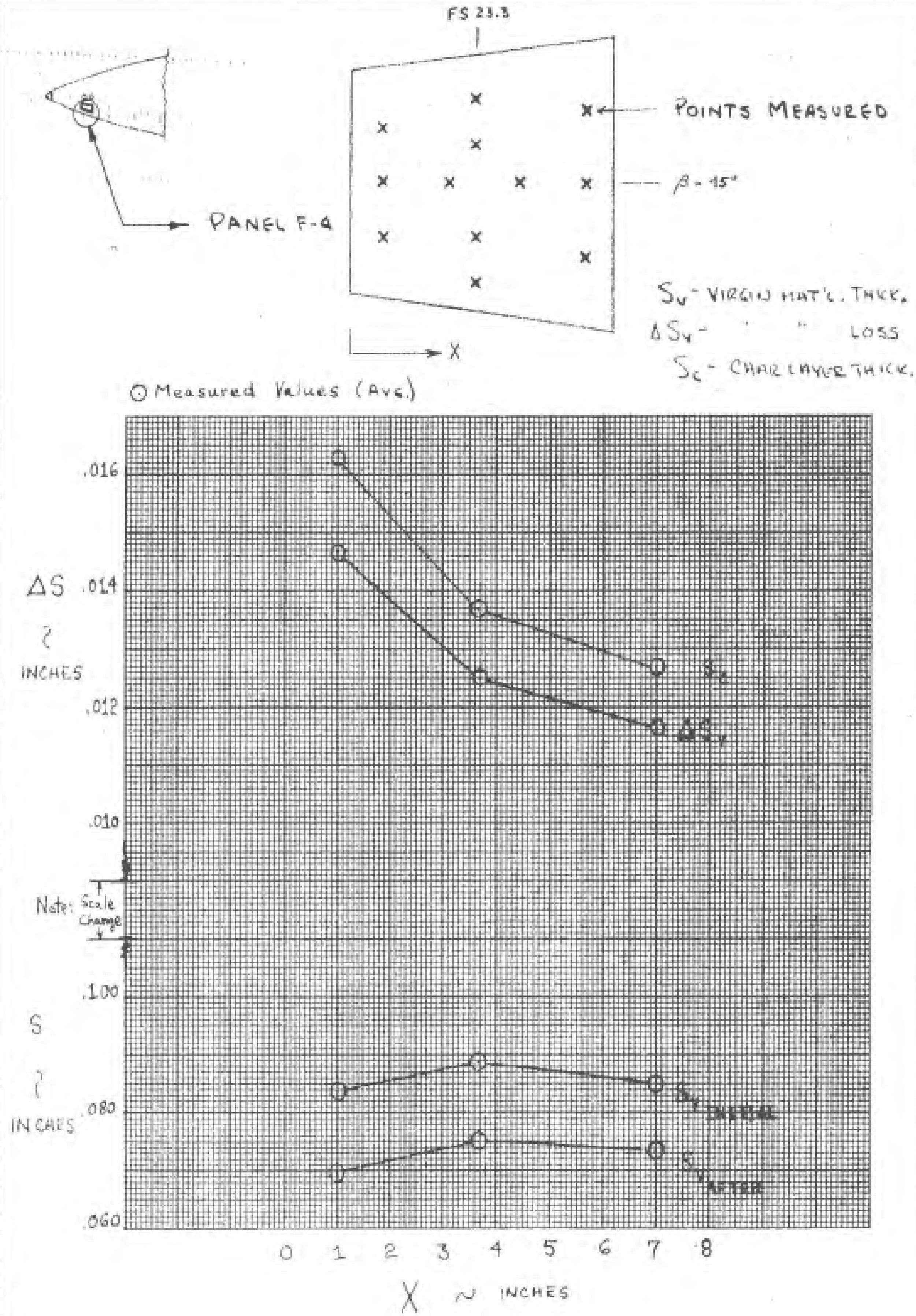

FORM 1021-S

PREPARED BY:	**NORTH AMERICAN AVIATION, INC.**	PAGE NO. 82 OF
CHECKED BY:	FLIGHT TEST # 6 (FLT. 3-25-42)	REPORT NO NA-64-177
DATE:	PANEL F-4 T-500 4A	MODEL NO.

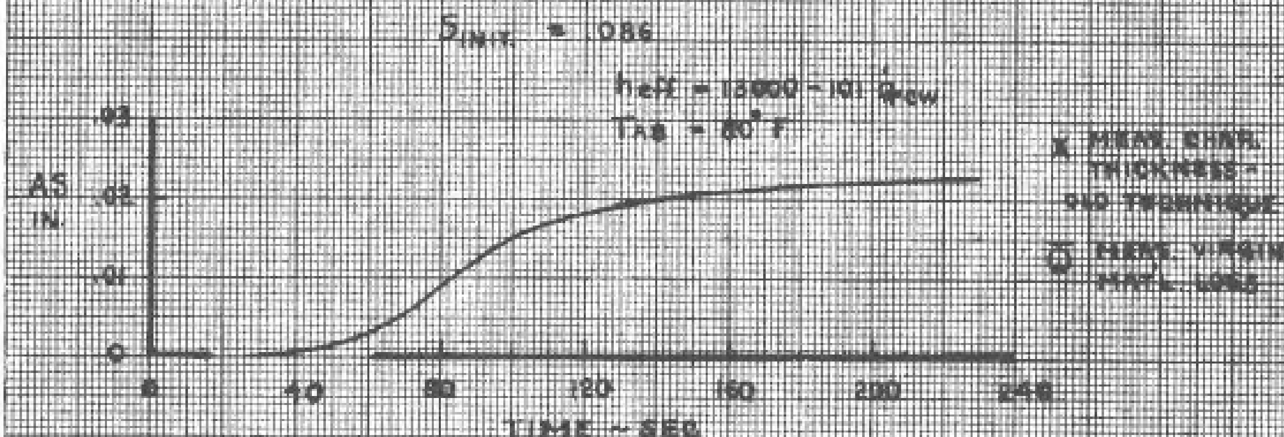

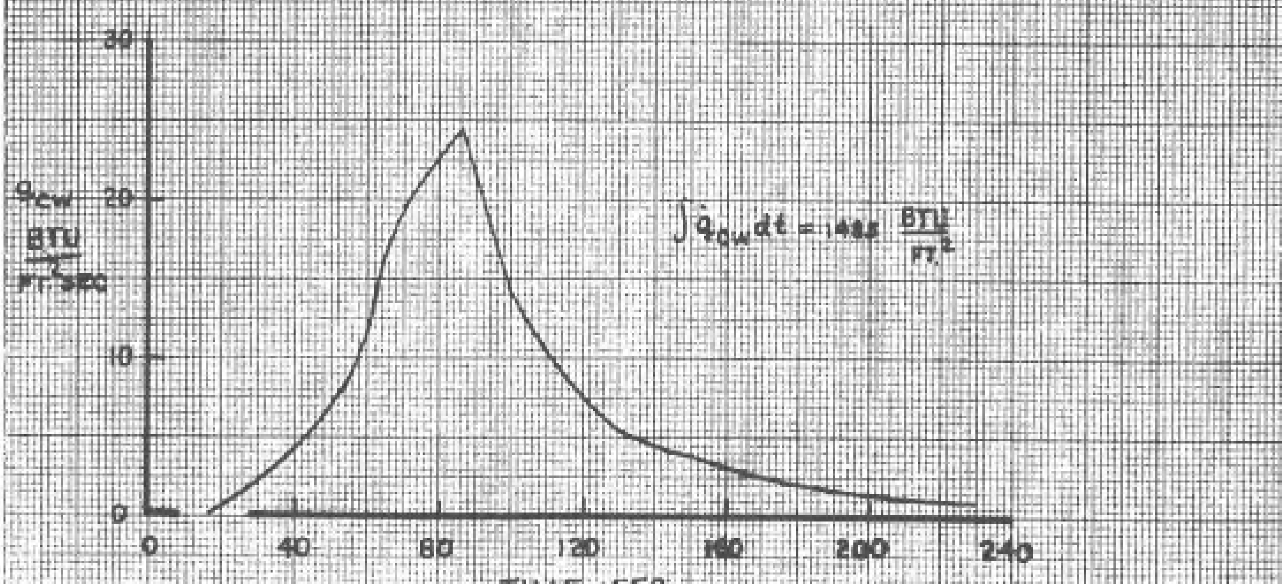

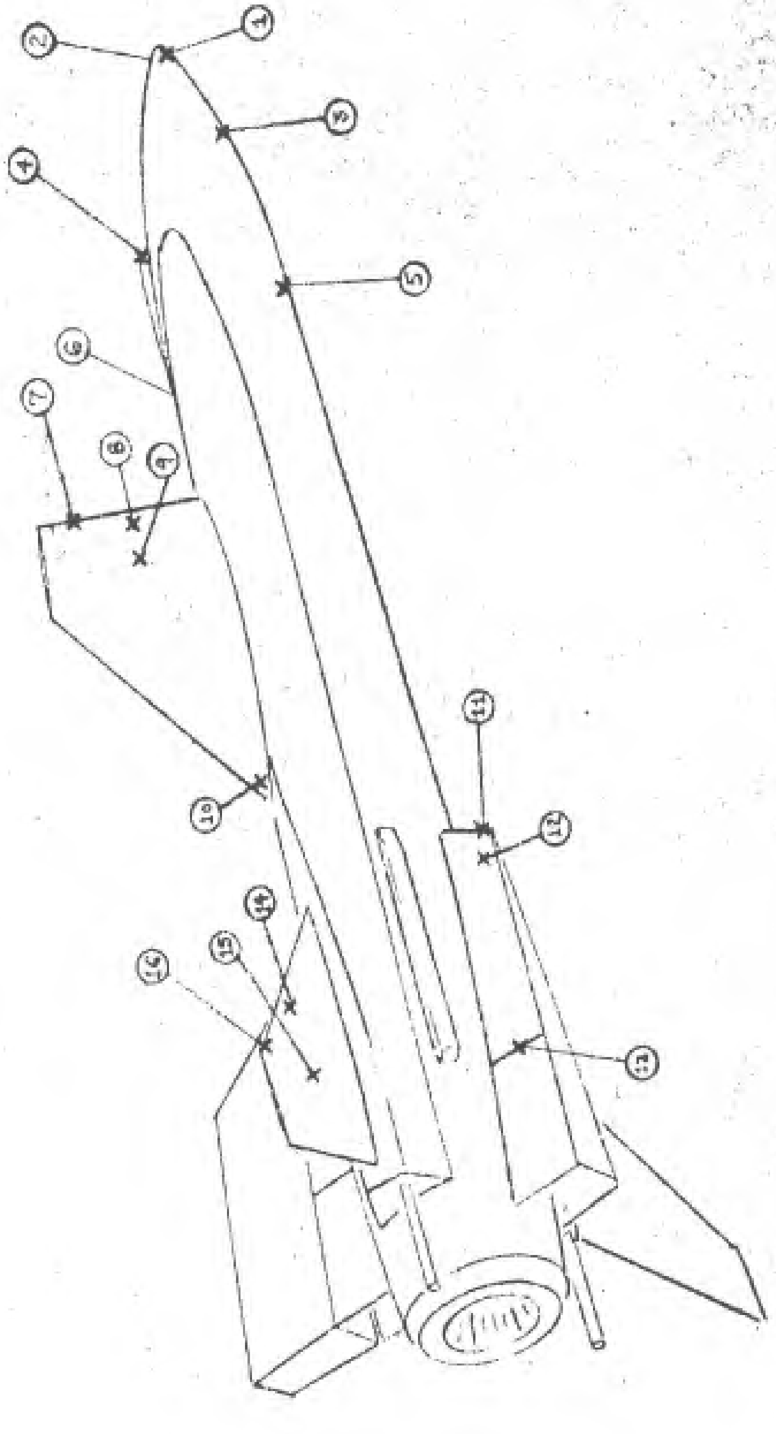

Figure 58 - Points on X-15 For Representative Heat Flux Calculations

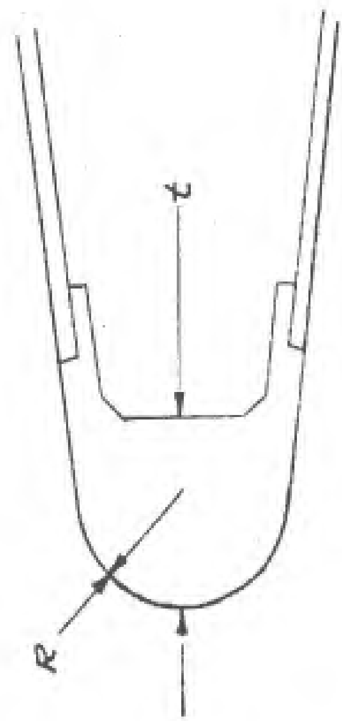

FIG 59 TYPICAL STAGNATION LINE SECTION

FIG. 60 STAGNATION LINE POINTS

POINT NO.	RADIUS ~ IN.	SKIN THICKNESS ~ IN.	Ω ~ SWEEP DEG.
4	.500	.125	60.00
7	.375	.688	36.75
11	.500	.594	30.00
16	.250	.375	50.78

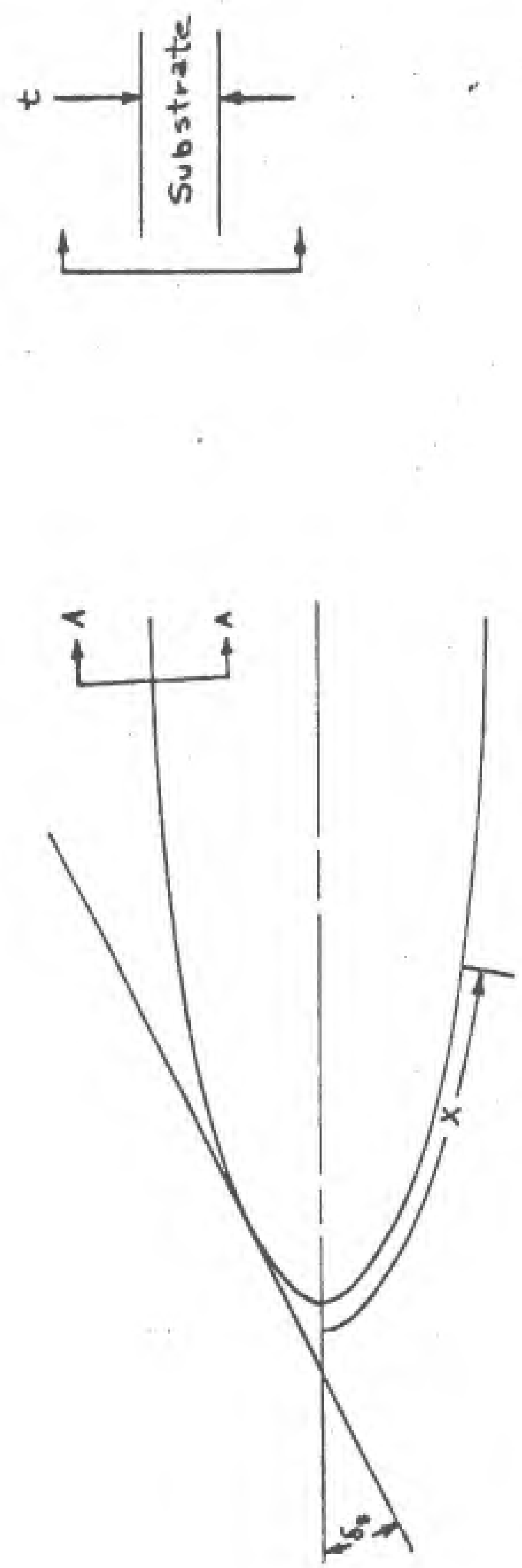

Fig. 61 Flat Plate Geometry Point Description

FIG. 62 FLAT PLATE POINTS

POINT No.	δ_S ~ DEG.	t ~ IN. (SUBSTRATE)	X~FLOW * LENGTH ~IN.
1 **	15.2	.125	16.11
2 **	15.2	.125	16.11
3	9.5	.071	81.85
5	0	.050	206.95
6	0	.050	206.95
8	6.0	.072	4.90
9	1.8	.057	18.00
10	4.0	.046	120.00
12	5.0	.037	6.00
13	5.0	.037	72.00
14	4.0	.050	6.00
15	0	.050	36.00

* FUSELAGE FLOW LENGTHS ARE MEASURED FROM THE ZERO ANGLE OF ATTACK STAGNATION POINT. THE TWO DIMENSIONAL FLOW LENGTHS ARE MEASURED FROM THE STAGNATION LINE.

** THESE POINTS ARE LOCATED ON THE NORTRONICS Q-BALL AIR DATA SYSTEM.

FORM 1021-S

PREPARED BY: P. Paxson	NORTH AMERICAN AVIATION, INC.	PAGE NO. ? 88 OF
CHECKED BY:		REPORT NO. NA-64-177
DATE: 9-26-63		MODEL NO. X-15A-2

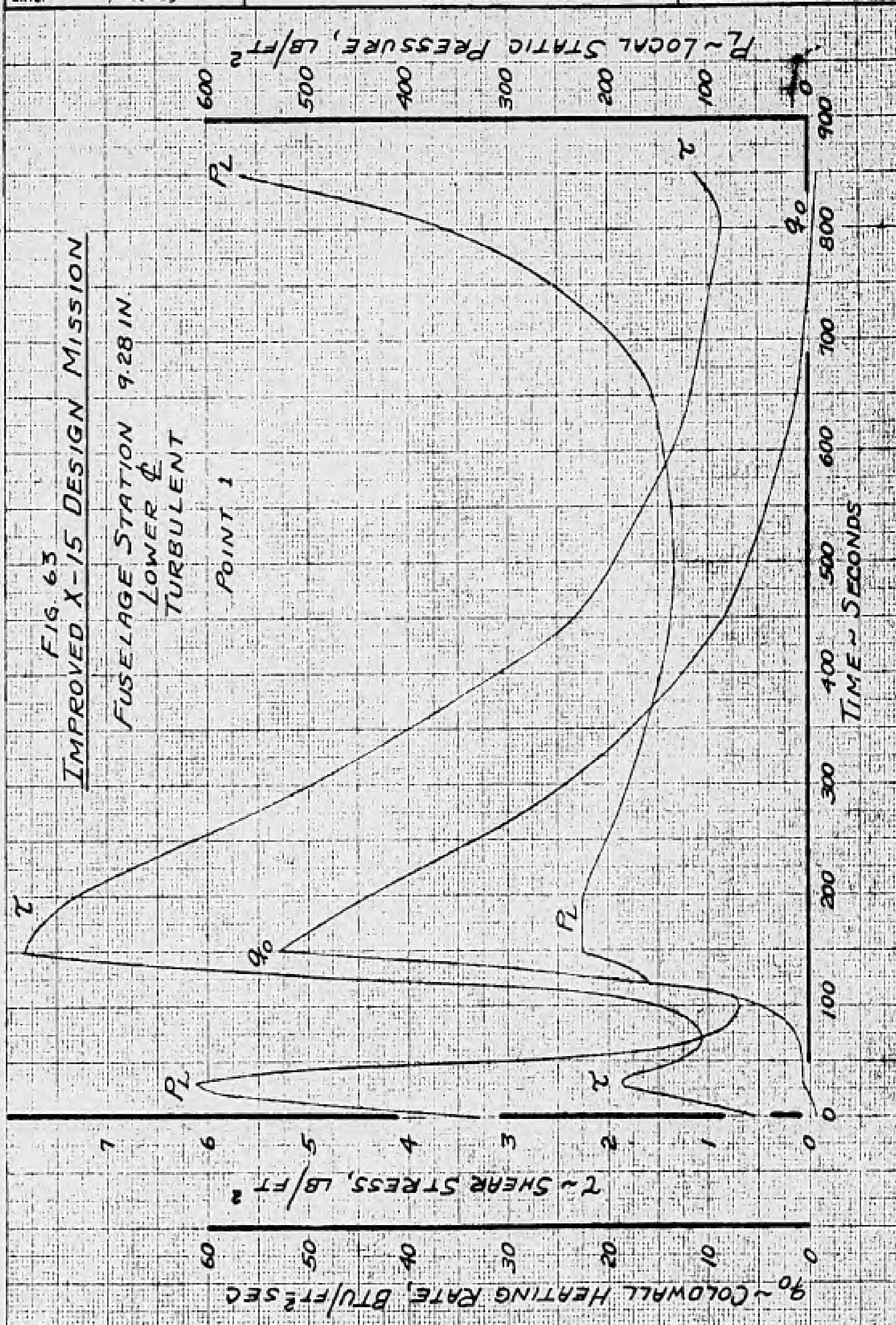

FORM 1021-B

PREPARED BY: P. Paxson	NORTH AMERICAN AVIATION, INC.	PAGE NO. 389 OF
CHECKED BY:		REPORT NO. NA-64-177
DATE: 9-26-63		MODEL NO. X-15A-2

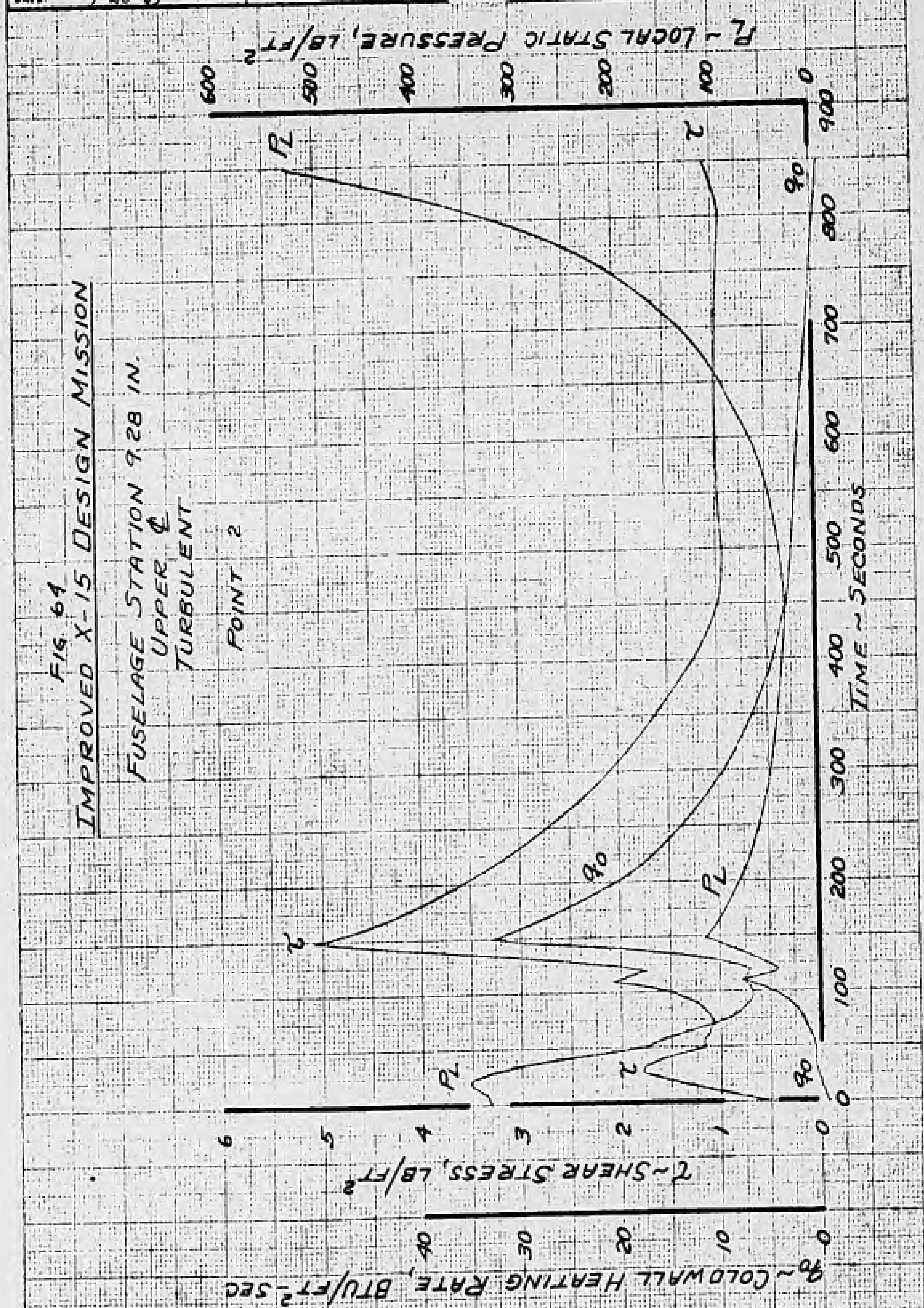

FORM 1021-5

PREPARED BY: P. Paxson	NORTH AMERICAN AVIATION, INC.	PAGE NO. 90 OF
CHECKED BY:		REPORT NO. NA-64-177
DATE: 9-26-63		MODEL NO. X-15A-2

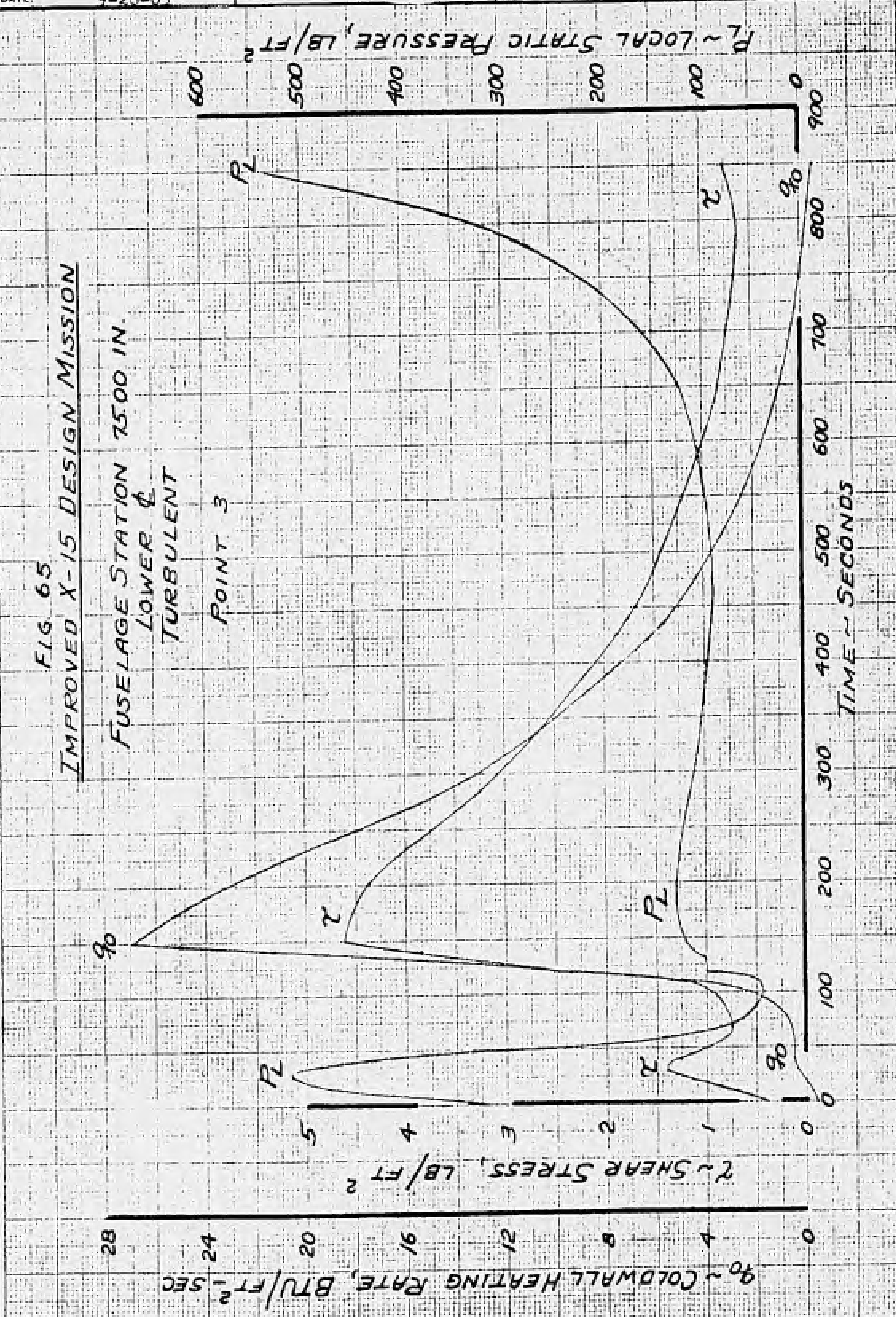

FIG 65

IMPROVED X-15 DESIGN MISSION

FORM 1021-8

NORTH AMERICAN AVIATION, INC.	
PREPARED BY: P. Paxson	PAGE NO. 91 OF
CHECKED BY:	REPORT NO. NA-64-177
DATE: 9-26-63	MODEL NO. X-15A-2

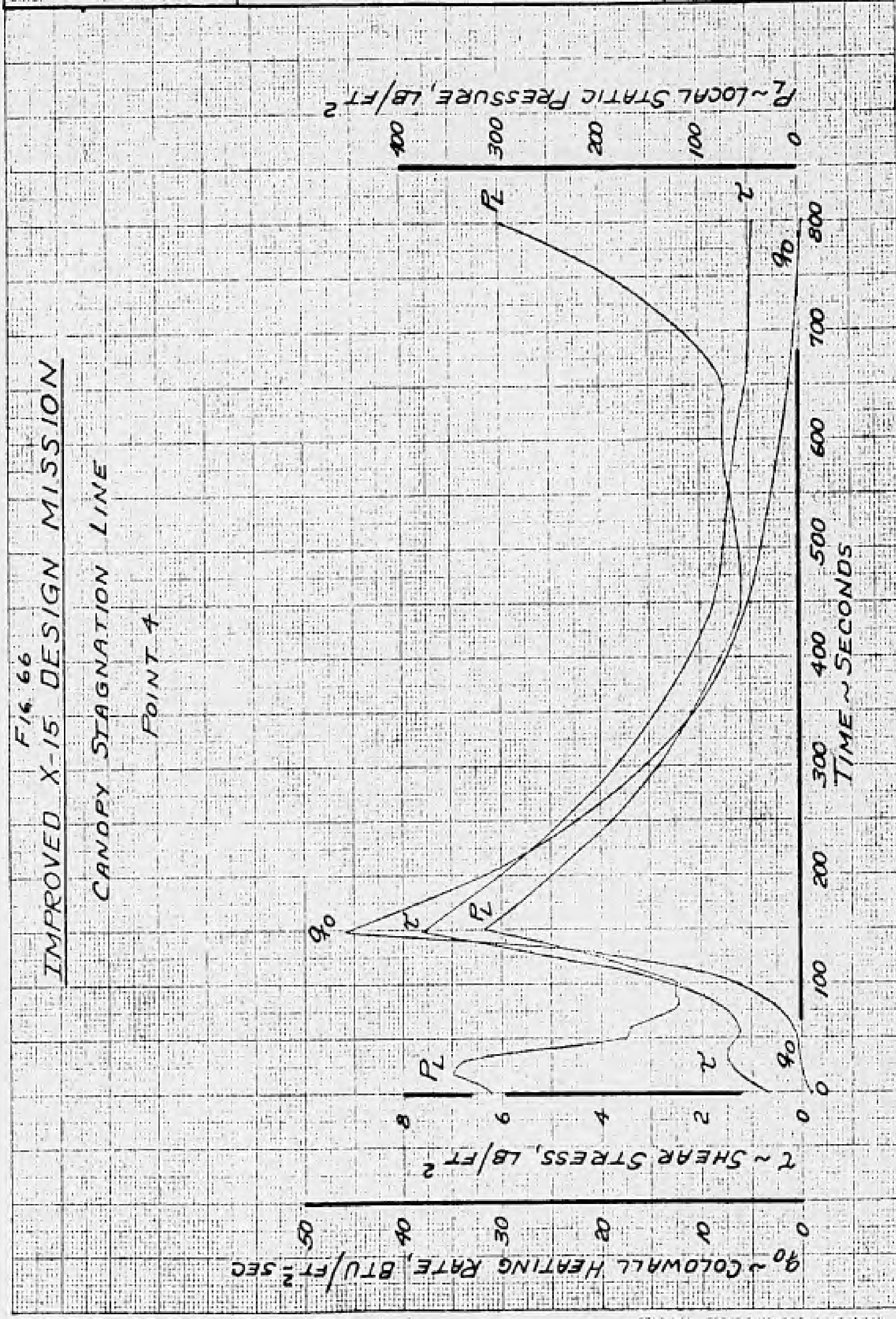

FORM 1021-8

PREPARED BY: P. Paxson	NORTH AMERICAN AVIATION, INC.	PAGE NO. 92 OF
CHECKED BY:		REPORT NO. NA-64-177
DATE: 9-26-63		MODEL NO. X-15A-2

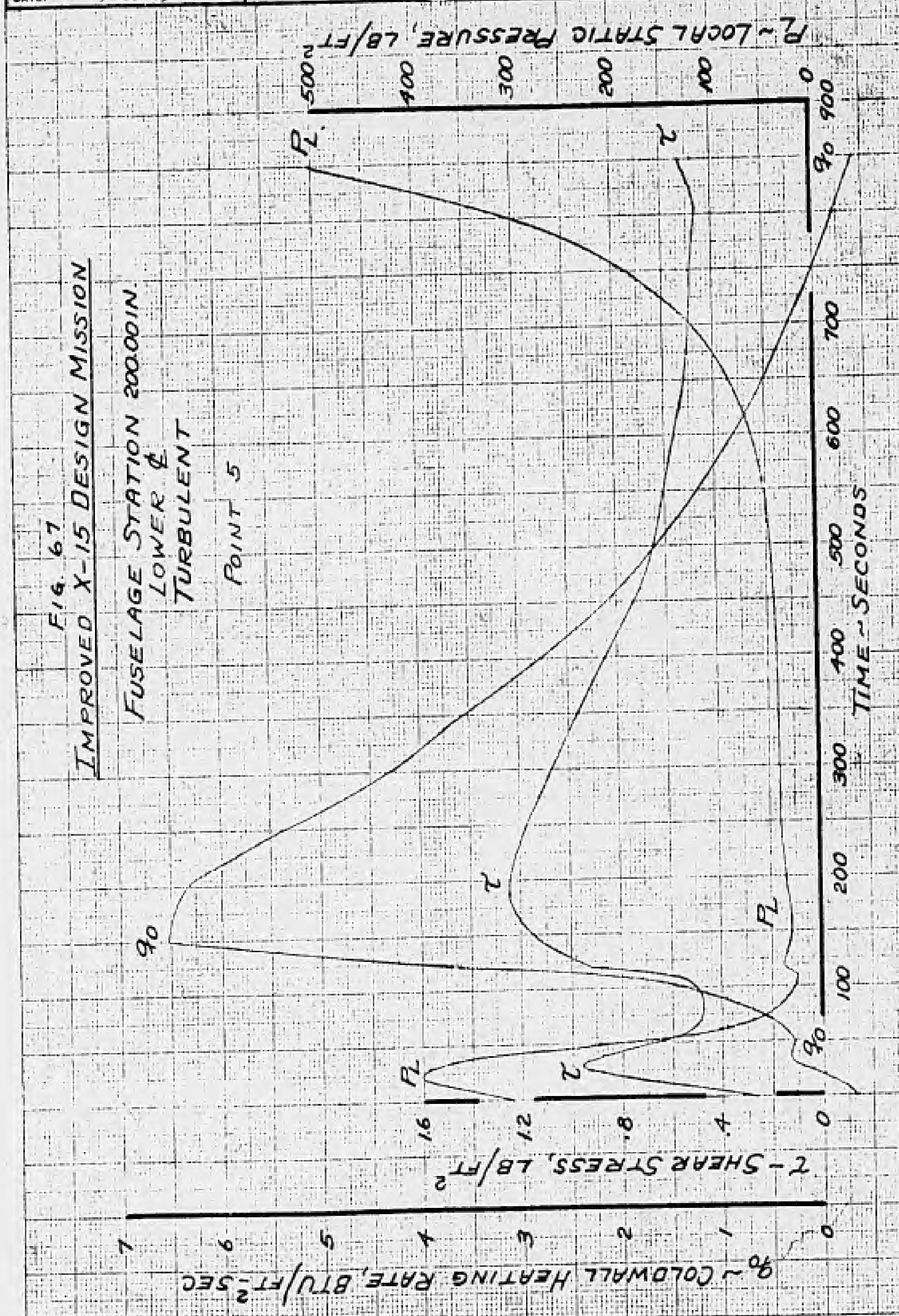

FORM 1021-S

PREPARED BY: P. Paxson	NORTH AMERICAN AVIATION, INC.	PAGE NO. 93 OF
CHECKED BY:		REPORT NO. NA-64-177
DATE: 9-26-63		MODEL NO. X-15A-2

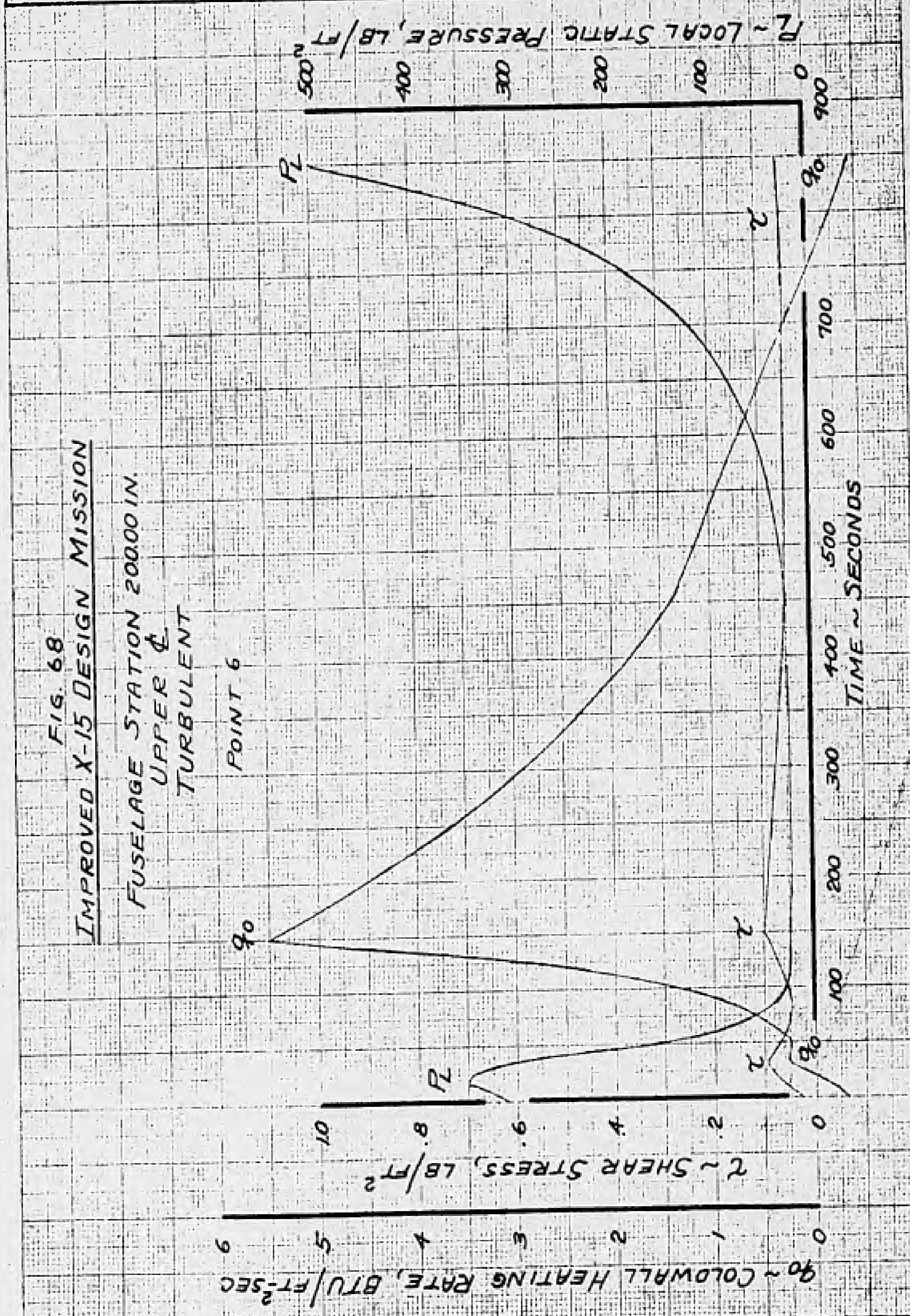

FIG. 68

IMPROVED X-15 DESIGN MISSION

FUSELAGE STATION 200.00 IN.
UPPER ℄
TURBULENT

POINT 6

FORM 1021-S

PREPARED BY: P. Paxson	**NORTH AMERICAN AVIATION, INC.**	PAGE NO. 94 OF
CHECKED BY:		REPORT NO. NA-64-177
DATE: 5-20-63		MODEL NO. X-15A-2

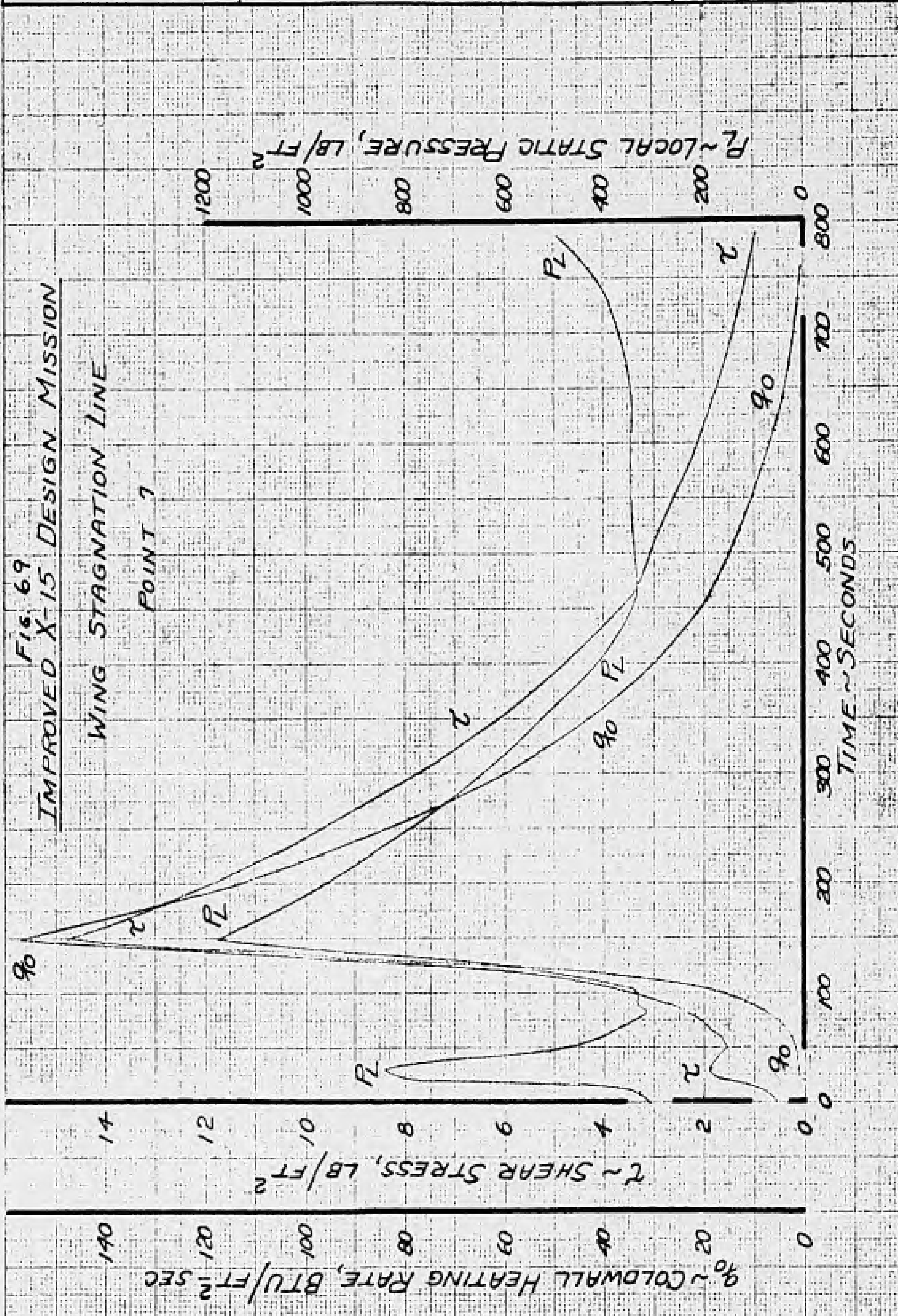

Fig. 69
IMPROVED X-15 DESIGN MISSION
WING STAGNATION LINE
POINT 1

FORM 1021-B

PREPARED BY: P. Paxson	NORTH AMERICAN AVIATION, INC.	PAGE NO. 95 OF
CHECKED BY:		REPORT NO. NA-64-177
DATE: 5-20-63		MODEL NO. X-15A-2

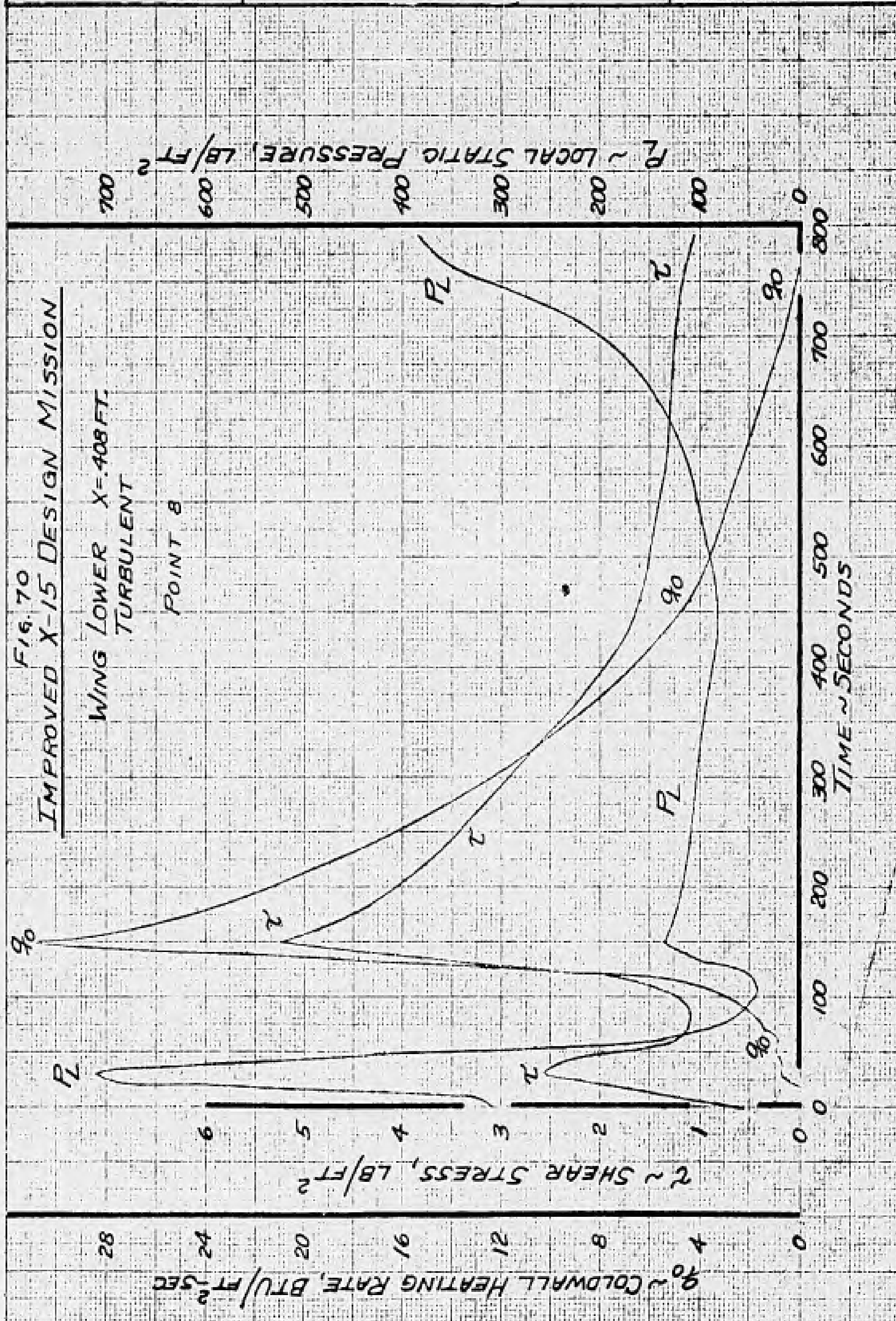

FORM 1021-B

NORTH AMERICAN AVIATION, INC.	
PREPARED BY: P. Paxson	PAGE NO. 96 OF
CHECKED BY:	REPORT NO. NA-64-177
DATE: 6-12-63	MODEL NO. X-15A-2

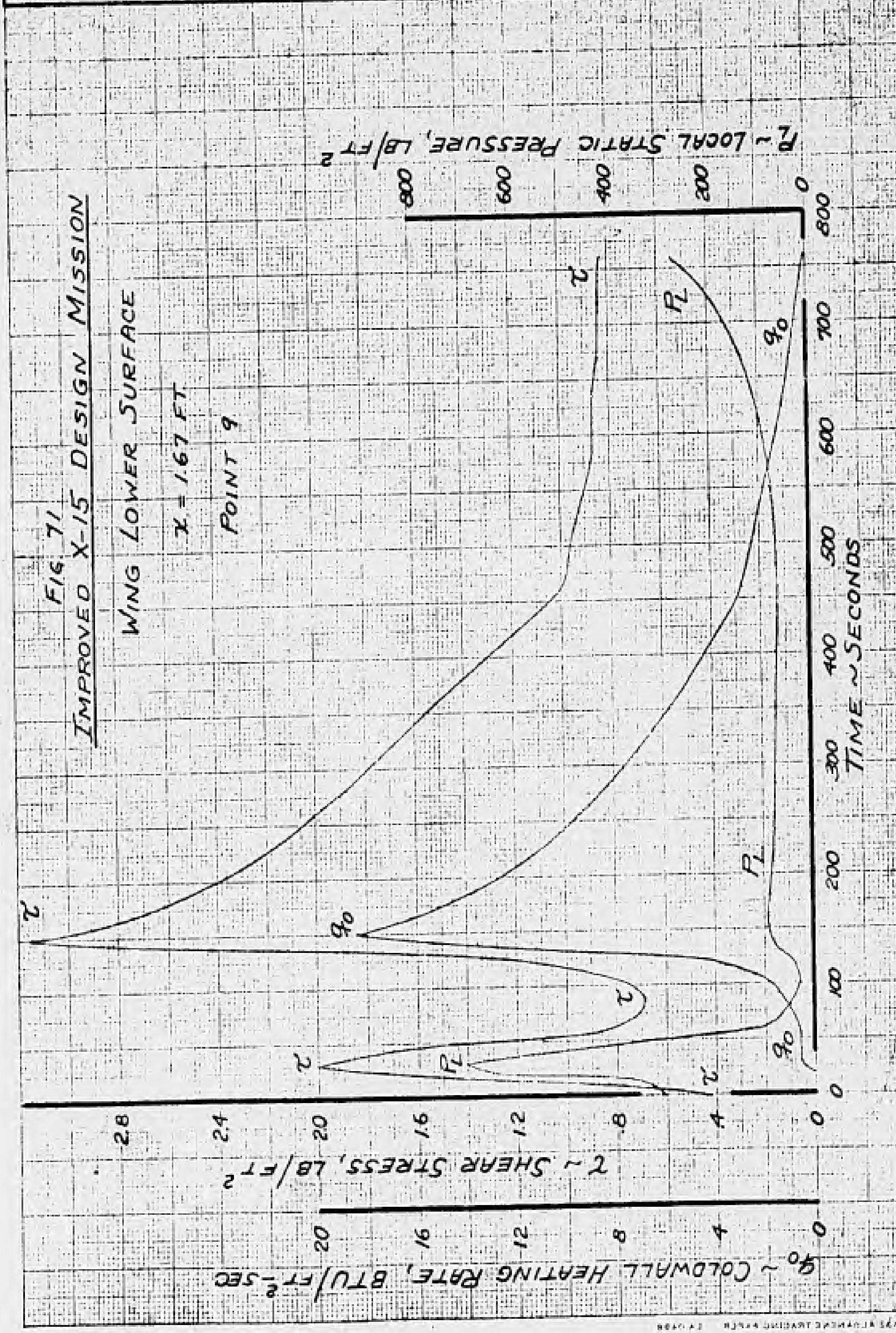

FIG 71
IMPROVED X-15 DESIGN MISSION
WING LOWER SURFACE
$x = 1.67$ FT.
POINT 9

FORM 1021-S

PREPARED BY: P. Paxson	**NORTH AMERICAN AVIATION, INC.**	PAGE NO. 96 OF
CHECKED BY:		REPORT NO. NA-64-177
DATE: 6-12-63		MODEL NO. X-15A-2

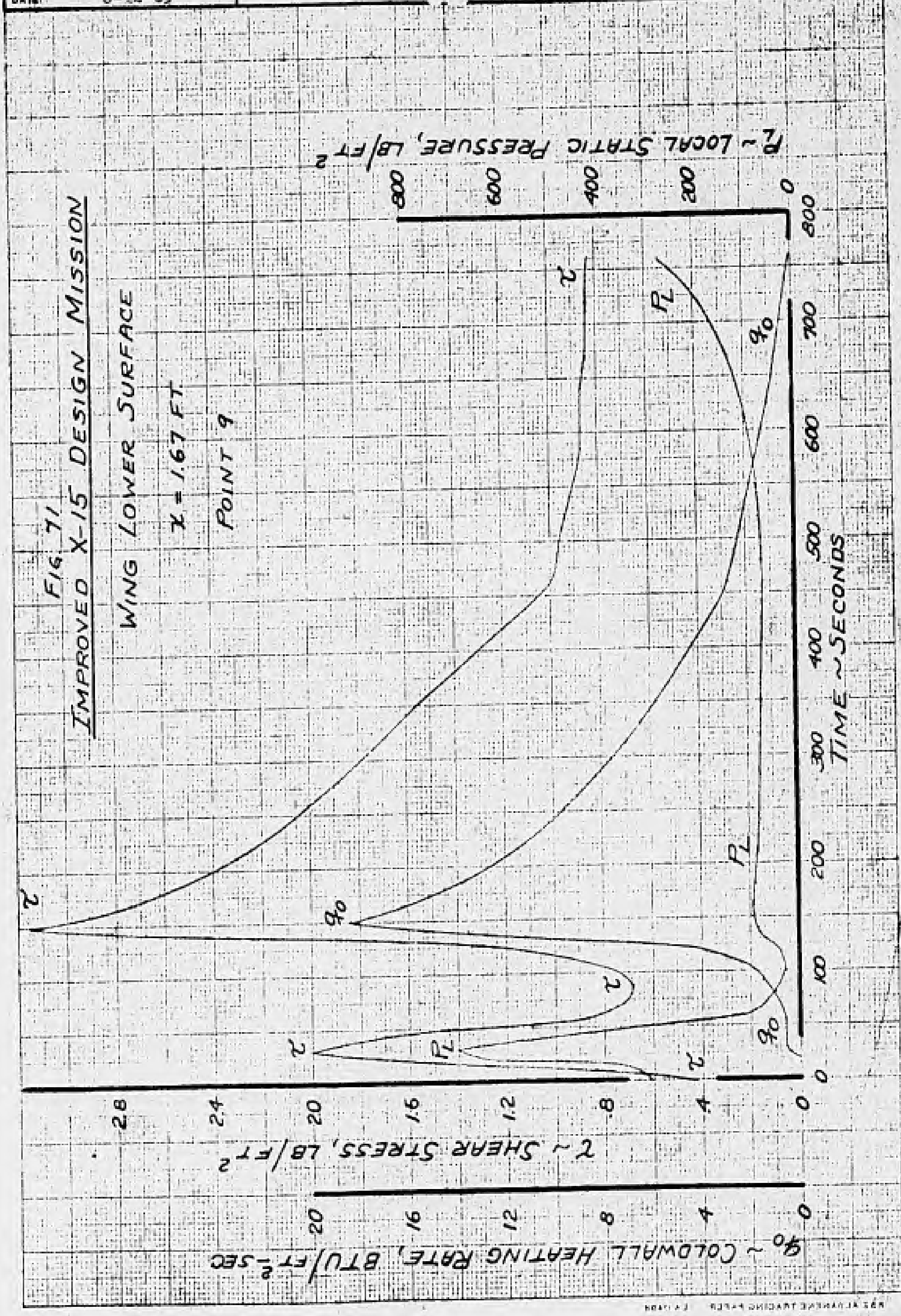

FORM 1021-5

PREPARED BY: P. Paxson	NORTH AMERICAN AVIATION, INC.	PAGE NO. 97 OF
CHECKED BY:		REPORT NO. NA-64-177
DATE: 5-20-63		MODEL NO. X-15A-2

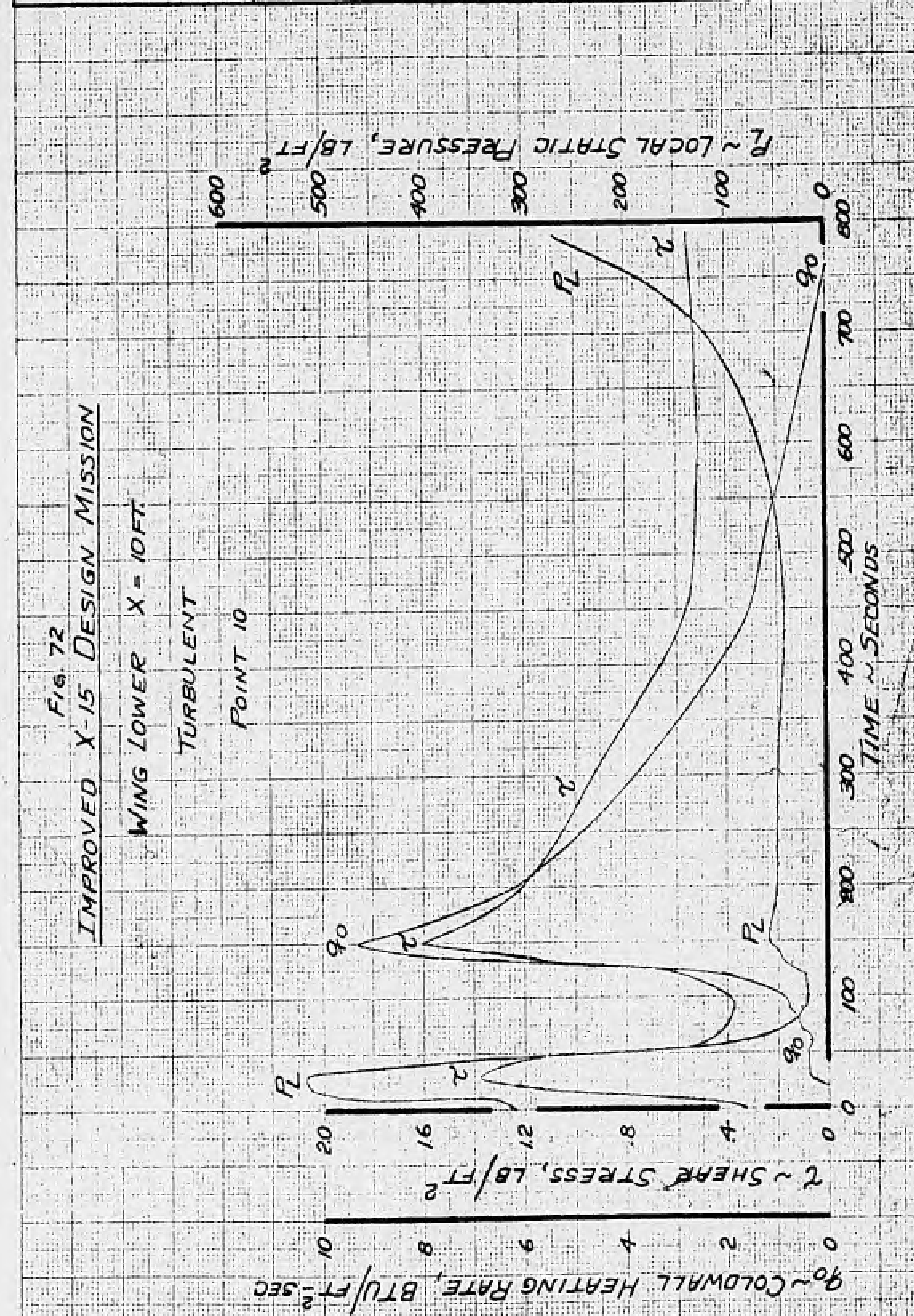

FIG. 72
IMPROVED X-15 DESIGN MISSION
WING LOWER X = 10 FT.
TURBULENT
POINT 10

FORM 1021-S

PREPARED BY: P. Paxson	NORTH AMERICAN AVIATION, INC.	PAGE NO. 98 OF
CHECKED BY:		REPORT NO. NA-64-177
DATE: 9-26-63		MODEL NO. X-15A-2

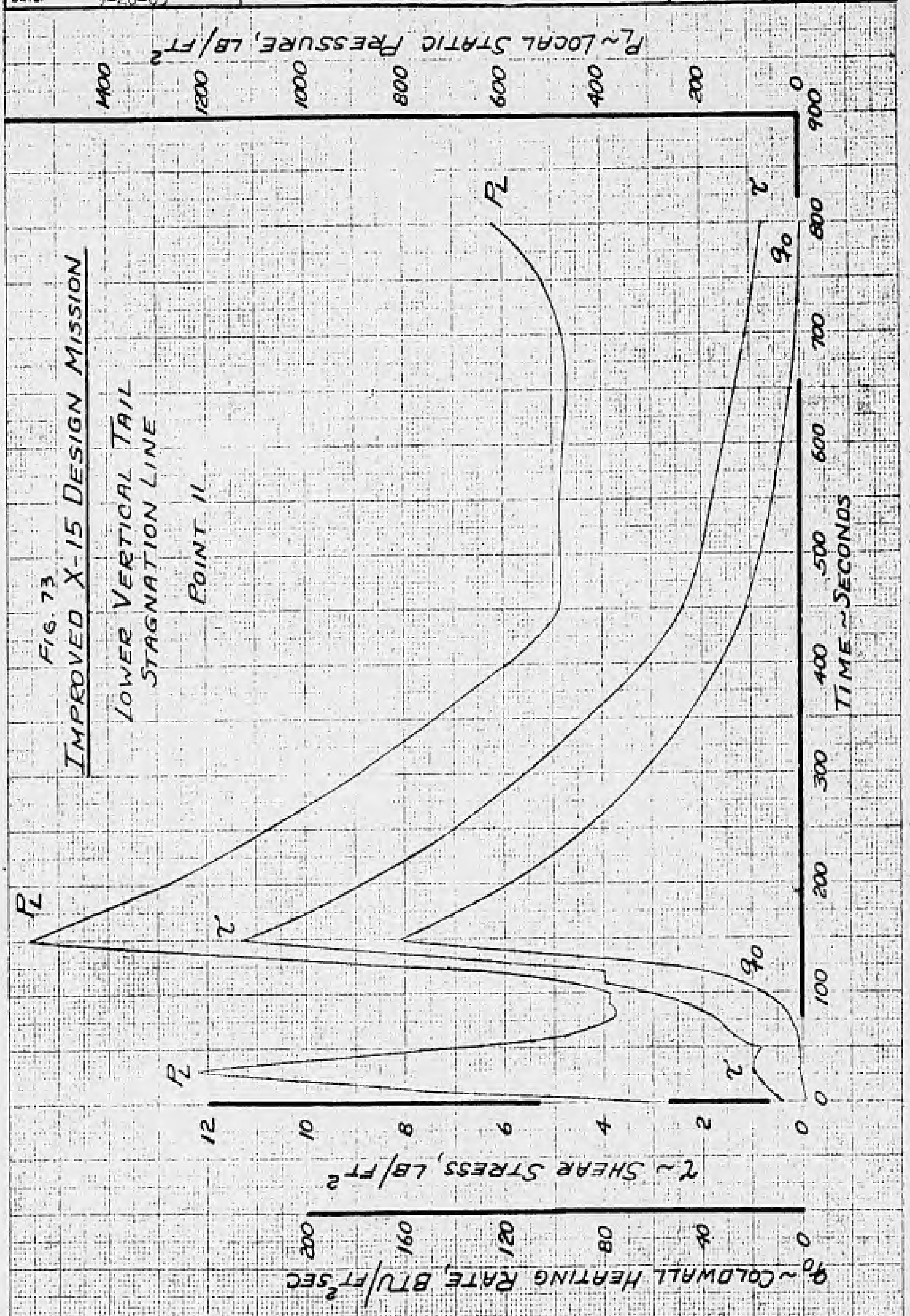

Fig. 73

FORM 1021-B

PREPARED BY: P. Paxson	NORTH AMERICAN AVIATION, INC.	PAGE NO. 99 OF
CHECKED BY:		REPORT NO. NA-64-177
DATE: 5-23-63		MODEL NO. X-15A-2

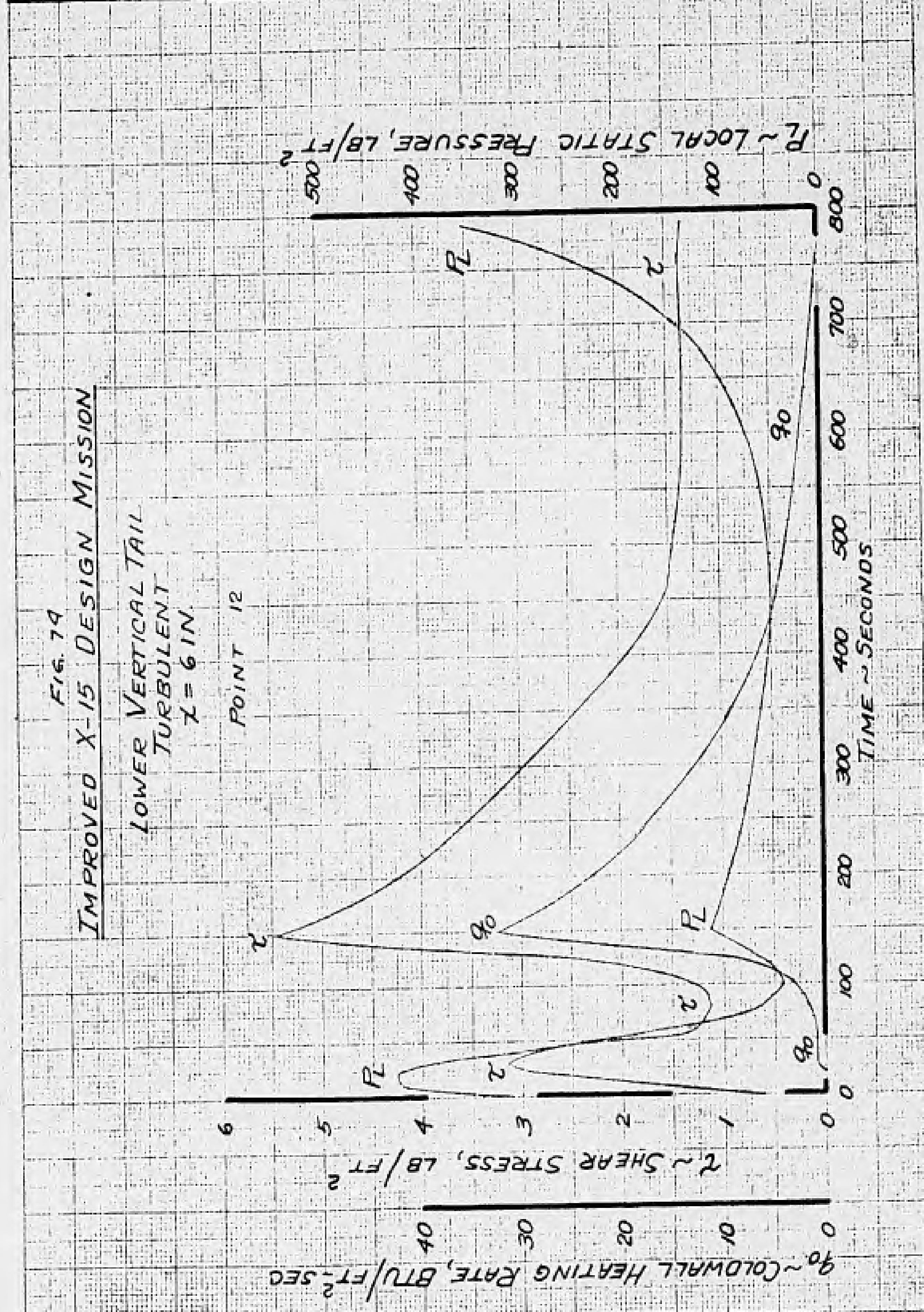

FORM 1021-6

PREPARED BY: P. Paxson	NORTH AMERICAN AVIATION, INC.	PAGE NO. 100 OF
CHECKED BY:		REPORT NO. NA-64-177
DATE: 9-26-63		MODEL NO. X-15A-2

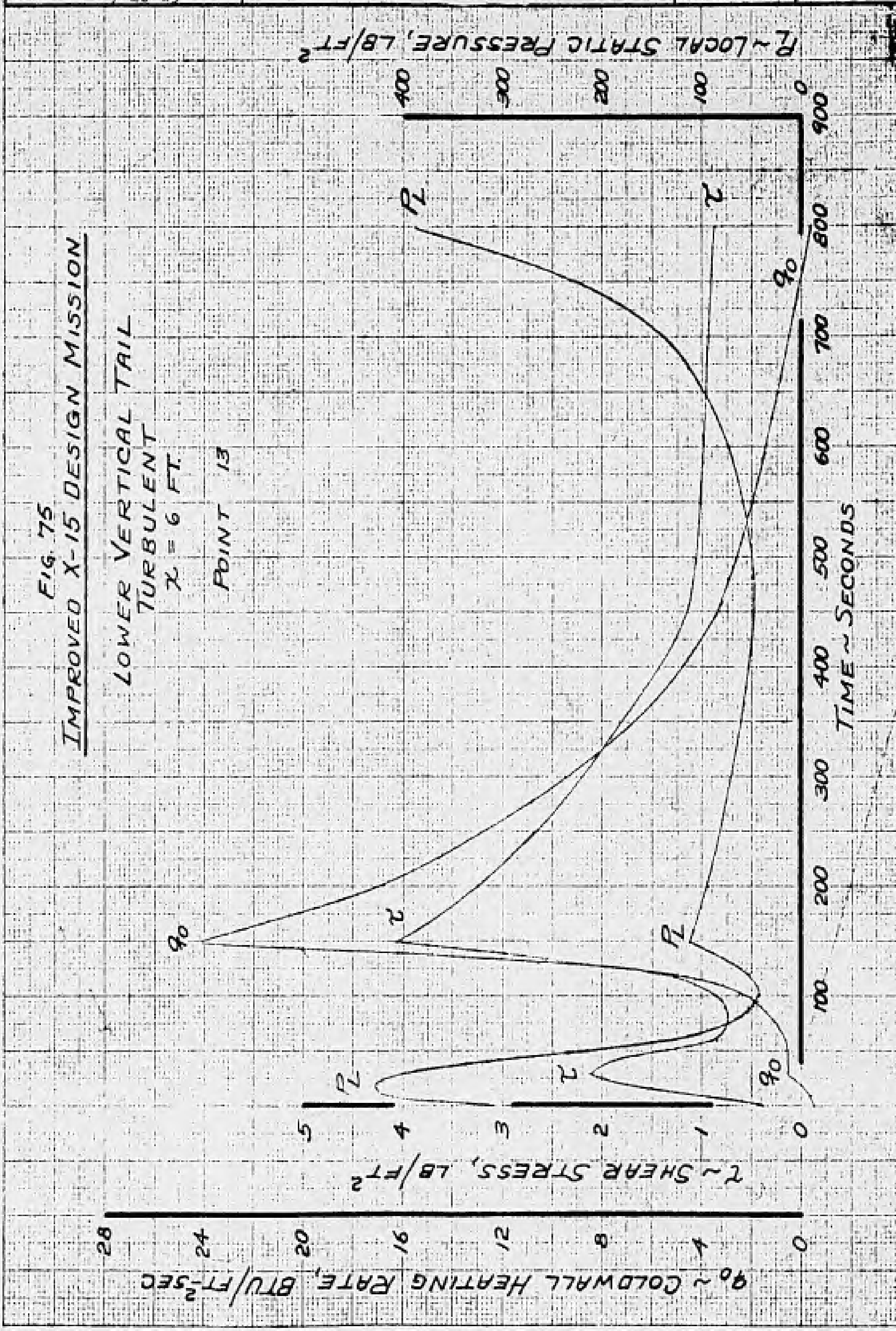

FORM 1021-S

PREPARED BY: P. Paxson	NORTH AMERICAN AVIATION, INC.	PAGE NO. 101 OF
CHECKED BY:		REPORT NO. NA-64-177
DATE: 9-26-63		MODEL NO. X-15A-2

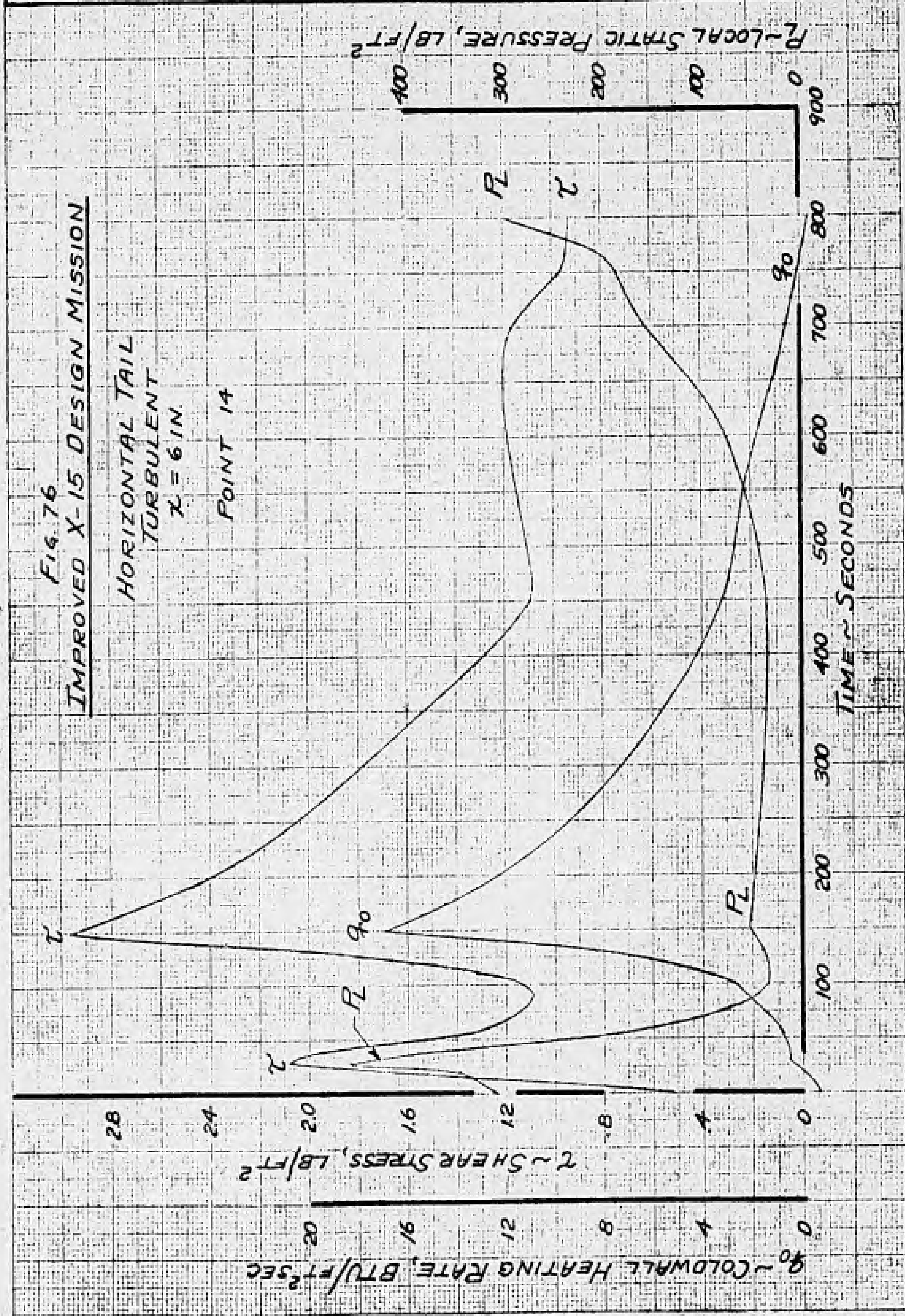

FIG. 76
IMPROVED X-15 DESIGN MISSION

FORM 1021-B

PREPARED BY: P. Paxson	NORTH AMERICAN AVIATION, INC.	PAGE NO. 102 OF
CHECKED BY:		REPORT NO. NA-64-177
DATE: 9-26-63		MODEL NO. X-15A-2

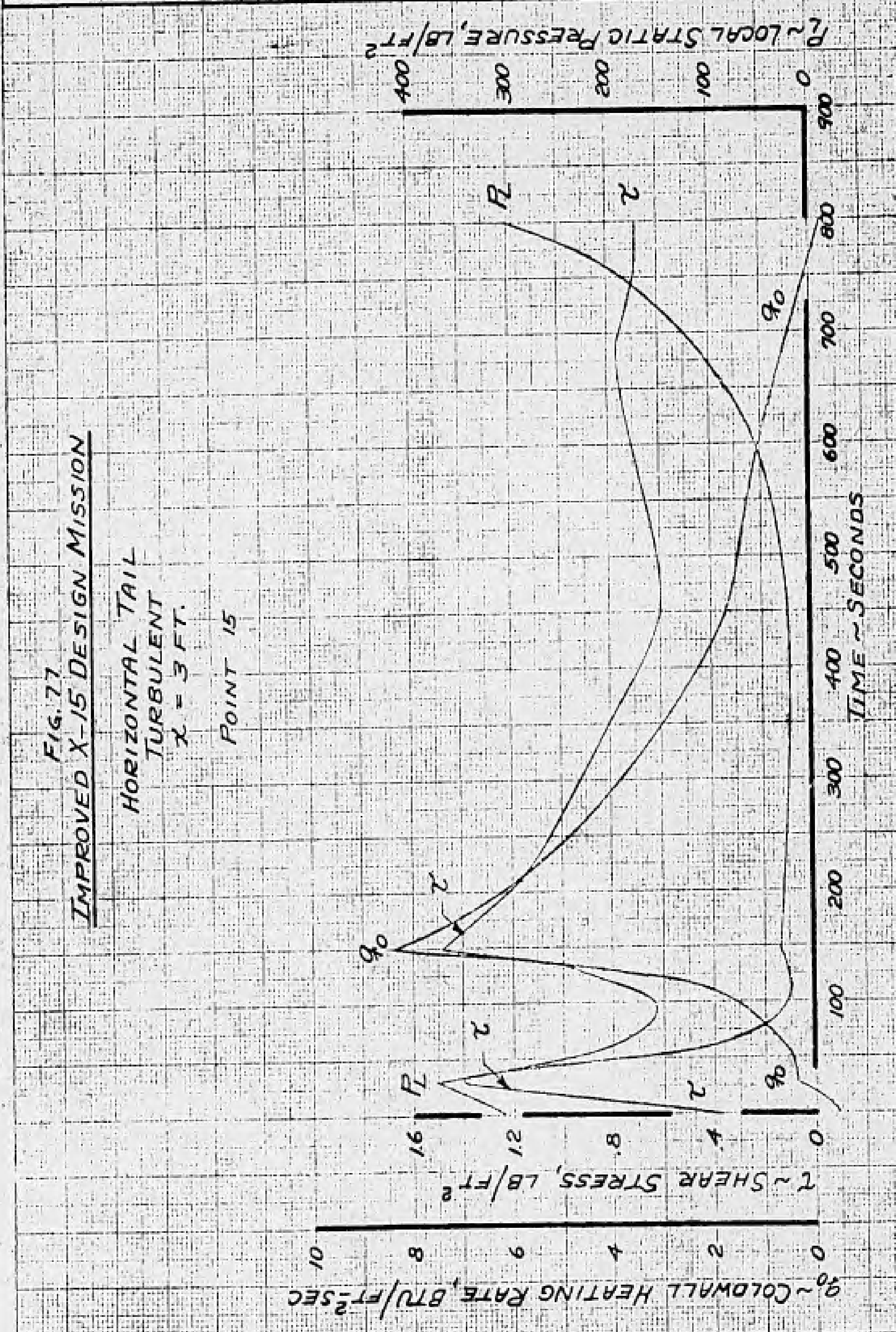

FORM 1021-B

PREPARED BY: P. Paxson	NORTH AMERICAN AVIATION, INC.	PAGE NO. 103 OF
CHECKED BY:		REPORT NO. NA-64-177
DATE: 9-26-63		MODEL NO. X-15A-2

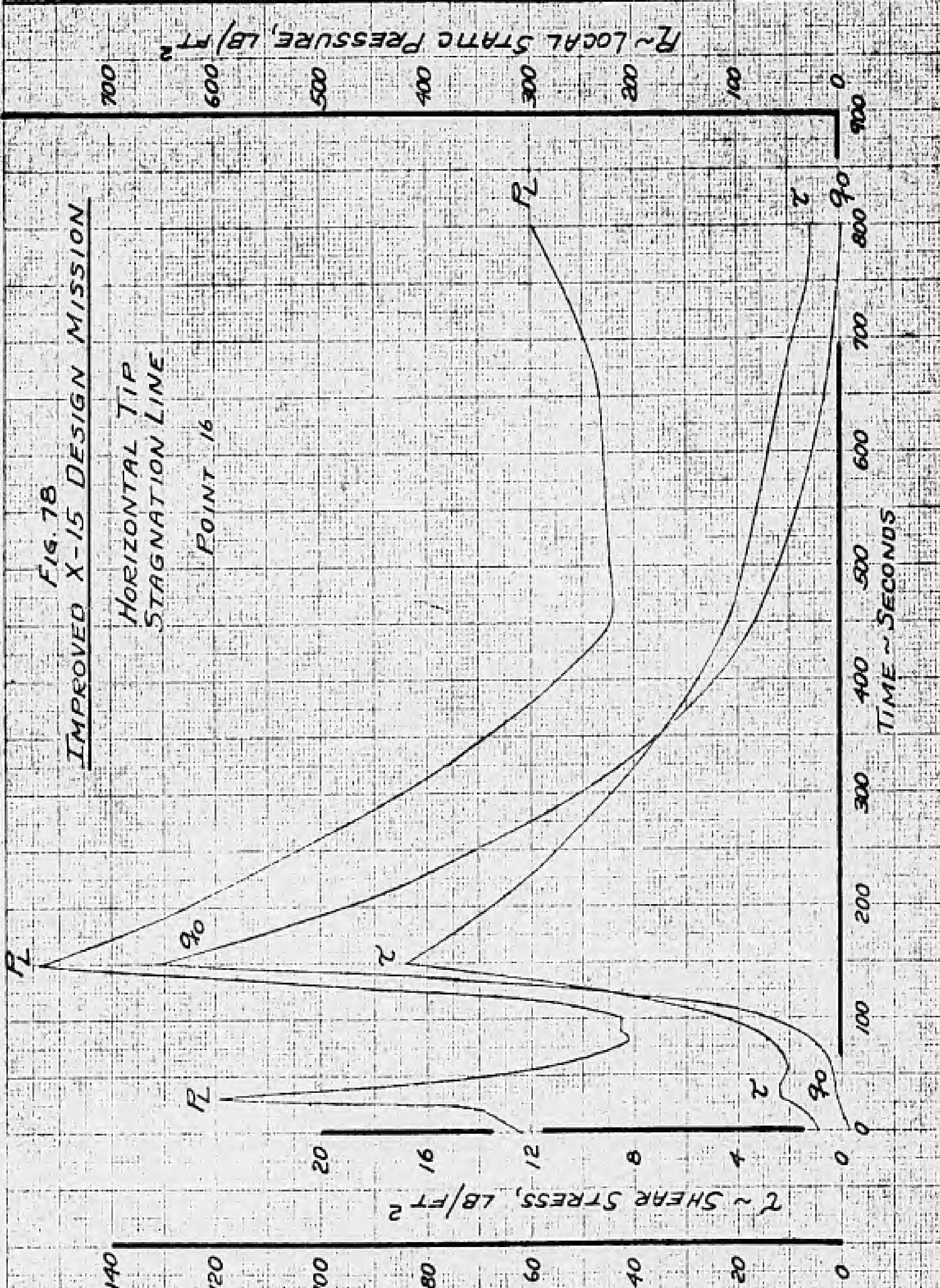

FORM 1021-B

PREPARED BY: P. Paxson	NORTH AMERICAN AVIATION, INC.	PAGE NO. 104 OF
CHECKED BY:		REPORT NO. NA-64-177
DATE: 9-26-63		MODEL NO. X-15A-2

FIG. 79

FUSELAGE CENTERLINE VARIATION OF HEAT FLUX

AT $t = 150$ SEC

FUSELAGE BOW SHOCK-WING LEADING EDGE SHOCK INTERACTION ANALYSIS

The presence of a system of shock waves caused by the nose of the airplane, side fairings, and canopy has been recognized and measured on the present X-15 airplanes. Due to the relatively large heat sink on the wing leading edge, the shock impingement on the leading edge has not caused any detectable high temperature regions. The shocks have been detected by pitot pressure measurements in the wing leading edge. On the Advanced X-15A-2, the ablation coating on the wing, because it does not have a "heat sink" capability comparable to the unprotected wing, must be designed to absorb the higher heating caused by shock impingement. The problem is to determine the additional ablation thickness required.

First, the most prominent shock, the one from the nose of the airplane, must be located. Figure 1 shows the location of the bow shock impingement on the wing leading edge as a function of Mach No. The information on Figure 1 has been obtained from wing tunnel and flight data on the current X-15 vehicles, corrected for the additional 29 inches of fuselage length between the wing and the nose on X-15A-2.

In reference 1, a method has been developed to calculate the increased heating at a shock impingement on a swept leading edge. The method has been applied to the X-15A-2 geometry and design mission and summarized in reference 2. The ratio of local heat flux at impingement to the undisturbed heat flux is shown in Figure 2.

From Figures 1 and 2 and the Mach No.-time history of the X-15A-2 design mission, Figure 3 was constructed. The location of the bow shock and the corresponding heat flux ratio are shown versus flight time. On this plot, additional lines of x/l may be drawn on either side of the curve shown to represent the region of influence of the bow shock. This was done for regions of shock influence of 1, 2, and 3 leading edge diameters (corresponds of x/l values of $\pm$ .00335, .0067, .01005 respectively). From this, it was possible, assuming the increased heating region to be step shaped, to determine the x/l value of the wing which was most affected by the bow shock, and for how long a period of time during the mission that the shock's presence would be felt. Having done this, the local heat flux was determined and the additional amount of ablation material required was calculated as a function of the assumed region of influence. This variation is shown in Figure 4; the location on the wing corresponds to the x/l most severly affected. The variation of material required as a function of x/l was determined in a similar manner and is shown in Figure 5 for a region of influence of 2 diameters.

The following arguments lead to a conclusion on the amount of additional ablation material required on the X-15A-2 wing leading edge to absorb the effects of the shock system.

1. It is recognized that shocks other than the bow shock exist.

2. Very little usable data exist on the magnitude of heat flux and region of influence of the shock impingement. Thus, a region of influence of two leading edge diameters, rather than one and one half, which available data indicate, will be used.

3. Some previous unpublished results indicated a higher stagnation line heating rate inboard of the shock.

In view of the above, an additional 0.09 inches of T-500-6A ablation material will be provided over the entire stagnation line of the leading edge to account for the shock system.

REFERENCES

1. TFD-63-653 "Summary Report of Fuselage-Bow Shock Interaction With A Wing Leading Edge Shock" by F. Hall and M. Glick.

2. FS-63-11-4 internal letter "Advanced X-15 Fuselage Bow Shock-Wing Leading Edge Shock Interaction Analysis" and TFD-63-887 "Enclosure 1".

FIG. 1 X-15A-2 SHOCK IMPINGEMENT POINT VERSUS MACH NUMBER[1]

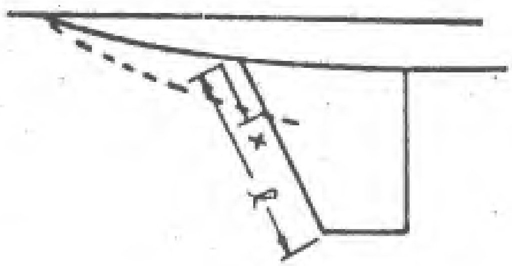

1 INCLUDES ALLOWANCE FOR 39 IN. EXTENSION

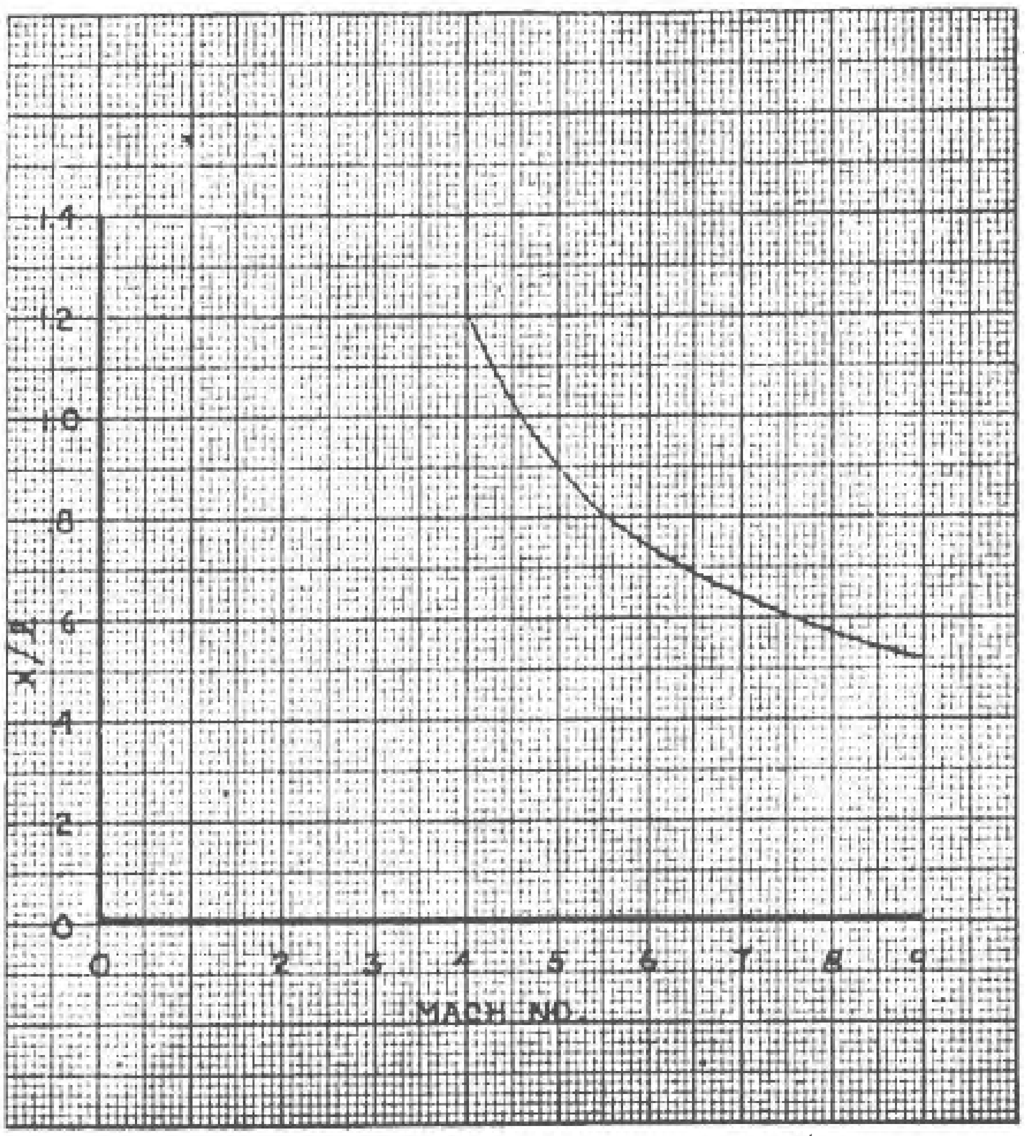

NORTH AMERICAN AVIATION, INC.	
PREPARED BY	PAGE NO 4A OF
CHECKED BY	REPORT NO NA-64-177 Appendix A
DATE	MODEL NO

FIG. 2 ADVANCED X-15 WING LEADING EDGE
HEAT TRANSFER RATIO VS MACH NUMBER
AT THE POINT OF SHOCK INTERSECTION

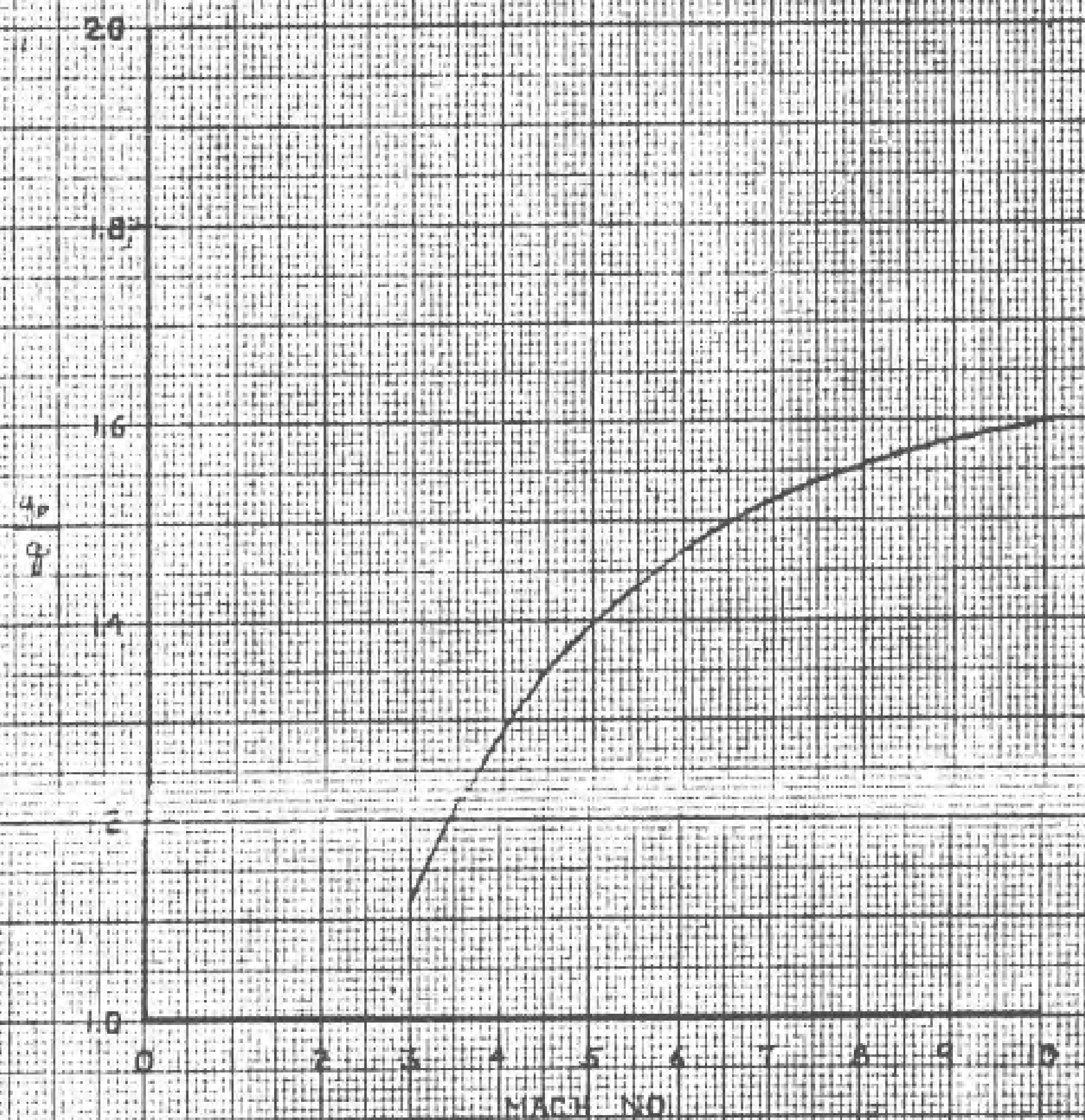

FORM 1021-B

PREPARED BY:	NORTH AMERICAN AVIATION, INC.	PAGE NO. 5A OF
CHECKED BY:		REPORT NO. NA-64-177 Appendix A
DATE:		MODEL NO.

Fig. 3

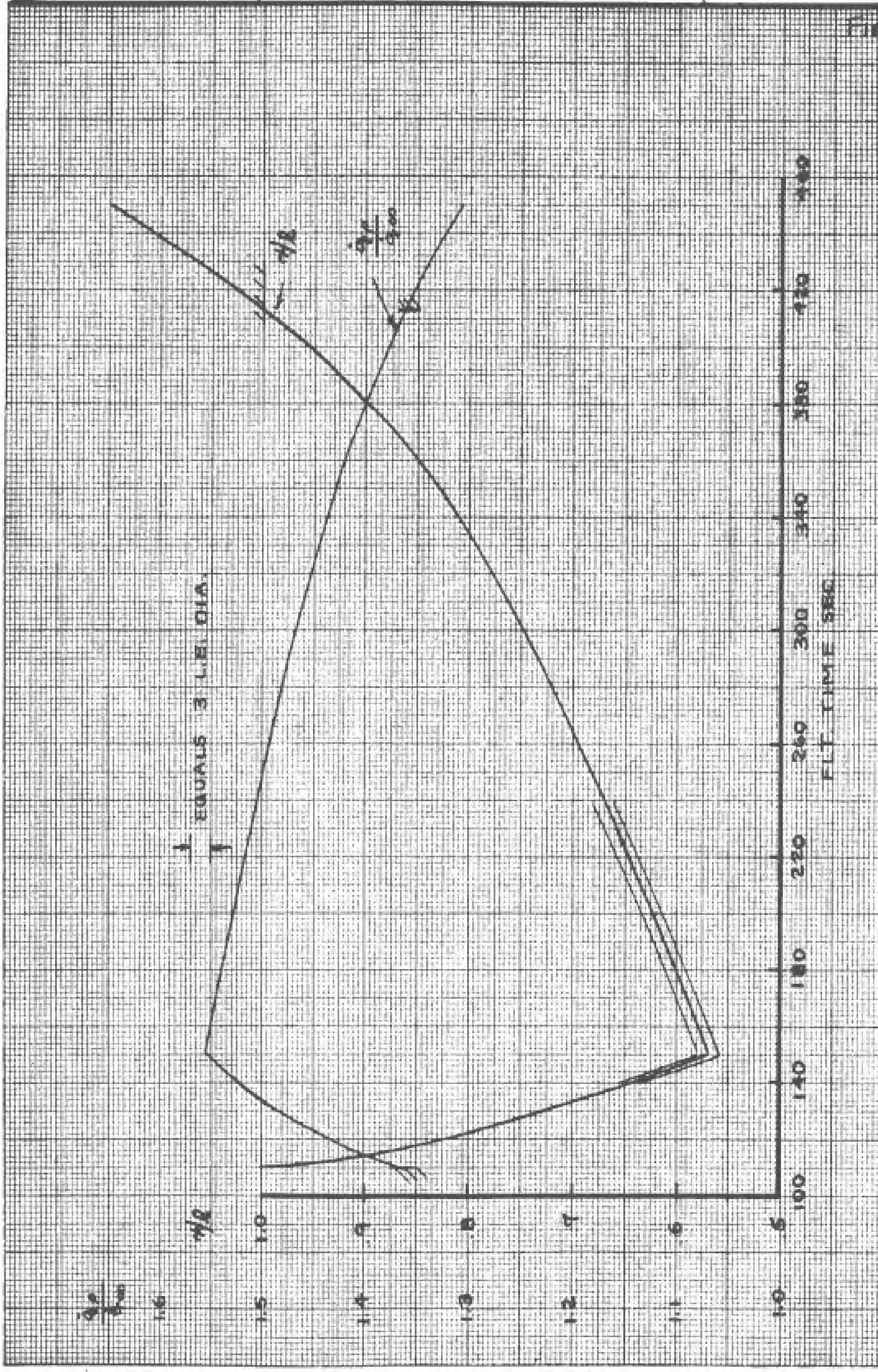

BOW SHOCK LOCATION AND HEAT FLUX RATIO - DESIGN MISSION

PREPARED BY:	**NORTH AMERICAN AVIATION, INC.**	PAGE NO. 6A OF
CHECKED BY:	Effect of Region of Influence of Bow	REPORT NO. NA-64-177 Appendix A
DATE:	Shock on Additional Ablation Thickness Req'd	MODEL NO. X-15A-2

FIG. 4

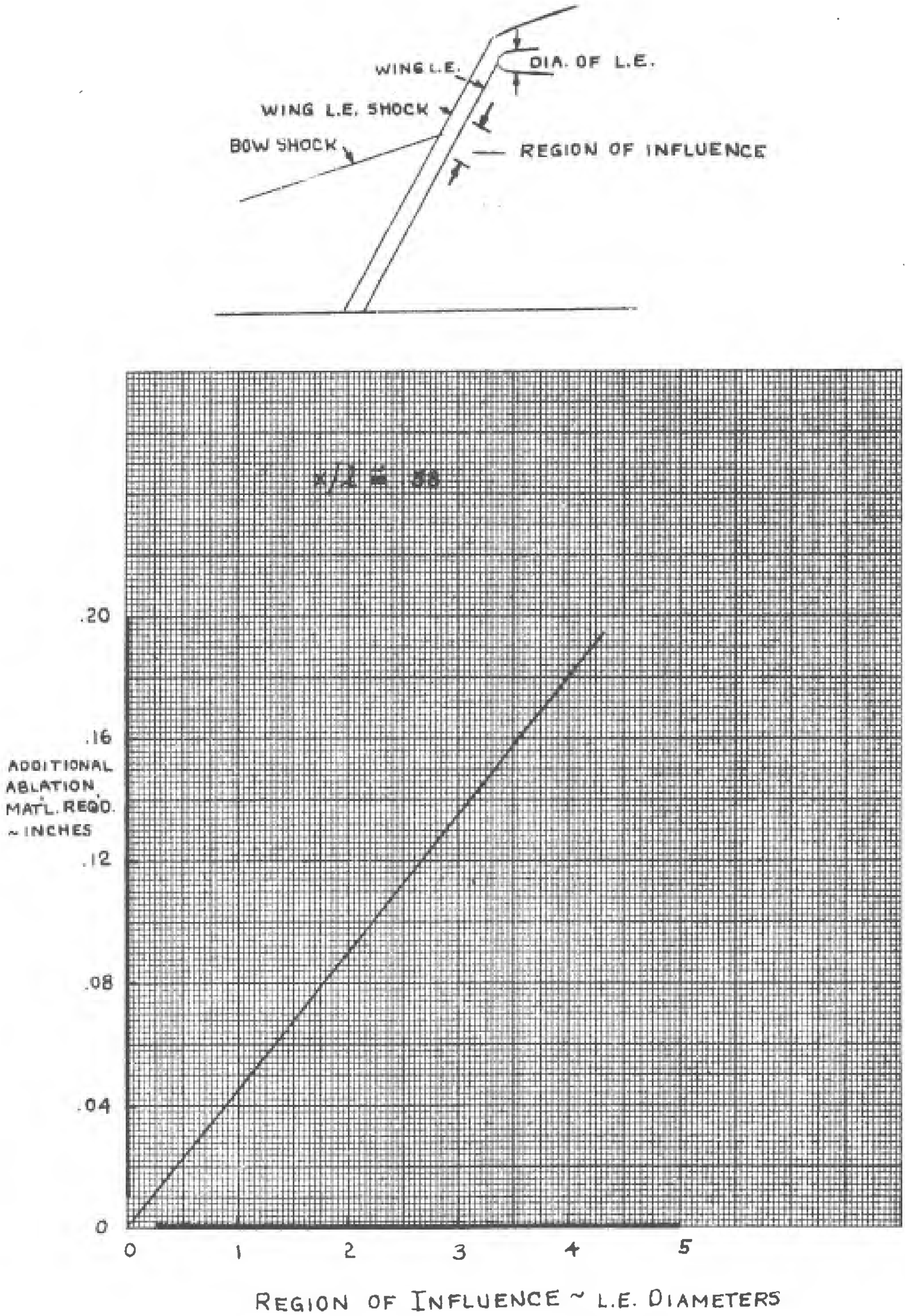

PREPARED BY:	NORTH AMERICAN AVIATION, INC.	PAGE NO. 7A OF
CHECKED BY:	Calculated Distribution of Additional	REPORT NO. NA-64-177 Appendix A
DATE:	Ablation Thickness Req'd Due To Bow Shock	MODEL NO. X-15A-2

FIG. 5

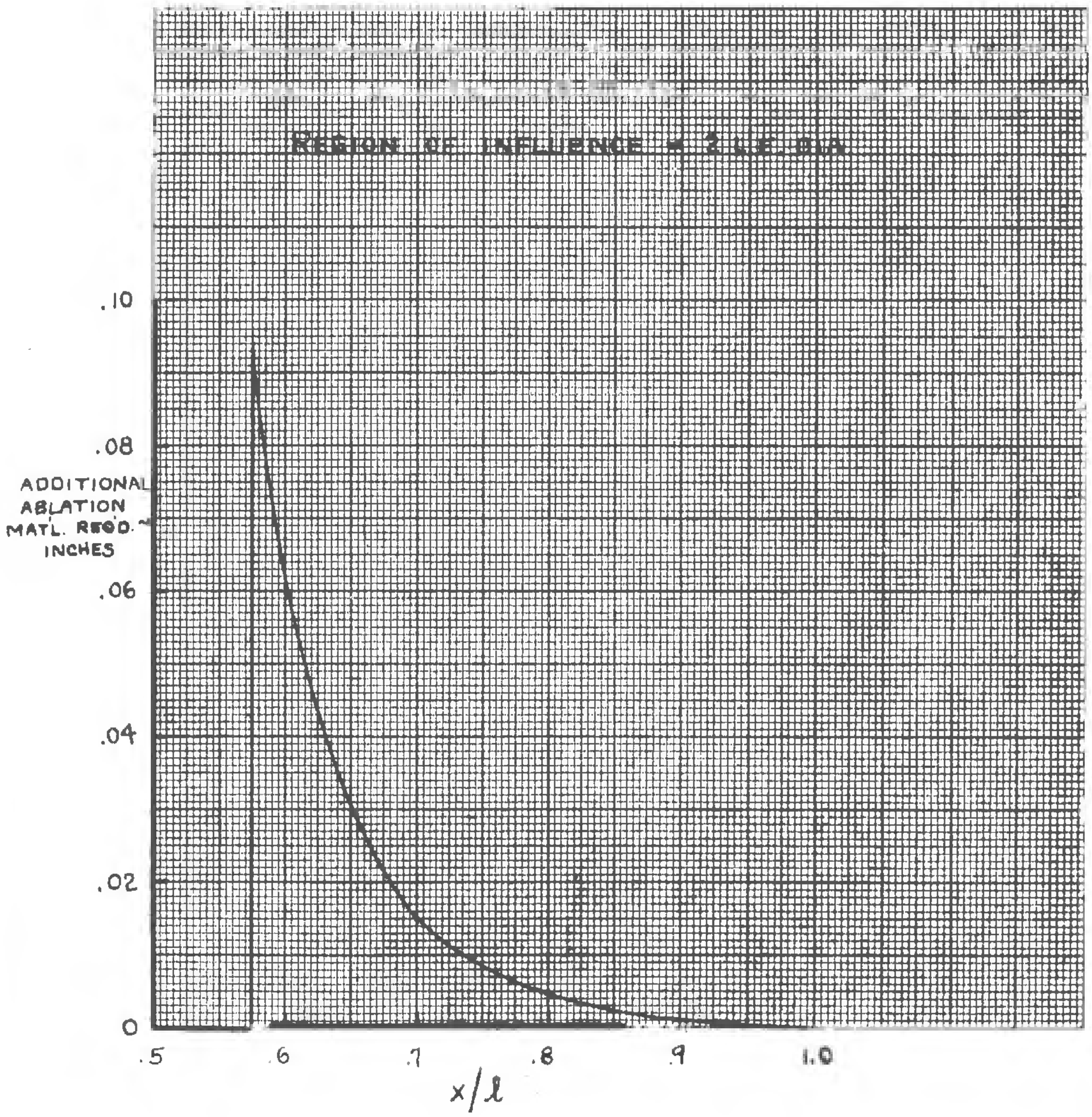

1002-X-9 NEW 6-62

PROTUBERANCE HEAT TRANSFER

Description of Protuberances

The following table shows the protuberances considered and the ablation thickness required on the fuselage adjacent to them.

TABLE I
PROTUBERANCE DESCRIPTION
AND ABLATION THICKNESS REQUIRED

	ITEM	FUS. STA.	SWEEP ANGLE	DIA.	AZIMUTH ANGLE, β	REQ'D THICK OF T-500-4a
1.	Pitot tube, forward of canopy	75	30° fwd.	.75 in.	180°	.764 in.
2.	APU exhaust stacks	190	0°	2 in.	135°	.209
3.	Antenna	200	30°	.75 in.	0°	.181
4.	Hydraulic vent stacks	215	0°	1 in.	30°	.271
5.	Lower vertical	469	30°	1 in.	0°	.115
6.	Upper vertical	469	30°	1 in.	180°	.078
7.	Landing skids	480	0°	6 in.	45°	.149

Theory

The following analysis treats the heating on the "flat" surfaces caused by the presence of a protuberance. Heating on the protuberances themselves is a separate problem. The theory developed by Yoshimura, in reference 1, the wind tunnel data from reference 2, and flight test data on X-15 ships 1 and 3 form the basis of the present analysis. Certain simplifications to the theory of reference 1 are incorporated herein.

Imagine a supersonic flow from left to right over a flat plate with no static pressure gradient in any direction and a turbulent boundary layer existing between the plate and free stream. This turbulent boundary layer is called the basic, or oncoming turbulent boundary layer. When a circular cylinder is inserted through the basic boundary layer, a phenomenon of three-dimensional boundary layer-shock interaction takes place in the vicinity of the forward half of the protuberance-plate junction and a pattern of "vorticies" is developed at the junction, as shown in Figure 1. A strong circulatory flow exists at the plate surface which flows radially outward from the junction; this is called the "reversed" flow, but the term "reversed" does not necessarily imply flow direction opposite to that of the free stream. The boundary layer developed by the "reversed" flow is considered to be laminar in the present case.

Peak Heating

The peak heating is considered to be located at X_1 and decreases to the undisturbed value at X_3. So far, the locations of X_1 and X_3 remain unspecified, but the value of peak heating at X_1 for an upright cylinder may be obtained from (1).

$$(1)\quad \left(\frac{h}{h_\infty}\right)_{X_1} = 51.83\,\frac{\left[1+0.51\,r_t\left(\frac{\gamma-1}{2}\right)M_\infty^2\right]^{.56}}{\left(\frac{V_\infty}{\nu_\infty}\right)^{1/4}\delta^{1/4}}\left(\frac{P_1}{P_\infty}\right)^{1/2}\frac{1}{\left[1+r_t\left(\frac{\gamma-1}{2}\right)M_\infty^2\right]^{.12}}$$

where:

$\left(\frac{h}{h_\infty}\right)_{X_1}$ - ratio of disturbed to undisturbed heat transfer coefficient at X_1.

r_t - recovery factor (.9 is taken for turbulent flow)

M_∞ - freestream Mach No.

$\frac{P_1}{P_\infty}$ - ratio of static pressure at X_1 to static pressure in freestream.

$\frac{V_\infty}{\nu_\infty}$ - freestream Reynolds No. per foot (called R_∞ hereafter)

δ - boundary layer thickness - ft.

$$(2)\quad \frac{P_1}{P_\infty} = \frac{P_n + P_\infty}{2P_\infty}$$

$$(3)\quad \frac{P_n}{P_\infty} = \frac{2\gamma M_\infty^2-(\gamma-1)}{\gamma+1} = \frac{7M_\infty^2-1}{6}$$ (static pressure across a normal shock)

$$(4)\quad \frac{P_1}{P_\infty} = \frac{7M_\infty^2+5}{12}$$

Equation (1) may be arranged as follows:

$$(5)\quad \left(\frac{h}{h_\infty}\right)_{X_1}(R_\infty)^{1/4}\delta^{1/4} = 51.83\left(\frac{P_1}{P_\infty}\right)^{1/2}\frac{\left[1+0.51\,r_t\left(\frac{\gamma-1}{2}\right)M_\infty^2\right]^{.56}}{\left[1+r_t\left(\frac{\gamma-1}{2}\right)M_\infty^2\right]^{.12}}$$

The above equation is shown in Figure 2 along with data points from References 1 and 2. Good agreement is noted in the Mach number range tested. Also shown are test points for a cylinder swept forward and aft; along with simple analytic expressions to represent the effects of sweep.

The following table shows (Table II) conditions for the X-15A-2 M = 8 design mission. Values of boundary layer thickness are obtained from Reference 3. The variation of $(h/h_\infty)_{X_1}\,\delta^{1/4}$ is shown in Figure 3.

TABLE II
DESIGN MISSION CONDITIONS

M_{∞}	Approx. Alt. 1000 ft.	R_{∞} 1/ft	$\left(\frac{h}{h_{\infty}}\right)_{x_1} \delta^{1/4}$ $ft^{1/4}$	δ (ft) @ $x \cong 6$ ft	δ (ft) @ $x \cong 18$ ft	δ (ft) @ $x \cong 42$ ft
2	69	108×10^4	2.98	.1025	.247	.487
4	96	48×10^4	8.69	.128	.308	.607
6	100	61.4×10^4	15.21	.1405	.338	.666
8	100	81.6×10^4	23.05	.1525	.368	.725

Heating Distribution

The variation of heating upstream of a protuberance is expressed as follows:

$$(6)\quad \left(\frac{h}{h_{\infty}}\right)_x = \left(\frac{h}{h_{\infty}}\right)_{x_1} \left(\frac{X_1}{X}\right)^{1/2} \left(\frac{P}{P_1}\right)^{1/2}$$

From previous arguments, equation (6) must equal $(h/h_{\infty})_{x_1}$ at $X = X_1$ and must equal unity at $X = X_3$. If P is set equal to P_{∞} at $X = X_3$, equation (6) may be solved at $X = X_3$ as:

$$(7)\quad \frac{X_1/D}{\delta^{1/2}} = \frac{X_3}{D} \frac{(P_1/P_{\infty})}{\left[\left(\frac{h}{h_{\infty}}\right)_{x_1} \delta^{1/4}\right]^2}$$

where D - protuberance diameter

Thus, at a given Mach and δ, if X_1 is specified, X_3 is determined, and vice-versa. From examination of test data, it appears preferable to select a value of X_3. A value of $\frac{X_3}{D} = 2$ will be tentatively selected. The static pressure is assumed to vary linearly between X_1 and X_3. Rewrite equation (6) as:

$$(8)\quad \frac{h_x}{h_{x_1}} = \left(\frac{X_1/D}{X/D}\right)^{1/2} \left(\frac{P}{P_1}\right)^{1/2}$$

The linear pressure distribution, assuming $\frac{X_3}{D} = 2$, is:

$$(9)\quad \frac{P}{P_1} = \left(\frac{\frac{P_{\infty}}{P_1} - 1}{2 - X_1/D}\right)\left(\frac{X}{D} - 2\right) + \frac{P_{\infty}}{P_1}$$

At high Mach numbers, both P_{∞}/P_1, and X_1/D tend to be small, hence a simplification of equation (9) is:

$$(10)\quad \frac{P}{P_1} = 1 - \frac{X/D}{2}$$

which when substituted into (8) yields

$$(11)\quad \frac{h_x/h_{x_1}}{(X_1/D)^{1/2}} = \left(\frac{1}{X/D} - \frac{1}{2}\right)^{1/2}$$

Equations (8), (7) and (9) have been solved for various representative design flight conditions (see also Table II) and plotted in Figure 4. Also, shown is the simplified equation (11). Due to the excellent agreement for a wide range of flight conditions, the simplified equation (11) will be used from here on.

From examination of Figure 4 consider the following.

Rather than attempt to tailor the ablation coating to a shape similar to the curve on Figure 4, consider a uniform thickness from X/D = 0 to X_3/D. The maximum value, $(h/h_\infty)_{x_1}$ since it affects a relatively small area, seems toohigh to use. Consider, then, an average value of heating ratio from the protuberance to X_3/D. This average value is obtained by integration between X/D = 0 and X_3/D and dividing the result by X_3/D. Groups of parameters will fall outside the integral and may be treater independently. The heat flux ($\dot q_x$) ratio is now defined as:

$$(12)\quad \frac{\dot q_x}{\dot q_\infty} \triangleq \frac{\int_0^{\bar x_3} (h_x/h_\infty)\, d\bar x}{\bar x_3}$$

where: $\dot q_x/\dot q_\infty$ - ratio of average heat flux near a protuberance to the undisturbed value.

$\bar x = X/D \;;\; \bar x_3 = X_3/D$

Repeating equation (6)

$$(6)\quad \frac{h_x}{h_\infty} = \left(\frac{h_{x_1}}{h_\infty}\right)\left(\frac{X_1}{X}\right)^{1/2}\left(\frac{P}{P_1}\right)^{1/2} = \left(\frac{h_{x_1}}{h_\infty}\right)\left(\frac{\bar X_1}{\bar X}\right)^{1/2}\left(\frac{P}{P_1}\right)^{1/2}$$

and, in general, the static pressure ratio (see also eq. (10)) can be written

$$(13)\quad \frac{P}{P_1} = 1 - \frac{\bar X}{\bar X_3}$$

Equation (7) can be rewritten as:

$$(14)\quad \frac{\bar x_1}{\bar x_3} = \frac{P_1/P_\infty}{(h_{x_1}/h_\infty)^2} \quad \text{or} \quad \left(\frac{\bar x_1}{\bar x_3}\right)^{1/2} = \frac{(P_1/P_\infty)^{1/2}}{h_{x_1}/h_\infty}$$

Thus (12) can be written as:

$$(15)\quad \frac{\dot q_x}{\dot q_\infty} = \int_0^{\bar x_3} \frac{1}{\sqrt{\bar x_3}}\left(\frac{h_{x_1}}{h_\infty}\right)\left(\frac{\bar x_1}{\bar x_3}\right)^{1/2}\left(1-\frac{\bar x}{\bar x_3}\right)^{1/2}\left(\frac{1}{\bar x}\right)^{1/2} d\bar x = \frac{(P_1/P_\infty)^{1/2}}{\sqrt{\bar x_3}} \int_0^{\bar x_3}\left(\frac{1}{\bar x} - \frac{1}{\bar x_3}\right)^{1/2} d\bar x$$

The integral, when evaluated, becomes:

$$(16) \quad \int_0^{\bar{x}_3} \left(\frac{1}{\bar{x}} - \frac{1}{\bar{x}_3} \right)^{1/2} d\bar{x} = \sqrt{\bar{x}_3} \left(\frac{\pi}{2} \right)$$

Finally, substituting (16) into (15) obtain:

$$(17) \quad \frac{\dot{q}_x}{\dot{q}_{x_\infty}} = \left(\frac{P_1}{P_\infty} \right)^{1/2} \left(\frac{\pi}{2} \right) = \frac{\pi}{2} \left[\frac{7 M_\infty^2 + 5}{12} \right]^{1/2} \qquad (\text{see eq. } (4))$$

Equation (17) is plotted in Figure 5. Note that eq. (17) is independent of $\bar{x}_3$. This is convenient, since it will permit latitude in the choice of the size of the region around the protuberance which will be protected, without affecting the required thickness of the ablation material.

Heat Flux and Ablation Thickness Evaluation at Protuberances

Using the information previously derived, the local heat flux values for the design mission may now be determined. Undisturbed values of cold wall heat flux are obtained from calculations made using an IBM program called AXFAC. For protuberances with zero sweep, the values of heating rate ratio shown in Figure 5, are used. To account for sweep, the following relations are used (see also Figure 2).

$$(18) \quad \frac{\dot{q}_{\Omega\,FWD}}{\dot{q}_{\Omega=0^\circ}} = \frac{1}{\cos^2 \Omega}$$

For a protuberance swept back

$$(19) \quad \frac{\dot{q}_{\Omega}}{\dot{q}_{\Omega=0^\circ}} = \cos^3 \Omega$$

The heat flux calculations are presented in Table III. Required thicknesses of Thermolag T-500-4a were determined using these heat flux values and a cold wall heat blockage based on $h_{eff} = 13800 - 101\ \dot{q}_{x_{cw}}$. The thicknesses (which are not added to the undisturbed values) are tabulated in Table I. Note that the heating rates and thickness required at the swept forward pitot tube are very high. It would appear desirable to remove this pitot tube and obtain the required pressure information from another source, such as the ball nose.

Due to the relatively large thicknesses of ablation material required, rather than spray heavier coats of T-500-4a in the protuberance regions when the rest of the airplane is being sprayed, pre-sprayed patches will probably be made in the lab and attached with an adhesive in the field. The patches will extend radially a distance of 3 diameters ($X_3/D = 3$) from the protuberance except for the landing skid which will use 2 diameters. For non-circular protuberances, such as the pitot, antenna, upper and lower verticals and landing skids, the protective ablation patch will still be circular, but cut out to fit around the protuberance. The added weight of ablation material required around protuberances will have a negligible (approximately 1%) effect on the total weight of the ablation system.

PREPARED BY: B	NORTH AMERICAN AVIATION, INC.	PAGE NO. 6B OF
CHECKED BY: R.J.	TABLE III	REPORT NO. NA-64-177 Appendix B
DATE:	HEAT FLUX AT PROTUBERANCES	MODEL NO.

TIME (sec.)	MACH No.	$\dot{q}$ PITOT	$\dot{q}$ HYD. VENT	$\dot{q}$ LOWER VENTRAL	$\dot{q}$ UPPER VERTICAL	$\dot{q}$ LANDING SKID	$\dot{q}$ APU EXHAUST	$\dot{q}$ ANTENNA
0	.826	0	0	0	0	0	0	0
30	1.638	.780	.526	.254	.216	.351	.49	.37
40	1.694	.922	.629	.304	.251	.426	.57	.44
49	1.766	.976	.657	.331	.276	.445	.61	.47
54	1.859	1.285	.729	.336	.336	.515	.74	.48
60	2.014	1.750	.972	.443	.443	.68	.97	.63
70	2.355	2.94	1.595	.718	.718	1.101	1.60	1.04
80	2.809	5.2	2.69	1.209	1.209	1.86	2.69	1.75
90	3.349	9.35	4.46	2.03	2.03	3.11	4.47	2.91
100	3.940	16.05	7.05	3.18	3.18	4.90	7.05	4.58
112	4.774	32.2	12.55	5.67	5.67	8.71	12.54	8.17
113	4.842	21.4	16.10	8.56	5.92	10.31	13.05	12.34
120	5.383	31.1	21.65	11.37	8.13	13.98	17.91	16.31
150	7.975	176.5	66.75	32.8	27.65	44.6	61.00	48.00
150.1	7.975	153.5	71.60	37.0	27.65	46.8	61.00	53.10
180	7.546	118.1	61.7	32.25	23.4	40.1	51.70	46.40
220	7.077	87.5	52.15	27.7	19.3	33.5	42.60	39.80
280	6.130	49.3	33.7	18.05	12.38	21.65	27.35	25.90
360	5.223	26.9	20.81	11.28	7.44	13.2	16.40	16.19
440	4.306	13.73	10.91	5.94	3.85	6.93	8.57	8.53
450	4.202	12.89	10.16	5.54	3.62	6.43	7.97	7.93
500	3.731	9.78	7.28	3.82	2.75	4.73	6.09	5.47
540	3.358	7.62	5.34	2.70	2.135	3.53	4.73	3.87
570	3.077	6.03	4.10	2.02	1.683	2.74	3.72	2.90
600	2.789	4.55	3.00	1.443	1.265	2.05	2.79	2.08
650	2.293	2.46	1.57	.728	.692	1.065	1.51	1.05
680	2.045	1.64	1.026	.473	.456	.70	1.00	.69
710	1.782	.803	.494	.224	.224	.344	.50	.32
836	1.012	0	0	0	0	0	0	0

FORM 18-G-28 (VELLUM)

REFERENCES

1. NA-61-174 "A Proposal For Analyses and Tests of Heat Transfer in the Vicinity of Surface Protuberances in Hypersonic Flows" dated 17 April 1964.

2. NASA TND-1372 "Heat Transfer and Pressure Measurements on a Flat-Plate Surface and Heat-Transfer Measurements on Attached Protuberances in a Supersonic Turbulent Boundary Layer at Mach Numbers of 2.65, 3.51 and 4.44" dated December 1962.

3. JAS Volume 18, No. 5 "Turbulent Boundary Layer in Compressible Fluids" dated March 1951.

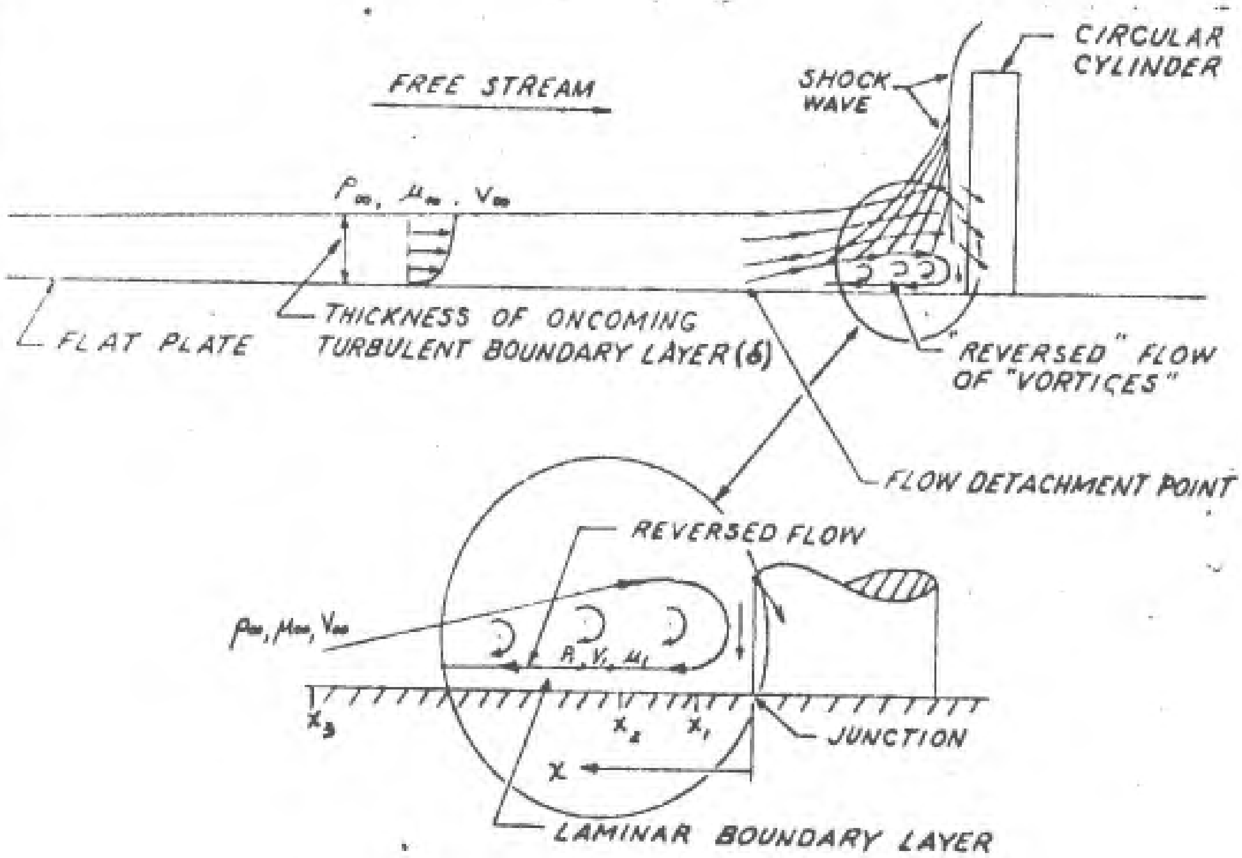

Figure 1

Sketch of Flow Near A Protuberance

FORM 1021-S

NORTH AMERICAN AVIATION, INC.

PREPARED BY:	PAGE NO. 9B OF
CHECKED BY:	REPORT NO. NA-64-177 Appendix B
DATE:	MODEL NO.

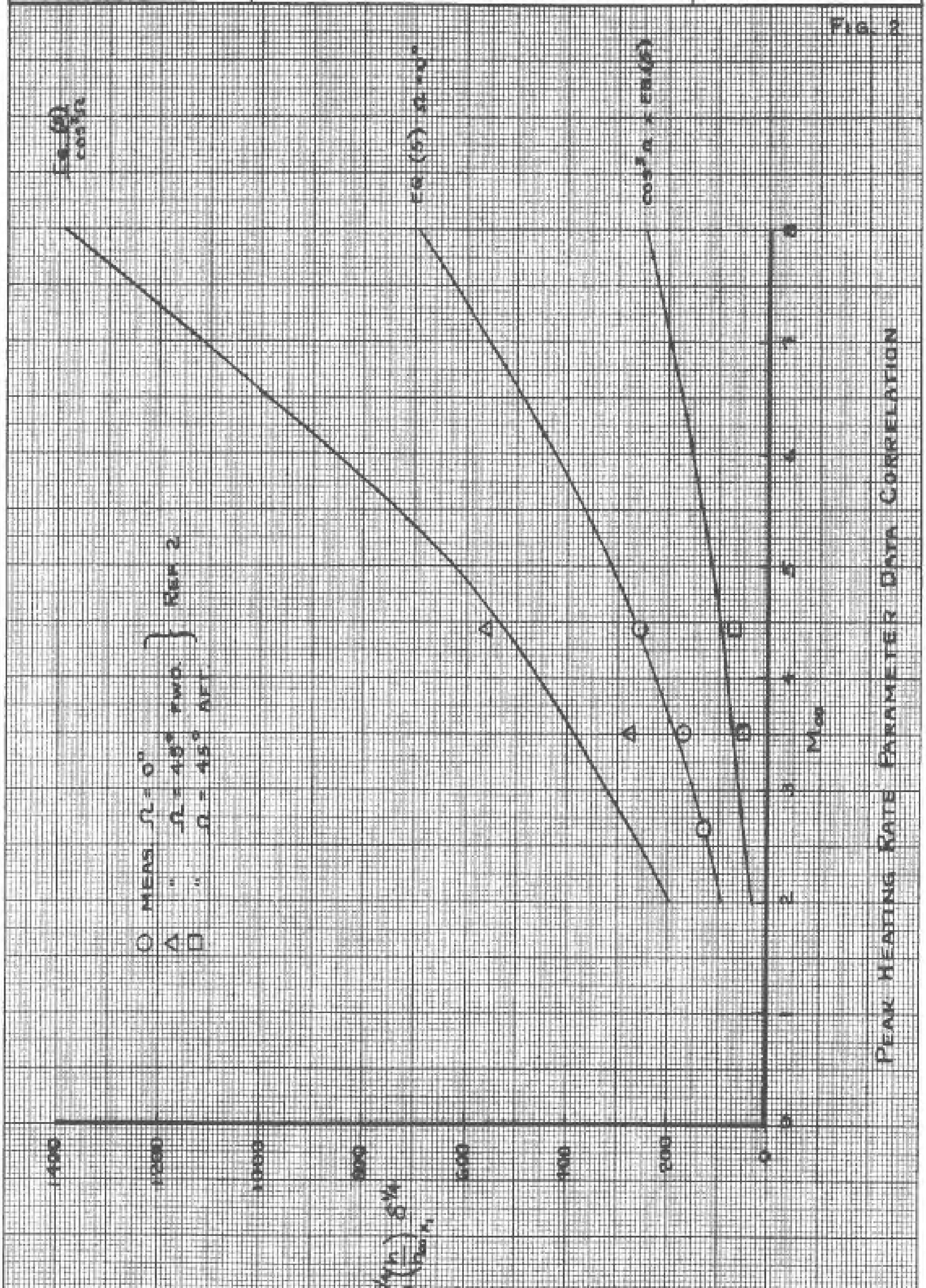

FORM 1021-S

PREPARED BY:	NORTH AMERICAN AVIATION, INC.	PAGE NO. 10B OF
CHECKED BY:		REPORT NO. NA-64-177 Appendix B
DATE:		MODEL NO.

FIG. 3

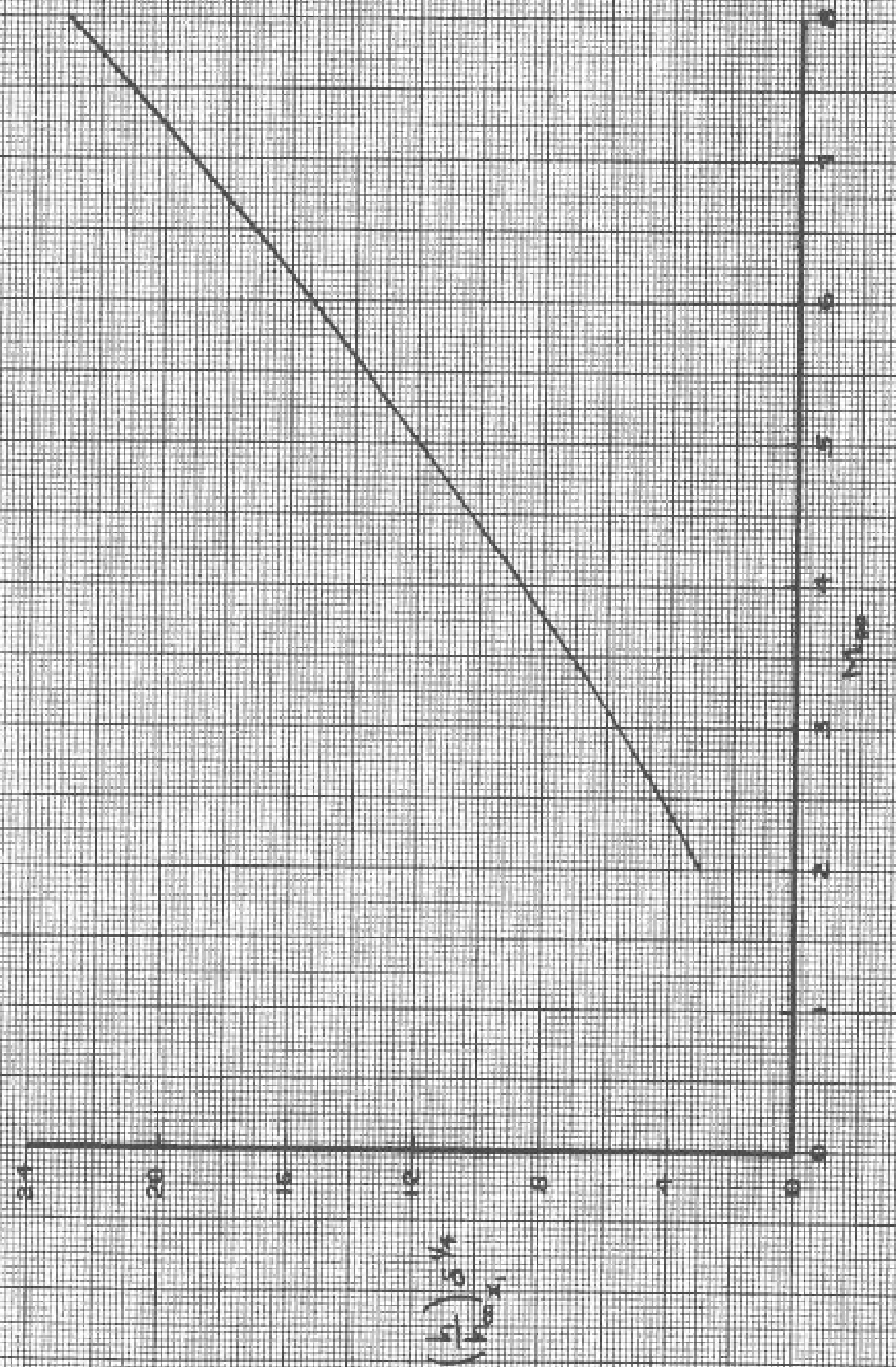

PEAK HEATING RATE RATIO ($\alpha = 0°$) - DESIGN MISSION

K&E ALBANENE TRACING PAPER LJ 0488

FORM 1021-5

PREPARED BY:	NORTH AMERICAN AVIATION, INC.	PAGE NO. 11B OF
CHECKED BY:		REPORT NO. NA-64-177 Appendix B
DATE:		MODEL NO.

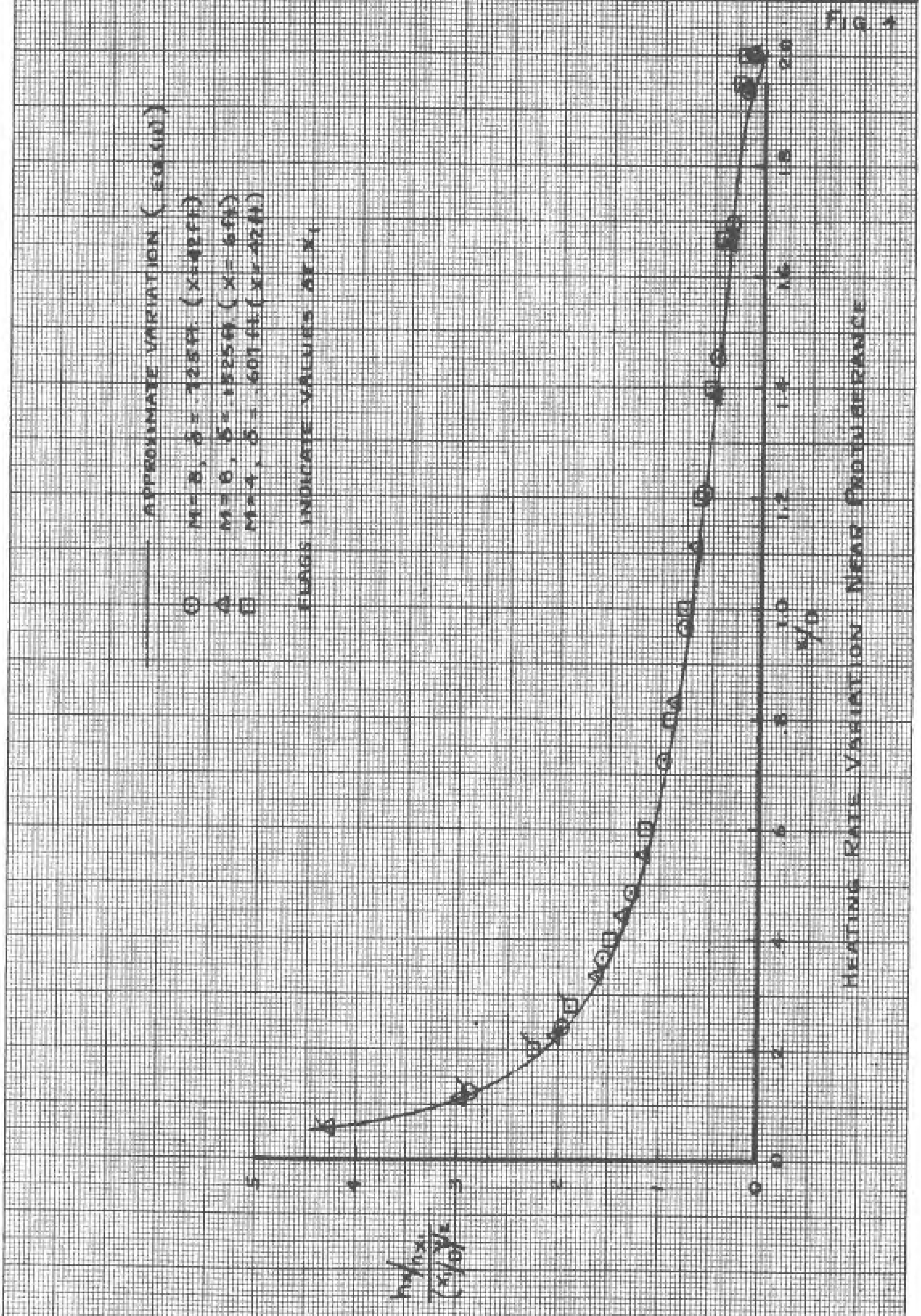

K&E ALBANENE TRACING PAPER LA 0498

FORM 1021-S

PREPARED BY:	NORTH AMERICAN AVIATION, INC.	PAGE NO. 12B OF
CHECKED BY:		REPORT NO. NA-64-177 Appendix B
DATE:		MODEL NO.

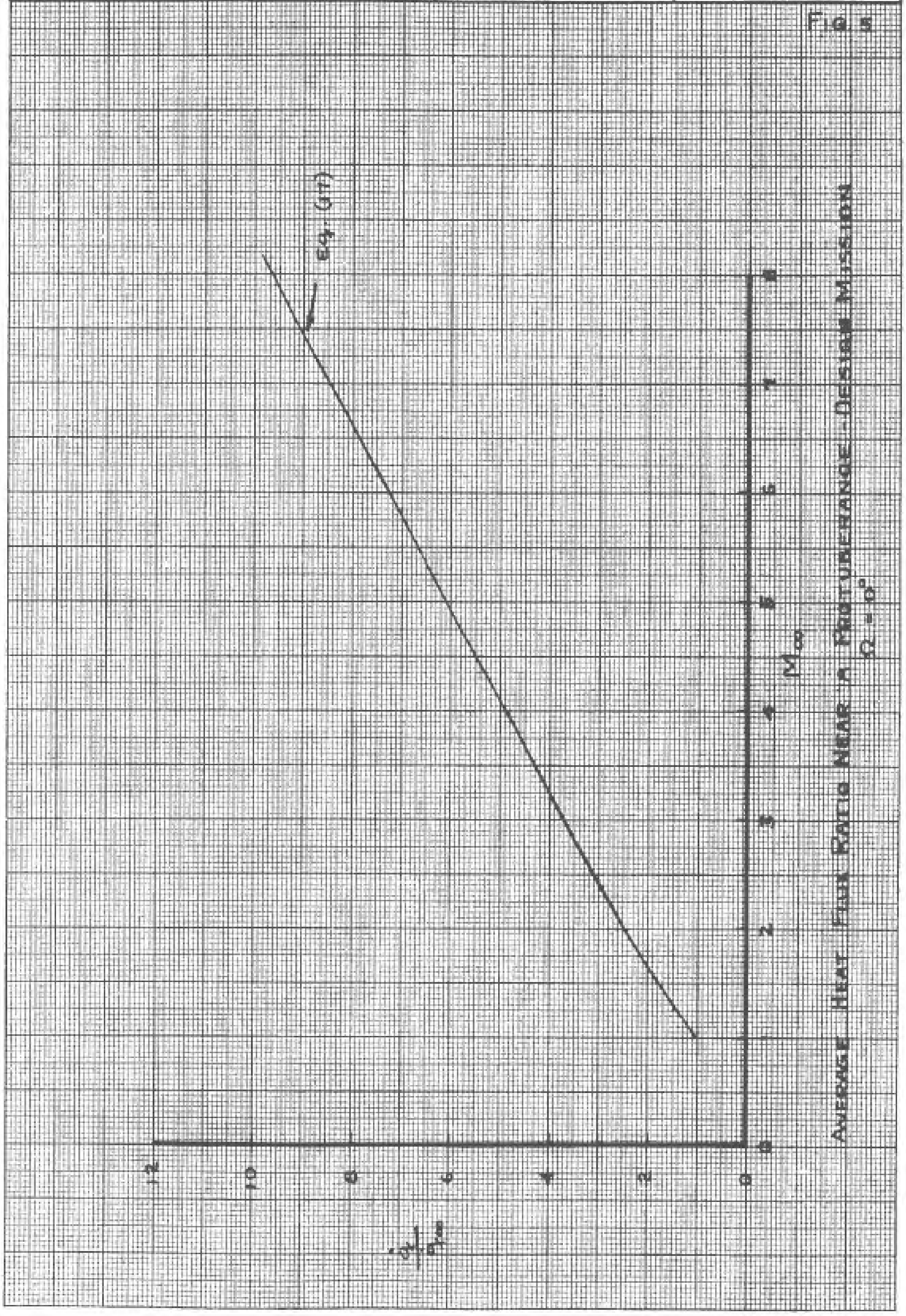

PLASMA TUNNEL MODEL PHOTOGRAPHS

Complete photographic coverage was made of the ablation tests. Page 2C shows a typical leading edge model before and after a test run. The model is shown mounted on the model holder in the "before" photograph. Page 3C shows a typical flat plate model before and after a test run. The photographs on page 4C show the mounting arrangement in the tunnel of a leading edge model and of a flat plate model. Note that the flat plate model is rotated 45° about the mounting axis. This facilitated motion picture coverage. The particular flat plate model shown is a cork model used for flow pattern tests.

Pages 5C through 45C show the leading edge and flat plate models after testing. They appear in the same order as they are listed in Table III and Table V of the body of this report.

The upstream apex of some leading edge specimens was filed off prior to testing to permit proper axial location of the model.

There were more than 3000 feet of 16mm motion pictures taken which are stored on five reels. They are identified by Photo-Instrumentation number PI-63-27 under the title "X-15A-2 Ablative Materials Evaluations (PT8)". The title appearing in the film on the first reel is "North American Aviation Advanced X-15A-2 Ablation Tests in the NAA 1MW Plasma Tunnel." These films may be requested from the X-15 Project Manager.

NA-64-177
Appendix C

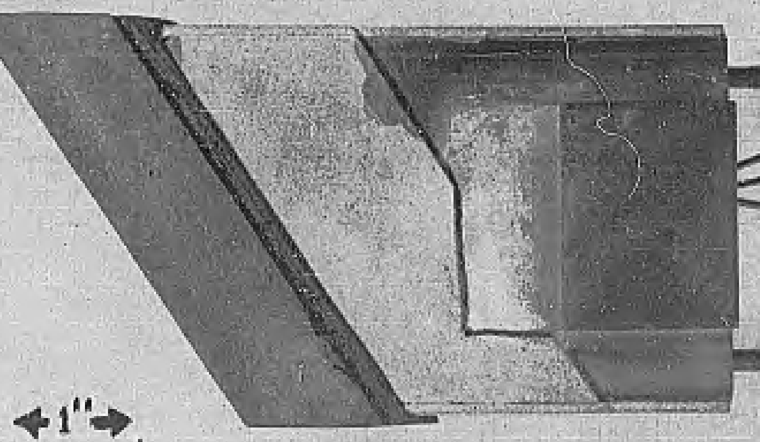

BEFORE TEST
Model Holder With A
TYPICAL LEADING EDGE MODEL

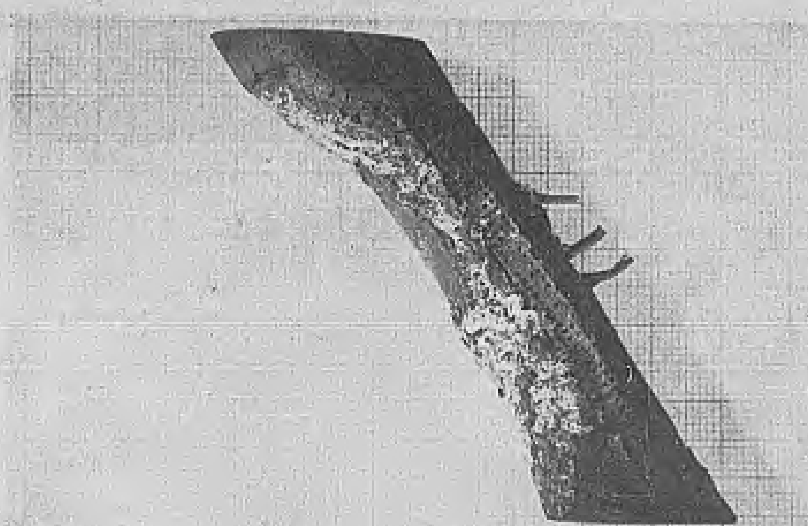

EMERSON ELECTRIC MODEL No: STAG LINE #9
PT-8 RUN No. 1

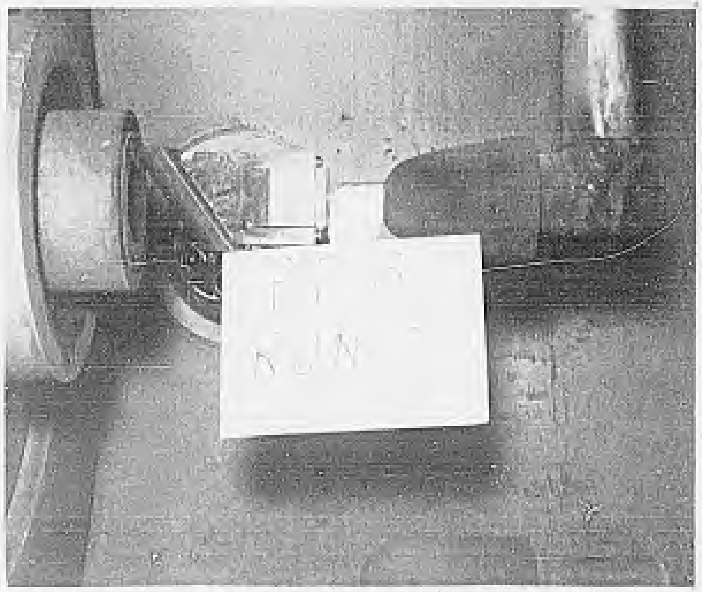
RUN

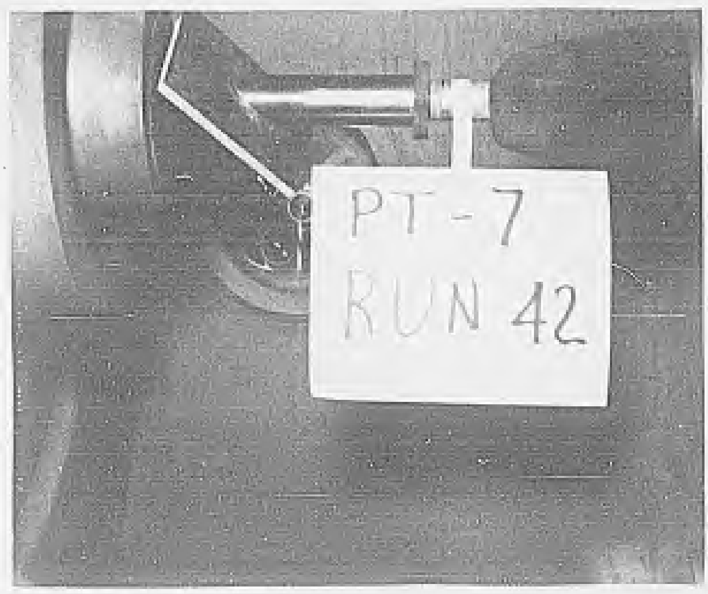
PT-7
RUN 42


PT-8
TYPICAL
FLAT PLATE
SPECIMEN

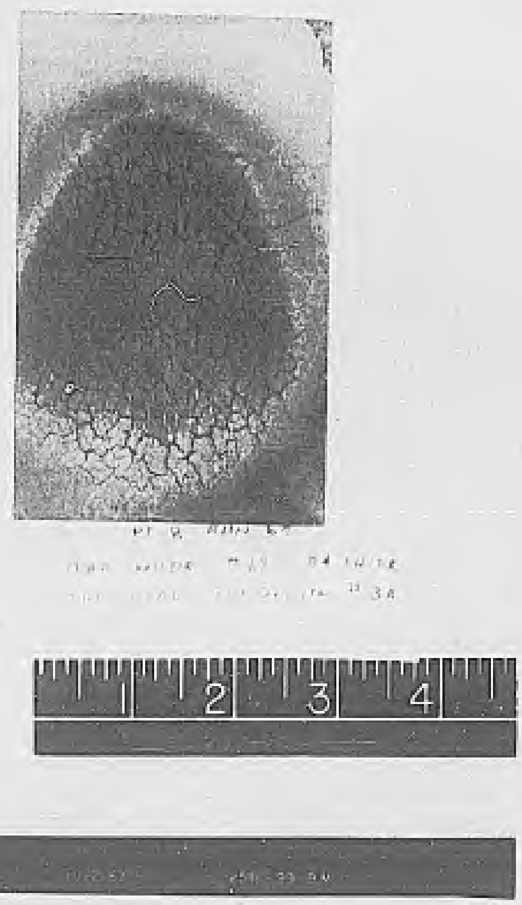
2
3
4

NORTH AMERICAN AVIATION, INC.
INTERNATIONAL AIRPORT
LOS ANGELES 9, CALIFORNIA

NA-64-177
Appendix C

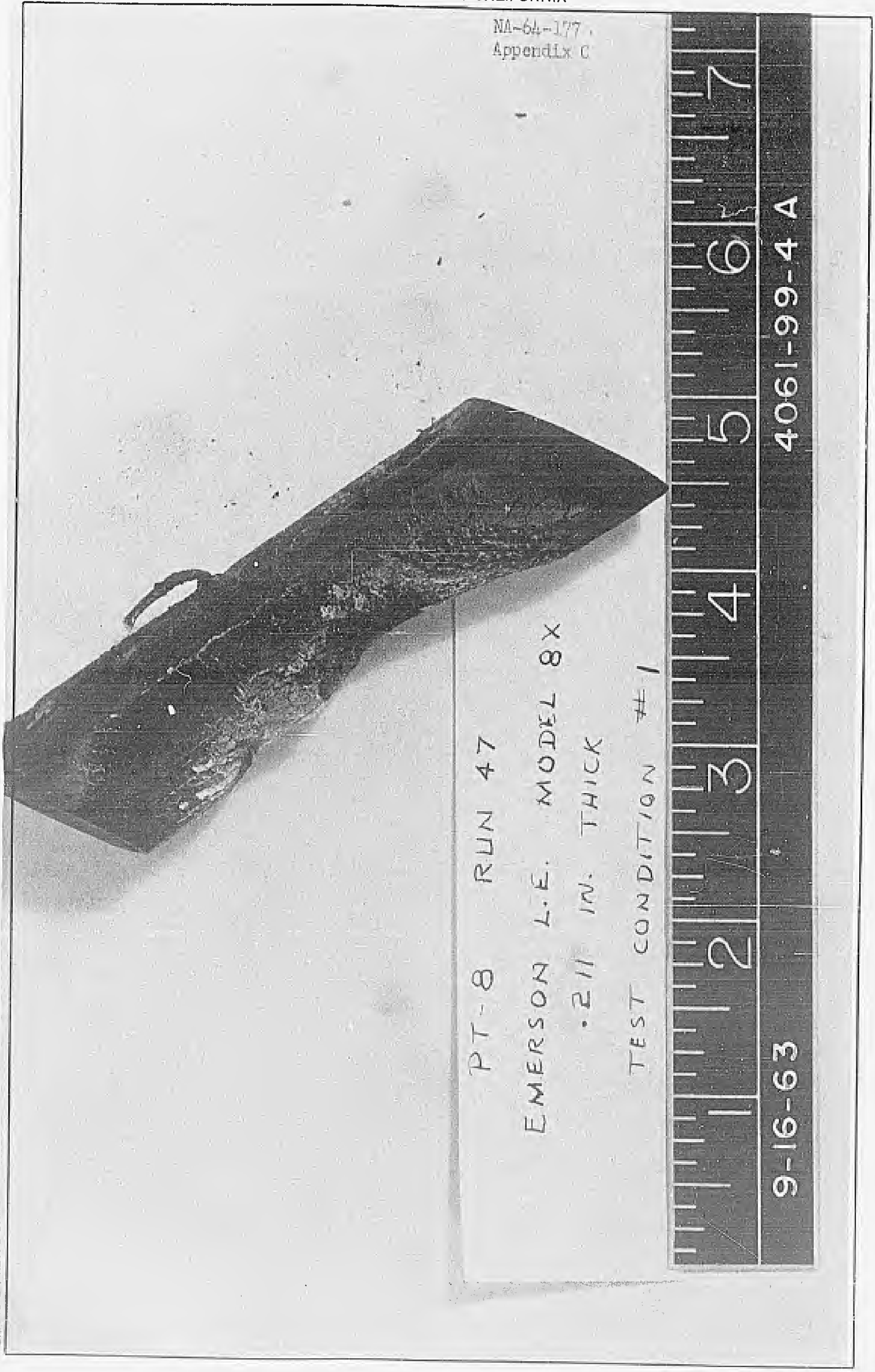

NORTH AMERICAN AVIATION, INC.
INTERNATIONAL AIRPORT
LOS ANGELES 9, CALIFORNIA

NA-64-177
Appendix C

FORM 18-C-1 REV. 9-61

NORTH AMERICAN AVIATION, INC.
INTERNATIONAL AIRPORT
LOS ANGELES 9, CALIFORNIA

NA-64-377
Appendix C

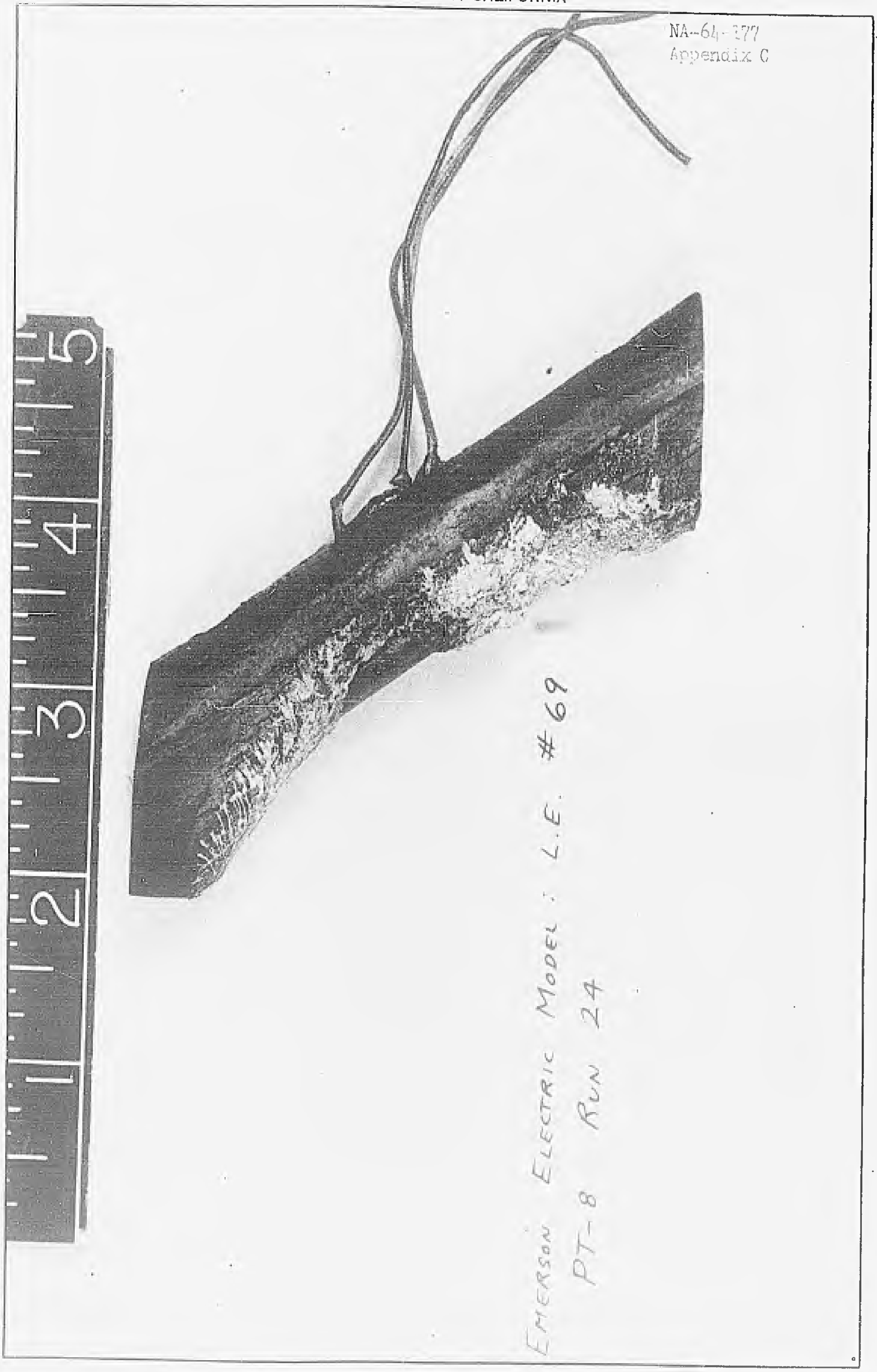

NA-64-177
Appendix C

NA-64-177
Appendix C

FORM 18-G-1 REV. 9-61

NA-64-177
Appendix C

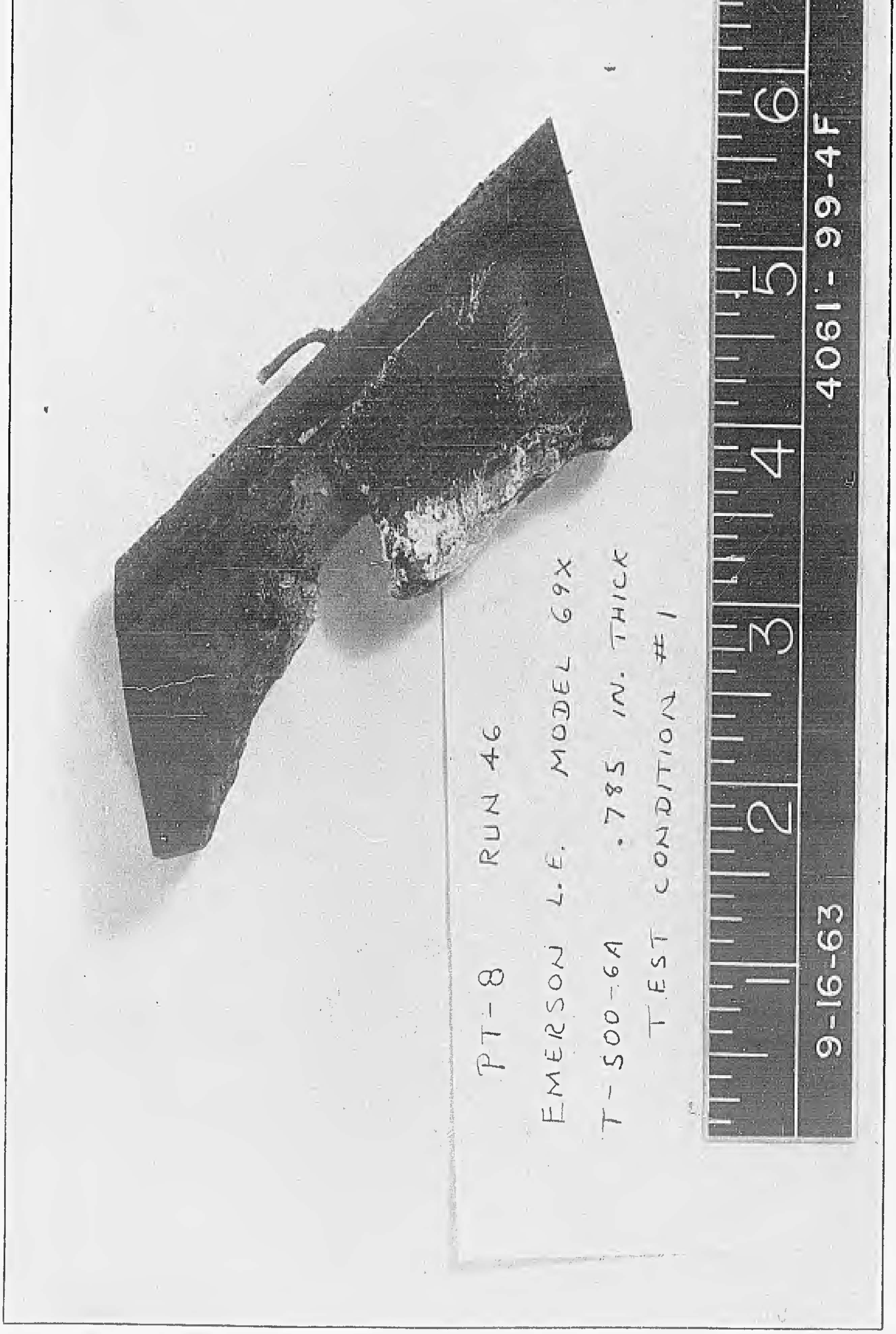

NORTH AMERICAN AVIATION, INC.
INTERNATIONAL AIRPORT
LOS ANGELES 9, CALIFORNIA

NA-64-177
Appendix C

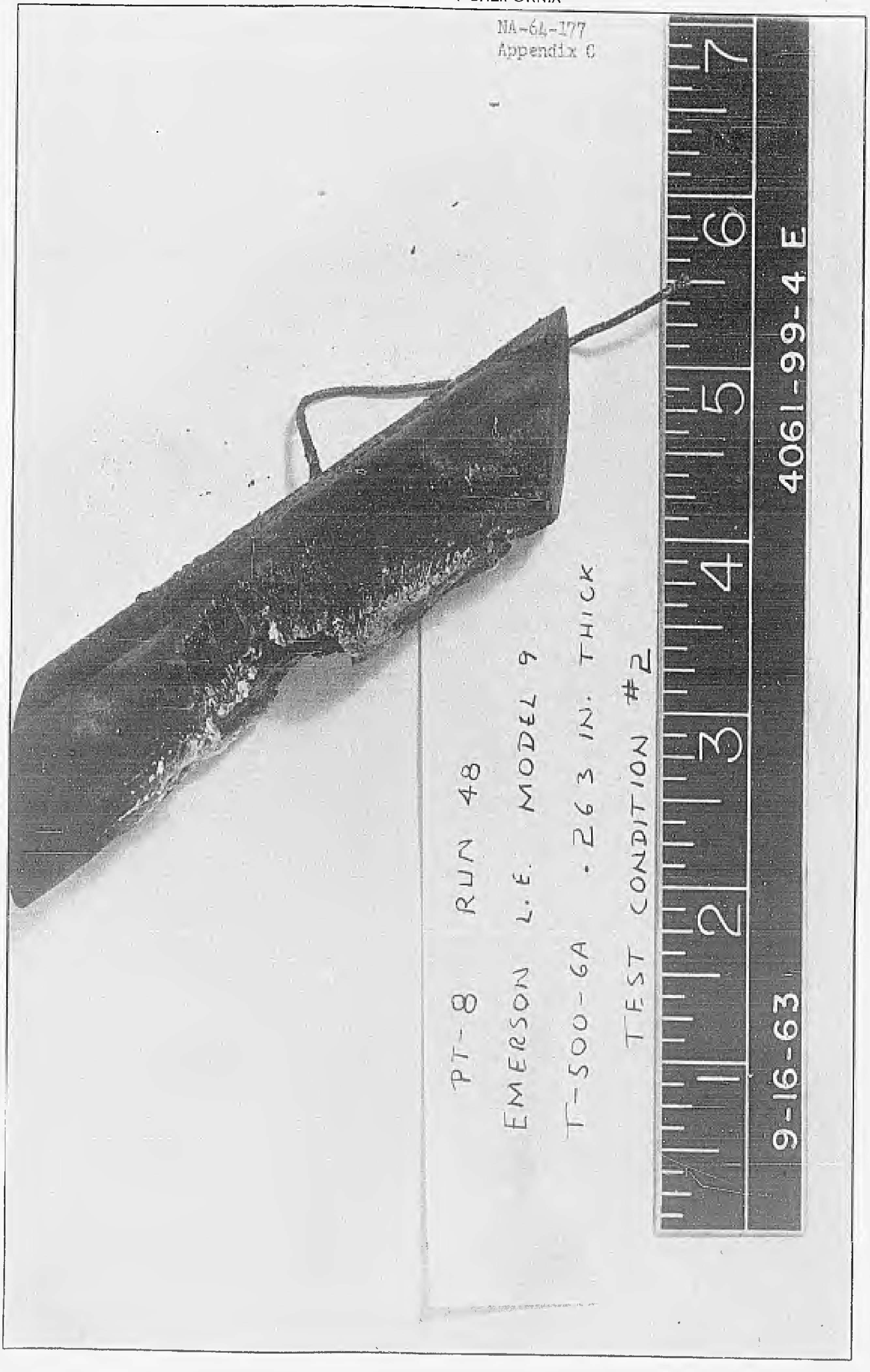

NA-64-177
Appendix C

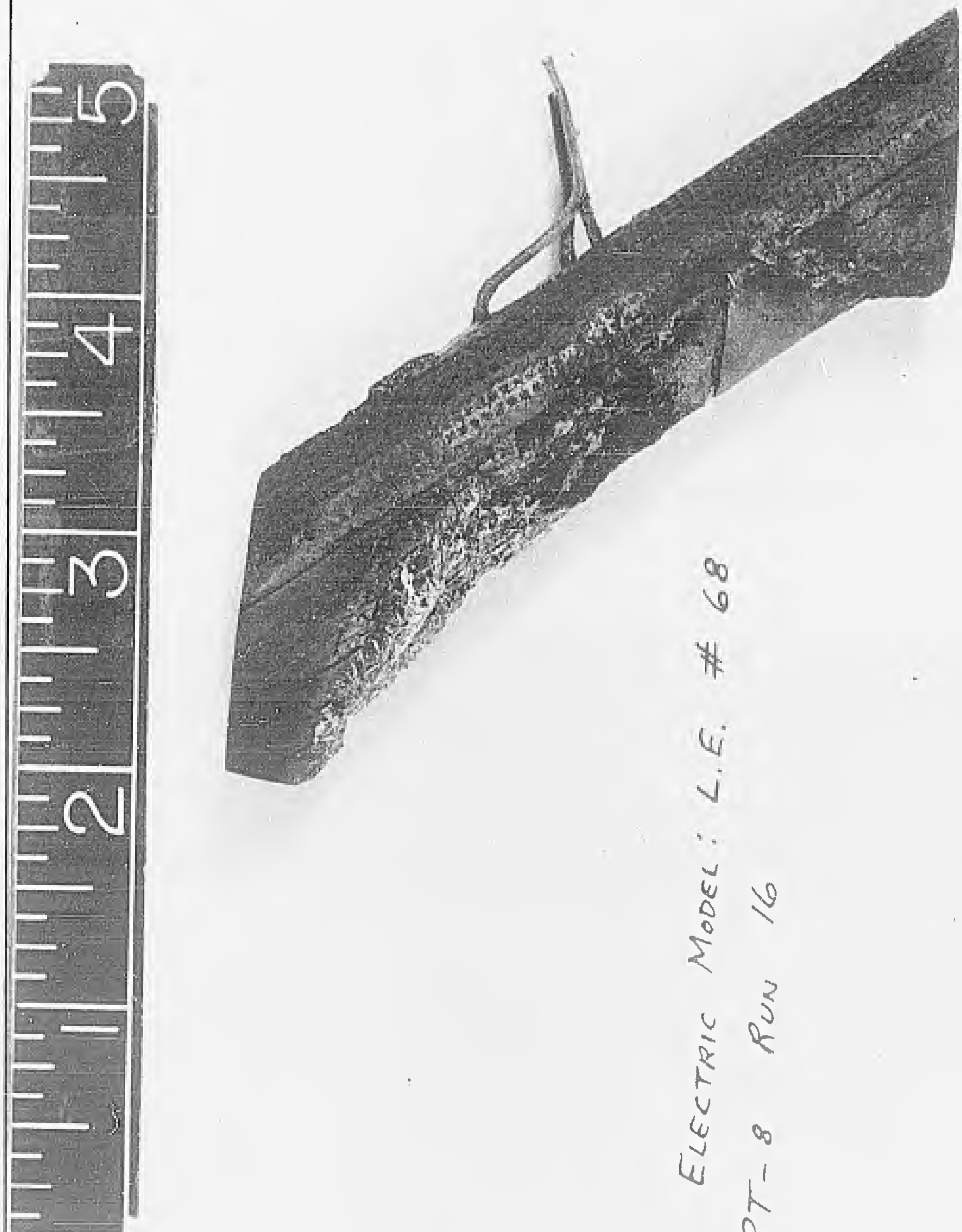

EMERSON ELECTRIC MODEL: L.E. # 68
PT-8 RUN 16

FORM 18-C-1 REV. 9-61


EMERSON ELECTRIC MODEL: L.E. #71
PT-8 RUN 17

NORTH AMERICAN AVIATION, INC.
INTERNATIONAL AIRPORT
LOS ANGELES 9, CALIFORNIA

NA-64-177
Appendix C

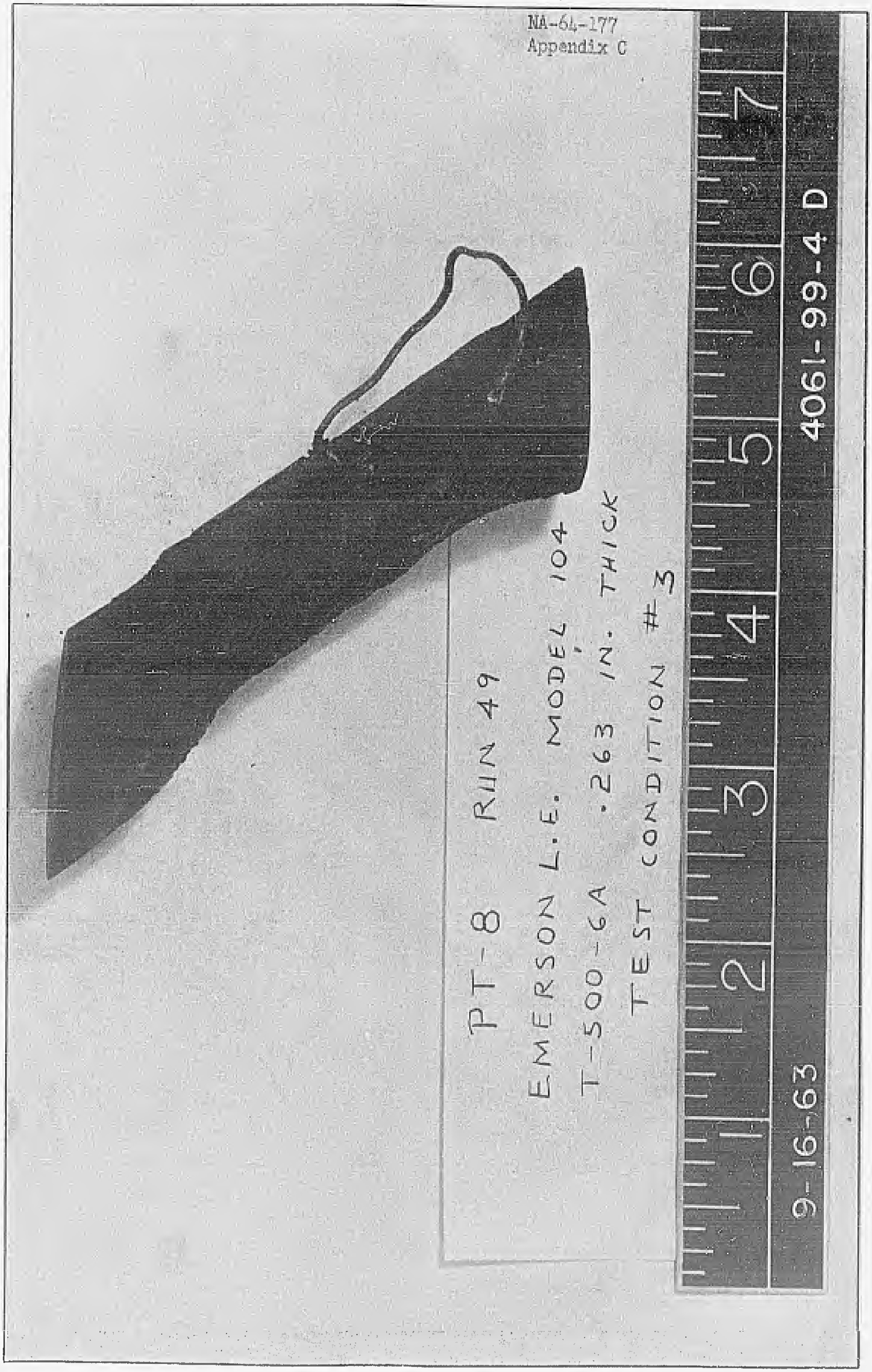

NORTH AMERICAN AVIATION, INC.
INTERNATIONAL AIRPORT
LOS ANGELES 9, CALIFORNIA

NA-64-177
Appendix C

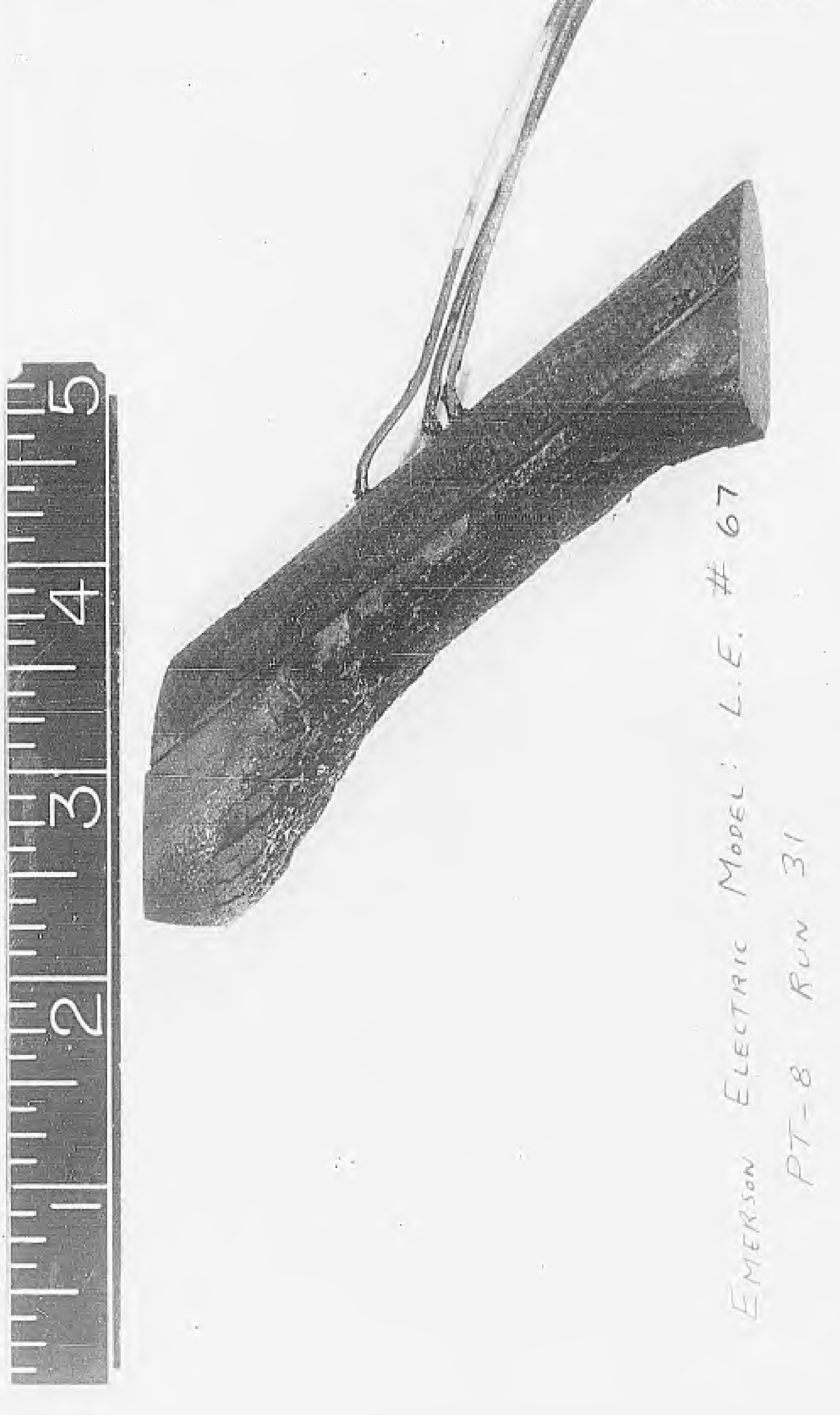

NA-64-177
Appendix C

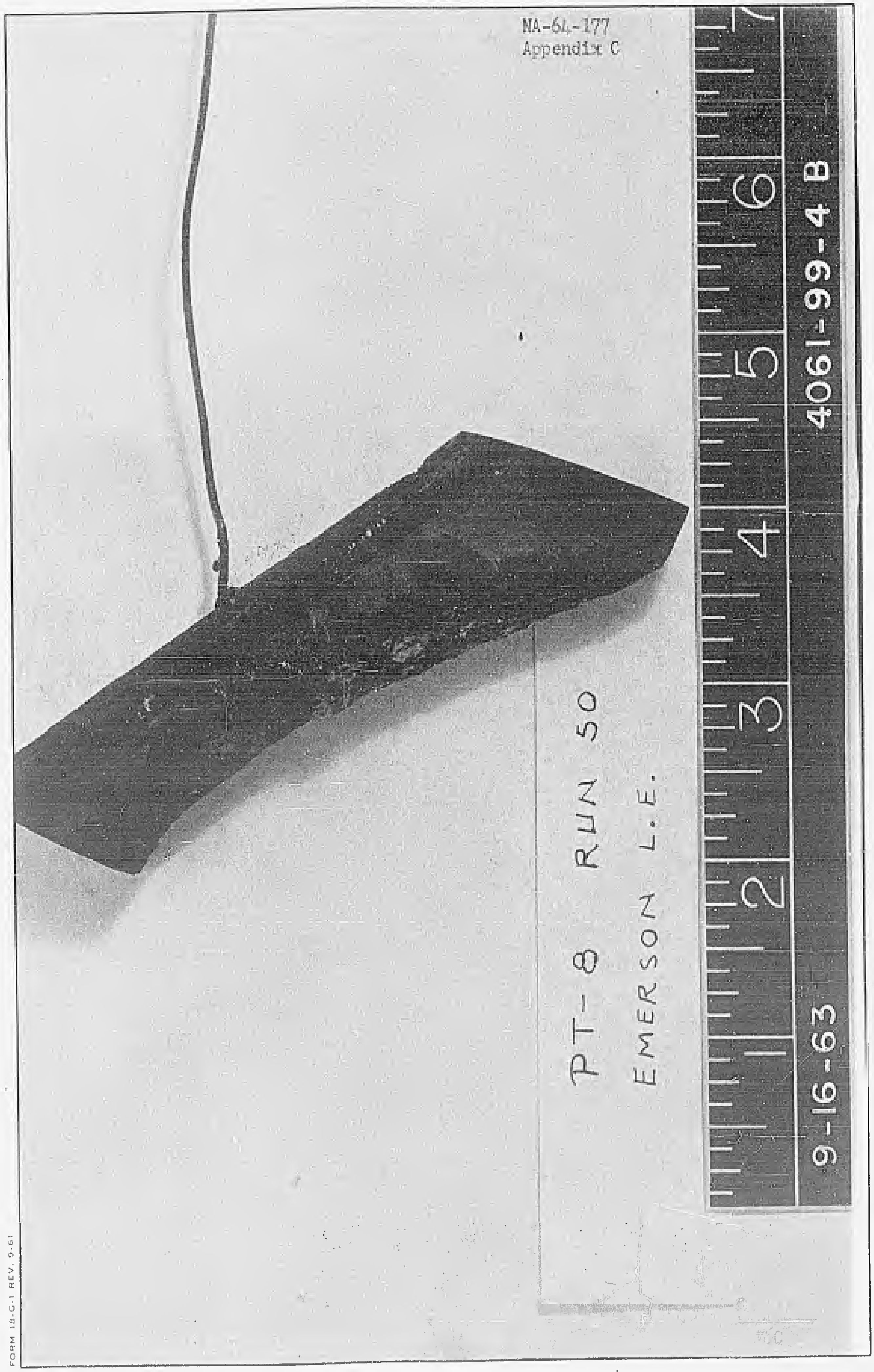

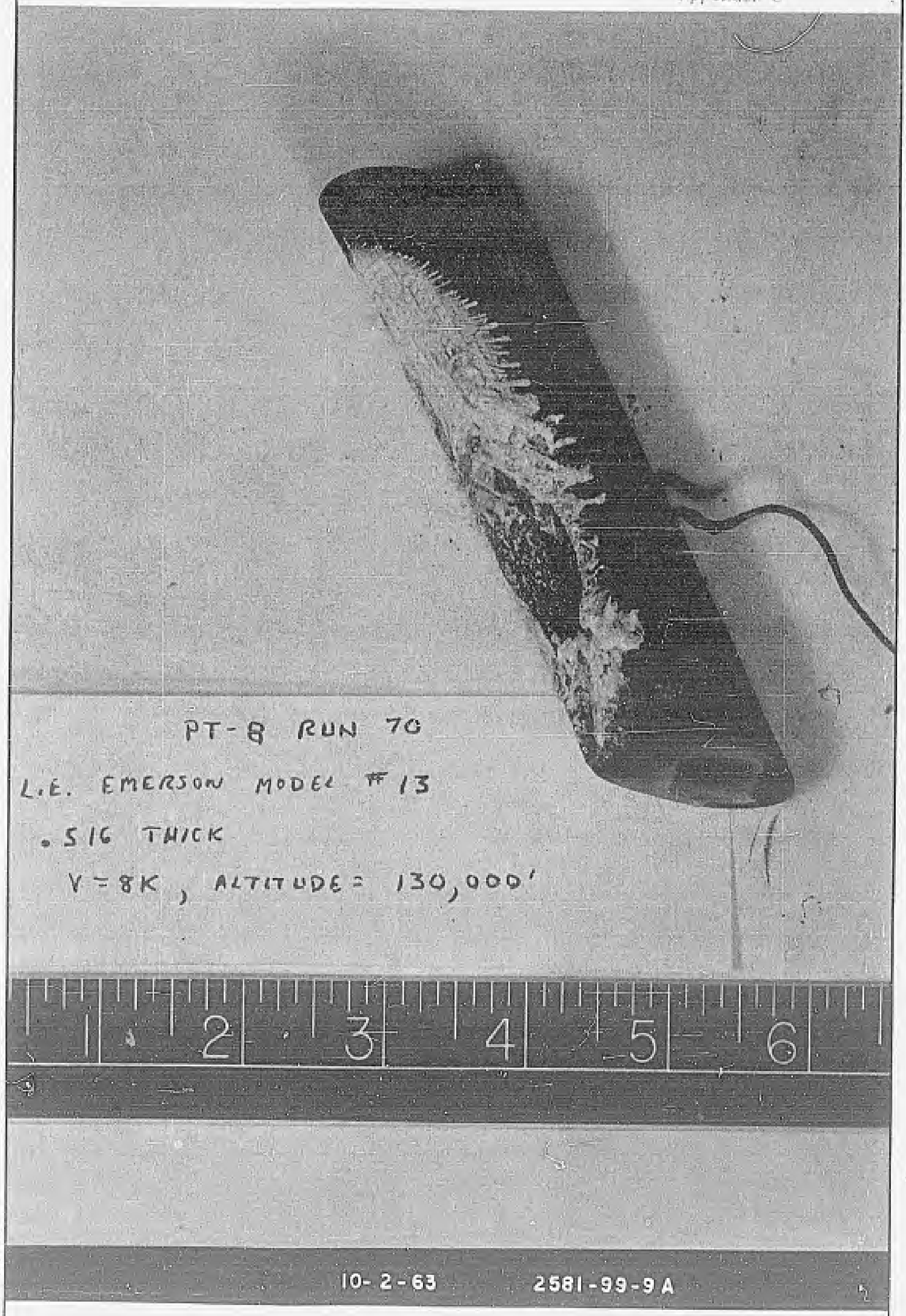
PT-8 RUN 70
L.E. EMERSON MODEL #13
.516 THICK
V = 8K , ALTITUDE = 130,000'
1 2 3 4 5 6
10-2-63 2581-99-9A

NA-64-177
Appendix C

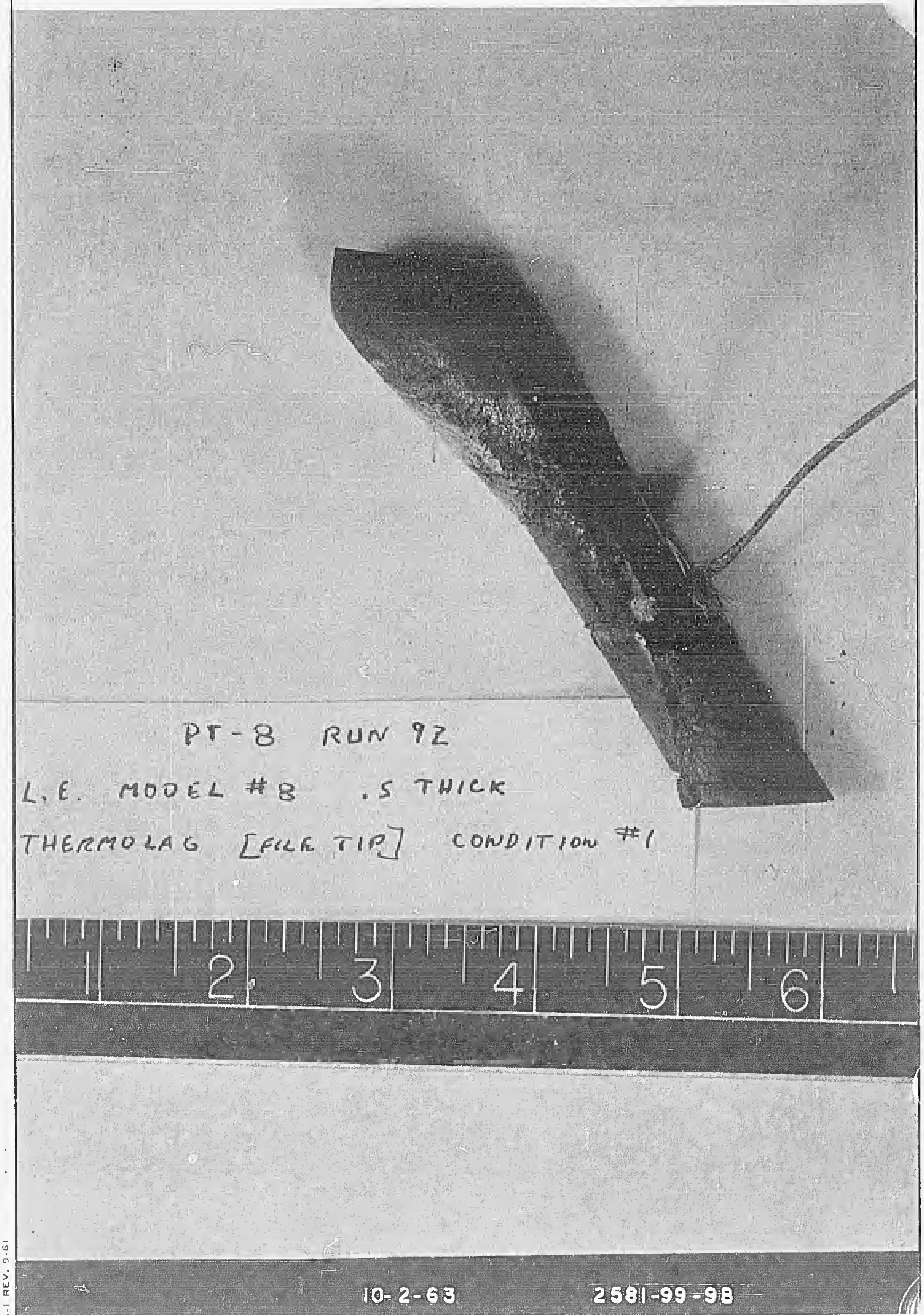

NA-64-177
Appendix C

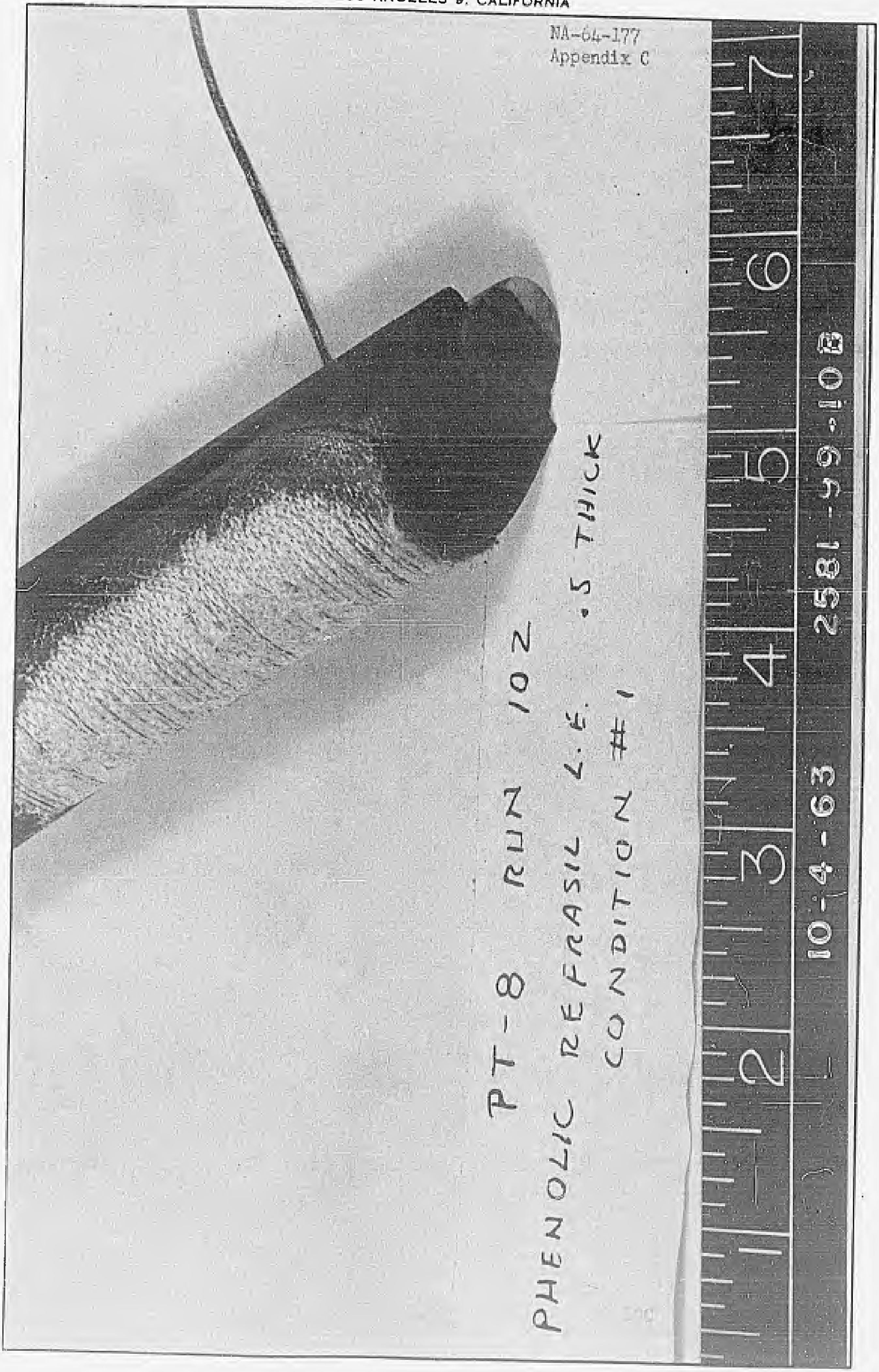

NORTH AMERICAN AVIATION, INC.
INTERNATIONAL AIRPORT
LOS ANGELES 9, CALIFORNIA

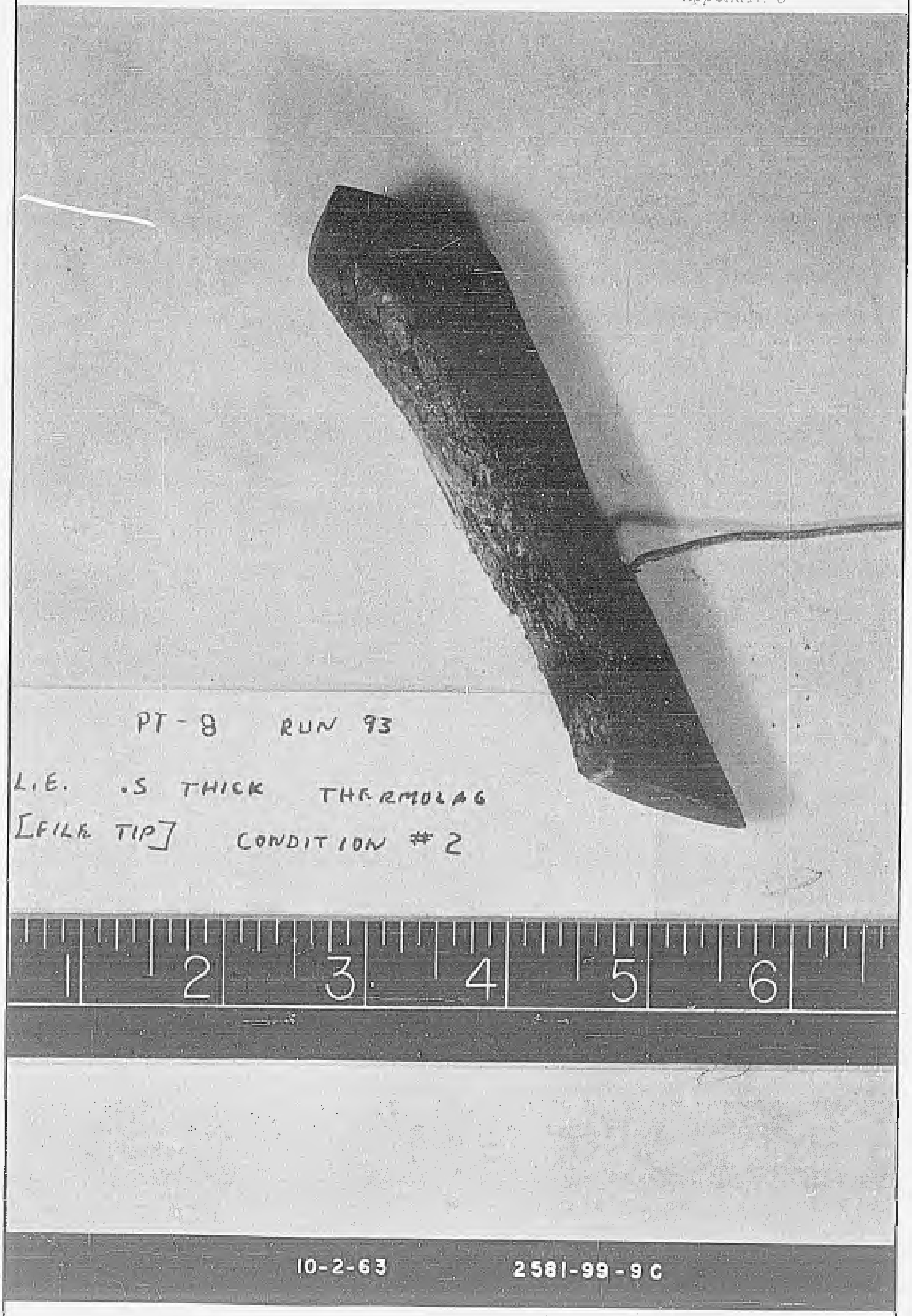

FORM 12-D-1 REV. 9-61

NORTH AMERICAN AVIATION, INC.

INTERNATIONAL AIRPORT
LOS ANGELES 9, CALIFORNIA

NA-64-77
Appendix C

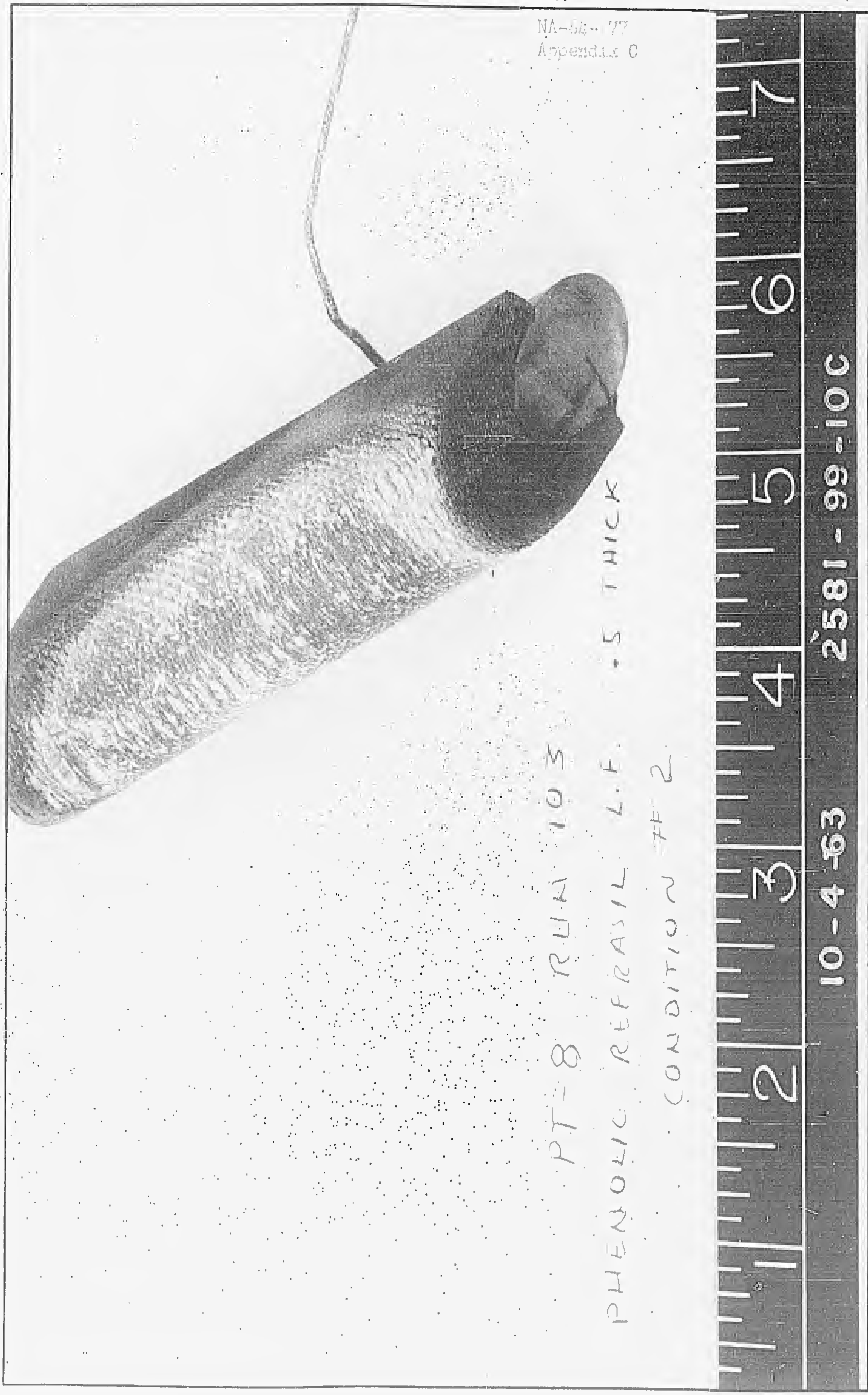

FORM 18-G-1 REV. 9-61

NA-64-177
Appendix C

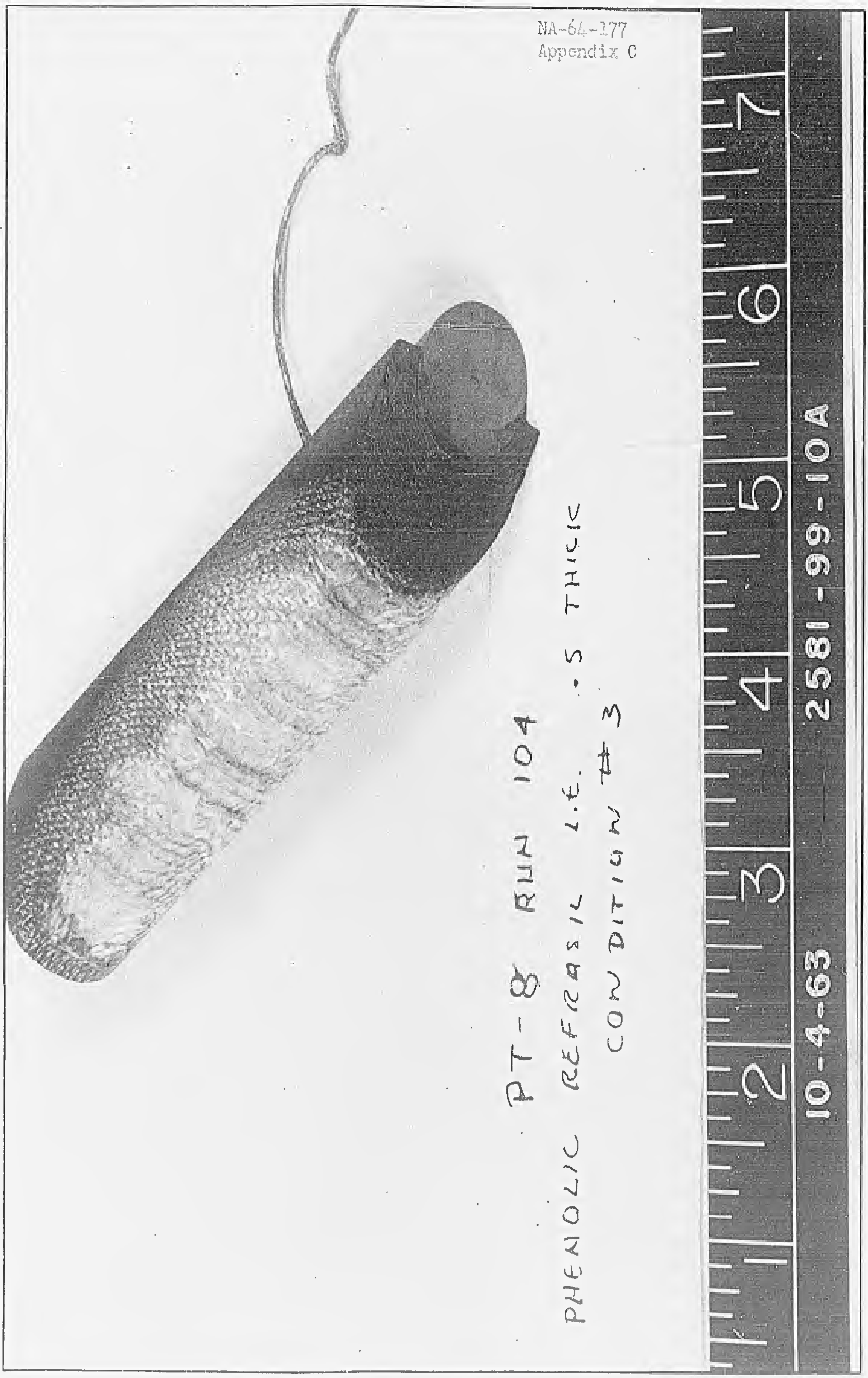

NORTH AMERICAN AVIATION, INC.
INTERNATIONAL AIRPORT
LOS ANGELES 9, CALIFORNIA

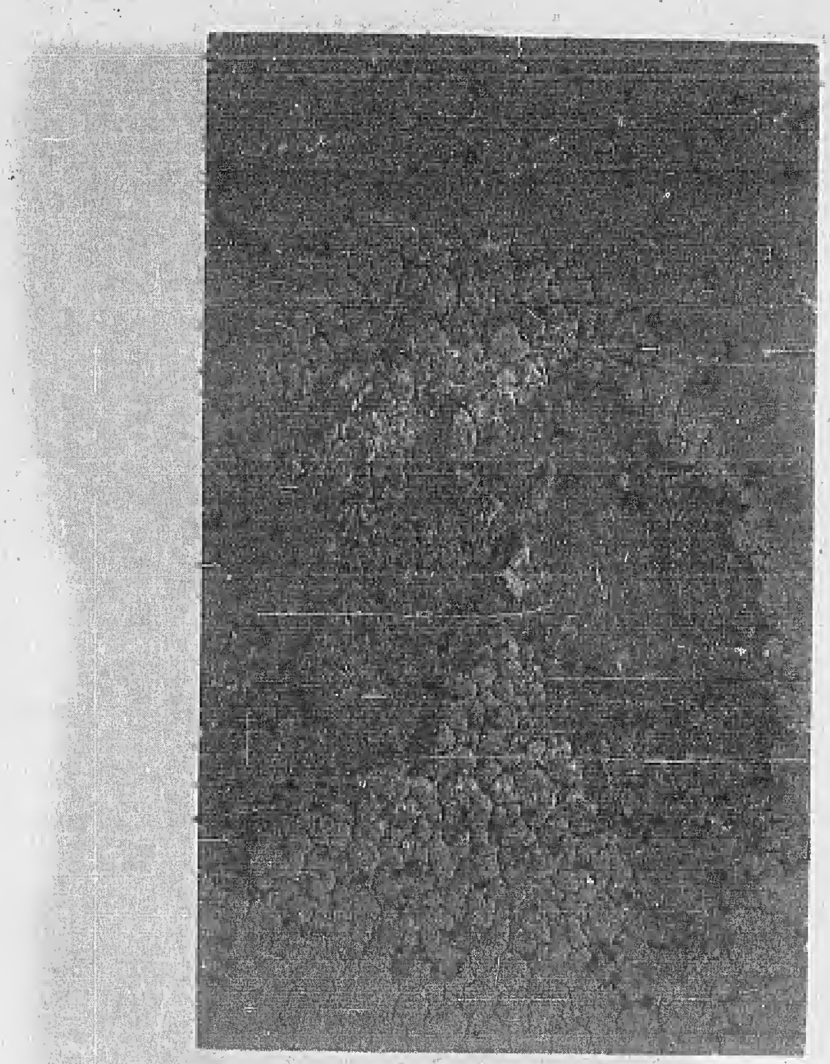

PT-8 RUN 71

MODEL #7 .10 THICK

T-500-4 CONDITION #2A

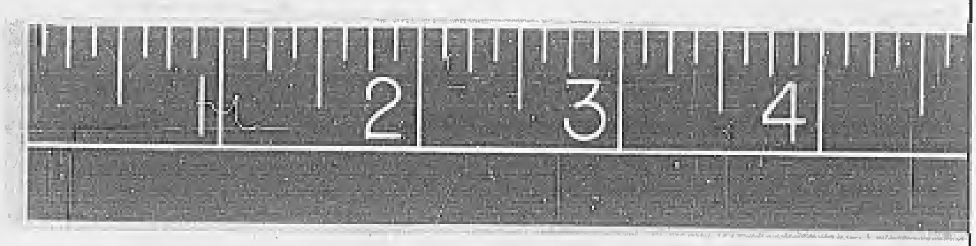

10-2-63 2581-99-9 J

FORM 18-G-1 REV. 9-61

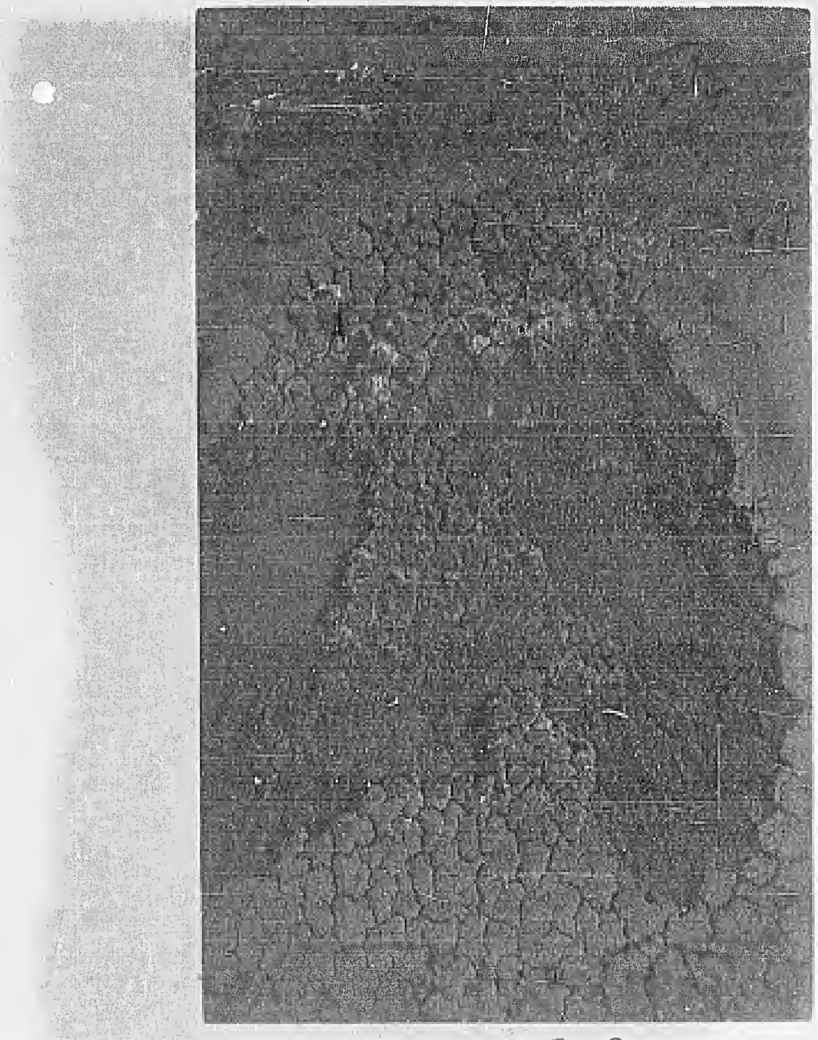

PT-8 RUN 72

MODEL #8 .010 THICK T-500-1

CONDITION #2A

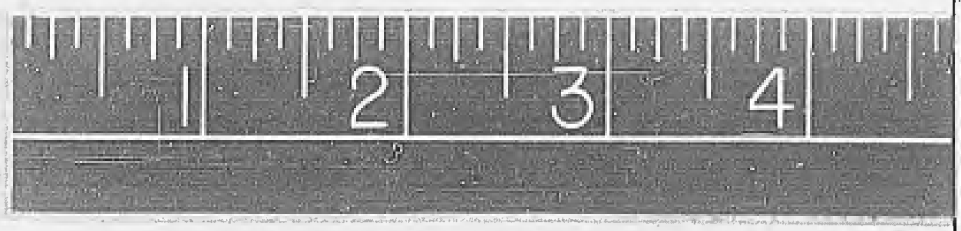

10-2-63 2581-99-9"0"

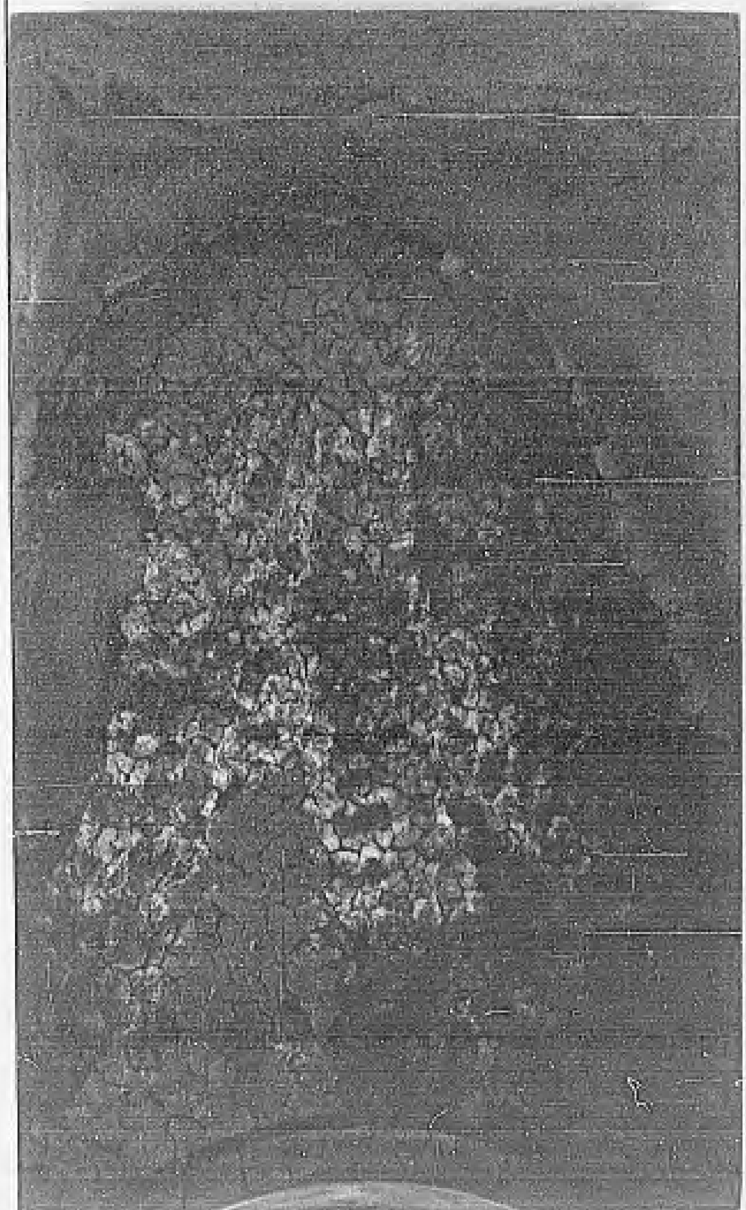

PT-8 RUN 85

EMERSON MODEL #22 .10 THICK

CONDITION #2A

10-3-63 2581-99-8F

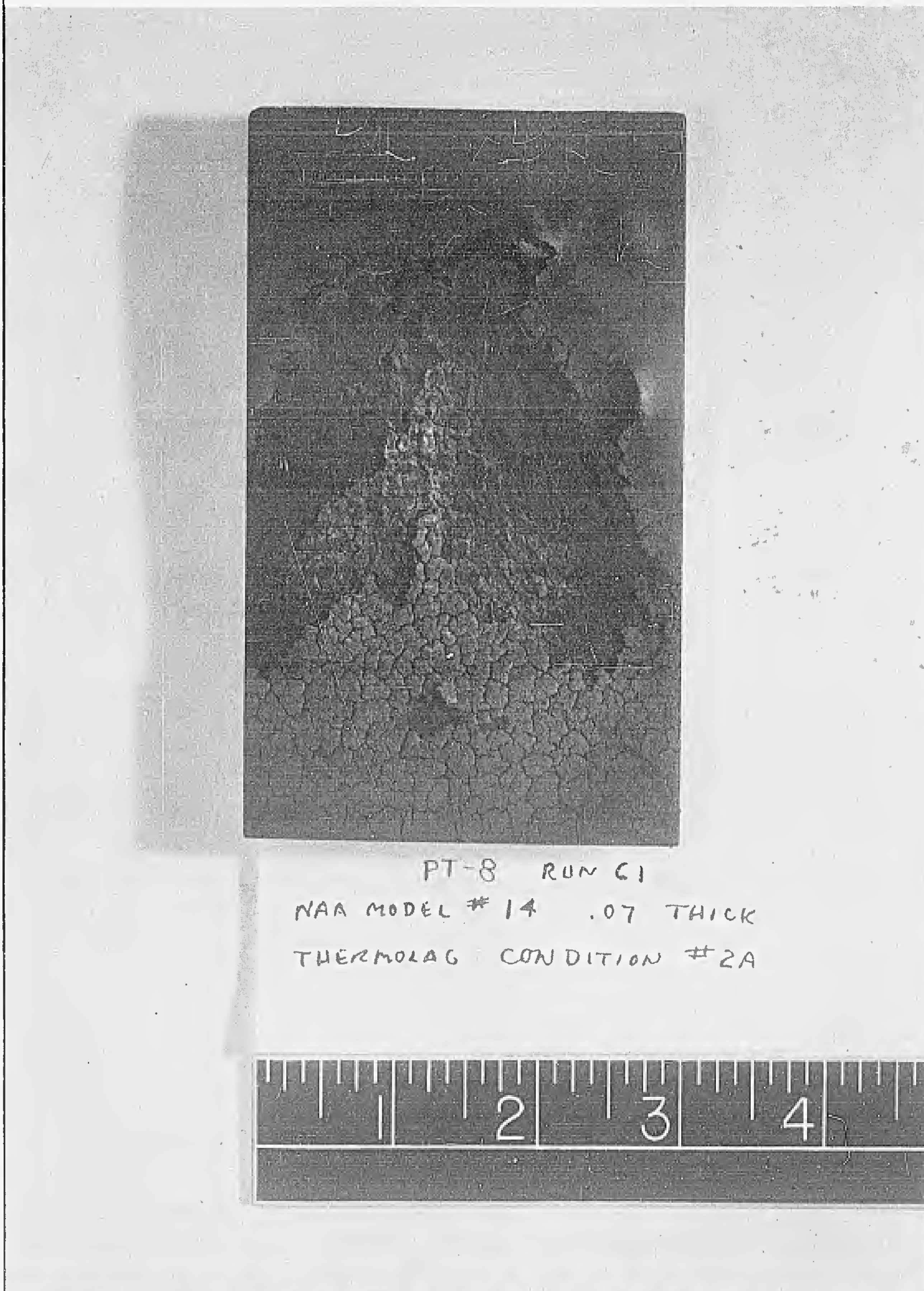

10-2-63 2581-99-9 H

FORM 18-C-1 REV. 9-61

NORTH AMERICAN AVIATION, INC.
INTERNATIONAL AIRPORT
LOS ANGELES 9, CALIFORNIA

NA-64-377
Appendix C

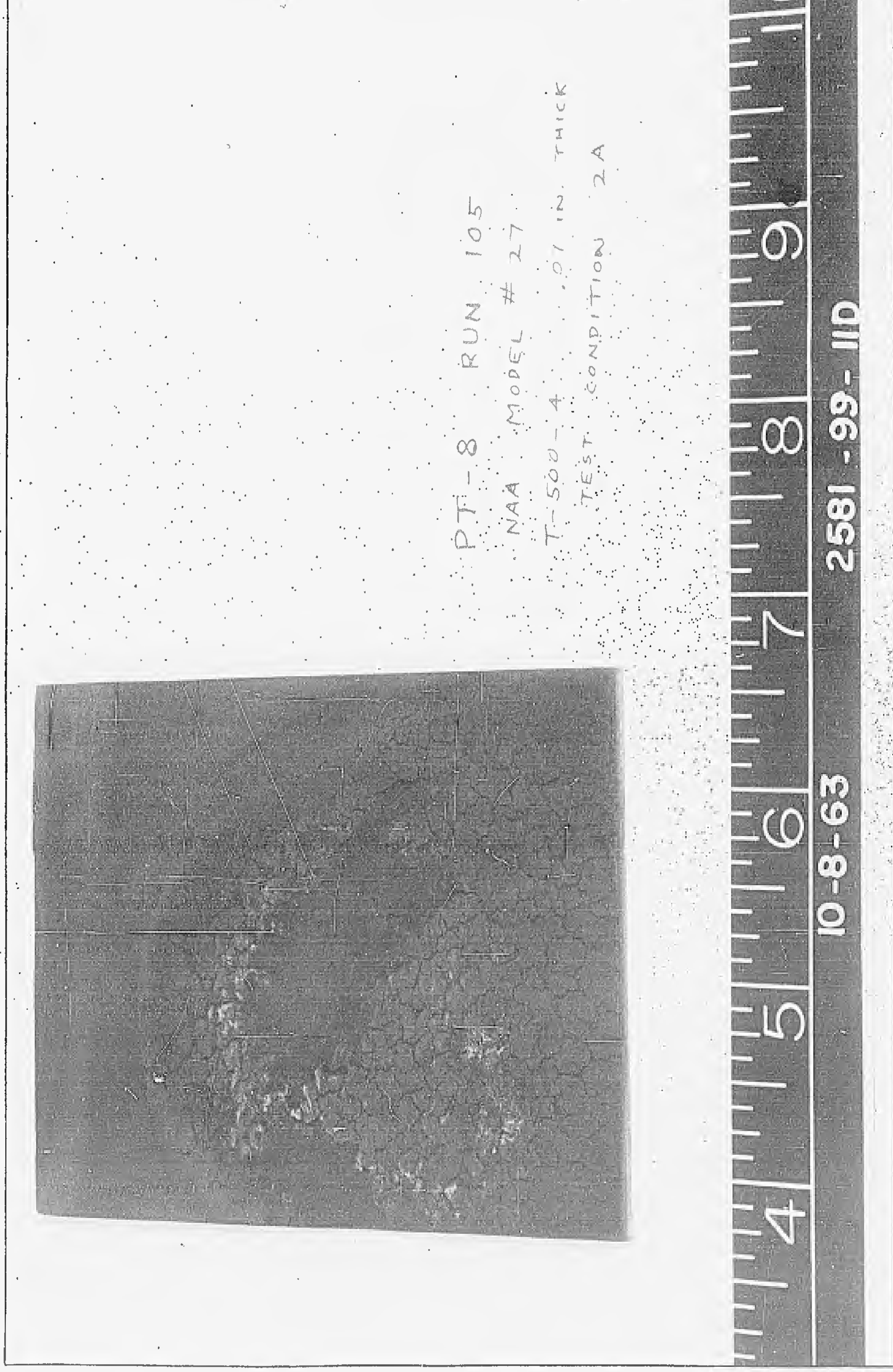

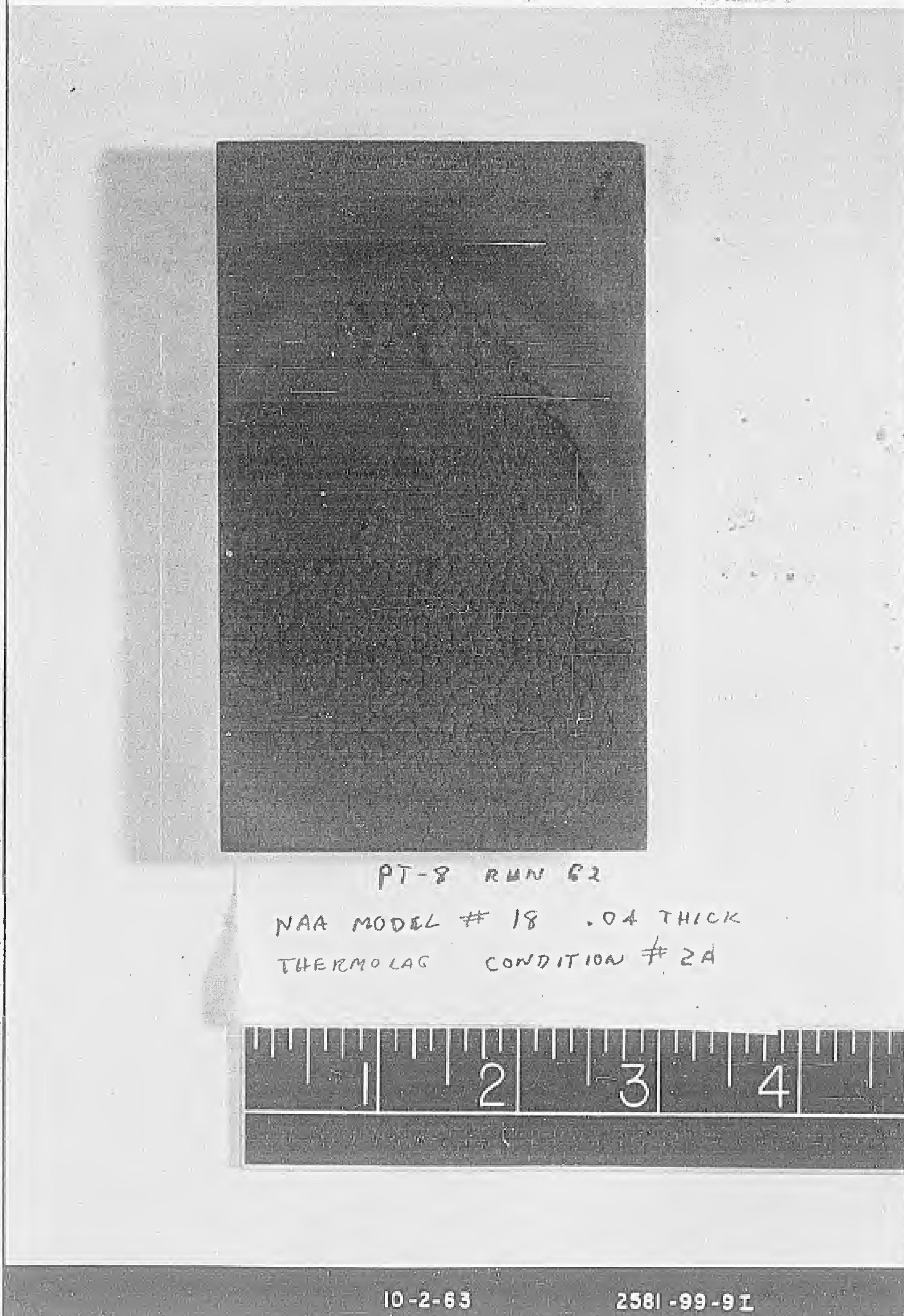
PT-8 RUN 62
NAA MODEL # 18 .04 THICK
THERMOLAG CONDITION # 2A
1
2
3
4
10-2-63
2581-99-9I

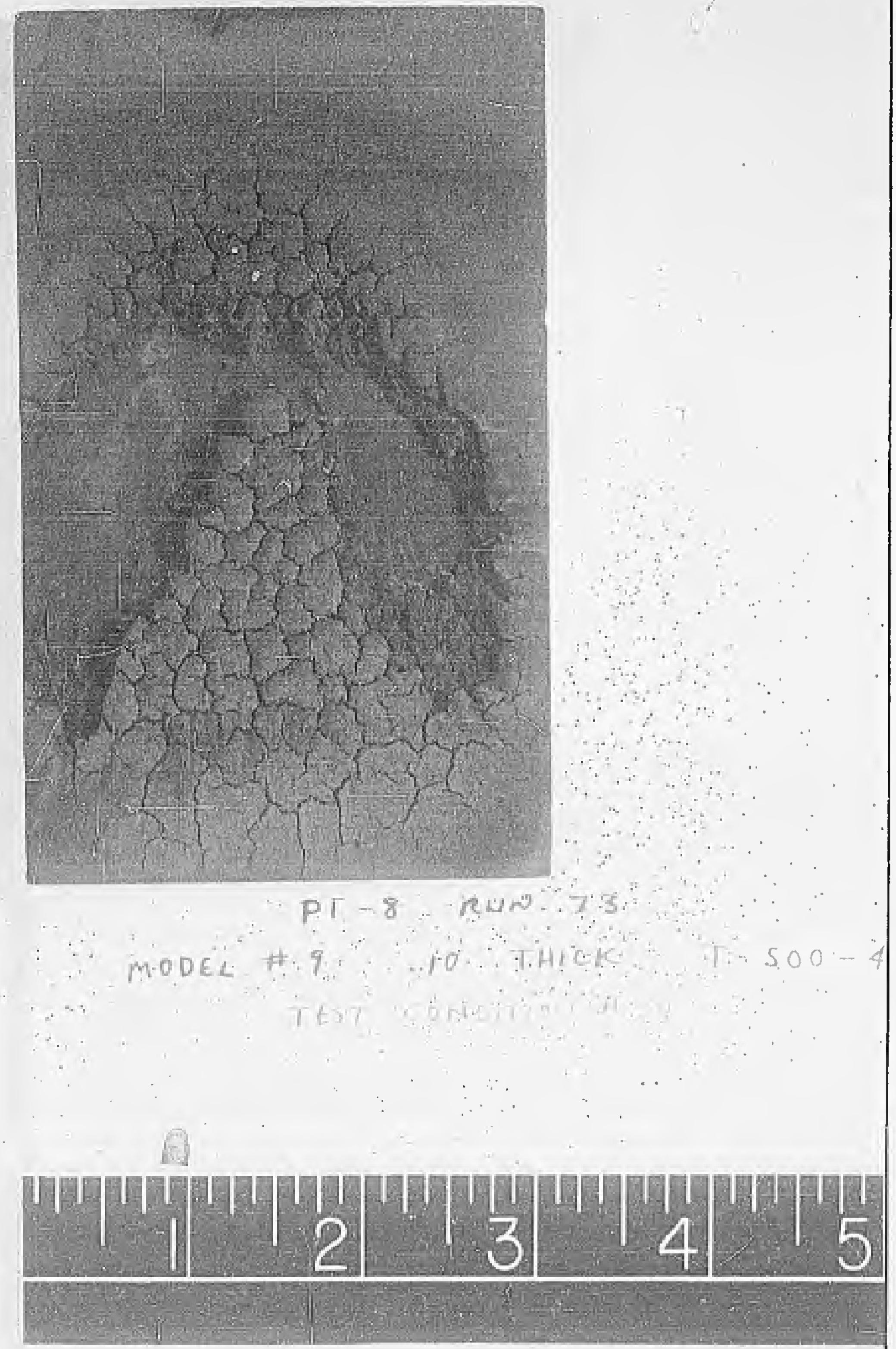

10-2-63 2581-99-9K

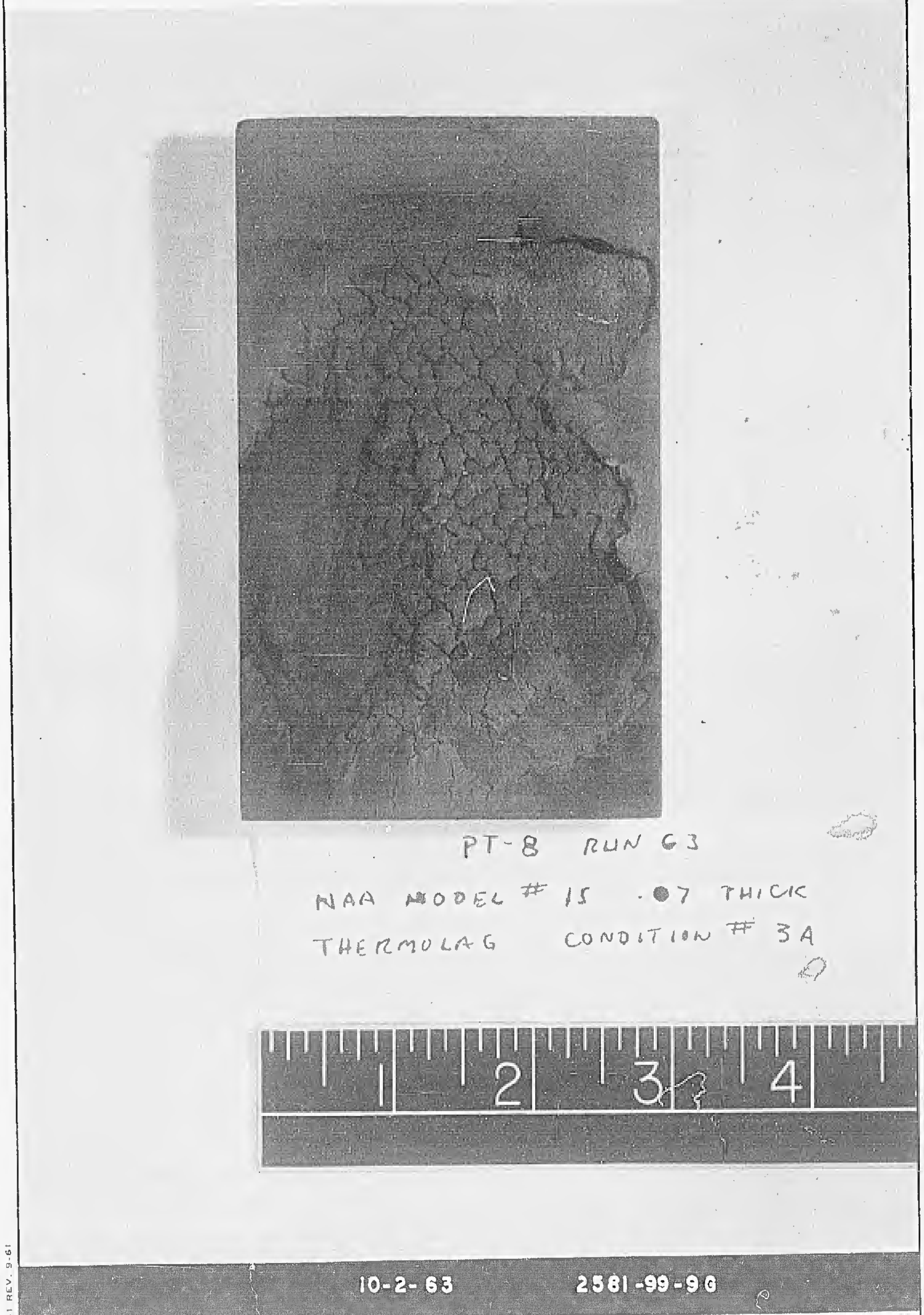
PT-8 RUN 63
NAA MODEL # 15 .07 THICK
THERMOLAG CONDITION # 3A
1
2
3
4
10-2-63
2581-99-96

NORTH AMERICAN AVIATION, INC.
INTERNATIONAL AIRPORT
LOS ANGELES 9, CALIFORNIA

NA-63-17
Appendix C

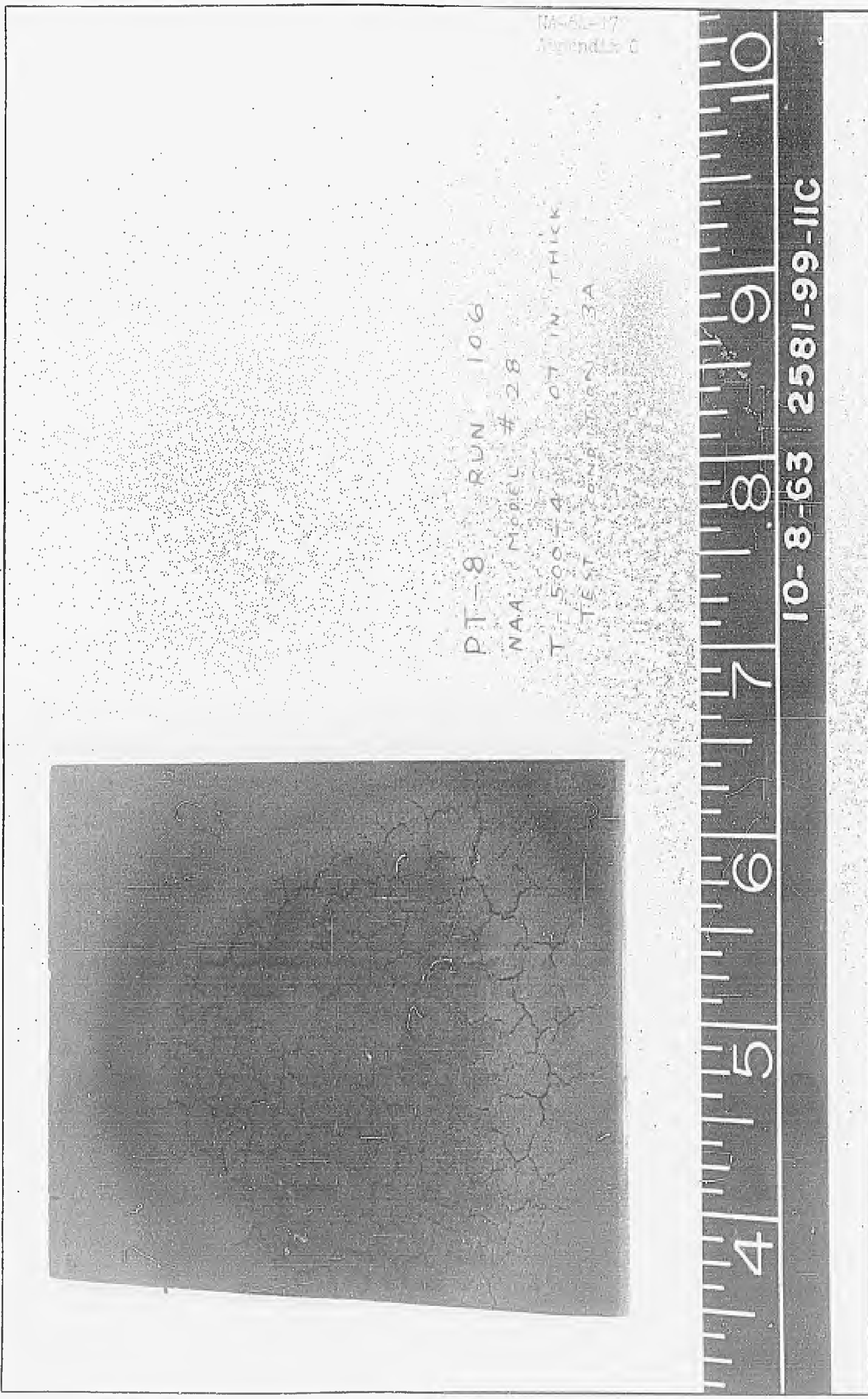

FORM 18-G-1 REV. 9-61

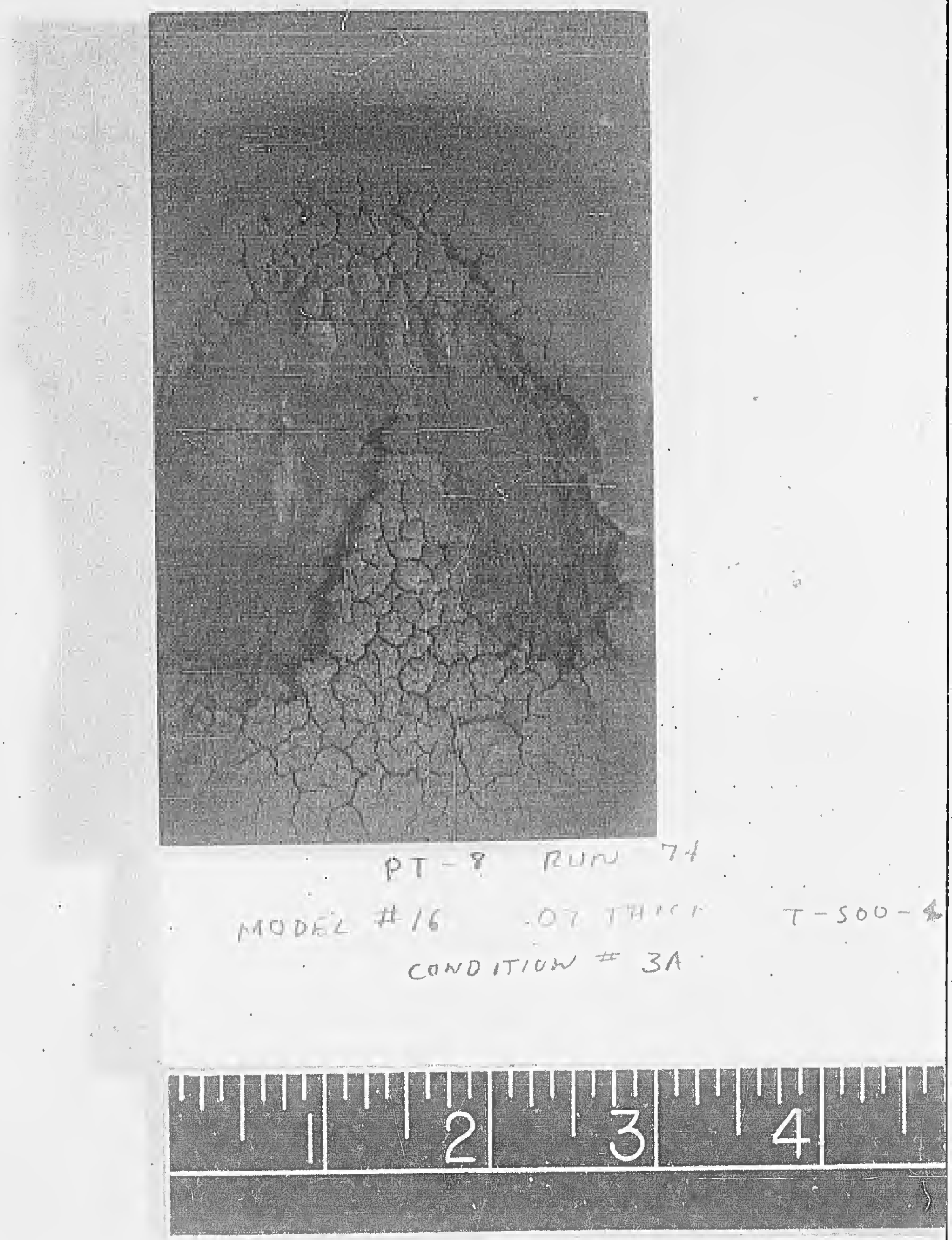

10-2-63 2581-99-90

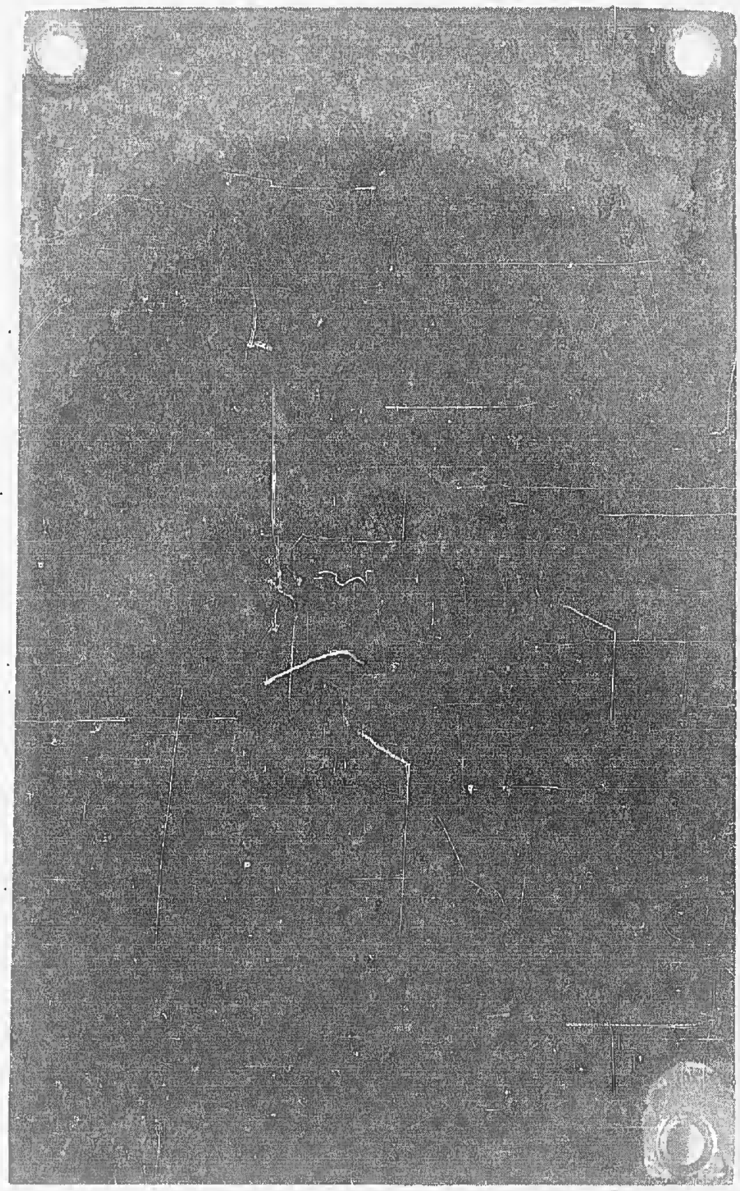

PT-8 RUN 84

EMERSON MODEL # 2A .07 THICK

CONDITION # 3A

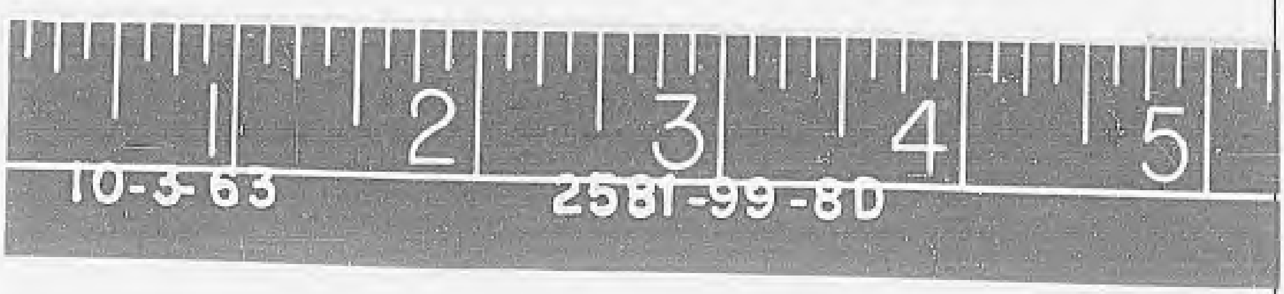

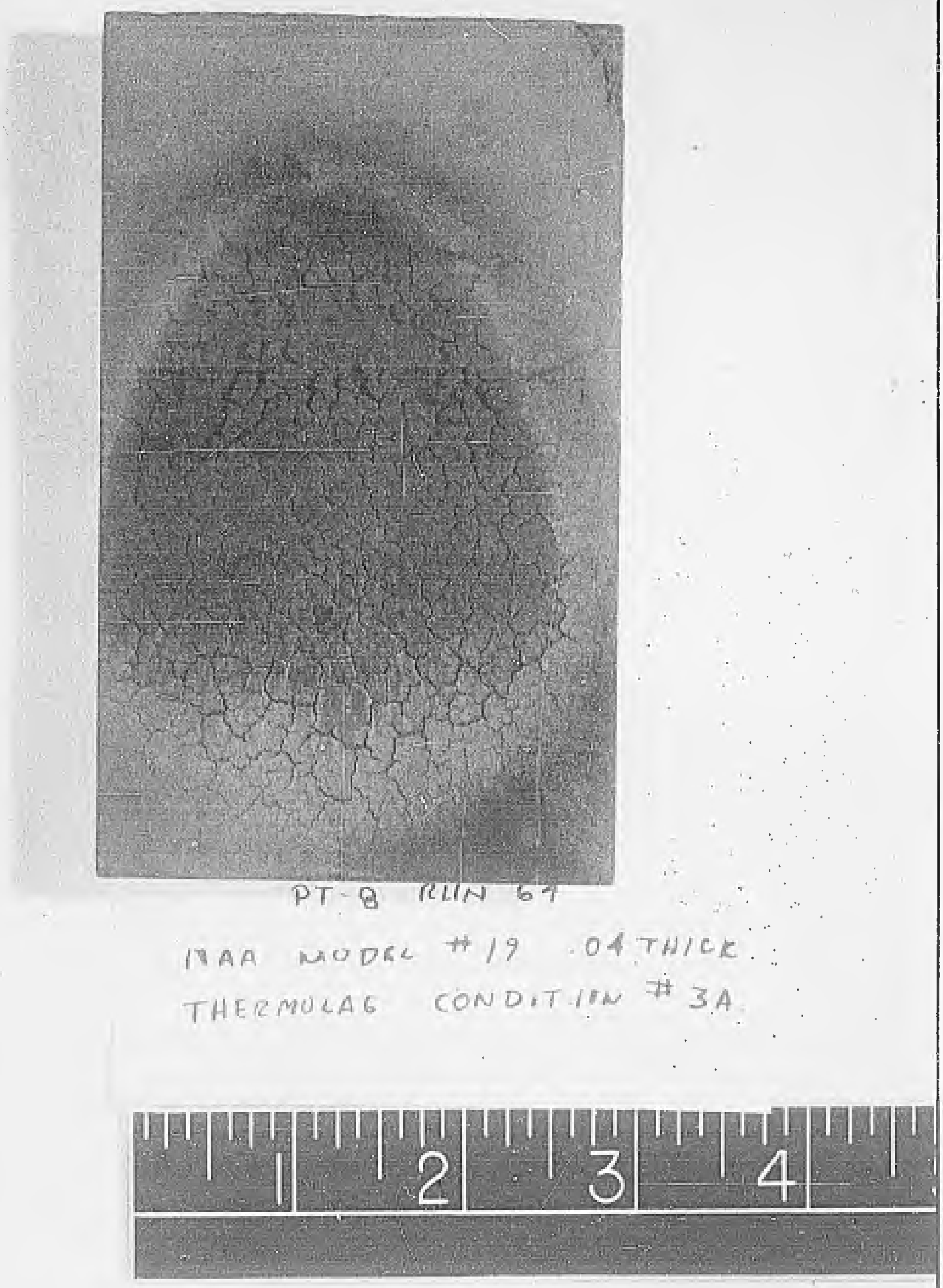

10-2-63 2581-99-9M

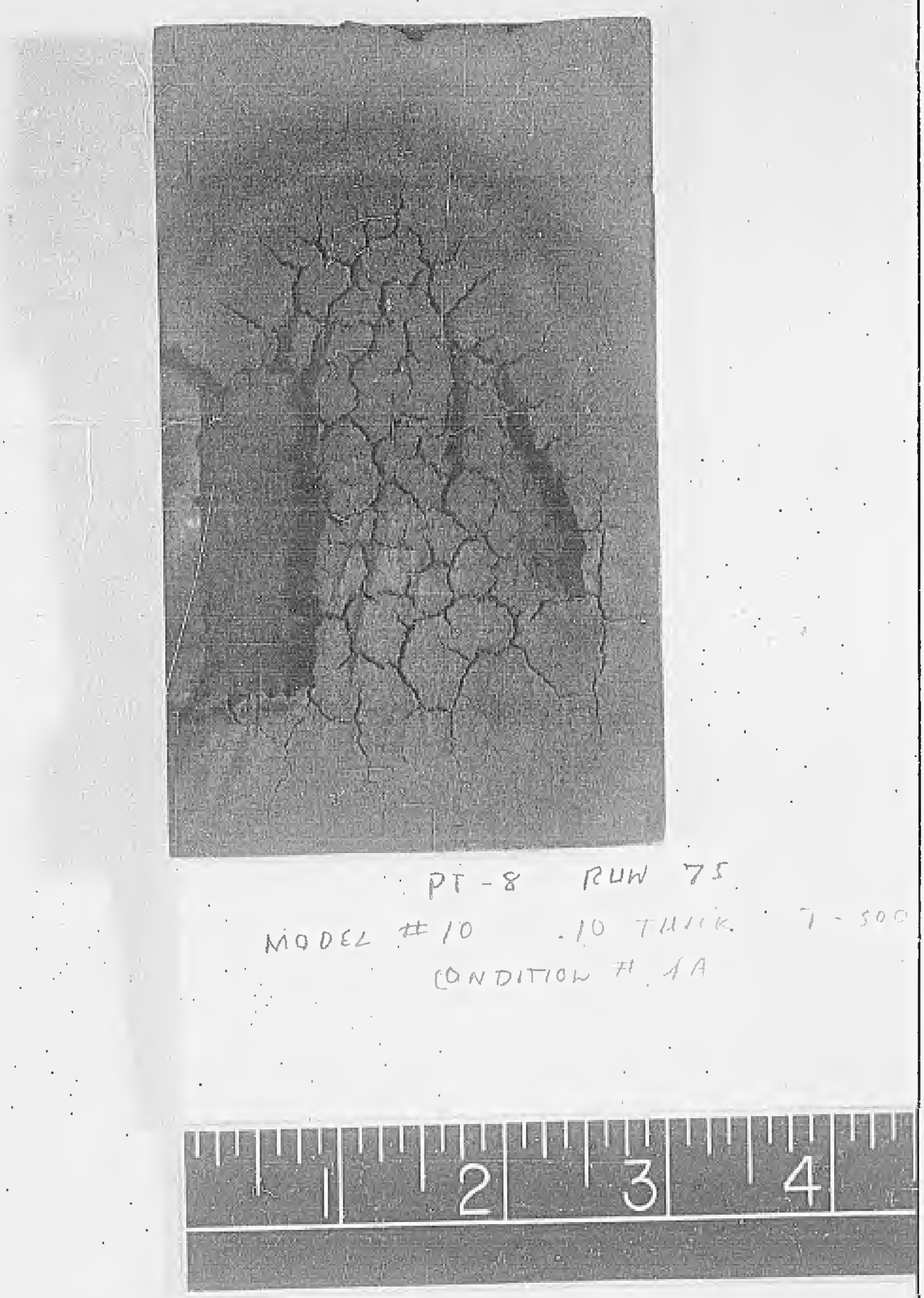

10-2-63 2581-99-9R

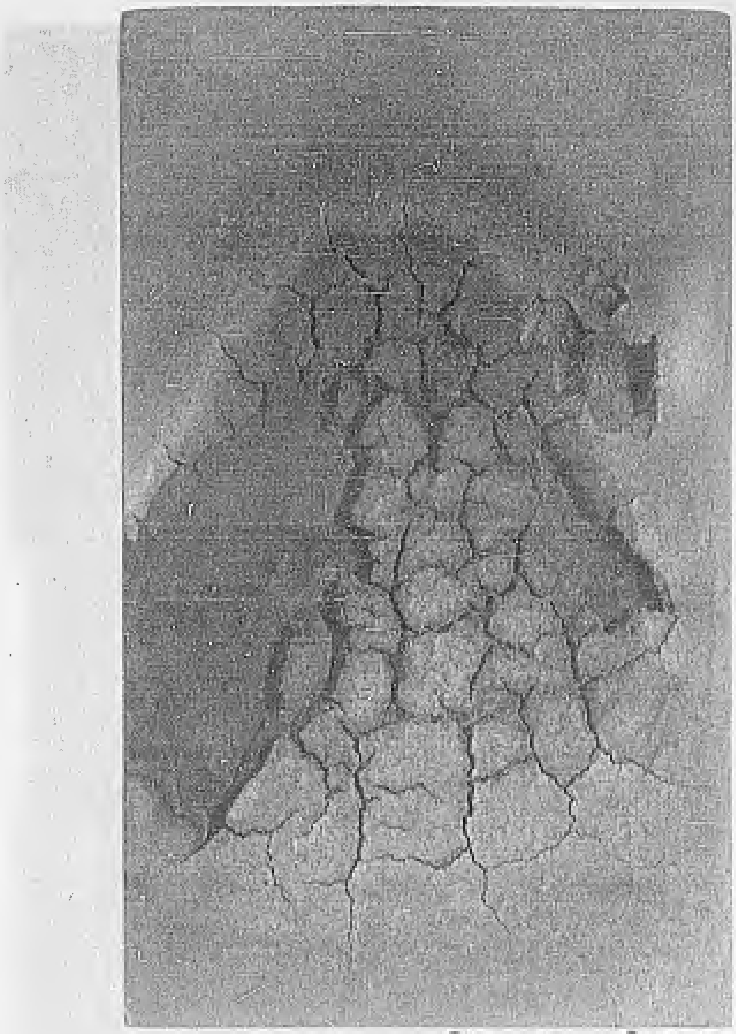

PT-8 RUN 65

NAA MODEL #17 .07 THICK
THERMOLAG CONDITION #4A

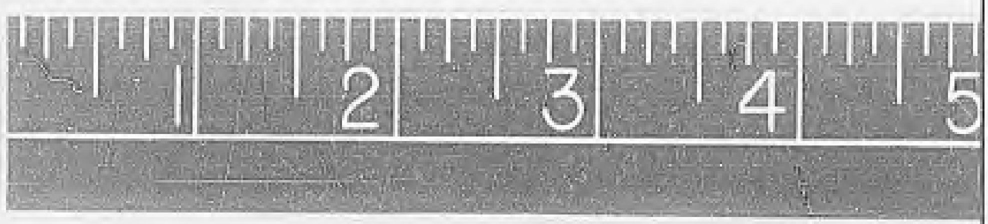

10-2-63 2581-99-9N

FORM 18-G-1 REV. 9-61

NORTH AMERICAN AVIATION, INC.
INTERNATIONAL AIRPORT
LOS ANGELES 9, CALIFORNIA

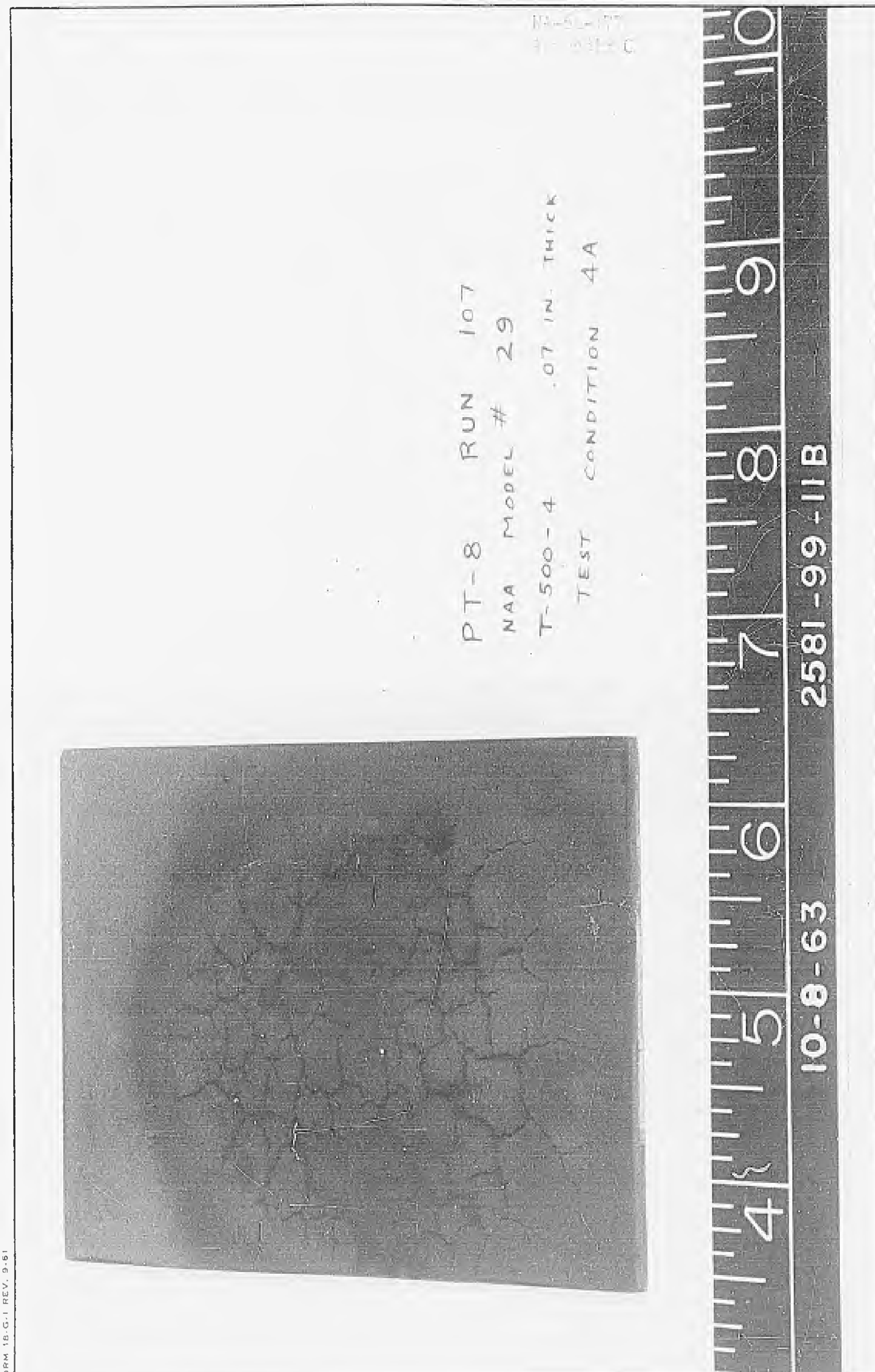

FORM 18.G.1 REV. 9-61

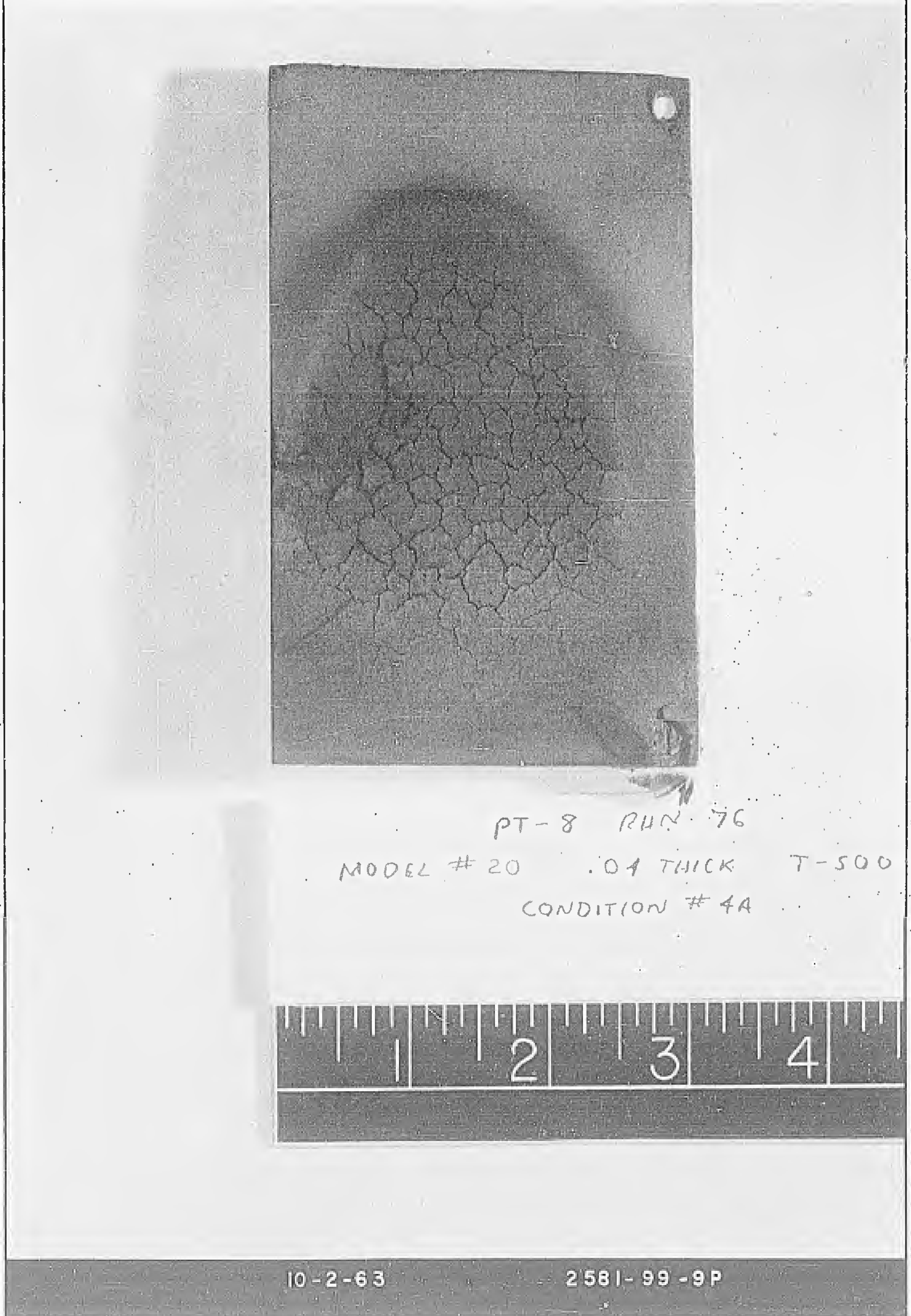

FORM 18-G-1 REV. 9-61

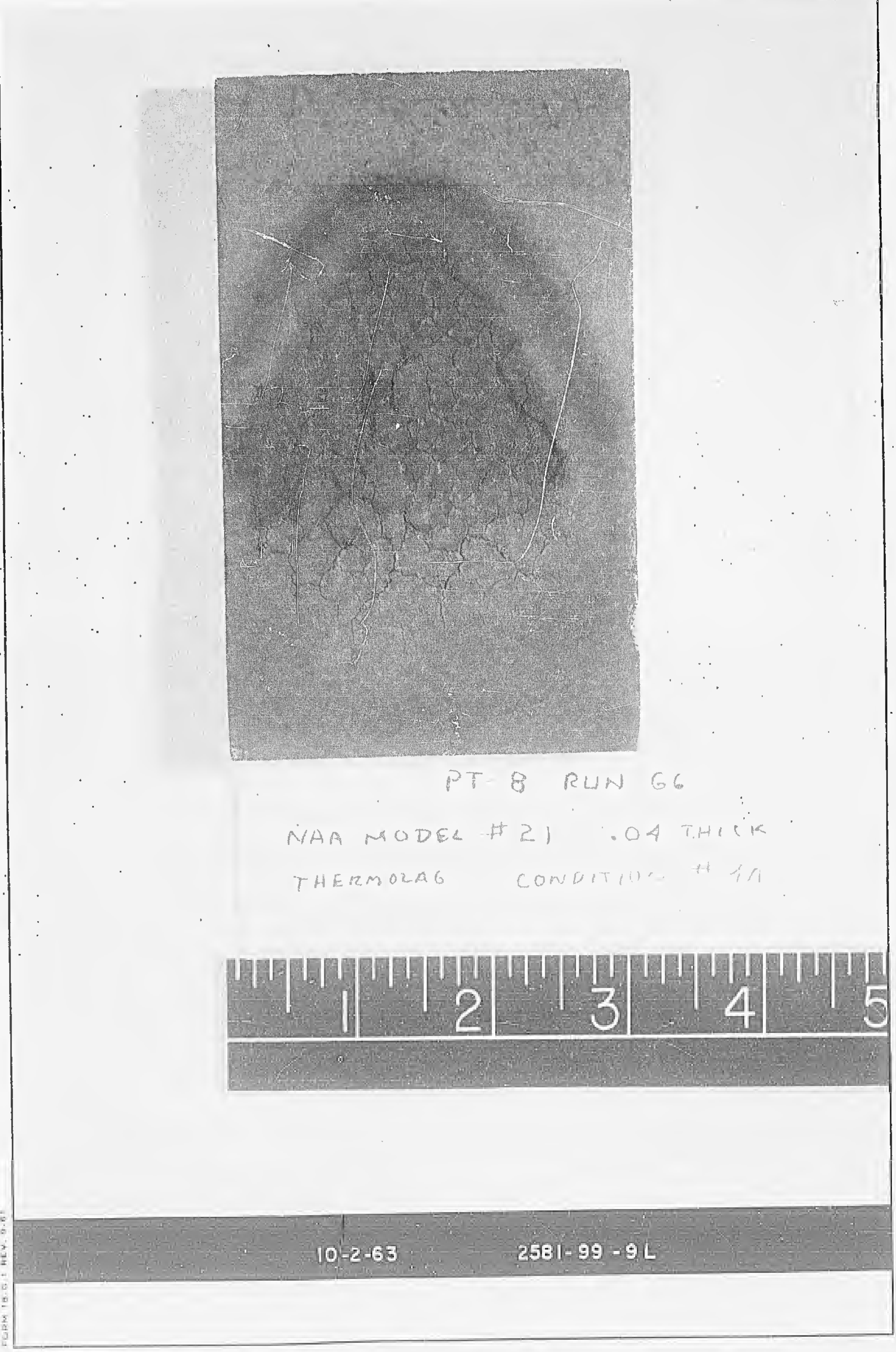
PT-8 RUN 66
NAA MODEL #21 .04 THICK
THERMOLAG CONDITION #11
1
2
3
4
5
10-2-63
2581-99-9L

NA-64-177
Appendix C

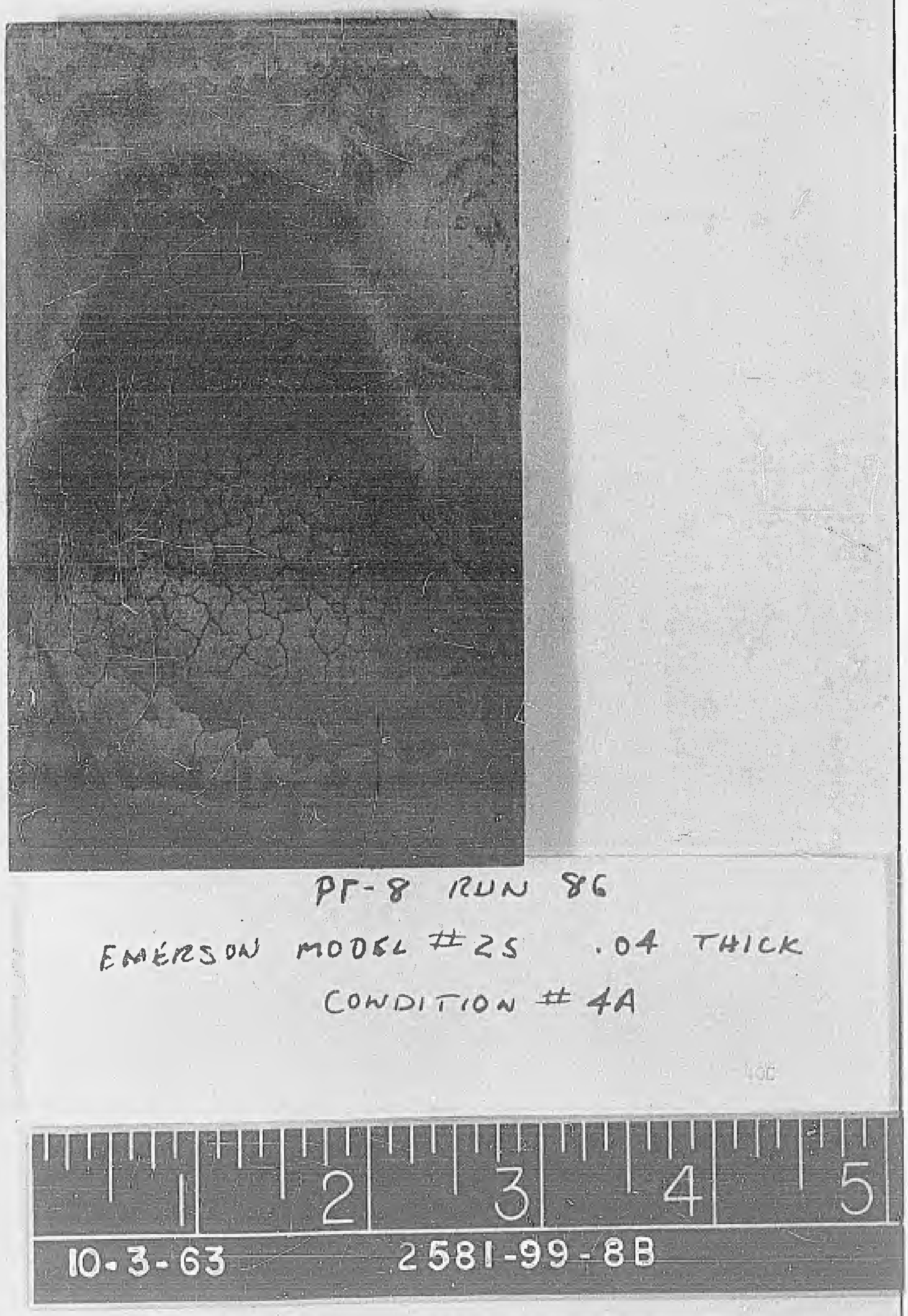

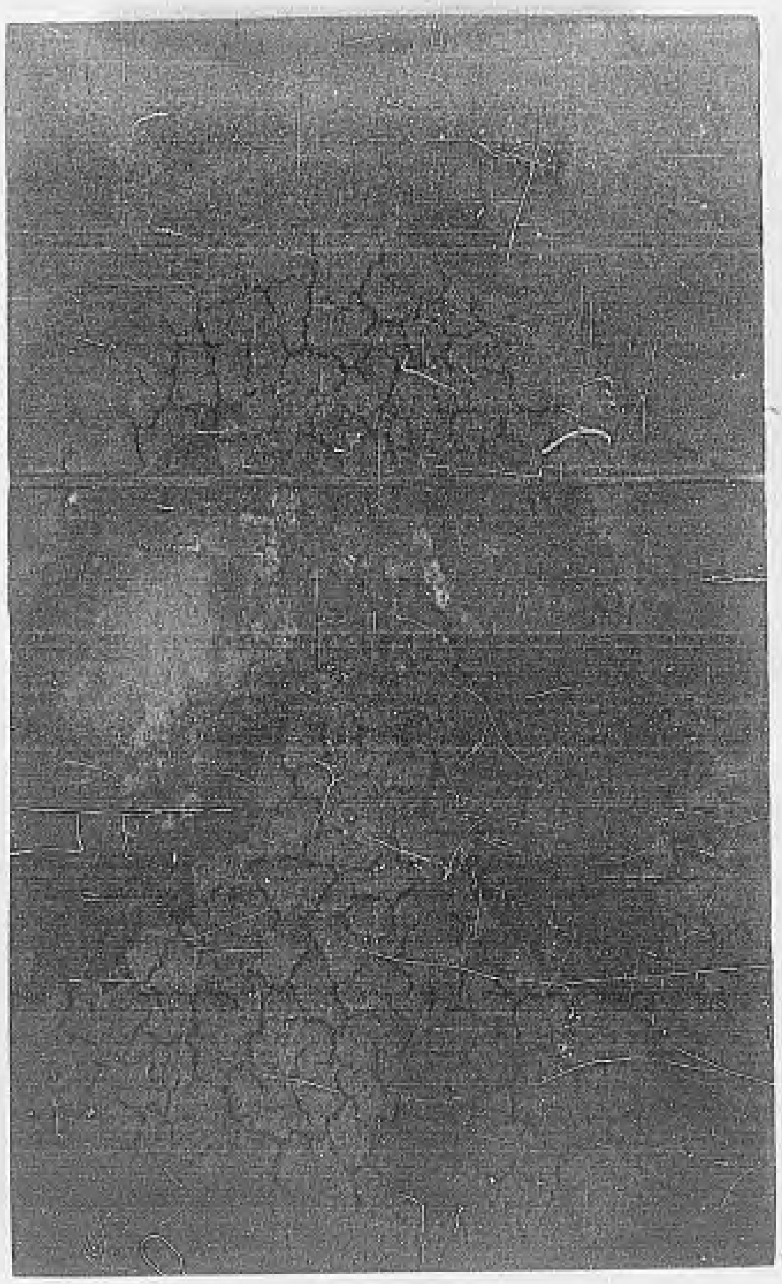

PT-8 RUN 87

NAA MODEL #3, .10 THICK

1/32" SLOT ⊥ WIND, CENTERED

AT MIDDLE OF BUTTON

CONDITION #3A

1 2 3 4 5

10-3-63 2581-99-8H

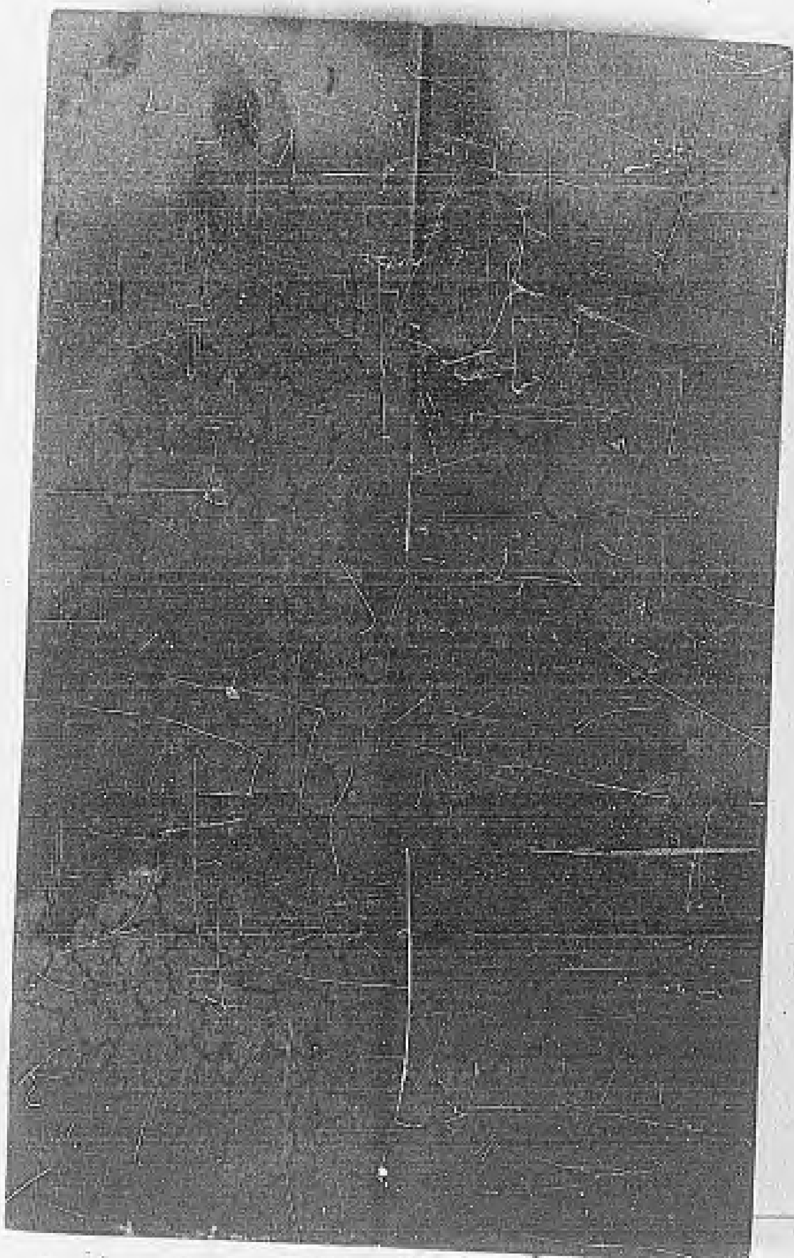

PT-8 RUN 88

NAA MODEL #11 .10 THICK

1/32" SLOT || TO WIND, CENTER @

MIDDLE OF BUTTON

CONDITION #3A

10-3-63 2581-99-8A

NA-64-177
Appendix C

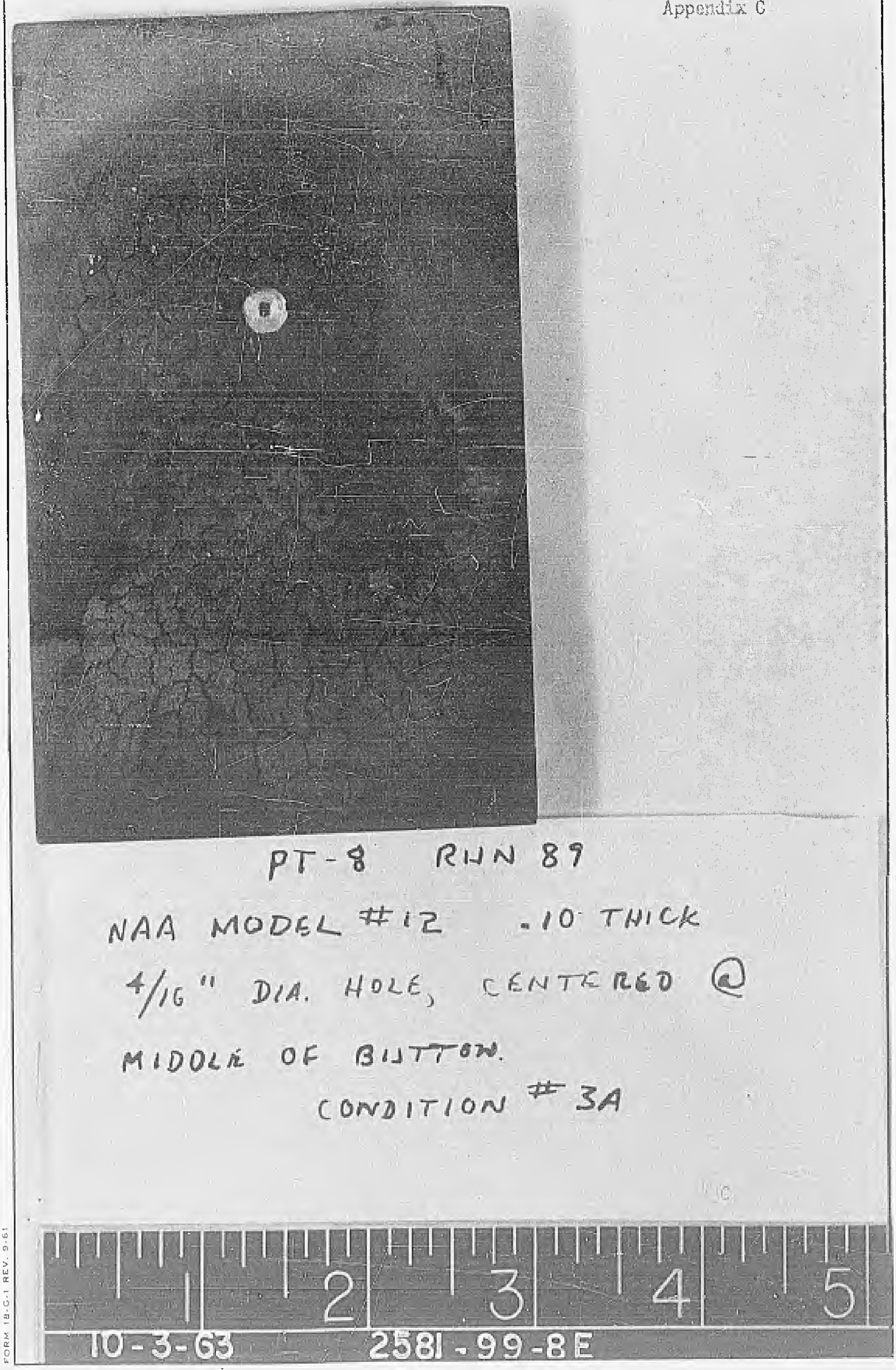

NA-64-177
Appendix C

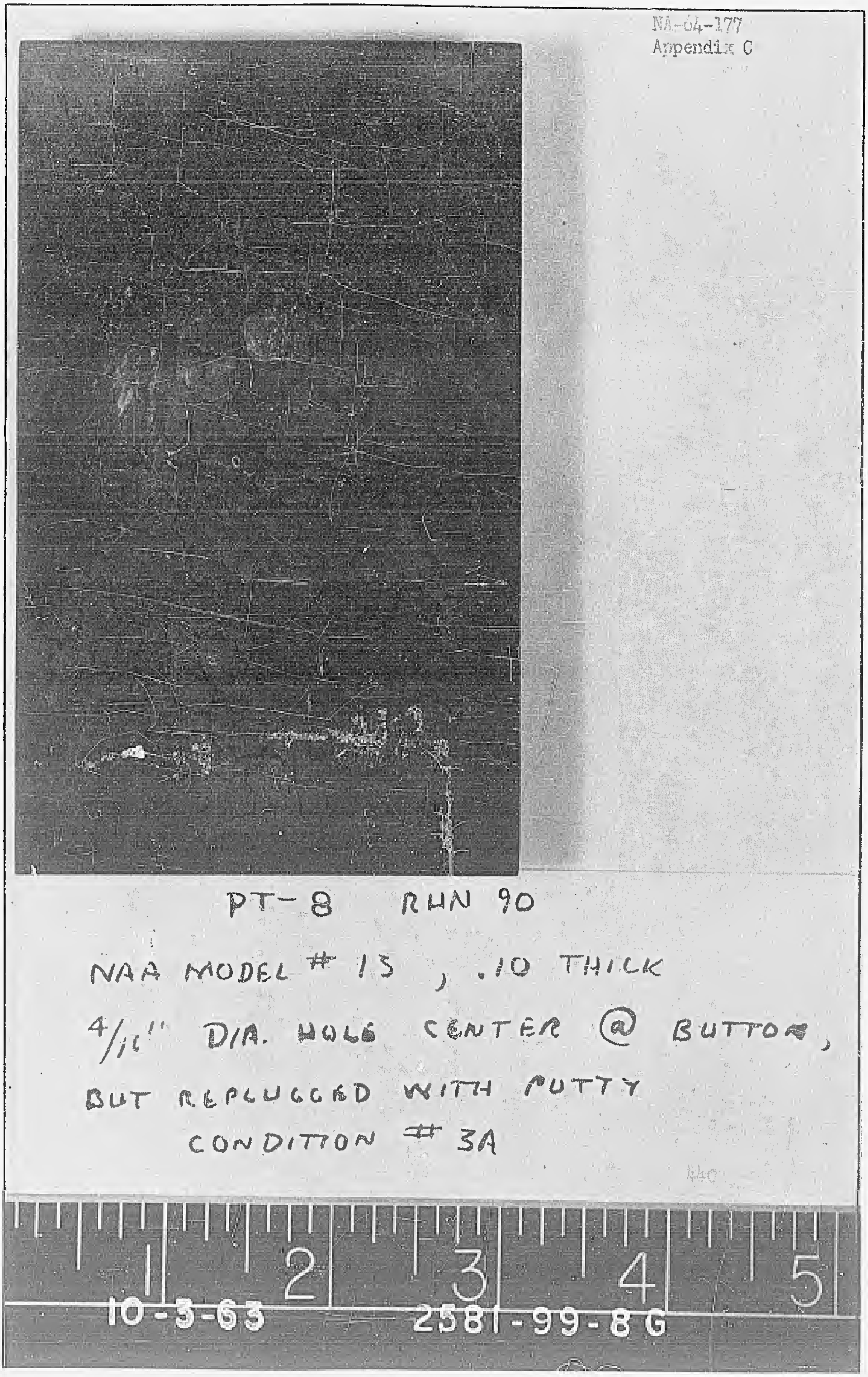

FORM 18-G-1 REV. 9-61

NORTH AMERICAN AVIATION, INC.
INTERNATIONAL AIRPORT
LOS ANGELES 9, CALIFORNIA

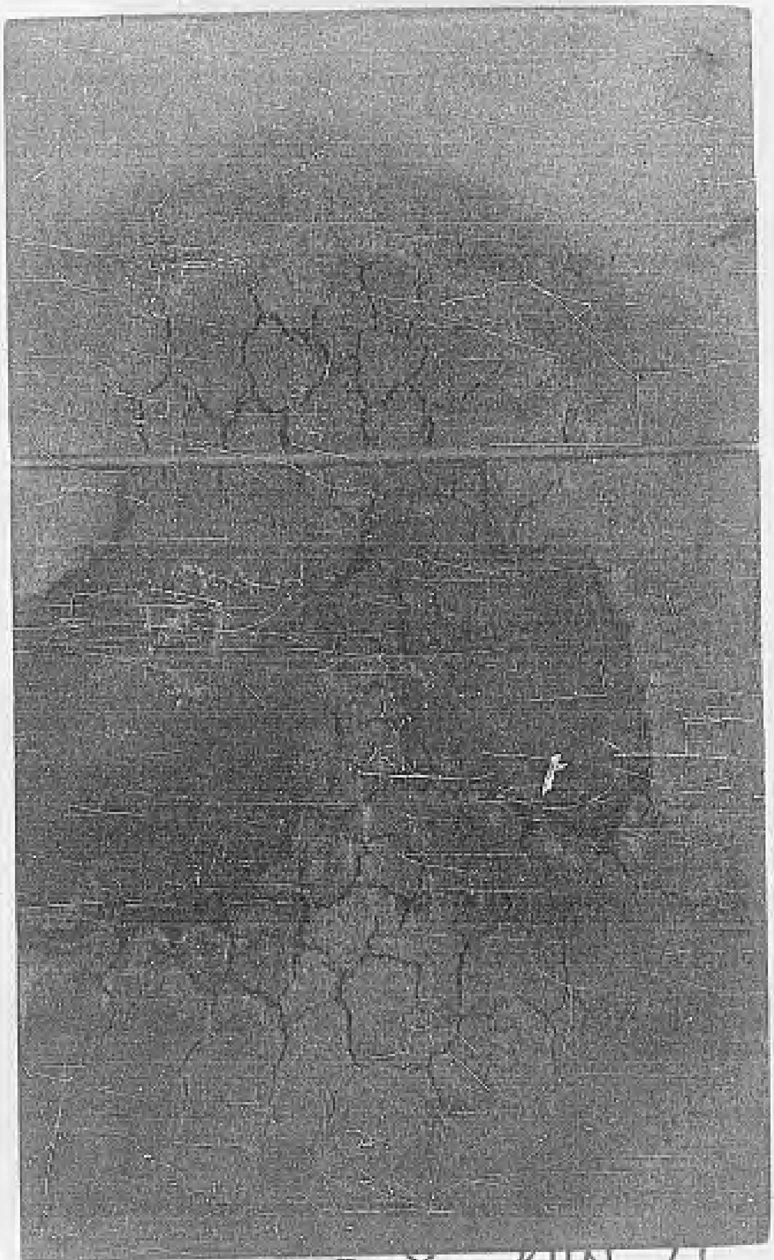

PT-8 RUN 11

NAA MODEL #4, 1/32" SLOT
⊥ WIND, CENTER @ BUTTON, SAME AS TEST #87

CONDITION #4A

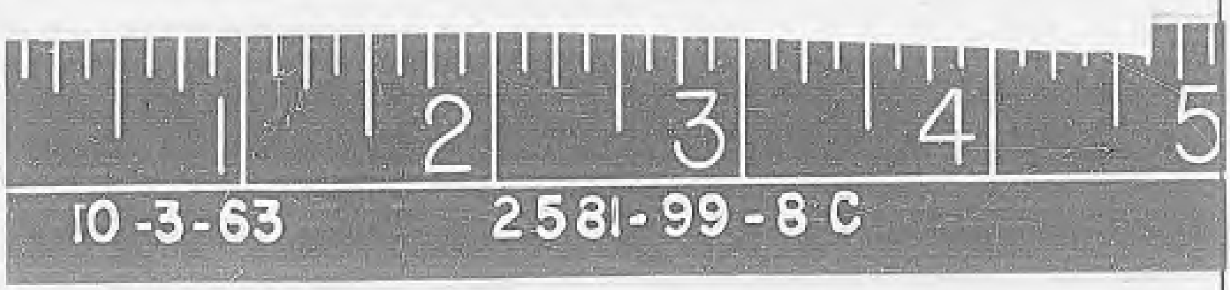

UNCLASSIFIED

UNCLASSIFIED